UNIVERSITY OF TRENTO - Italy

International PhD Program in Biomolecular Sciences
Centre for Cellular, Computational and Integrative Biology

XXXI Cycle

"Exploiting extracellular vesicles for ultrasensitive detection of cancer biomarkers from liquid biopsies"

Tutor
Prof. Alessandro QUATTRONE
CIBIO - University of Trento

Advisor
Dr. Vito Giuseppe D'Agostino
CIBIO - University of Trento

Ph.D. Thesis of

MICHELA NOTARANGELO

Department of cellular, computational and integrative Biology (DCIBIO)
University of Trento

Academic Year 2018 - 2019

Original authorship

Declaration:

I, Michela Notarangelo, confirm that the experimental work described in this thesis is my original work and that all materials obtained from other sources have been properly and fully acknowledged.

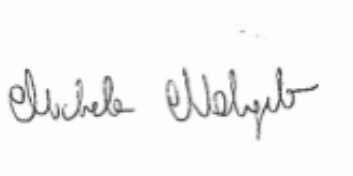

ABSTRACT

Extracellular vesicles (EVs) are small membrane-surrounded structures containing trans-membrane proteins and enclosing cytosolic proteins and nucleic acids. They are released in the extracellular space by both normal and neoplastic cells and play an important role in cell-cell communication in numerous physiological processes and pathological conditions, through the transfer of their functional cargo to recipient cells. EVs are highly abundant in biological fluids, and even more represented in cancer patients' biofluids, therefore many studies suggested that they can be instrumental in liquid biopsies as prognostic markers or for early detection of tumors. Moreover, being secreted by potentially all the cells, they can serve in oncology to represent the tumor heterogeneity, which is underestimated by the current diagnostic tools. Given their small size, EVs are difficult to isolate in a high-throughput way and, therefore, one of the main obstacles to their clinical application, is that the existing isolation methods are impractical.

During these years, I worked at the development and optimization of a novel technique that allows purification of heterogeneous EVs from biological fluids in an efficient, fast and reproducible way. This technique, named Nickel-Based Isolation (NBI), is a biochemical assay that allows obtaining polydisperse EVs in a physiological pH solution, therefore, preserving their morphology, heterogeneity, and stability. We tested and optimized this assay in protein-enriched systems and comparing it to the techniques currently used to characterize and measure EVs, such as flow cytometry and Tunable Resistive Pulse Sensing. We challenged the reproducibility of this method by isolating EVs from different biological fluids. Interestingly, the EVs purified with NBI result more intact and stable compared to the ones obtained with other methods, and can be studied in a clinical setting and used as an innovative tool for detection of molecules associated with diseases. We demonstrated the specificity of the procedure by using individual isolated vesicles in biochemical and molecular assay, optimized to characterize the biological content of EVs. We were able to detect picomolar concentration of PSMA on 10^5 EVs isolated from plasma of prostate cancer patients and BRAF-V600E transcript in just 10^3 EVs from the plasma of colon cancer patients, reaching unprecedented matching with tissue biopsy results. We also investigated the transcriptome of EVs isolated from glioblastoma cancer stem cells, in order to exploit the potential of EVs as diagnostic markers.

TABLE OF CONTENTS

THESIS SUMMARY

This Ph.D. thesis summarizes the main results of almost four years of work on the application of extracellular vesicles (EVs) in liquid biopsies. This research work is part of a larger project that aims at discovering novel biomarkers with a diagnostic, prognostic and predictive value, using non-invasive tests based on molecular analysis of circulating molecules in liquid biopsies of cancer patients.

Chapter I contains a general introduction. To start, I illustrate the biology of extracellular vesicles, with particular attention to their RNA content. Later, I report the evidence on the clinical significance of extracellular vesicles as biomarkers. Finally, I describe an overview of the methods to isolate extracellular vesicles for the sake of contextualizing the nickel-based isolation method as a useful tool to exploit extracellular vesicles in liquid biopsies.

Chapter II focuses on Y-RNAs associated with extracellular vesicles released by glioblastoma cancer stem cells. I explain the reasons why we are focusing on glioblastoma. Then I illustrate the features of cancer stem cells, chosen as a model of the study. Finally, I give some details on non-coding Y-RNAs with insights on their potential as EV-associated biomarkers.

The results related to **Chapter I** refer to a published manuscript (attached), whose details are given in the section “Scientific production.” The results related to **Chapter II** constitute the backbone for a project that is still ongoing, which started after the optimization of the NBI procedure.

ABBREVIATIONS

CTCs: circulating tumor cells
ctDNA: circulating tumor DNA
EVs: extracellular vesicles
NSCLC: non-small cell lung cancer
Exo: exosomes
MVs: microvesicles
ABs: apoptotic bodies
ILV: intra luminal bodies
MVB: multivesicular bodies
ESCRT: endosomal sorting complex required for transport
ARF6: ADP-ribosylation factor 6
TME: tumor microenvironment
exRNA: extracellular RNA
ZP: zeta potential
RBP: RNA binding protein
UC: differential ultracentrifugation
LDL: low density lipoprotein
HDL: high density lipoprotein
Ago2: argonaute 2
PD-L1: programmed death-ligand 1
GBM: glioblastoma
NACT: neoadjuvant chemotherapy
GPC1: glypican 1
WHO: World Health Organization
TMZ: temozolomide
MGMT:O-6-Methylguanine-DNA Methyltransferase
IDH1/2: isocitrate dehydrogenase 1 and 2
CSCs: cancer stem cells
TICs: tumor initiating cells
RNPs: ribonucleoproteins
FACS: fluorescence activated cell sorting
CFDA-SE:carboxyfluorescein-diacetate succinimidyl ester
NBI: nickel-based isolation
CA: citric acid
TRPS: tunable resistive pulse sensing
DLS: dynamic light scattering
TEM: transmission electron microscopy
LVs: large vesicles
SVs: small vesicles
dFBS: depleted of fetal bovin serum
PSMA: prostate specific membrane antigen
ddPCR: digital droplet PCR
FFPE: formalin-fixed paraffin-embedded
RBCs: red blood cells
WBCs: white blood cells
PLTs: platelets
APOA1: apolipoprotein A1
APOB100: apolipoprotein B100
hiPSCs: human induced pluripotent stem cells
AHA: L-azidohomoalanine

BACKGROUND

THE CORE OF PRECISION MEDICINE: CANCER TARGETED THERAPY

Accurate diagnosis and optimization of the available medical treatments are the aims of precision medicine, as every tumor is unique (Bilkey et al., 2019). To determine the most suitable combination of treatments, the clinical history of each patient should be assessed carefully. Screening and detection of molecular alterations in the genomic make-up of individuals indicates the best therapeutic strategy among combinations of surgery, chemotherapy and/or radiation therapy (Siravegna, Marsoni, Siena, & Bardelli, 2017).

The term “biomarker” refers to any feature that can be objectively measured and evaluated in the body or its products as an indicator of physiological processes, pathogenic processes or pharmacologic responses to a therapeutic intervention (Biomarkers Definitions Working Group., 2001; WHO, 2001). Biological markers are therefore classified on their ability to provide information on the cancer prognosis (prognostic markers), as HER2 and K-RAS mutations (Slamon et al., 2001; Van Cutsem et al., 2009), response to therapy (predictive markers) (Goossens, Nakagawa, Sun, & Hoshida, 2015) and to identify the initial signs of a pathological condition (diagnostic markers) (Steffen et al., 2015). During the progression of a pathological condition, the analysis of the molecular variability defines the most effective therapies according to the molecular evolution of the disease (Oldenhuis, Oosting, Gietema, & de Vries, 2008).

In the clinical management of cancer patients, proteins and nucleic acids are usually obtained by needle-biopsy or after a surgical intervention but they need to be implemented in detection rapidity and sensitivity for the assessment of therapeutic benefits over time (Finotti et al., 2018). The evaluation of alternative tools is therefore necessary to upgrade the patient care in the era of a genomic driven-oncology.

INTRODUCTION

CHAPTER I

ULTRASENSITIVE DETECTION OF CANCER BIOMARKERS BY NICKEL BASED ISOLATION

THE ROLE OF LIQUID BIOPSIES IN ONCOLOGY

Tumor status evolves dynamically. The dynamism is reflecting its diverse genetic structure due to the presence of multiple and molecularly different cell subpopulations within the tumor (Siravegna et al., 2017). The genetic instability within tumor populations would confer to cells the ability to develop mutations, intrinsic to every step of carcinogenesis (J. Zhang & Zhang, 2017). These molecular alterations arise to counteract the surveillance mechanisms that non-tumorigenic cells activate to prevent the growth and proliferation of the tumor (Casás-Selves & Degregori, 2011; Gerdes et al., 2014). Together, these features render the genomic make-up of the cancer quite hard to depict.

The clinical management of the tumor progression is mostly based on the analysis on surgical biopsies consisting of solid tissues. The analysis of tissue biopsies represents, though, a single snapshot of the tumor genomic landscape during the course of the disease. The prognostic and predictive value of biomarkers, analyzed within solid samples, is, therefore, lacking information regarding tumor subpopulations, characteristic of the intra-tumor heterogeneity. In this scenario, liquid biopsies can implement the diagnostic and prognostic power of surgical biopsies cost-effectively and sustainably for patients and clinicians (Castro-Giner et al., 2018; Mathai et al., 2019).

A liquid biopsy consists in the collection of liquid biological tissues (e.g. blood, cerebrospinal fluid, saliva, urine) and in the analysis of molecular material that can be informative such as circulating tumor cells, cell-free tumor DNA and, most recently, extracellular vesicles. Liquid biopsies are advantageous as blood draws can be systematically scheduled at consecutive time points during the course of the disease. Moreover, sampling biological fluids are more accessible and less invasive for the patients compared to tissue biopsies. The ability to portray the molecular evolution of the tumor appoints liquid biopsy as a powerful tool to monitor tumor progression and response to the therapy and could represent invaluable support for precision medicine (Castro-Giner et al., 2018; Siravegna et al., 2017).

CIRCULATING MOLECULES AS POTENTIAL DIAGNOSTIC TOOLS

A wide range of tumor-derived material can be isolated from biological fluids. In particular, circulating tumor cells (CTCs), circulating cell-free tumor DNA (ctDNA) and, most recently, extracellular vesicles (EVs) are extracted and interrogated for their transcriptome, genome, methylome, and proteome (Castro-Giner et al., 2018; Siravegna et al., 2017). Currently, ctDNA is the only diagnostic tool derived from a liquid biopsy that is applied in clinical laboratory practice from 2016. In particular, it is used to discriminate which, among patients with non-small cell lung cancer (NSCLC), bear EGFR mutation and are therefore eligible to receive anti-EGFR treatment (Siravegna et al., 2017).

Circulating tumor cells (CTCs)

Circulating tumor cells are intact tumor cells derived from primary lesions and metastatic sites that are actively shed or pushed into the bloodstream by external forces, such as tumor growth (Fidler, 2003). CTCs are highly rare and under-represented in the blood stream as compared to all the non-tumoral blood cells, although their presence has been detected in early-stage cancers (Racila et al., 1998) therefore they can provide vital information on the disease status. The isolation and analysis of CTCs represent a challenge in diagnostic. It has been reported that in the blood of patients with advanced metastatic cancer there is approximately one CTC per $1*10^9$ blood cells and that this quantity is variable among cancer types (Siravegna et al., 2017; Haber & Velculescu, 2014). Moreover, another challenge is to identify which subpopulation of CTCs displays the potential of helping the tumor spreading metastasis (Krebs, Hou, Ward, Blackhall, & Dive, 2010); therefore the molecular characterization of CTCs would be crucial to estimate the risk for metastatic progression of cancer in patients.

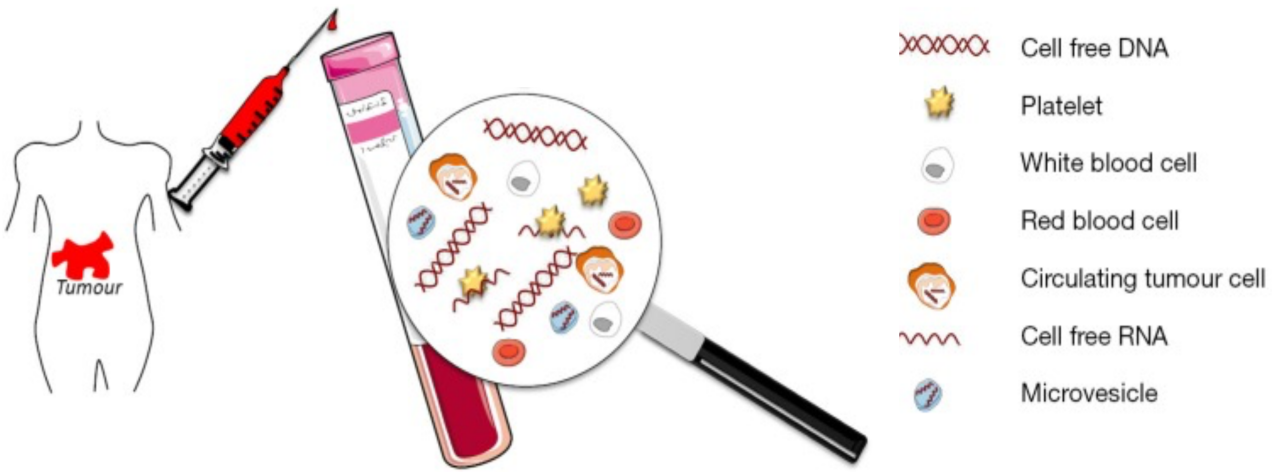

Figure 1. Circulating molecules in liquid biopsies. *Blood cells, circulating tumor cells (CTCs), extracellular vesicles and cell-free nucleic acids circulate in the blood and represent potential biomarkers that can be obtained with liquid biopsies (adapted from Karachaliou, Mayo-de-Las-Casas, Molina-Vila, & Rosell, 2015).*

Cell-free tumor DNA (ctDNA)

Fragments of circulating cell-free tumor DNA, first described in 1948, are released from necrotic and apoptotic cells in the circulation and during cellular turnover (Haber & Velculescu, 2014). Several studies reported that mutations in ctDNA match mutations of the primary tumor and that the relative abundance of ctDNA in the blood increases with tumor growth, indicating its value as a highly sensitive and specific biomarker (Mathai et al., 2019). Furthermore, ctDNA is considered a convenient option whenever tissue biopsies are challenging to obtain surgically (Mathai et al., 2019), as in the case of tumors of the brain or internal organs. The diagnostic disadvantage of ctDNA is that it is very prone to degradation and, since it represents a small fraction of the total DNA in the circulation, its extraction needs to be handled very carefully to preserve it. Despite these issues, the analysis of ctDNA constitutes a specific approach to study the primary tumor since the tumor-specific alterations detected in ctDNA are absent in healthy cells (Haber & Velculescu, 2014).

Extracellular vesicles (EVs)

Extracellular vesicles have recently emerged as an innovative diagnostic tool in liquid biopsy. Extracellular vesicles are nanosized membranous particles that differ in size and biogenesis (Zaborowski, Balaj, Breakefield, & Lai, 2015) and play an important role in cell-cell communication (Skog et al., 2008). Different types of extracellular vesicles are released from normal and tumor cells into biological fluids, and it has been reported an increased abundance of EVs in the blood of cancer

patient, especially after chemotherapy administration (Aubertin et al., 2016). This characteristic renders EVs attractive markers for cancer treatment monitoring. Accumulating evidence indicates that the EV-diagnostic potential is associated to the proteins and nucleic acids that they contain, well protected in a lipid membrane bilayer, that could be exploited as cancer biomarkers (György et al., 2011; Meldolesi, 2018). In particular, the EV cargo reflects the state of its cell of origin and therefore, may provide a reliable photograph of the state and progression of cancers (La Marca, & Fierabracci, 2017). Despite this evidence, longitudinal studies and extensive clinical trials still need to be carried out to demonstrate the diagnostic potential of extracellular vesicles as tumor biomarkers.

EXTRACELLULAR VESICLES

CLASSIFICATION, BIOGENESIS, CELL RELEASE AND UPTAKE

The term “extracellular vesicles” encompasses a heterogeneous population of membranous particles secreted virtually by all types of cells into extracellular space and in bodily fluids. EVs have been isolated in most body fluids from blood to ascites fluid and bile (Raposo & Stoorvogel, 2013). As I mentioned earlier, extracellular vesicles are being extensively studied and characterized by their properties and structures. Despite the increasing attention, the EV field is still coping with inconsistencies in the terminology because the name of vesicles has been mostly customized according to the research context. Here, I will use the term extracellular vesicles to indicate the entire heterogeneous vesicles subpopulation, and I will describe three main types of vesicles, which mostly differ for their biogenesis and size: exosomes (Exo), microvesicles (MVs) and apoptotic bodies (ABs), (Gould & Raposo, 2013).

In general, extracellular vesicles contain proteins, lipids, and nucleic acids. It is still largely unknown whether the EV cargo might be accurately sorted through an organized mechanism, or if the cellular components are randomly shuttled inside vesicles. For example, in some cases, the RNA enclosed in EVs appeared different respect to the cells of origin, suggesting a specific packaging mechanism (Abels & Breakefield, 2016). Moreover, the recurrence of particular proteins in all EV subtypes might suggest a regulated loading mechanism, but further studies are needed to exploit this aspect (Jeppesen et al., 2019). An updated compendium of all the species of RNA, proteins and lipids discovered inside EVs is the Exocarta database (www.exocarta.org, Mathivanan & Simpson, 2009) which represents an useful tool to approach the molecular composition of extracellular vesicles (Keerthikumar, Gangoda, Gho, & Mathivanan, 2017). With a variability depending on the membrane composition of the cells of origin, EV membranes have been found enriched in lipids as sphingomyelin, gangliosides, phosphatidylcholine, cholesterol and endosomal proteins such as Alix,

Syntenin, TSG101, and tetraspanins like CD63 and CD81 (Kowal et al., 2016). Most of the proteins mentioned above were initially associated with exosomes, although there is no consensus on their specificity for vesicles subtypes. In fact, their expression may vary according to the cell types, physiological conditions and biogenesis mechanism (Kalra, Drummen, & Mathivanan, 2016; Théry, Zitvogel, & Amigorena, 2002; Laulagnier et al., 2004; Abels & Breakefield, 2016) therefore, at the moment, there are no reliable markers able to discriminate each vesicle subclass.

Despite the differences in the mechanisms of formation and cargo composition, once released in the extracellular space, EVs can be incorporated into cells via both general or specific mechanisms. For example, they can be internalized into cells by fusion with the plasma membrane, or via endocytosis, and alternatively by phagocytosis. Moreover, EVs can interact with cells through cell-specific mechanisms, defined by the binding of a ligand present on the surface of EV-membrane with a receptor located on particular types of cells (Zaborowski et al., 2015).

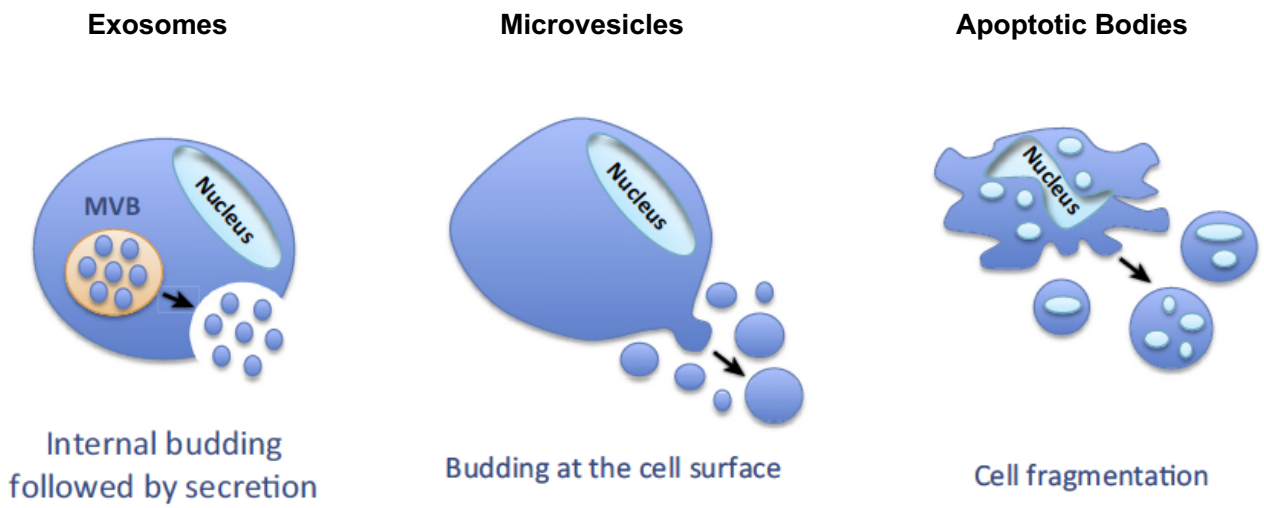

Figure 2. Main classes of extracellular vesicles with relative biogenesis mechanisms*. The vesicular subtypes mainly differ for their mechanisms of formation, which affect their cargo composition (adapted from Kanata et al., 2015)*

In the next three paragraphs, I will focus on each of the main types of extracellular vesicles, with particular attention to their mechanisms of formation and cargo composition.

Exosomes: biogenesis and composition

Exosomes are the smallest vesicles found in the extracellular space with a dimension that varies between 30 and 100 nm. These EVs contain a cargo composed of membrane and cytosolic proteins, a large variety of lipids, glycoproteins, and nucleic acids (RNA and single-stranded or

double-stranded DNA) (Théry et al., 2002). The first evidence that exosomes were released in the extracellular space was observed in the sheep reticulocyte maturation, more than thirty years ago (Pan & Johnstone, 1983) and, initially, they were classified as cellular debris or a way to dispose of cellular waste (Kalra et al., 2016).

Exosomes' biogenesis does not follow the classical secretory pathway since they do not contain any proteins of nuclear, mitochondrial, endoplasmic-reticulum, or Golgi-apparatus origin (Théry et al., 2002). In particular, exosomes are formed within the cell through endocytosis (Morelli et al., 2004) in two main steps: the internalization of proteins and membrane-associated molecules, with the formation of the early endosome, and their maturation and release through multivesicular bodies (MVB) (H Rashed et al., 2017). Precisely, during maturation in the endosomes, the proteins can follow two faiths: they can either be sent back into the plasma membrane and remodeled or incorporated inside endosomes to form intraluminal vesicles (ILVs). When endosomes are packed with ILVs, they can be referred to as multivesicular bodies, whose formation is regulated by the endosomal sorting complex required for transport (ESCRT) complexes that promote the invagination of the endosomal limiting membrane (Hurley, 2008; Colombo, Raposo, & Théry, 2014). At this point MVBs may fuse with lysosomes for degradation of their contents or integrate with the plasma membrane through a Calcium-dependent mechanism, unloading their components into the extracellular space, in the form of exosomes (Kowal, Tkach, & Théry, 2014; Colombo et al., 2014; Kalra et al., 2016; Savina, Furlán, Vidal, & Colombo, 2003). The role of the ESCRT complexes in the regulation of the exosome formation is still not completely clarified, but it clearly plays a crucial role in sorting and recycling specific proteins into MVBs, as TSG101, CHMP4 and ubiquitinated proteins that are found particularly enriched in exosomes (Kowal et al., 2014; Kalra et al., 2016; Théry et al., 2002). Of particular relevance is the synergy between the Syndecan proteoglycan family of proteins with Syntenin and Alix, soluble proteins and ESCRT-interactors, which promotes the membrane remodeling during the formation of ILVs, precursors of exosomes (Hessvik & Llorente, 2018; Baietti et al., 2012).

Microvesicles: biogenesis and composition

Microvesicles, also known as ectosomes or shedding vesicles, are bigger vesicles whose size ranges from 100 nanometers (nm) to a few microns (μm). Differently from exosomes, microvesicles originate from the plasma membrane (Tricarico, Clancy, & D'Souza-Schorey, 2017). Contrarily to exosomes, the biogenesis of microvesicles has been far less characterized. To date, the complexity of MVs' cargo indicates that their release is anticipated by a vertical trafficking and a lateral redistribution of outer molecules directed to the plasma membrane. This process causes the

remodeling of the membrane composition, resulting in the budding event (D'Souza-Schorey & Clancy, 2012; Tricarico et al., 2017). As for exosome biogenesis, the formation of MVs involves the endosomal machinery regulated by the Ras-related ARF family of small GTP-binding proteins and components of the ESCRT system (Tricarico et al., 2017). In particular, ADP-ribosylation-factor-6 (ARF6) has been found involved in the modulation of microvesicle release into the surrounding environment (Muralidharan-Chari et al., 2009).

As I mentioned before, It is still under debate whether the vesicle cargo is selectively packaged inside EVs or not. While some components are randomly incorporated into MVs, protein and nucleic acids may also be selectively recruited (D'Souza-Schorey & Clancy, 2012; Tricarico et al., 2017). A recent evidence, from Jeppesen and colleagues, suggested that annexin A1, a membrane-localized protein that binds phospholipids, might be a specific marker of microvesicles, as the result of the budding from the plasma membrane (Jeppesen et al., 2019) but more studies are required to define a distinctive pattern in EV subtypes.

Apoptotic bodies: biogenesis and composition

Apoptotic bodies (ABs) are large subcellular particles of a diameter between 800 - 5000 nm, which are also present in body fluids. Contrarily to exosomes and microvesicles, ABs are released from apoptotic and necrotic cells (Crescitelli et al., 2013). The formation of apoptotic bodies is the result of the dying cell disassembly, a mechanism necessary to guarantee the homeostasis of a multicellular organism. Hence, their content is packed with cellular components such as DNA, RNA, histone-proteins, and loaded with autoantigens, as observed by Schiller et al., 2008 in patients affected by systemic lupus erythematosus (SLE).
Apoptotic bodies mostly overlap in size and protein composition (e.g., CD63, LAMP1) with MVs derived from viable cells thus, their main distinction remains the biogenesis mechanism which for ABs is dependent on the sphingosine-1-phosphate/sphingosine-1-phosphate receptors (S1P/S1PRs) signaling (S. J. Park et al., 2018). Interestingly, Annexin V protein, whose expression is typically tested in may apoptotic assays, has been found associated with the other main types of extracellular vesicles, and recently exploited to characterize EVs in biological fluids, despite their mechanism of formation (Igami et al., 2019). Despite the morphological and biogenetic differences, at the moment there is no a systematic way to isolate independently apoptotic bodies from larger vesicles, excluding the cross-contamination of the two vesicles (Crescitelli et al., 2013).

INNER AND OUTER SIDES OF EXTRACELLULAR VESICLES

In this paragraph, I will focus on two main components of extracellular vesicles, which have been exploited and investigated during my research work. In detail, I will focus on the properties and composition of the membrane of extracellular vesicles, which have been employed by several techniques to target EVs, or exploited to use EVs as drug delivery tools. Later, I will summarize the characteristics of RNA associated with extracellular vesicles, which is extensively analyzed in liquid biopsies, as a source of informative genetic messages derived from the cells of origin.

MEMBRANE OF EXTRACELLULAR VESICLES

Extracellular vesicles are submicron particles surrounded by a lipid bilayer, whose composition may be variable between the different subtypes. Generally, the lipid composition of the vesicles' membrane partially reflects the architecture of the cell membrane with some structural differences. For example, the exosomal membrane is characterized by a lack of asymmetry in phospholipids between the two membrane leaflets and consistent higher trans-bilayer movements as compared to the plasma membrane (Kastelowitz & Yin, 2014). Exosome membrane has also been proved to be less fluid than cell membrane, due to an increased distribution in saturated fatty acids along with phosphatidylcholine and phosphoethanolamine species (Skotland, Sandvig, & Llorente, 2017). This rigidity is not hampering the flip flop rate of lipids: on the contrary, this feature is common to other membranes of subcellular organelles, such as endoplasmatic reticulum (ER), characterized by an increased membrane dynamics (Laulagnier et al., 2004).

The membrane of vesicles is also typically more enriched in sphingolipids and contain less cholesterol than the plasma membrane (Kastelowitz & Yin, 2014). Further studies demonstrated that both exosomes and microvesicles contain ceramide (Trajkovic et al., 2008) and are enriched in phosphatidylserine on the outer membrane leaflet that confers them a net negative charge (Laulagnier et al., 2004). Another peculiarity of EV membrane is the high degree of membrane curvature due to their substantial anionic lipid density (Kastelowitz & Yin, 2014) and the presence of electrostatic interactions between molecules embedded in the membrane (Bigay & Antonny, 2012). Because of this aspect, under physiological conditions (pH 5), heterogeneous EVs display negative fluctuations of zeta potential (ZP), establishing a net negative surface charge (Salgın, Salgın, & Bahadır, 2012).

For all these reasons, the composition and shape of the EV membrane may render possible the biophysical interaction of EVs with different molecules (Konoshenko, Lekchnov, Vlassov, & Laktionov, 2018). This aspect is particularly relevant, suggesting that the biophysical properties of extracellular vesicles may be exploited for isolation and targeting of these particles in biological fluids. Therefore, despite their heterogeneity, EV collectively share similar biophysical features such as ZP, offering scientists the opportunity to target them for multiple applications.

RNA LANDSCAPE OF EXTRACELLULAR VESICLES

In this paragraph, I will describe the main species of RNA associated with extracellular vesicles, highlighting their importance, and describe some suggested loading mechanisms of RNA inside EVs. Generally, the term extracellular RNA (exRNA) identifies all the RNA species that are contained in the extracellular space whose presence has been found in biological fluids (X. Chen, Liang, Zhang, Zen, & Zhang, 2011). In detail, the RNA is present in the extracellular space as cell-free RNA, high-density lipoprotein-bound RNA, RNA encapsulated inside EVs and RNA associated to Argonaut 2 (D D Taylor & Gerçel-Taylor, 2005).

The discovery of stable forms of extracellular RNA protected by enzymatic RNAse degradation allowed to understand that RNA is also present within vesicles that defend it, arousing great interest in the field. Valadi and colleagues, in 2007, were the first to report the evidence of RNA contained inside extracellular vesicles. They also demonstrated that extracellular messenger RNA (RNA) and microRNA (miRNA) are still functional when transferred to recipient cells (Valadi et al., 2007). In other groundbreaking studies, tumor EVs were found enriched of mRNAs respect to donor cells (Skog et al., 2008) and the oncogenic transcript EGFR vIII, shuttled via microvesicles, induced translation of functional proteins after uptake into the recipient cells (Al-Nedawi et al., 2008).

Knowing that cells can communicate via extracellular vesicles and exchange genetic information, opened up new possibilities regarding the role of EVs, suggesting a considerable potential of particles in cellular crosstalk. To interpret and unravel the nature and purpose of RNA transfer in cell-cell communication, in 2013 it was established the Extracellular RNA Communication consortium, a program supported by NIH Common Fund, with particular attention on EV-RNA (Ainsztein et al., 2015).

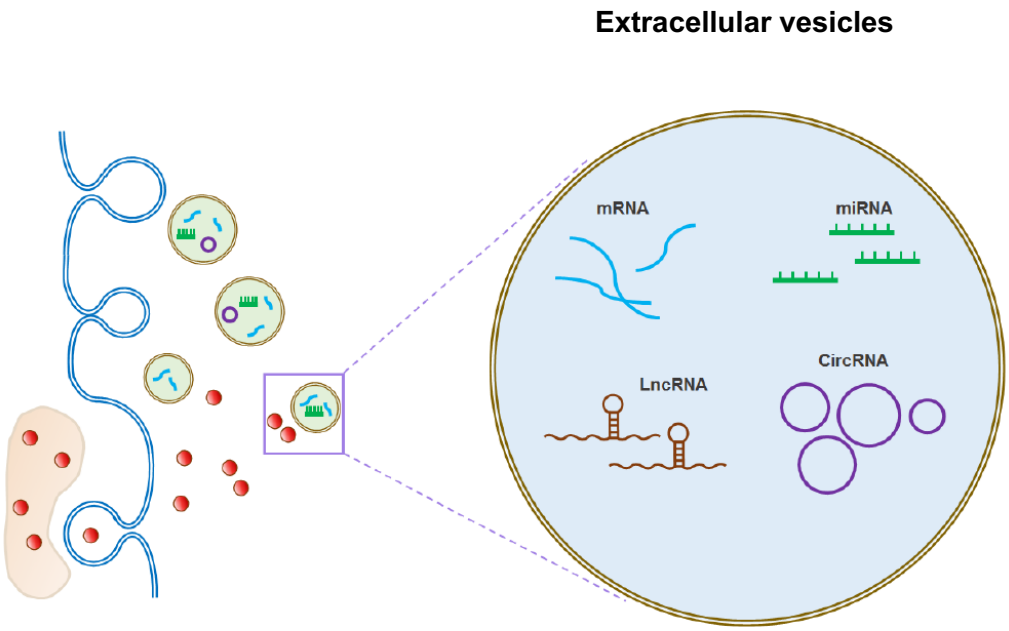

Figure 3. Most represented species of RNA enriched in extracellular vesicles *(adapted from Kim et al., 2017)*

Since 2007, many studies focused on the analysis of the EV transcriptome. The first RNA species observed in extracellular vesicles were mRNA and miRNA (Valadi et al., 2007); several non-coding RNA species (smaller than 200 nucleotides), were further identified by deep RNA sequencing (Nolte-'t Hoen et al., 2012) including transport RNA (t-RNA), piwi-interacting RNA (piRNA), ribosomal RNA (rRNA), long non coding RNA (lncRNA), circular RNA (circRNA) and small nuclear (snRNA) and nucleolar (snoRNA). Coding RNA species were observed in both short full length and fragmented forms that mostly reflected the cellular transcriptome (Wei et al., 2017). The presence of transcripts enclosed in EVs represents a rare event. It has been reported that one copy of full-length mRNA can be found in approximately ten EVs, and the same ratio applies to miRNA as well (Wei et al., 2017b).

Little is known about the mechanism of RNA encapsulation inside EVs. Given the enrichment or the exclusive presence of some RNA species inside EVs compared to deriving cells, selective loading mechanisms have been proposed (Skog et al., 2008; Kim, Abdelmohsen, Mustapic, Kapogiannis, & Gorospe, 2017). A study of Janas and co-workers hypothesized that RNA loading probably occurs prior the exocytosis/budding event during MVB formation, in proximity to the cytosolic side of MVB delimiting membrane (Janas, Janas, Sapoń, & Janas, 2015). Other studies suggest that RNA loading into EVs may be mediated by RNA binding proteins (RBPs). The involvement of RBPs might contribute, in fact, to explain the stability of EV-RNA, which is well protected by RNAse degradation in the extracellular space (Douglas D. Taylor & Shah, 2015). To date, specific binding motifs, called EXOmotifs, have been identified in miRNA as binding sites of the RNA binding protein

heterogeneous nuclear ribonucleoprotein A2B1 (hnRNPA2B1) (Villarroya-Beltri et al., 2013). In this case, sumoylation seemed to affect the localization of hnRNPA2B1, by favoring its recruitment inside EVs; suggesting that post-translational modification can regulate the binding between RNA binding proteins and EV-RNA (Villarroya-Beltri et al., 2013). Another study investigated the role of Y-Box Protein 1 (Y-BX1) in the sorting of mir223, a microRNA abundantly present in exosomes from donor cells (Shurtleff, Temoche-Diaz, Karfilis, Ri, & Schekman, 2016). One more evidence comes from Batagov and colleagues, which applied an *in-silico* approach to predict potential RNA secretory motifs in the RNA loaded inside EVs. These motifs correlated with the presence of EV-RNAs, although not sufficient to explain the sorting of specific RNA species packaged into EVs (Batagov, Kuznetsov, & Kurochkin, 2011). Despite the efforts made so far, further investigations are needed to decipher the mechanisms of RNA recruitment inside EVs, and better understand the role of the horizontal transfer of genetic material between cells.

OVERVIEW OF METHODS TO ISOLATE EXTRACELLULAR VESICLES

The search for reproducibility and the need to isolate EVs for biomarker discovery and diagnostic analysis, is one of the biggest challenges to the clinical utilization of extracellular vesicles. Extracellular vesicles are more or less a hundred time smaller than a cell (Bathini et al., 2018), and brand-new techniques are increasingly required to guarantee a targeted enrichment of these particles, surpassing the contamination by extracellular contaminants. The ideal EV isolation method would allow specific isolation of extracellular vesicles, in a high-throughput manner, with optimal yield and in a reproducible way. These characteristics are necessary to obtain a sample that can be adequately characterized and analyzed. To address this goal, the scientific community is putting efforts to set up standardized procedures and technical tools to consistently isolate EVs. To centralize the knowledge in the field, the International Society of Extracellular Vesicles (ISEV) is the reference organization that publishes guidelines and protocols to help scientists in exchanging information and standardize the experimental procedures from 2012 (Araldi et al., 2012). Lately, in 2017, a collateral consortium (http://evtrack.org/) was also born to collect and interpret all the issues fostered in the scientific community, for the sake of ensuring a proper experimental reproducibility (EV-TRACK Consortium, Van Deun et al., 2017).

Brand-new technologies are evolving over time to find the most optimal way to isolate EVs. When it comes to the choice of the method, each technique has its limitations and advantages indeed. The more frequently adopted EV-isolation methods include differential ultracentrifugation, eventually coupled to density gradient, immunocapture with or w/o magnetic beads, filtration, size exclusion,

polymeric precipitation with hydrophobic agents, and microfluidics-based techniques (Gardiner et al., 2016).

The **differential ultracentrifugation** (UC) is the most widely applied technique (Momen-Heravi et al., 2013) and long considered the *gold standard*. UC concentrates the vesicles and allows for size-based sedimentation of EVs according to the g-force applied without interferences from chemical additives, essential in light of downstream applications. Briefly, the samples are progressively centrifuged at different speeds to get rid of cells, debris, extra-vesicular protein aggregates and apoptotic bodies, then further centrifuged at 10,000xg x 30 minutes to pellet larger vesicles and finally spun at 100,000×g for 70 minutes to pellet the smaller vesicles (Théry, Clayton, Amigorena, & Raposo, 2006; Takov, Yellon, & Davidson, 2019; Di Vizio et al., 2012). The main issues of this technique are the presence of non-vesicular contaminants and the required amount of time. Many studies have reported a co-sedimentation of lipoproteins and EVs when using UC, especially in the case of EV isolation from body fluids where both particles are abundantly present (Sódar et al., 2016). Contaminants are mostly proteins and lipoproteins due to the similar density of EVs and lipoproteins (e.g., low-density lipoproteins or LDL and high-density lipoproteins or HDL), ranging between 1,063 and 1,21 g/ml^{-1} (Witwer et al., 2013; Yuana, Levels, Grootemaat, Sturk, & Nieuwland, 2014).

To overcome this issue, ultracentrifugation steps have been implemented with a fractionation step using **density gradients of sucrose or iodixanol** (Optiprep). Gradients allow recovering particles of interest according to their floatation speed and density without excluding heterogeneous populations of extracellular vesicles (Witwer et al., 2013; Kowal et al., 2016). However, Yuana and colleagues in 2014 showed that EVs and HDL also resulted co-purified to some extent in plasmatic EV preparations obtained from plasma samples with sucrose density gradient centrifugation, proving the failure of the technique in targeting specifically EVs. To this end, following steps using size exclusion strategies or filtration may be needed to ensure that the obtained results in the downstream analysis can be attributed to EVs (Yuana et al., 2014; Menard, Cerezo-Magaña, & Belting, 2018).

Isolation techniques	Category	Principles	Evidences of clinical application	Disadvantages for clinical application	References
Differential ultracentrifugation	Differential ultracentrifugation	EV are concentrated by g-force.	Yes	Protein contamination Laborious Low-throughput	(Gardiner et al., 2016; Osti et al., 2019)
Sucrose density gradient Iodixanol density gradient (Optiprep™)	Density gradient ultracentrifugation	EVs migrate according to their equilibrium buoyant density in a continuous or discontinuous gradient and are pelleted by g-force.	Yes	Laborious Low-throughput	(Kawakami et al., 2017; Kowal et al., 2016)
PureExo exosome isolation kit™ Polyethylene glycol (PEG) PROSPR (PRotein Organic Solvent PRecipitation) Acetate Ammonium sulphate Total Exosome Isolation™ Exoquick™ Exo-spin™	Polymeric precipitation	The addition of water-excluding precipitants allows to concentrate EVs	Yes	Protein contamination	(Konoshenko et al., 2018; Tang et al., 2017)
ExoChip™ Immunological separation Nanowire-based traps	Microfluidics	EV are immobilized on surfaces and separated according to size, markers or acoustic, electrophoretic and electromagnetic fields.	Yes	Expensive Technical expertise required	(S.-C. Guo, Tao, & Dawn, 2018; Kanwar, Dunlay, Simeone, & Nagrath, 2014)
Antibody coated magnetic beads	Immuno-affinity	EV are captured using a specific antibody coupled to beads are separated	Yes	Expensive Lack of specific markers	(Balaj et al., 2015; Ghosh et al., 2014; Kawakami et al., 2017)

Antibody coated latex beads Heparin affinity		by centrifugation or magnetically.			
Sepharose gel Sephadex gel Izon qEV™ column Bio-gel A™	Size exclusion	EVs are separated based on their size.	Yes	Lipoprotein contamination For large scale application it may require pre-concentration steps	(Buschmann et al., 2018; Lane, Korbie, Trau, & Hill, 2017; Monguió-Tortajada et al., 2019)
Charge based precipitation AIEX anion exchange column	Charge based precipitation	Negative charge of EV charge is exploited to capture them.	No	Lipoprotein contamination Usually it is coupled with further passages	(Deregibus et al., 2016a; Heath et al., 2018)
Ultrafiltration	Microfiltration	EVs are separated using semipermeable membranes with defined pore size or molecular weight.	Yes	EV integrity may be affected	(Xu, Greening, Rai, Ji, & Simpson, 2015; Xu, Greening, Zhu, Takahashi, & Simpson, 2016)
Asymmetrical Flow Field-Flow Fractionation (AF4) Hollow-Fiber-Flow Field-Flow Fractionation (HF5)	One-phase chromatography	EVs are separated based on their electrophoretic mobility by electrostatic force, size or molecular weight.	Yes	Laborious Technical expertise required	(Giddings, Yang, & Myers, 1976; Marassi, Roda, Zattoni, Tanase, & Reschiglian, 2014; H. Zhang & Lyden, 2019)

Table 1. Classification of the main methods applied to isolate extracellular vesicles based on their properties and utility for clinical applications.

Generally, the majority of techniques are time-consuming, low-throughput, expensive, and labor demanding, representing limitations to the application of EVs into the everyday clinical routine. To overcome these issues, **antibody-based strategies** and **EV-targeting nano-probes** have been developed to recognize the vesicles for subsequent analysis of their content (Liang et al., 2017; Wan et al., 2017). These techniques are advantageous to discover clinically relevant markers co-

expressed with proteins that generally decorate the surface of EV membrane. A drawback of this system is represented by the structural differences of the composition of EVs, which may be potentially influenced by the cell status and need to be assessed over time and between cellular types. As a result, these techniques might select subpopulations of vesicles, relying on their affinity with two specific antigens, with the risk to bypass relevant diagnostic information.

Other commonly used methods are **commercial kits**, such as ExoQuick™ and Total Exosome Isolation™, based on polymeric precipitation solutions. Despite the enrichment of EVs obtained with these kits, the purity of the sample obtained may be not sufficient for diagnostic applications. For example, using these methods Van Deun and colleagues observed the presence of protein aggregates as Argonaute 2 (Ago2) together with EVs, in comparison to a preparation of EVs isolated by Optiprep density gradient ultracentrifugation (Van Deun et al., 2014).

Alternative quick EV-isolation procedures, proven to reduce protein contaminants in comparison with ultracentrifugation, exploited the **negative surface charge of EVs** (Deregibus et al., 2016; Kosanović, Milutinović, Goč, Mitić, & Janković, 2017; Heath et al., 2018). As previously mentioned**,** EVs with different size (polydisperse) are known to have negative fluctuations of zeta potential (ZP), a physicochemical parameter that quantifies the surface charge of biological particles (Salgın et al., 2012). In these cases, ZP is exploited to capture EVs through interactions with positively charged molecules. These assays present the advantage of allowing EV purification in a fast and less laborious manner, despite in some cases it is still necessary to proceed with further passages to get rid of sticky contaminants such as lipoproteins, affecting the overall simplicity of the assay (Deregibus et al., 2016).

Many technical challenges need to be overcome to isolate specifically EVs. And the standardization of the isolation methods is of utmost priority in the field since the sensitivity and specificity of the results are highly dependent on the methods used to enrich them (Van Deun et al., 2014; Gardiner et al., 2016). Furthermore, the employment of EVs as potential diagnostic resources in a clinical setting requires suitable technologies and quality controls that could be daily managed by the hospital staff or delegated to specific facilities. The translation of extracellular vesicles as a potential source of biomarkers in a clinical scenario still requires a suitable isolation method, compared to the most labor-requiring techniques (refer to Table.1).

CLINICAL SIGNIFICANCE OF EXTRACELLULAR VESICLES

THE ROLE OF TUMOR DERIVED EXTRACELLULAR VESICLES AS PROMISING CANCER BIOMARKERS

A large number of existing studies demonstrated that tumor cells influence the extracellular environment and transform healthy cells to establish the prevalence of a cancer phenotype (Hanahan & Weinberg, 2011). To sustain their proliferation, cancer cells build a network within the tissue environment, supported by the release of soluble factors (e.g., cytokines, growth factors) and secretion of extracellular vesicles.

Extracellular vesicles, critical players in cell-cell communication, are known to be released in the tumor microenvironment (TME) and to induce a neoplastic reprogramming of non-tumoral cells (Abd Elmageed et al., 2014; Maacha et al., 2019; Guo et al., 2017). In particular, *in vitro* studies of glioblastoma multiforme, melanoma, colorectal, breast and prostate cancer cell lines, described a massive release of extracellular vesicles compared to healthy cells (Xu et al., 2018). Several studies demonstrated that the tumorigenic potential of EVs is also intrinsic to their bioactive content and that nucleic acids and proteins contained in EVs have a role in promoting the tumor growth, angiogenesis, invasion of normal tissues and resistance to anti-tumor drugs (Melo et al., 2014; Zhao, Wang, Xiong, & Liu, 2018).

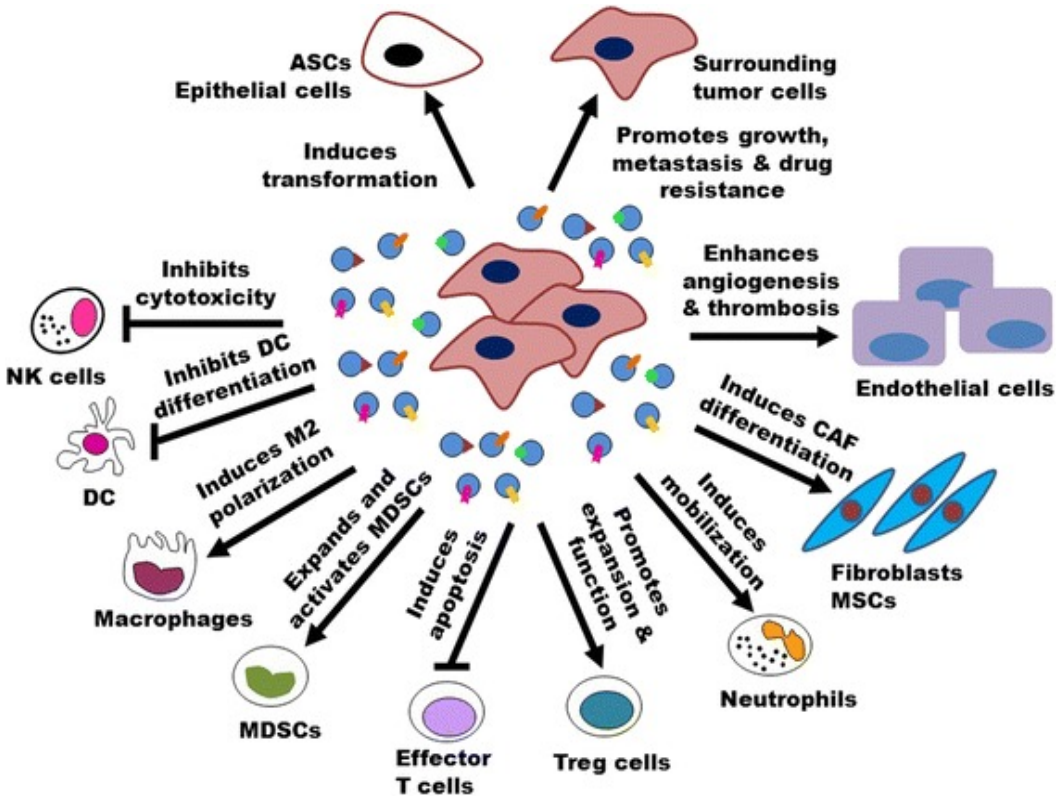

Figure 4. Illustration of the multiple functions exerted by extracellular vesicles in the tumor microenvironment (X. Zhang et al., 2015).

A key feature of cancer is its heterogeneous composition. Within a single tumor, several tumor niches exist, with different morphology and functions. In this scenario, aggressive populations of tumor cells can spread their oncogenic material (mostly composed of proteins and RNA) to non-tumorigenic or less aggressive tumor cells via EVs, therefore increasing their oncogenic activity and invasiveness.

One of the first evidence of RNA shuttled by extracellular vesicles, involved the transfer of oncogenic EGFR vIII transcript by microvesicles derived from patients to glioblastoma recipient cells, resulting in their increased tumor cell growth (Al-Nedawi et al., 2008). Alternatively, the transfer of EV-membrane proteins has been observed to protect the tumor by evading the functions of the immune system. A recent study demonstrated that metastatic melanomas secrete EVs expressing PD-L1 (programmed death-ligand 1), which seems to impair the effects of T cells and NK cells to favor the tumor growth (Xu et al., 2018). Tumor cells can internalize EV containing proteins with anti-apoptotic activity such as the protein survivin, that protects the tumor by inhibition of apoptotic cell death (Khan et al., 2011). Furthermore, tumor EVs can mediate the expulsion of drugs, therefore, playing a role in drug resistance. For example, Safaei and colleagues observed an increased secretion of exosomes expressing cisplatin transporters in drug-resistant cells compared to sensitive ones, promoting the cisplatin efflux in drug-resistant ovarian carcinoma cells (Safaei et al., 2005). Recent evidence underlined how tumor cells could disseminate EVs to distant organs, predisposing a

hosting microenvironment for tumor growth called pre-metastatic niches (Peinado et al., 2017). In line with this, Hoshino and colleagues performed a proteomic profile on cells and EV of several cancer types with a higher propensity to metastasize and identified a strong correlation between the expression of integrins, proteins of the EV surface, and the initial formation of metastatic sites. Most importantly, they discovered that the formation of these pre-metastatic niches mediated by EV-integrins was organ dependent, indicating that they might represent organotropic markers that allow predicting the metastatic sites (Hoshino et al., 2015). Finally, tumor EVs help the tumor cells to build new blood vessels, required for tumor invasion, by transferring pro angiogenic factors such as VEGF, PDGF and angiopoietins to surrounding endothelial cells. This process has been described in glioblastoma (Kucharzewska et al., 2013) and also in other tumors (L. Zhang et al., 2015; J. E. Park et al., 2010).

Whether the tumorigenic properties of extracellular vesicles are connected to a particular subtype of EV is still a question to be addressed, since even within a single EV subtype there is a large variability in structure and cargo composition (Tauro et al., 2013; Willms et al., 2016). Larger microvesicles have been objects of considerable attention from a clinical perspective. Di Vizio and colleagues, in 2012, were the first to observe the presence of larger vesicles (approximately 1-10 μm of diameter) in the blood of prostate cancers mouse models. These so-called "*oncosomes*" were most abundant in the circulation of mice with metastatic tumors (Di Vizio et al., 2012) and have been identified by recent studies as carriers of DNA that resemble the genomic architecture of the deriving cells (Vagner et al., 2018). Also, Wright PK, in 2014, reported *"...the discovery of giant (3-42 μm) intracellular and extracellular vesicles..."* in both immortalized and patient-derived breast cancer cell lines, indicating that they can be an exciting subject of study from a diagnostic perspective related to tumor progression state (Wright et al., 2014).

EXTRACELLULAR VESICLES IN LIQUID BIOPSIES: STATE OF ART

The interest in EV as potential cancer biomarkers highly increased in the last decade, and the biological fluids of cancer patients are more and more investigated for their abundance in EVs. The presence of extracellular vesicles has been extensively documented in body fluids such as blood, urine, semen, saliva, amniotic fluid, breast milk, cerebrospinal fluids, bile, ascites and even tears (L. Guo & He, 2017).

Notably, the simple higher abundance of EV in biological fluids of patients compared to healthy donors is considered a specific and sensitive marker of clinical significance *per se* (Xu, Greening, Zhu, Takahashi, & Simpson, 2016; (König et al., 2018). An increased release of EVs has been

reported in the plasma of glioblastoma (GBM) patients at diagnosis, compared to thirty-three healthy donors, and when compared to patients with other brain lesions, the EV enrichment was proven to be glioblastoma specific (Osti et al., 2019). Moreover, the relative abundance of EVs did not correlate with canonical GBM markers, or with tumor size (Osti et al., 2019), suggesting that EVs can represent an additional source of diagnostic information, to the existing clinical parameters. Plasmatic levels of GBM EVs decreased post-surgery and raised with relapse (Osti et al., 2019) suggesting that EVs can recapitulate and describe the tumor evolution. Similarly, elevated levels of EVs in the circulation of breast cancer (BC) patients before the neoadjuvant chemotherapy (NACT) were associated with a negative therapeutic outcome, while a higher EV count post NACT correspond with disease-free survival (König et al., 2018).

Apart from being indicators of clinical status *per se,* EVs are also carriers of informative molecules that have been exploited in clinical studies. At present, there are six registered interventional studies ongoing in different countries focused on the interaction between EVs and cancer (see Table.2). High levels of the protein Glypican-1 (GPC1) have been detected in serum EVs of breast cancer (BC) and pancreatic cancer patients, compared to healthy controls (Melo et al., 2015). Notably, in pancreatic carcinoma, the different expression of GPC1 associated with EVs was able to discriminate patients with early and late stage cancer (Melo et al., 2015). Besides, it is possible to detect mutation in the nucleic acids carried by vesicles, as the case of BRAFV600E mutation, KRAS expression and EGFR alterations, discovered in exosomal DNA of patients with melanoma, lung cancer and pancreatic carcinoma respectively (reviewed by Fais et al., 2016). Importantly, abundant levels of plasmatic EVs double positive for caveolin-1 and CD63 in stages III and IV melanoma patients revealed to be more specific than classical markers in retrospective studies (Logozzi et al., 2009; Fais et al., 2016).

The association of multiple circulating microRNAs with pathological conditions raised a great interest in the field (Douglas D Taylor & Gercel-Taylor, 2013). Extracellular miRNAs are highly stable in body fluids, at room temperature and resist to freeze-thawing cycles (reviewed by Gudbergsson, Johnsen, Skov, & Duroux, 2016), therefore representing markers that can be relatively easily obtained and processed. Circulating miR-21 and miR-1246 expressions were detected in higher amount in plasma of patients with BC, with respect to healthy controls, indicating that they could represent diagnostic indicators of the disease (Hannafon et al., 2015). Likewise, the presence of multiple microRNA as let-7a, miR-1229, miR-1246, miR-150, miR-21, miR-223, and miR-23a allowed to discriminate patients with colorectal cancer and healthy controls (Ogata-Kawata et al., 2014).

In conclusion, inner and outer EV features present a clinical significance and therefore, can be interrogated in liquid biopsies as diagnostic tools.

Project	Pathological condition	Focus of Intervention	Status
Pimo Study: Extracellular Vesicle based Liquid Biopsy to Detect Hypoxia in Tumors	Cancer	Hypoxia marker	Recruiting
Olmutinib Trial in T790M (+) NSCLC Patients Detected by Liquid Biopsy Using BALF Extracellular Vesicular DNA	Non-Small Cell Lung Cancer	Drug: Olmutinib	Active
Pilot Study with the Aim to Quantify a Stress Protein in the Blood and in the Urine for the Monitoring and Early Diagnosis of Malignant Solid Tumors	Cancer	Blood/Urine samples	Recruiting
A Phase III Trial of Pertuzumab Retreatment in Previously Pertuzumab-Treated Her2-Positive Advanced Breast Cancer	HER2-positive Breast Cancer: locally advanced or metastatic	•Drug: Trastuzumab •Drug: Pertuzumab •Drug: Docetaxel •Drug: Paclitaxel •Drug: Nab-paclitaxel •Drug: Vinorelbine •Drug: Eribulin •Drug: Capecitabine •Drug: Gemcitabine	Recruiting
ncRNAs in Exosomes of Cholangiocarcinoma	Cholangiocarcinoma Benign Biliary Stricture	N/A	Recruiting
GMCI, Nivolumab, and Radiation Therapy in Treating Patients with Newly Diagnosed High-Grade Gliomas	Glioma, Malignant	•Biological: AdV-tk •Drug: Valacyclovir •Radiation: Radiation •Drug: Temozolomide •Biological: Nivolumab •Other: Laboratory Biomarker Analysis	Recruiting

Table 2. Registered clinical trials based on extracellular vesicles: an updated report from the NIH database *(ClinicalTrials.org).*

CHAPTER II

EXPLORING THE ROLE OF EXTRACELLULAR Y-RNAs IN GLIOBLASTOMA CANCER STEM CELLS

THE DISEASE: GLIOBLASTOMA

Glioblastoma multiforme (GBM) is one of the most malignant tumors of the central nervous system. It accounts for 54% of all glioma types and it is mainly diagnosed in adulthood (Ostrom et al., 2014). In 2016, the World Health Organization (WHO) classified GBM as a grade IV glioma (Louis et al., 2016) because of its elevated invasive nature (Hatoum, Mohammed, & Zakieh, 2019). In fact, even though GBM can be considered a rare type of cancer, with a worldly incidence of about 3.9 per 100,000 people, it is one of the deadliest tumors, with a survival rate of 15 months after diagnosis, representing a social healthcare emergency, given the poor clinical outcome (Hanif, Muzaffar, Perveen, Malhi, & Simjee, 2017b).

Glioblastoma is characterized by a high grade of inter and intra-tumor heterogeneity, both molecular and cellular; which underlies to the GMB resistance to therapies and to a high frequency of recurrence after surgery (Pesenti et al., 2019). The current standard of care for glioblastoma is based on a careful surgical resection of the tumoral area, often concomitant to radiotherapy to kill the residual tumor cells, and adjuvant chemotherapy with temozolomide (TMZ). Temozolomide is a methylating agent, which represents the only effective chemotherapy drug for GBM patients, since the majority of the GBM therapeutic drugs showed more side effects than clinical benefits (Hanif et al., 2017b).

Recurrent molecular signatures have been detected in glioblastoma, although the major factors are sporadic. In particular, genetic hallmarks of GBM are the overexpression of epidermal growth factor receptor (EGFR), the presence of mutations in isocitrate dehydrogenase-1 (IDH1 and IDH2), and high levels of methyl guanine methyl transferase (MGMT), which correlates positively with the resistance to TMZ (Kitange et al., 2009; Hanif et al., 2017, Wick et al., 2019).
Despite the efforts made so far in investigating new potential effective treatments, more interventions are required at a research level to understand possible mechanistic causes of GMB onset and discover potential biomarkers for early tumor detection.

THE MODEL: CANCER STEM CELLS

The tissue complexity of cancer is a reflection of its heterogeneous cellular composition, comprised of cellular hierarchies which mimic the organization of healthy tissues. Many reports demonstrated that even a single tumor is composed of highly diverse cellular niches with tumorigenic properties. This intra-tumoral heterogeneity is particularly complex in glioblastoma, a study of Patel and colleagues detected up to 430 different cells in five primary glioblastomas (Patel et al., 2014), representing a challenge from a therapeutic perspective.

Contrarily to normal cells, cells with tumorigenic properties display a distinctive uncontrolled growth, even in the absence of factors essential to cellular proliferation (Hanahan & Weinberg, 2011b). From this point of view, cancer cells are resembling stem cells rather than differentiated cell types and in fact, within tumors, included glioblastomas, multiple studies identified rare subset of tumor cells with distinctive stemness features (Bonnet & Dick, 1997; Singh et al., 2003), which have been called “cancer stem cells” (CSCs) or “tumor-initiating cells” (TICs) (Aum et al., 2014).

These stem-like tumor cells are high proliferative, possess a high tumorigenic potential since when injected in mice can give rise to a tumor (Mummery, Stolpe, Roelen, & Clevers, n.d.). Moreover, cancer stem cells harness the ability of self-renew and are characterized by multipotent properties since they may differentiate in neural cell lineages phenotypically different (i.e., mature neurons, astrocytes, and oligodendrocytes), which support the growth of other tumor cells (Zong, Parada, & Baker, 2015). Furthermore, cancer stem cells are held responsible for cancer resistance to therapies. In glioblastoma, CSCs have shown an improved mechanism of DNA repair damage, unresponsiveness to cell cycle regulation (Ropolo et al., 2009), and therapeutic resistance to TMZ, due to an increased expression of MGMT, establishing a phenotype less tolerant to TMZ (Auffinger, Spencer, Pytel, Ahmed, & Lesniak, 2015).

To target CSCs, multiple markers have been proposed as surface antigens CD15, CD133, A2B5, and the cell adhesion molecule L1CAM (Brescia, Richichi, & Pelicci, 2012; Lathia, Mack, Mulkearns-Hubert, Valentim, & Rich, 2015). In particular, the glycoprotein CD133 has been proposed as a marker of stem cell types, proving to be useful in sorting glioblastoma cells with stem-like properties by flow cytometry (Brescia et al., 2012). Furthermore, CD133 appeared to have a prognostic value in studies with glioblastoma patients (R.-Q. Zhang et al., 2016). Despite its clinical utility, the specificity of therapies targeting CD133 as a marker of tumor-initiating stem cells is still under debate whether not all the GCSs express CD133 (Brescia et al., 2013), thereafter more efforts are needed to find new promising markers of CSCs in glioblastoma, to design more effective therapies against tumors.

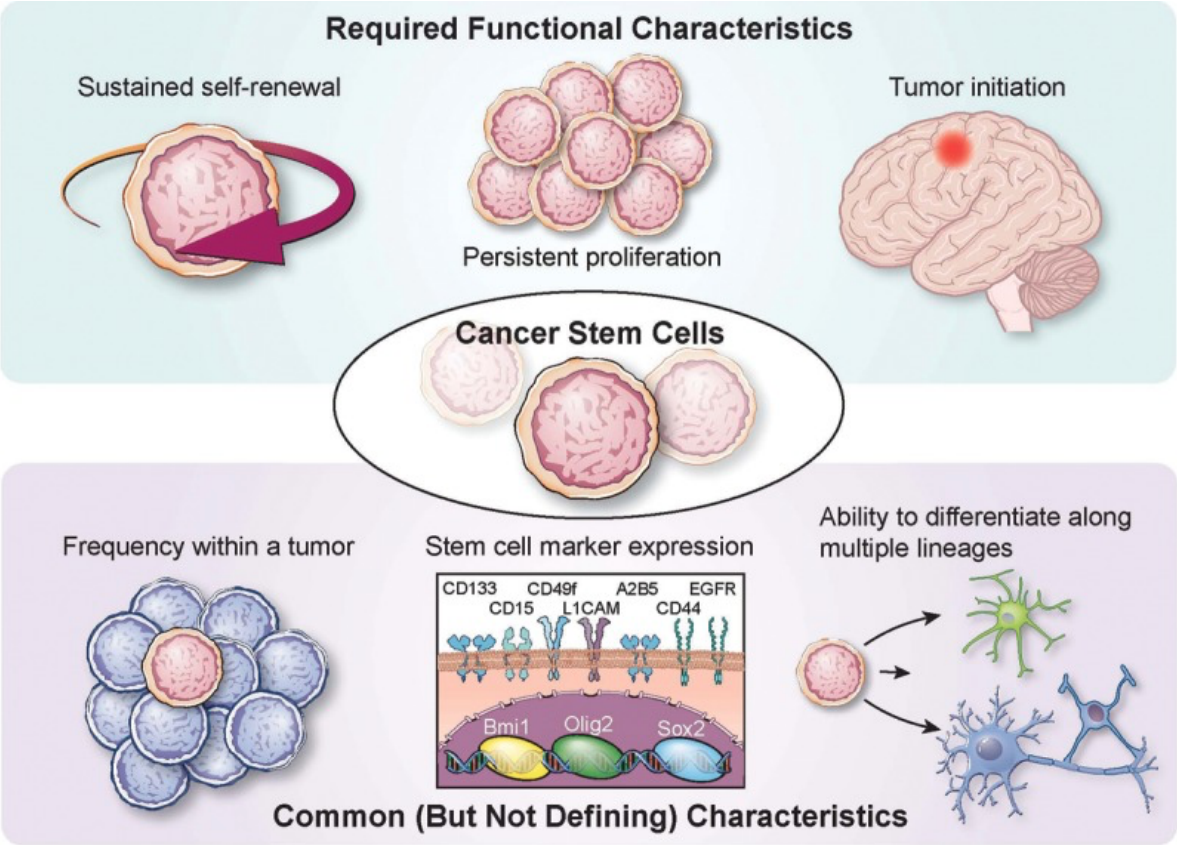

Figure 5. Illustration of the functional characteristics of Cancer Stem Cells (CSCs)*. CSCs are a rare population of cells defined a sustained self-renewal, persistent proliferation, and tumor initiation upon transplantation in animal models. Besides, other common characteristics of CSCs are their frequency within a tumor, expression of stem cell markers (in this case markers are referred to neural cancer types), and the multipotent ability to generate neural cell lineages. (adapted from Lathia et al., 2015).*

FOCUS ON A CLASS OF NON-CODING RNA: Y- RNAs

Y-RNAs are a family of small non-coding RNAs discovered in 1981 in patients suffering from autoimmune diseases, as part of ribonucleoproteins (RNPs) associated with Ro60 (60 kDa protein) and La antigens (Lerner, Boyle, Hardin, & Steitz, 1981). Y-RNAs, a well-conserved family of RNA, are found in all the vertebrates investigated so far. Moreover, the existence of similar small non-coding RNAs has been reported in nematodes, insects and in some prokaryotes (Kowalski & Krude, 2015a). Humans possess four Y-RNA species: Y1, Y3, Y4 and Y5 (Lerner et al., 1981). Y2 is missing as it represents a product of Y1 degradation (Kowalski & Krude, 2015a) while Y3 is the most consistently present across species (Farris, O'Brien, & Harley, 1995).

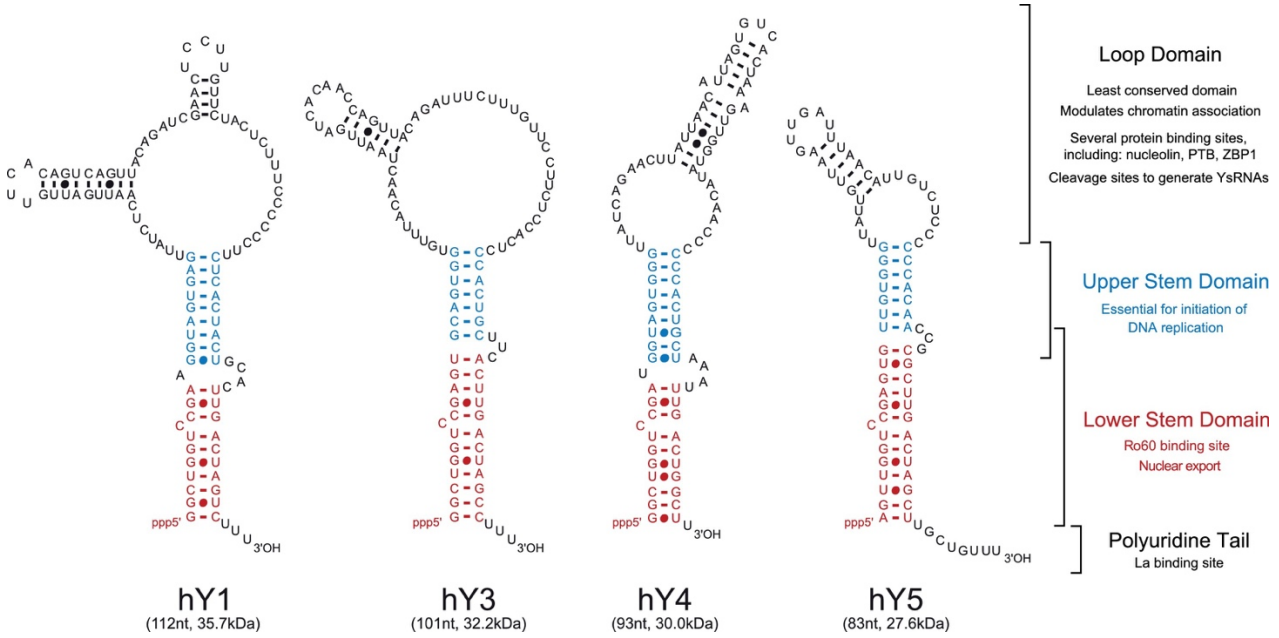

Figure 6. Structure of Y-RNAs *(adapted from Kowalski & Krude, 2015).*

Human Y-RNAs are 84–113 nucleotide long and are expressed in extracellular and cellular fractions, although mostly enriched in the extracellular share (Hendrick, Wolin, Rinke, Lerner, & Steitz, 1981; Wei et al., 2017b). Y-RNAs genes are located on chromosome 7q36, and each Y-RNA has its specific promoter recognized by RNA Polymerase III (Köhn, Pazaitis, & Hüttelmaier, 2013). Y-RNAs have a characteristic stem-loop structure with double-stranded stem regions that contain 5'- and 3'-sequences. The lower stem and the polyuridine tail domains are conserved across species and contain binding sites for Ro60 and La proteins (Teunissen, 2000; Kowalski & Krude, 2015b). The binding of Y-RNAs to Ro60 and La is essential to form Ro Ribonucleoproteins (Ro RNPs) that are involved in RNA stability and cellular responses to stress (Langley, Chambers, Christov, & Krude,

2010). It has been demonstrated that the export and stabilization of Y-RNA in the cytoplasm is dependent on Ro60 binding, while La is not necessary for the export (Simons, Rutjes, Van Venrooij, & Pruijn, 1996). The internal loop domain is pivotal in the initiation of chromosomal replication. The sequence variability in the loop sites distinguishes the four Y-RNAs and is essential to recruit RNA binding proteins (Teunissen, 2000).

RNA sequencing analysis revealed that the majority of RNAs associated with EVs are non-coding RNAs. Among all, miRNA and Y-RNAs were the most represented RNA species (Wei et al., 2017a). Interestingly, all Y-RNAs species were abundantly detected inside extracellular vesicles, both full length and as fragments (Wei et al., 2017a; Nolte-'t Hoen et al., 2012).

The structural conformation of Y-RNAs is favoring the binding with RBPs. Driedonks & Nolte-'t Hoen recently reviewed some reports of the association between the Y-RNAs and different RBPs. In these reports, the mass spectrometric analysis found twenty-three RNA binding proteins associated with Y-RNAs, suggesting that these RBPs might play a role in delivering RNA to recipient cells, via EVs (Driedonks & Nolte-'t Hoen, 2019). Among the twenty-three proteins, eighteen have been identified as present inside EVs and six have been further confirmed by western blotting. Mass spectrometric analysis digests peptide fragments, and a validation step with antibodies that involves the recognition of antigens of interest is required to verify the specific protein expression (Driedonks & Nolte-'t Hoen, 2019; Shao et al., 2018). Among the validated RNA binding proteins, remarkably YBX1 has been proposed to deliver Y-RNAs inside EVs, although this function was not found specific for Y-RNAs only (Shurtleff et al., 2016).

In conclusion, the abundance of Y-RNAs inside EVs suggests that they may play a role in cellular crosstalk acting as messengers, but further studies are necessary to elucidate the packaging of Y-RNA inside EVs and the functional roles of Y-RNAs.

THE DIAGNOSTIC POTENTIAL OF Y- RNA ASSOCIATED TO EVs

Recent studies showed the presence of high level of Y-RNAs associated with extracellular vesicles in biological fluids (reviewed by Driedonks & Nolte-'t Hoen, 2019). Alterations in plasma levels of extracellular Y-RNA were observed in pathological conditions such as cancer and neurological diseases (Driedonks & Nolte-'t Hoen, 2019), suggesting the potential utility of Y-RNA as biomarkers. High expression of the different Y-RNAs has been detected in the circulation of patients with breast cancer (Dhahbi, Spindler, Atamna, Boffelli, & Martin, 2014) glioblastoma (Wei et al., 2017a) and leukemia (Haderk et al., 2014).

Besides this evidence, little is known on the conditions that may trigger tumor cells to release EVs packed with Y-RNAs and on the functions that Y-RNA may exert on recipient cells in the tumor microenvironment. The first clinical evidence derives from studies that analyze small cohorts of patients. Moreover, extracellular Y-RNAs can also be associated with Ribonucleoproteins, other than EVs. To avoid misleading indications, a major standardization is required in sample processing and RNA analysis to confirm the correlation between EVs and Y-RNAs (Langley et al., 2010), and to better investigate the role of Y-RNAs in the TME.

AIM OF THE WORK

Extracellular vesicles are vehicles of biological signals between cells in physiological and pathological conditions. They are key players in the intercellular communication and contribute to elucidating in real time the status of pathological processes. Most importantly, they offer the possibility to detect novel targets for therapeutic monitoring.

Circulating molecules are interrogated in liquid biopsies to track the tumor dynamics. The abundance and bioactive content of heterogeneous EVs in biological fluids qualify them as an attractive source of diagnostic and prognostic markers. However, the lack of reproducible and efficient isolation methods is an obstacle to the applicability of EVs in clinical practice.

The overall aim of my Ph.D. studies was to assess whether extracellular vesicles isolated from liquid biopsies could be used as an innovative tool for detection of molecules associated with cancer, to be applied in a clinical setting. To this end:

- We challenged the technical limitations developing a novel procedure to isolate EVs in body fluids, which is compatible with a clinical utilization.
- We implemented different molecular assays to characterize the RNA and proteins enclosed in EVs.
- We validated the performance of NBI to detect cancer biomarkers associated to EVs that could discriminate cancer patients from healthy subjects in retrospective studies.
- We investigated the EV-RNA content of glioblastoma cancer stem cells to identify molecules with clinical significance to be used in medical research as promising biomarkers.

The ultimate goal of the project is to identify cancer biomarker associated to EVs in liquid biopsies and for this reason we are currently investigating the transcriptome of EVs derived from plasma of breast cancer patients, collected in an ongoing prospective study, to assess their potential as prognostic biomarkers.

RESULTS

OPTIMIZATION OF TECHNICAL PROCEDURES TO ANALYZE EXTRACELLULAR VESICLES

Approaches to analyze large vesicles in flow cytometry

Extracellular vesicles are approximately two orders-of-magnitude smaller than the cells they originate from. For these reasons, over these years, the research in the EV field dedicated much effort to develop new techniques and adapt existing protocols to characterize EV preparations. Morphological and biophysical properties of EVs as size, molecular composition, concentration, and optical density can be exploited for EVs characterization.

One of the most commonly applied techniques to characterize the molecular phenotype of EVs is flow cytometry, as it allows analyzing multiple markers expressed on the vesicle membrane, at the same time (Shao et al., 2018). Briefly, particles suspended in a fluid are individually analyzed at their passage through a laser beam, when an electronic detection system measures light scatter and fluorescence intensity of particles. Despite the technological advancements in the field, standard flow cytometers fail to target smaller vesicles because of a poor scattering signal, and the presence of the swarm effect (Van Der Pol, 2012). Swarm effect is a confounding phenomenon, which leads to underestimating the count of small particles. In this case, multiple vesicles are counted as a single event when the laser hits the surface of small particles (Van Der Pol et al., 2012). Therefore, it has been observed that only MVs and ABs can be properly analyzed at a conventional flow-cytometer, having a diameter ≥ 0.5 μm, less prone to swarm effect (Van Der Pol et al., 2012).

To visualize large vesicles (LVs) at a conventional flow cytometer, we designed a gate using polystyrene beads of 1 and 10 μm, (Fig. 7 a). We optimized FACS parameters on extracellular vesicles isolated by U87 cell line by differential centrifugation (UC). U87-MG cell line was chosen since these cells were known to release a massive amount of EVs (Di Vizio et al., 2012). Specifically, we analyzed the pellet obtained after the second ultracentrifugation at 10000xg, according to Di Vizio protocol to isolate large vesicles (Di Vizio et al., 2012).
Another way to visualize LVs at FACS (flow activated cell sorting), is staining vesicles with a fluorescent dye. We compared two permeable dyes commonly used to stain vesicle membrane: Nile Red (also known as Nile blue oxazone) and Carboxyfluorescein diacetate succinimidyl ester (CFDA-SE) (Morales-Kastresana et al., 2017). We observed the formation of aggregates made of unbound

dye using Nile Red, while CFDA-SE alone did not form aggregates and the stained pool of LVs had similar size compared to unstained LVs (Fig. 7 b). We assessed that CFDA-SE is the best labeling method since we were able to appreciate a bright fluorescent signal of MVs using CFDA-SE staining at a low concentration of 0.1 μM, without any formation of dye aggregates (Fig. 7 c).

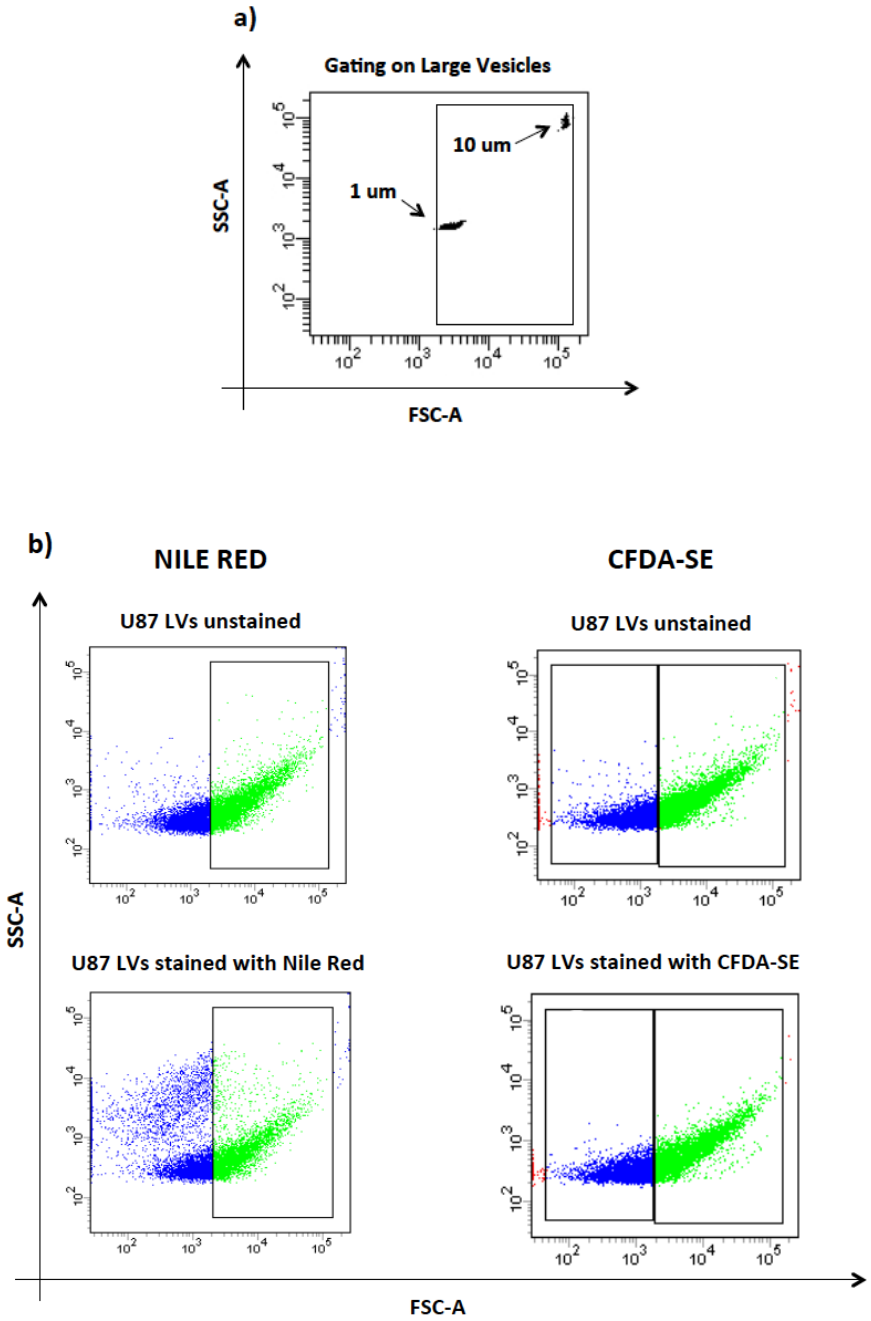

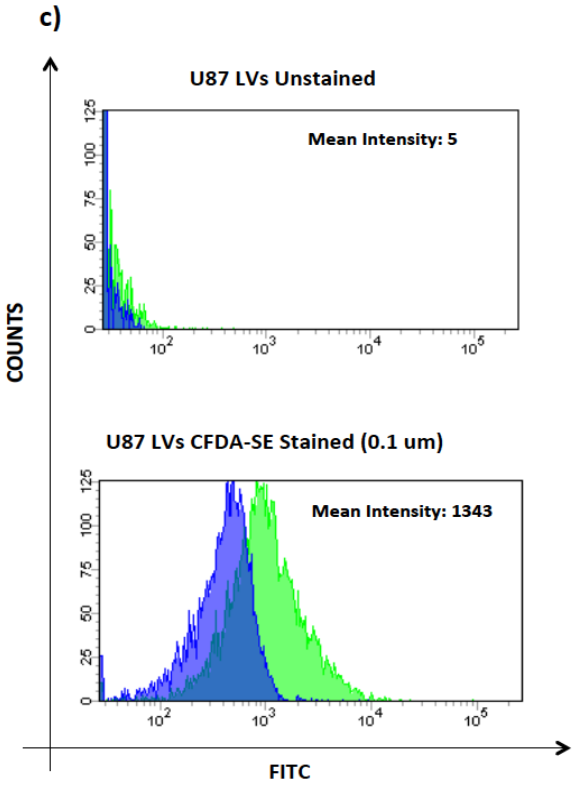

Figure 7. Flow cytometry analysis of large vesicles. a) *Gating strategy used to analyze large vesicles at FACS using silica beads.* ***b)*** *Optimization of staining conditions to visualize LVs membranes. Comparison between Nile Red and CFDA-SE dyes. 1000 events were counted by FACS Canto cytometer for each condition.* ***c)*** *CFDA-SE staining is chosen as the best labeling method.*

Optimization of extraction and analysis of RNA from extracellular vesicles

Extracellular RNA associated with EVs is well protected by a membrane bilayer of EVs from the degradation of external agents, and it proved to be of diagnostic interest (Hill et al., 2013). To purify RNA efficiently in terms of quantity and quality of RNA, we tested five different protocols of RNA extraction, selected from a literature analysis between the most performant commercial kits.

In detail, we isolated EVs from melanoma cells A-375 (ATCC® CRL-1619™), and we extracted RNA starting from the same number of EVs. We tested five different protocol for RNA extraction: RNA purification with TRIzol® Reagent; RNA purification with TRIzol® Reagent followed by treatment with DNAse Qiagen® and purification on a Norgen column (Single Cell RNA Purification Kit); RNA purification on a Norgen column (Single Cell RNA Purification Kit) followed by treatment with DNAse Qiagen®; RNA purification with miRCURY™ Exiqon® Kit, followed by treatment with DNAse Qiagen® and lastly, RNA purification with TRIzol® Reagent followed by treatment with DNAse TURBO DNA-free™ Kit.

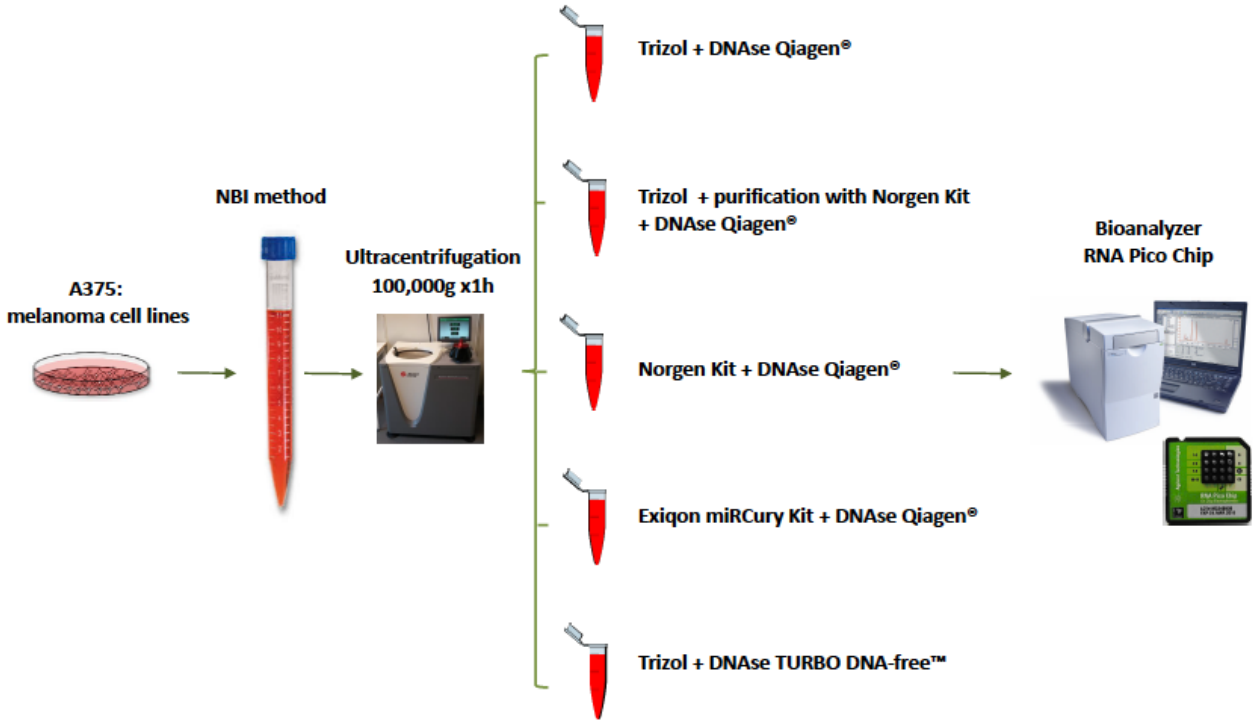

Figure 8. Illustration of extraction and analysis of extracellular RNAs. *The workflow of EV-RNA extraction and analysis. EVs were pelleted after NBI isolation to avoid buffer interference during extraction passages.*

After the purification, RNA has been analyzed at Bioanalyzer, using RNA Pico assay (Agilent), the most sensible approach to test the quality and quantity of EV-RNAs, through nucleic acid separation by capillary electrophoresis on a microchip device, starting from picograms of RNA. As expected, Bioanalyzer analysis revealed variability in the amount of purified RNA, between the different protocol tested, ranging from 15 pg/μL to 8000 pg/μL (Fig. 9). Qualitatively, the electropherograms showed, in all the samples, except the RNA extraction with TRIzol® Reagent followed by treatment with DNAse TURBO DNA-free™ Kit, a recurrent presence of defined peaks correspondent to a small number of nucleotides, indicating enrichment of small RNAs in EVs, as reported in the literature (Enderle et al., 2015). Afterward, we performed a sequencing analysis on total RNA, using SMARTer® Stranded RNA-Seq Kit (Clontech) on an Illumina MiSeq platform. The result of these experiments indicated that the Trizol protocol, followed by purification on a Norgen column was the best procedure to extract RNA from extracellular vesicles, to proceed with next-generation sequencing approaches and efficiently detect molecular alteration in liquid biopsies. This work has been fundamental to identify a standard protocol which can be translated to other molecular diagnostics assays.

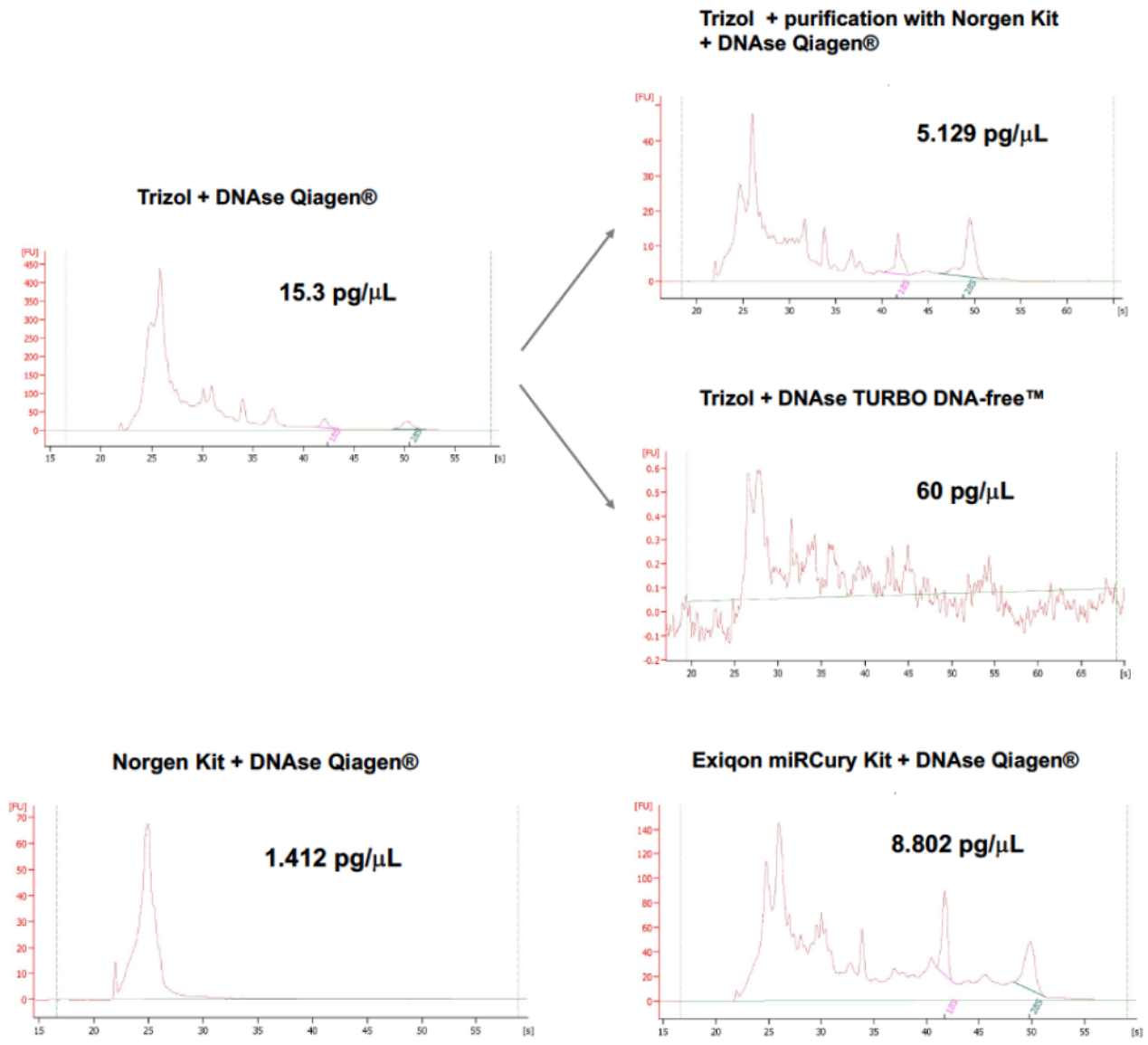

Figure 9. Bioanalyzer profiles of RNA extracted with the different protocols. *Size distribution of total EV-RNA, extracted from A375 melanoma cell line, with the different methods listed previously.*

CAPTURE AND COMPETITIVE ELUTION OF EXTRACELLULAR VESICLES BY NICKEL-BASED ISOLATION (NBI)

NBI is designed to exploit the charge of EV membrane

To efficiently apply the potential of EVs in clinical practice, we worked at a fast procedure to capture extracellular vesicles in biological fluids. To target EVs in biological fluids, we exploited their

biophysical properties. As I mentioned in the introduction, the vesicle membrane is characterized by a net negative charge (or ZP) of −40 to −7 mV in PBS at pH 7.4. Previously, other methods employed ZP to isolate EVs, although the proposed techniques required subsequent passages as polymer-based precipitation (Deregibus et al., 2016a) to pellet EVs, or density gradients, to get rid of lipoproteins (Heath et al., 2018).

We alternatively propose a procedure called nickel-based isolation (NBI), which consists of two main steps and take place in less than one hour (Fig. 9). Heterogeneous EVs are captured by nickel cations (50–300 mM) bound to a matrix of agarose beads. The binding is efficiently reverted using a tailored buffer, composed by chelating agents (EDTA and citric acid) in PBS buffer (pH 7.4). In this way, polydisperse EVs could be efficiently isolated in physiological solution with rapidity, preserving their integrity and stability.

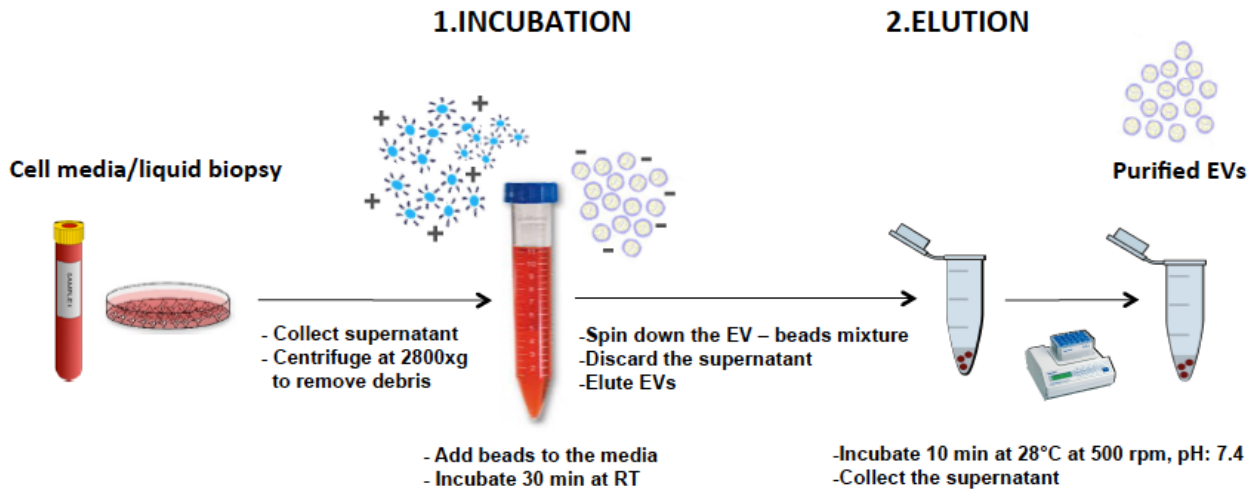

Figure 10. Workflow of Nickel-based Isolation (NBI) procedure. *The main passages of NBI method are illustrated.*

NBI relies on Nickel cations to recover negatively charged particles

To have an indication of the number of particles recovered by NBI, we compared the performances of the novel technique with the gold standard differential ultracentrifugation. U87 were cultured for 48 hours, before changing with a serum-free media. After 24 hours, we isolated EVs both with differential ultracentrifugation and Nickel-Based Isolation from 10 mL of serum-free supernatant of U87 glioma cells, for each condition. For NBI, we incubated the U87 cell culture media with a diluted suspension of nickel-functionalized agarose beads (1:50 v/v). Differential

ultracentrifugation had been performed at 10,000 and 100,000 of *g* force. We analyzed with a conventional flow cytometer the number of large particles (≥ 0.5 µm) recovered from UC, NBI, and, as a negative control, non-functionalized beads. We observed that the number of isolated particles was comparable between the two methods, while we noticed that non-functionalized beads were not able to recover any particle**.** NBI performance is therefore dependent on the affinity of Nickel cations for negatively charged particles.

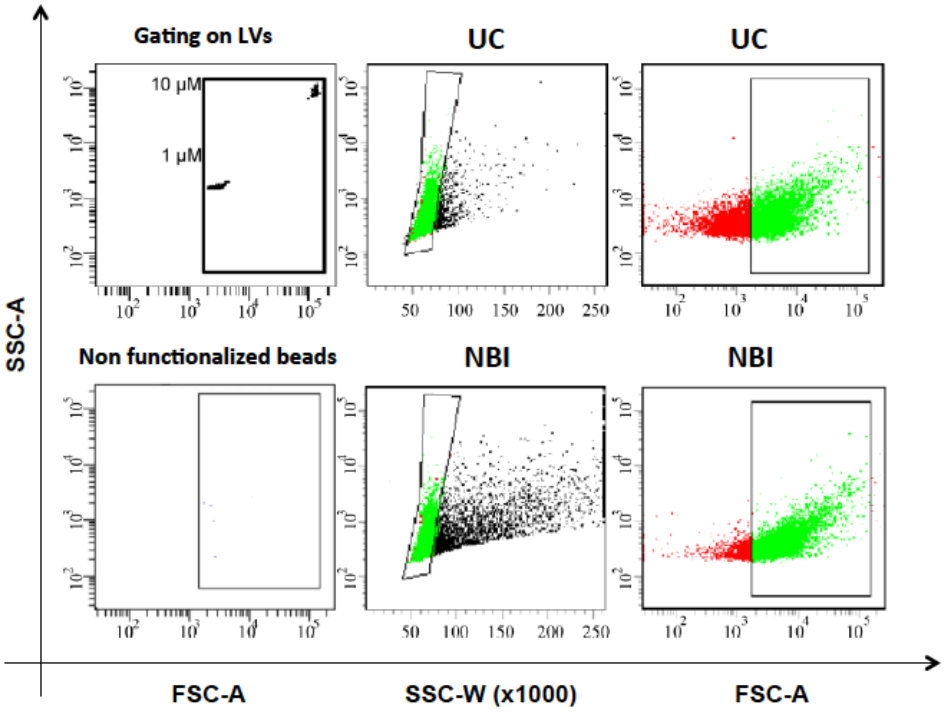

Figure 11. NBI efficiently recovers a number of particles (>0.5 µm) comparable to UC. *FACS Canto Instrument (BD) calibrated with polystyrene beads (F13838, Life Tech) of 1 and 10 µM. A suspension of 20 mg/ml of nickel-functionalized agarose beads was diluted 1:50 (v/v) in the cell culture media. The number of particles ≥ 0.5 µm (gate) is equivalent between ultracentrifuge (56.6%) and NBI (58.8%) using agarose beads functionalized with nickel sulphate. Plots are representative of two independent experiments.*

NBI buffer is designed to target EVs in the secretome

As I reported in the introduction, the net negative charge of membrane-enclosed particles, at pH values >5, makes them susceptible to electrostatic interactions. Aiming to isolate EVs in a complex matrix as the secretome, we optimized the conditions to elute specifically EVs, overcoming the interference of Nickel charged beads with other molecules present in the cellular matrix. We used 10 mL of U87 cell supernatant to optimize the composition of the elution buffer, composed of a phosphate buffered saline (PBS) solution containing chelating agents like EDTA and citric acid (CA), to revert the binding of EVs from the functionalized beads, over proteins, RNA, and DNA. Next, we

measured the number of recovered particles by Tunable Resistive Pulse Sensing (TRPS), using qNano. Simultaneously, the absorbance and fluorescence of both elution buffers and beads were monitored (in this case by further normalizing the signal to the 350 nm peak of nickel beads). To distinguish the affinity of nucleic acids for the beads, absorbing UV light at 260 nm, we pre-stained the beads with Pyronin Y, a fluorescent probe able to bind both double single and double-stranded RNA (Bao, Rhee, & Tsourkas, 2009) to measure a specific fluorescence signal for the RNA. We eluted a consistent number of particles (2–5 × 10^9/mL), with a diameter of 50–700 nm) from the stationary functionalized beads using a low concentration of chelating agents (1-3 mM). Meanwhile, we did not detect any absorbance or relevant fluorescence signals from controls, when nucleic acids (A260), proteins (A280), or pre-stained RNA were pre-incubated with nickel-agarose beads. Conversely, at increasing concentrations of EDTA (>3 mM), the specificity of the elution buffer for EVs resulted affected (Fig. 12).

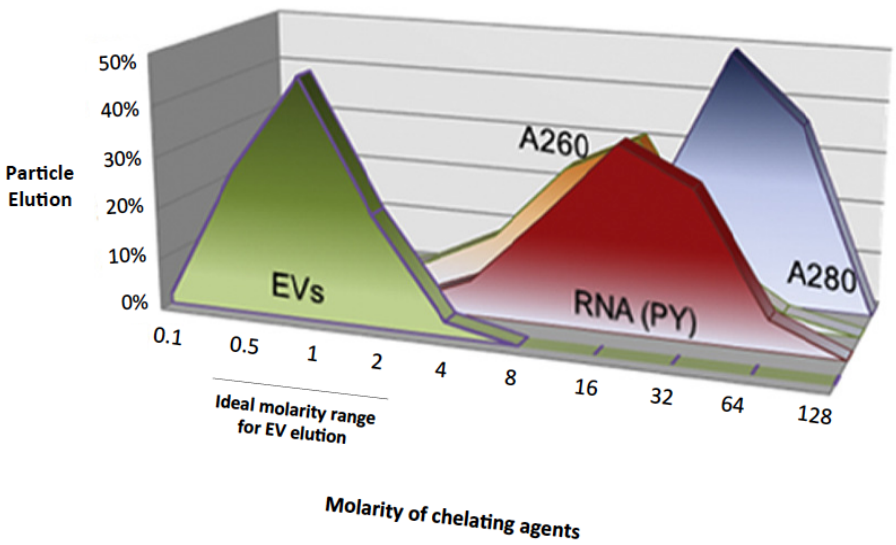

Figure 12. Optimization of elution buffer composition to target EVs. *At pH ≥ 5, using 1–3 mM of chelating agents, particles are selectively eluted from a functionalized stationary phase in contrast to nucleic acids (A260), proteins (A280), or pre-stained RNA (with Pyronin Y), pre-incubated with nickel-agarose beads. The optimal molar ratio of EDTA:CA is ~1:70, which corresponds to elution buffer 1×. TRPS analysis has been performed at qNano using three different nanopores (NP200, NP400, NP800).*

Preferential elution of EVs in a protein-enriched system

To validate the previous observations, we tested the performance of NBI to elute EVs in a protein enriched-environment. Ni^{2+} ions are exploited in protein purification, in the form of Ni-NTA

Resin (Crowe et al., 1994). For this reason, we supplemented the medium of U87 with purified Histidine-tagged proteins (tag known to confer the most robust interaction with Ni) and crude extracts of DH5α *E. coli* cells (from pelleted bacteria). At that point, we performed NBI by eluting EVs at increasing buffer concentrations, while keeping as reference the 1X elution buffer. TRPS analysis evidenced that samples eluted with 0.5X and 1X solutions were the most concentrated ones, confirming the previous observations. We also detected 20–25 µg/mL of proteins in 0.5X + 1X condition by BCA and Bradford assays, reflecting the protein content of the particles quantified at qNano. In the meantime, we observed an increased elution of proteins from 1.5X solution by SYPRO Ruby staining, SDS-PAGE, and Western blotting using an Anti-His antibody to recognize the recombinant proteins. Although, at increasing concentrations (mM) of chelating agents, we detected a lower number of particles measured by TRPS (Fig. 13).

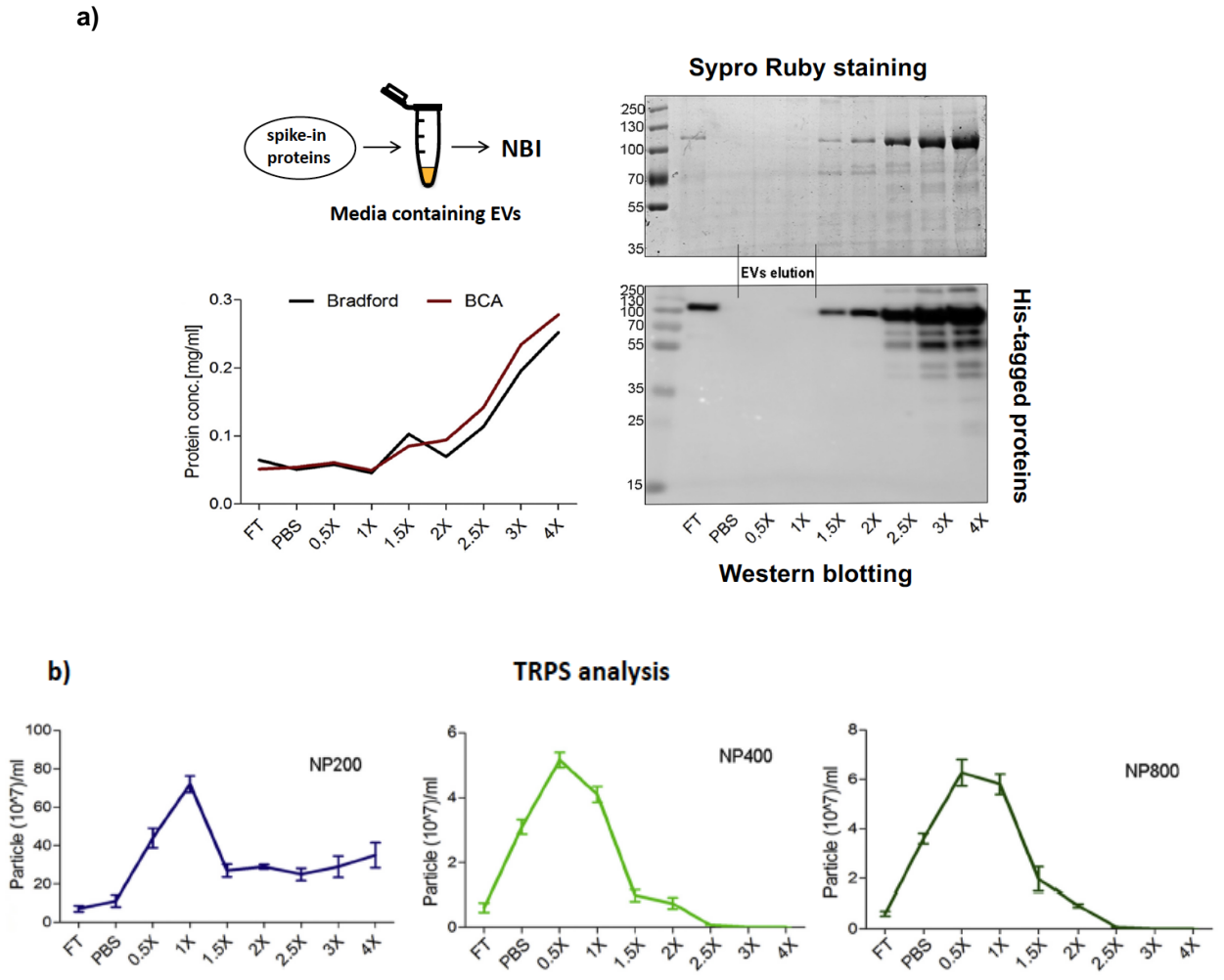

Figure 13. NBI Competitive assay in protein-enriched serum-free medium. a) *500 µg/ml of DH5α protein extract and of 50 µg/ml each of purified His-tagged proteins (T7p07, HuR, YTH domain) were added to the medium. Two parallel gels were exposed to SYPRO Ruby or blotted on PVDF membrane to detect histidine.* ***b)*** *qNano analyses with indicated nanopores were performed and SD refers to two independent*

experiments. The 1X solution is the optimized buffer and the flow-through (FT) is the medium after beads sedimentation.

Characterization of EVs isolated by Nickel Based Isolation

To verify the nature of the isolated particles, we evaluated the morphology of the particles isolated with the elution buffer 1X by Transmission Electron Microscopy (TEM). We could appreciate a broad heterogeneity of vesicles in the wide-field acquisitions, mostly enriched in objects with dimensions of 80–120 nm. Notably, the apparent size and shape of vesicles appear to be artifacts of fixation and drying associated with electron microscopy. Even though we optimized the sample preparation, using a reduced concentration of formaldehyde and dry time to minimize the shrinkage effects (van Niel, D'Angelo, & Raposo, 2018), we could observe this phenomenon. Therefore, we used Dynamic Light Scattering (DSL) to calculate the dispersity index (0.61 ± 0.05), which validate the measurements obtained by TRPS (Fig.14 a).

To endorse the nature of the purified vesicles, we performed western blotting on those samples, using antibodies that recognize EV enriched proteins (Kowal et al., 2016). We found that NBI-isolated vesicles were positive to endosome-associated proteins, such as Alix and CD63 markers, or membrane proteins such as Flotillin-1, and negative to Golgi markers (GM130), indicating the presence of exosomes and microvesicles in the mixed populations of the vesicles we isolate (Fig.14 b).

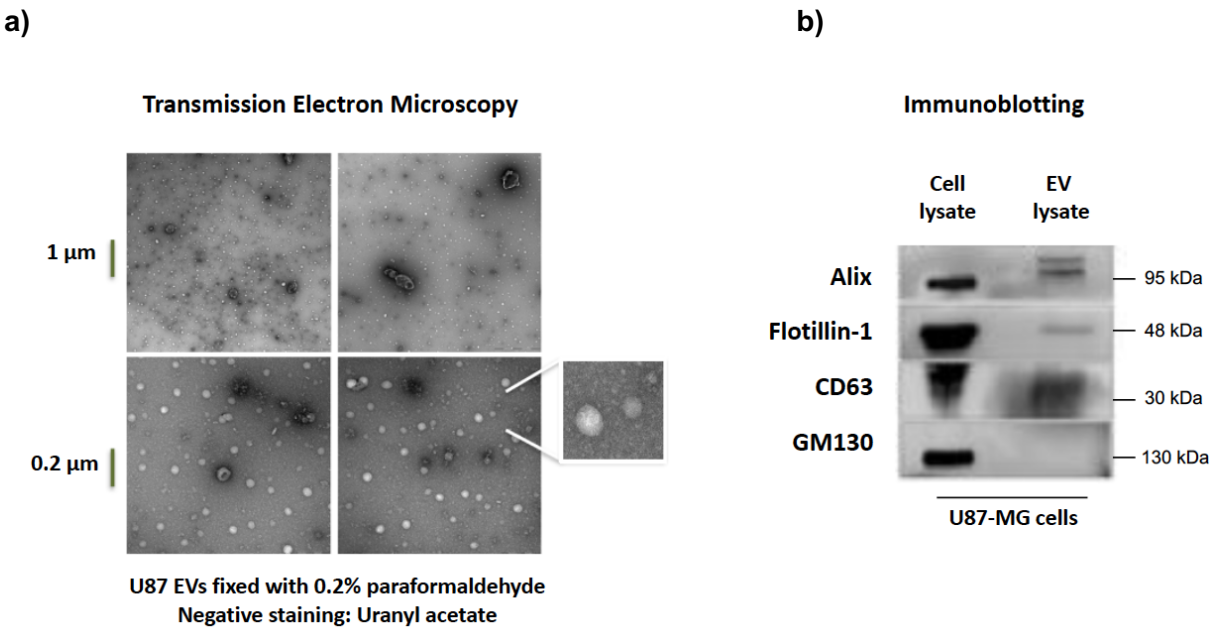

Figure 14. NBI-isolated vesicles are polydisperse and express typical EV enriched proteins. a) *Transmission electron microscopy (TEM) acquisitions, with three fields at 20.500× (1 µm) + 5× magnification*

and three fields at 87.000× (200 nm) + 5× magnification, of NBI samples fixed with 2.5% paraformaldehyde in the elution buffer. The original scale bars are embedded in the figure at the bottom right, but also added manually on the left side for better visualization. ***b)*** *Western blot analyses on EV lysate (recovered by 14 × 10^6 cells) and on 1% total cell lysate (TCL) of U87.*

To estimate the reproducibility of NBI in cell-based assays, we purified EVs released by U87, seeded at different densities in 6-well plates, as indicated in Fig 15 a). Later, we analyzed the distribution of purified particles by TRPS using NP400, NP200, and NP100 nanopores, to cover all the vesicular subpopulations. Isolated EVs displayed a continuous distribution, from approximately 50 to 700 nm in diameter, characterized by at least two main vesicle populations of ~200 and ~600 nm of mean diameter.

Being aware of the unknown sub-cellular origin of individual NBI-isolated EVs, we referred to these two EV populations as small EVs (SVs) and large EVs (LVs), respectively (Fig. 15 b). In particular, we observed a linear release of small EVs as a function of cell density, and an faster release of large EVs, as already suggested for microvesicles (van Niel et al., 2018), possibly related with different biogenetic mechanism, intrinsic stability and/or cell-mediated turnover that correlate with particle size or composition (Abels & Breakefield, 2016)**.** Interestingly, the efficient isolation of EVs from small volumes allowed us to follow the release of vesicles using as low as 10^3 cells/cm^2 (Fig. 15 b).

A good isolation method should ensure a proper experimental reproducibility, essential to both research and clinical applications. We appraised the consistency of NBI procedure, noticing the overall number of isolated vesicles was proportional to the number of seeded cells, with a global coefficient of variation (*CV*) of 6.14% ($n = 9$ for NBI 1, 2, and 3) for both SVs (197 ± 26 nm) and LVs (595 ± 37 nm). Moreover, we did not observe a statistically significant variation ($P = 0.459$) comparing EVs from EV-depleted serum (dFBS) (Wei et al., 2016) and serum-free media (NBI 1), indicating that a reliable EV isolation can be started from relatively viscous solutions upon dilution with PBS (Fig. 15 c).

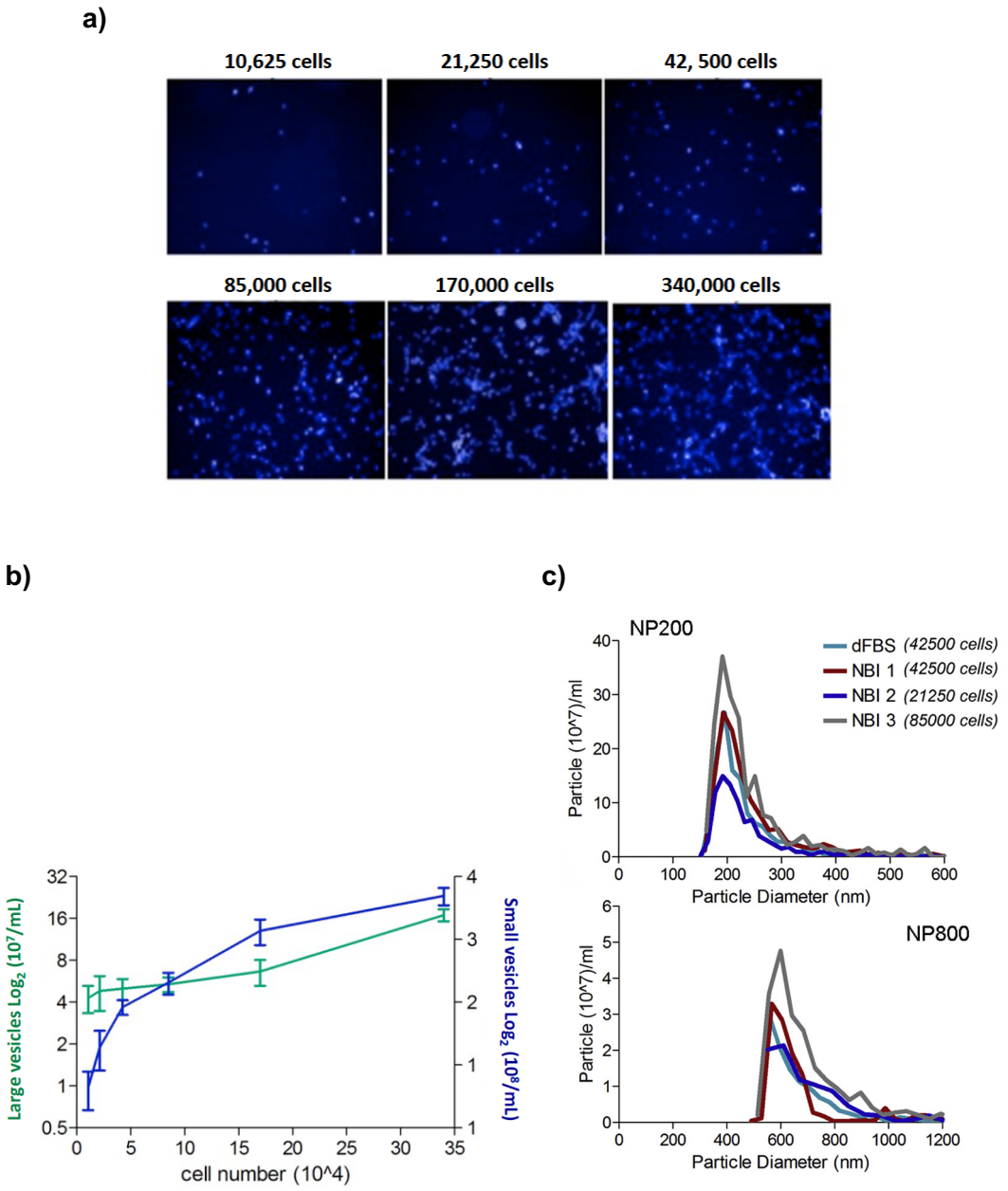

Figure 15. EVs recovered according to cell density, reveal two different releasing dynamics. a) *U87 cells were seeded at different density, as indicated, in 6-well plates. Media (1 ml) were recovered after 24 h, and cells were stained with 10ng/ml Hoechst 33342.* ***b)*** *Media were processed by NBI, and the number of EVs, indicated here as* Log_2*, was assessed by TRPS with qNano instrument (IZON Science). Standard deviation refers to three independent experiments.* ***c)*** *The reproducibility of NBI has been tested in serum-free media of U87 seeded at different density, in 6-well plates, as indicated (NBI 1, 2, and 3). Ten % ultracentrifuged FBS (dFBS) condition showed substantial overlap with NBI-1 results. Plots are representative of three independent experiments, and the global CV was 6.1%.*

NBI preserves the integrity and stability of EVs

Multiple studies reported how the membrane composition of extracellular vesicles is accounting for their reduced immunogenicity (Murphy et al., 2019), suggesting the utilization of extracellular vesicles as promising tools for therapeutic purposes (Fais et al., 2016). In light of this application, the preservation of the structural integrity of EVs represents a prerequisite to translate their biological functions into a solid clinical reality. Along with improvements of the conditions to ensure EV stability (Kusuma et al., 2018), isolating intact EVs would be valuable to these purposes.

To exploit this perspective, we verified whether the composition of the elution buffer would affect the integrity of NBI-purified vesicles. We tested increasing concentration of elution buffer, starting with the 1X solution, although this time supplemented with salts, to resemble the conditions reported in other ion exchange protocols (Kosanović et al., 2017) and we used the addition of SDS as a control for the integrity loss of EVs. We demonstrated that the synergy of EDTA with citric acid provided a valuable alternative to preserve the pH and the biological samples from high concentrations of salts (Kosanović et al., 2017) that can affect vesicles' integrity, as shown in Fig. 16.

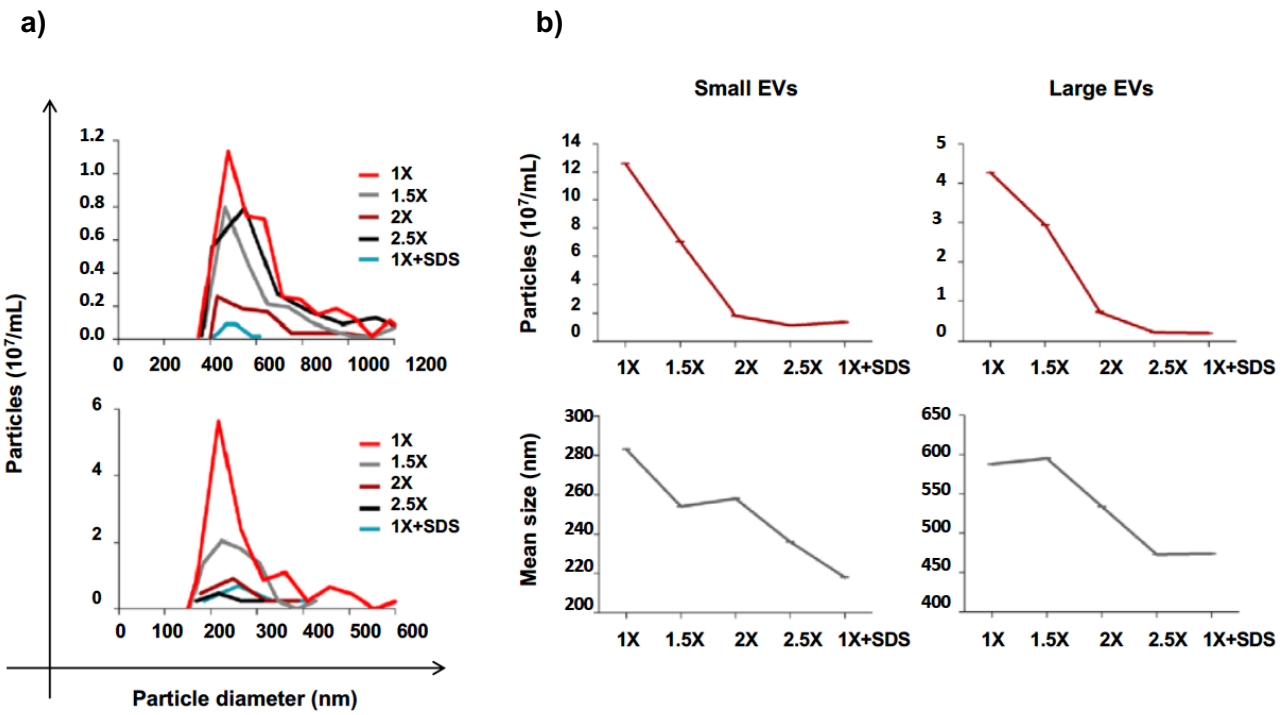

Figure 16. Increasing concentration of salts in the elution buffer affects the integrity of EVs. a) *The number and mean diameter of particles, analyzed by qNano instrument (IZON Science) are affected by different elution buffers containing higher concentrations of salts (NaCl 100 mM).* ***b)*** *In comparison with 1x elution buffer, the increasing ionic strength causes detrimental effects on the integrity (inferred by the reduced*

number) of beads-eluted vesicles, with detected variations also in the mean size of TRPS-measured particles. Graphs are representative of two independent experiments.

Being composed of a lipid bilayer, the membranes of extracellular vesicles are characterized by a curvature degree, influenced by their composition in different protein and lipid species (Haraszti et al., 2016). Even if it had not been completely clarified yet, centrifugation-based methods might affect the structural shape of EVs, using high g-forces for prolonged times (Douglas D. Taylor & Shah, 2015).

To investigate the impact of mechanical forces exerted during the NBI procedure, we chose, as models, liposomes with an "exosome-like" lipidic composition (adapted from Llorente et al., 2013; Haraszti et al., 2016). We spiked a pool of liposomes in 10 mL of DMEM, and we proceeded with the isolation, comparing NBI with UC. We also tested the same samples, this time stained prior the isolation, with the lipophilic phosphatidylethanolamine-rhodamine (PE-Rho), a fluorescent lipid dye used to study membrane fusion and surface aggregation (Chang, Reich, Brunzell, & Will, 1998). Both methods were able to recover almost all the spiked particles (98.6%), with a mean size of ~190 nm, although we measured a slight shift of ~10 nm of diameter in UC samples. Similarly, in PE-Rho stained liposomes, we could observe a coalescent effect (>40 nm shift) in ultracentrifuged liposomes, compared to the ones processed by NBI. These data, shown in Fig. 17, demonstrate that the elution buffer used for NBI minimizes particles aggregation.

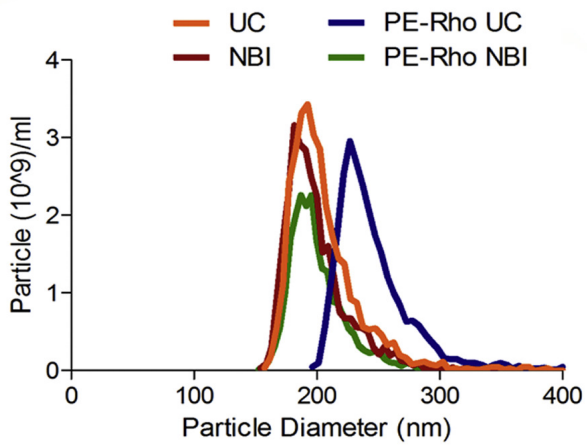

Figure 17. NBI minimizes particles aggregation. *Similar to the EVs in the same conditions, the average zeta potential of these preparations was −15.2 mV, as determined by DLS.*

Different studies questioned the importance of the storage conditions to preserve the biological and physical properties of EVs (Welch et al., 2017; Maroto et al., 2017; (S. J. Park et al., 2018). It has been demonstrated that factors as time and temperature could affect the biological activities and

impact on the number of particles, resulting in vesicle aggregation (S. J. Park et al., 2018; Bosch et al., 2016).

To investigate the effect of these parameters on NBI physical properties, we interrogated the turnover of vesicles stored at 4 °C after purification by NBI or UC (Fig. 18). We chose to focus on particles ≥300 nm, more vulnerable than smaller vesicles to different storage conditions (Yuana et al., 2015). In UC samples, at 24 days post-isolation (*t24*), the 600 nm population initially present was virtually replaced by a population of ~300 nm. Strikingly, NBI samples retained the 86% of the original EV population, still detectable using the same nanopore. A kinetic analysis evaluating the size-shift of the 600 nm test population, revealed a half-life of >50 days for NBI EVs, in contrast to 7.35 days for UC EVs (Fig. 18, on the right).

Collectively, these data indicate that NBI recovered EVs can preserve their stability in a near physiological pH solution for short-time storage at 4°C. Most importantly, the application of EVs in a clinical context would be subjected to volume restrictions, and an ideal isolation method should be scalable. While for therapeutic purposes it is required a large-scale production of EVs, the employment of EVs in liquid biopsies is limited to the availability of the volume of biofluids derived from patients at different time points along the course of the disease. In this scenario, NBI represents a valuable tool since it can be applied to a wide range of volumes, as we demonstrated so far.

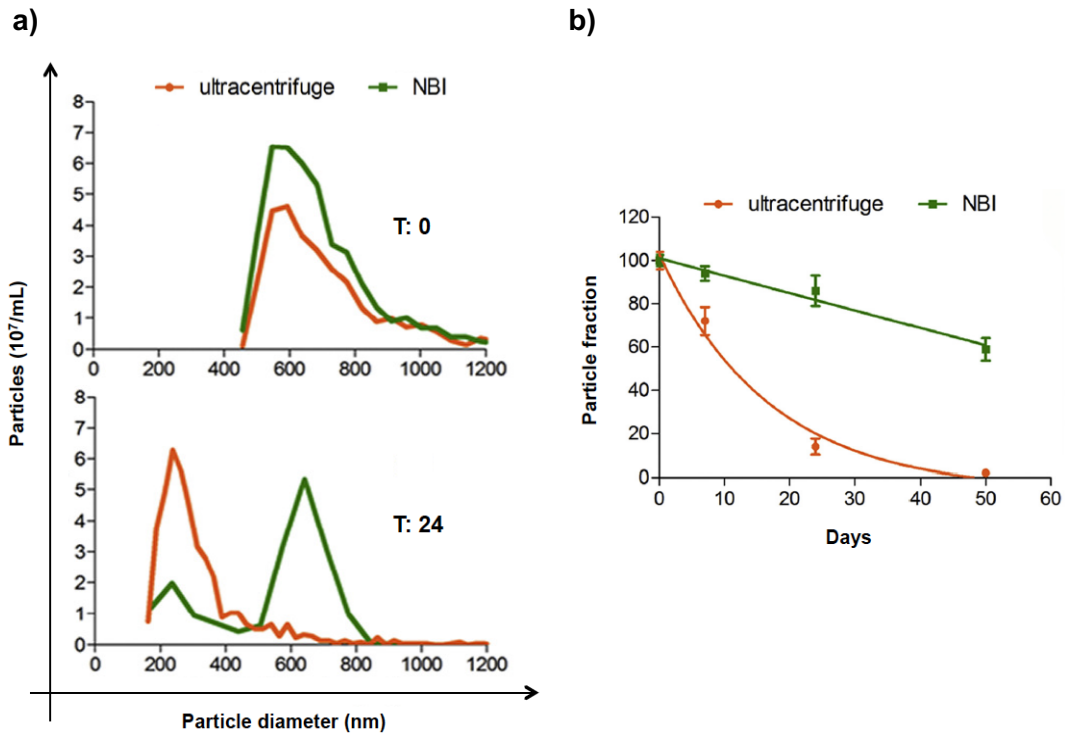

Figure 18. NBI-isolated EVs preserve their stability in solution. a) *EVs were isolated by UC or NBI from 3 ml of serum-free medium of U87 and analyzed at (t0) or after 24 days (t24, stored at 4 °C).* ***b)*** *Repeated*

measurements by TRPS have been performed until 52 days post-purification, and the relative half-live of the 600 nm populations have been calculated with GraphPad Prism software v.5.

SCALABLE AND REPRODUCIBLE ISOLATION OF POLYDISPERSE EVs FROM CANCER CELL LINES AND PLASMA OF HEALTHY VOLUNTEERS

In light of being employed for clinical applications, a suitable EV isolation method should guarantee reproducibility to standardize the results. Therefore, we evaluated the NBI procedure on a panel of immortalized, and well characterized, cancer cell lines. In detail, we characterized the EVs recovered from MCF-7, PC-3, MDA-MB-231, and SH-SY5Y tumor cell lines (Fig.19). We observed a consistent distribution of isolated EVs in terms of size and concentration, except the SH-SY5Y cells that demonstrated a lower tendency to release both small and large vesicle populations.

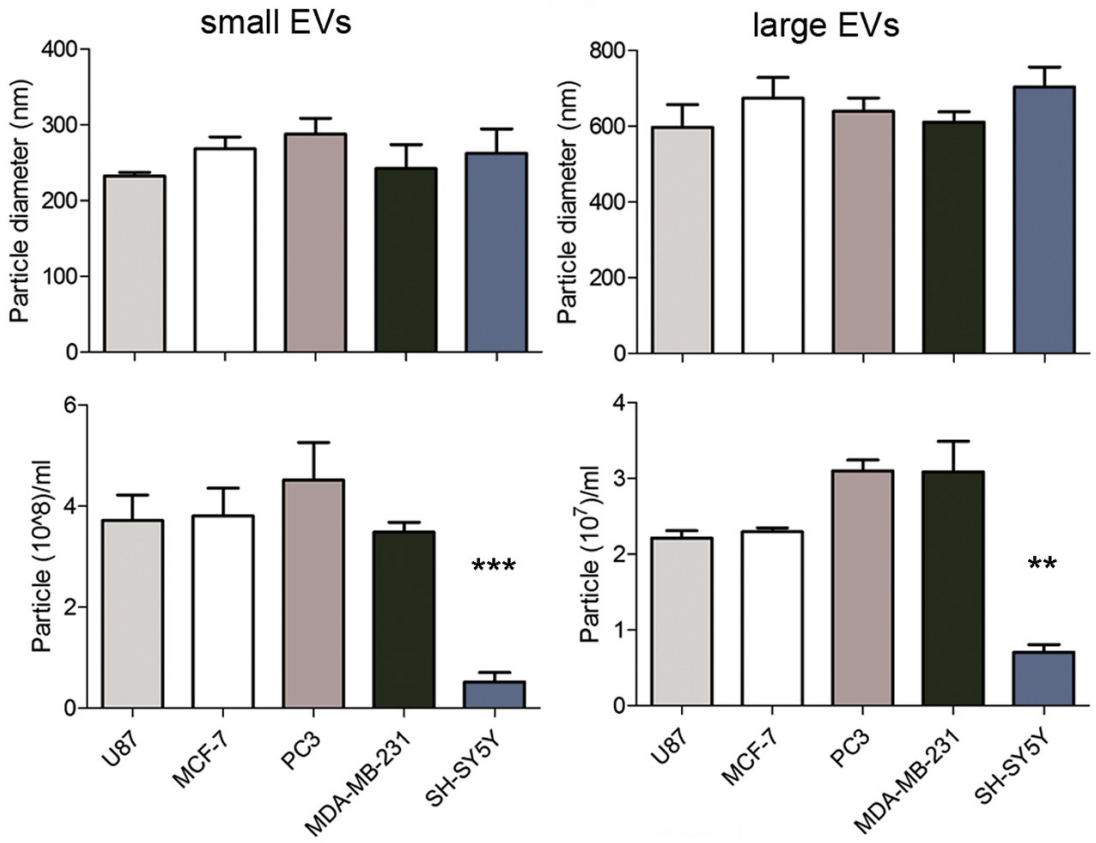

Figure 19. NBI efficiently isolates EVs with high reproducibility from different cell lines. *The distribution of NBI-isolated EVs has been analyzed for different cell lines, as indicated. SH-SY5Y cells showed a substantial reduction in releasing both vesicle populations (**P-value = .006, F = 70.13, and *** < 0.0001, F = 30.84, using one-way ANOVA and Bonferroni's post-test). SD refers to 3 independent experiments.*

At the same time, we verified the consistency of NBI performance on EVs isolated biological fluids. To this aim, plasma and serum fractions of nine healthy donors were subjected to NBI, and the relative abundance of LVs was analyzed by flow cytometry. We observed a 6-fold enrichment of EVs purified from plasma compared to serum EVs (in Fig. 20 a) a representative case is shown). Given the enrichment in EVs in the plasmatic fraction, we isolated EVs from the plasma of forty-seven healthy donors, assessing the distribution of EVs by TRPS. The profile of NBI-isolated EVs was characterized by at least two enriched populations showing a quantitative ratio of ~55:1: the first one with a mean diameter of 249.5 ± 36.71 nm (SVs) and a concentration of 30.56 ± 25.78 × 10^9 per milliliter of plasma; the second one with a mean size of 564.4 ± 57.3 nm (LVs) and a concentration of 5.49 ± 3.09 × 10^8 per milliliter of plasma, as indicated in Fig. 19 b). As reported by previous studies (Abels & Breakefield, 2016), smaller vesicles were more abundant than larger ones, and a similar trend was also observed in the distribution of cell-derived EVs.

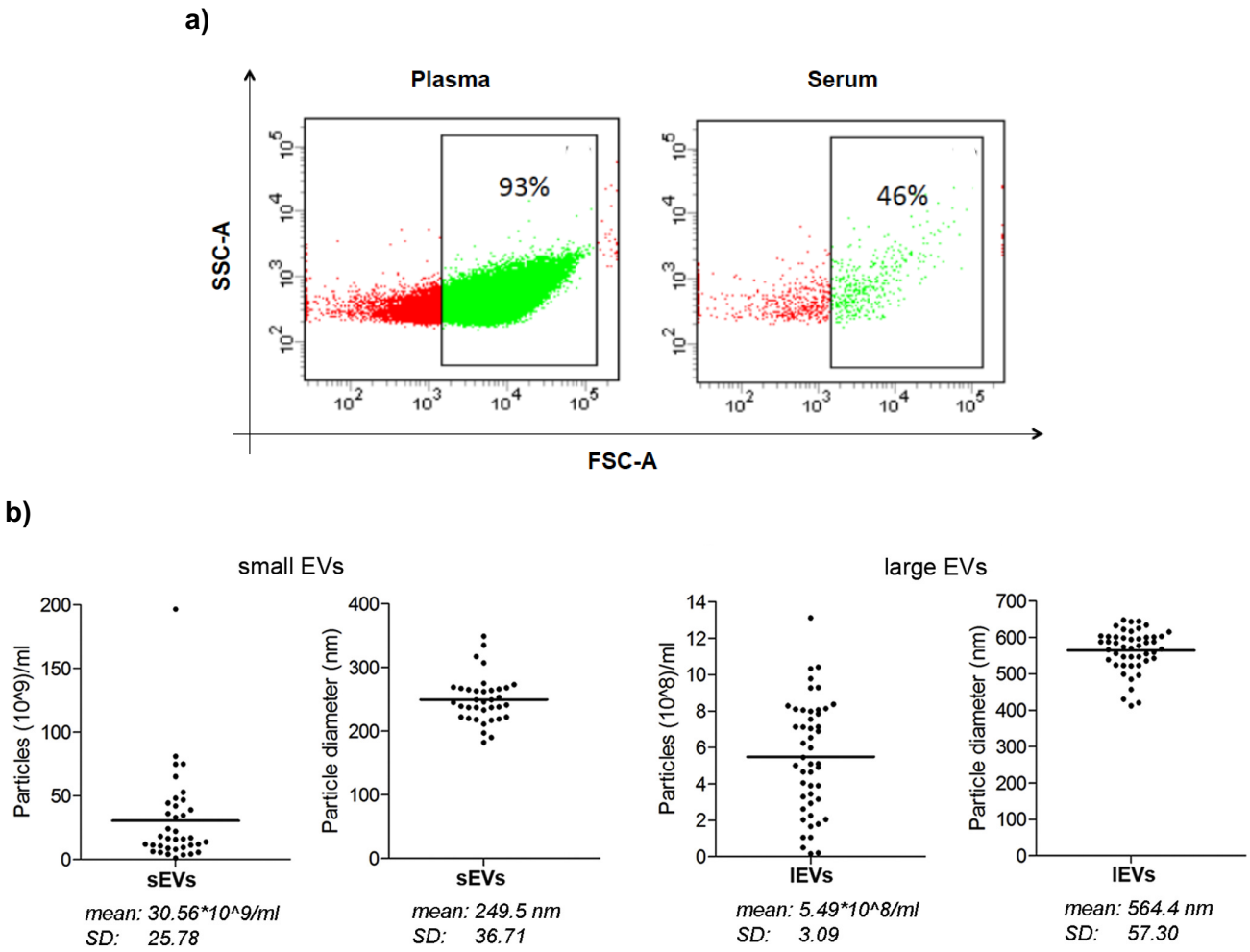

Figure 20. NBI efficiently isolates EVs with high reproducibility from the blood of healthy donors. a) *Representative percentages of LV distribution in plasma and serum fractions of one donor is shown. 1000 events were recorded for each condition. The abundance of LVs was assessed by flow cytometry (BD, FACS*

Canto). ***b)*** *NBI was applied to 0.5 mL of plasma obtained from 46 healthy volunteers. The mean age of the volunteers was 45 ± 10 years. The relative distribution of EVs has been evaluated by TRPS analyses using three nanopores with the obtained concentrations, per milliliter of plasma, of the small and large EV populations.*

Characterization of plasma EV lineages by combined immune-capture

As I mentioned in the introduction, an advanced stage of the tumor correlates with a high degree of hardly detectable cell heterogeneity. As an opportunity, tumor-EVs released by different cellular subtypes can reflect the tumor heterogeneity (Willms et al., 2016; Willms, Cabañas, Mäger, Wood, & Vader, 2018). One challenge in liquid biopsies is the presence of EVs that are secreted by non-cancer cell types as blood cells; therefore the assessment of EV subtypes is necessary to define specific lineages to unravel the messages carried by EVs (Greening & Simpson, 2018)

In line with other reports (Nomura, 2017; Wolf, 1967), mixed populations of circulating vesicles in healthy individuals are positive to hematopoietic or endothelial cell markers. To recognize specific EV lineages from a liquid biopsy, we analyzed a pool of NBI-isolated vesicles derived from plasma of healthy volunteers. Hence, we used an immune-capture strategy exploiting hematopoietic cell markers expressed on the surface of blood cells, to understand if they could be instrumental for the characterization of isolated EVs. In detail, we analyzed a mixture of EVs immunodepleted of CD235a (a marker of erythrocytes) and CD41a (a marker of platelets) (Valkonen et al., 2017; Vagida et al., 2017). We measured the number of vesicles before and after the immune-depletion experiment, observing a 20% diminution of the original population of microvesicles, and about 60% reduction of SVs using the CD235a. Viceversa, we detected an opposite trend using the CD41a, which showed preferential recognition of LVs (Fig. 21). These results indicate that plasmatic EVs expose markers that are specific of distinct cell lineages, underlying the derivation from different cells/progenitors. Besides, these results are in line with other reports indicating that platelet-derived microvesicles (range of size >300 nm) are abundant in the blood of healthy individuals (Vagida et al., 2017; (Aatonen et al., 2014).

a)

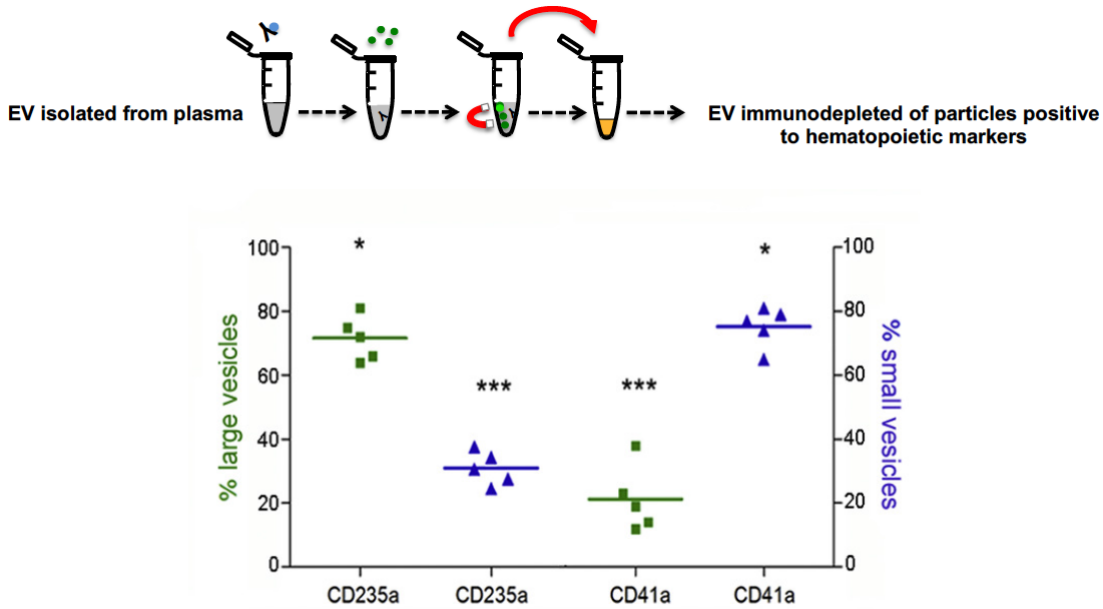

b)

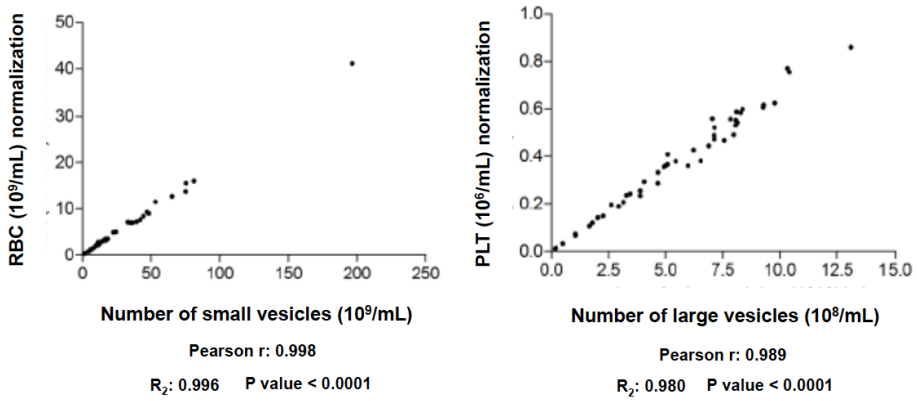

c)

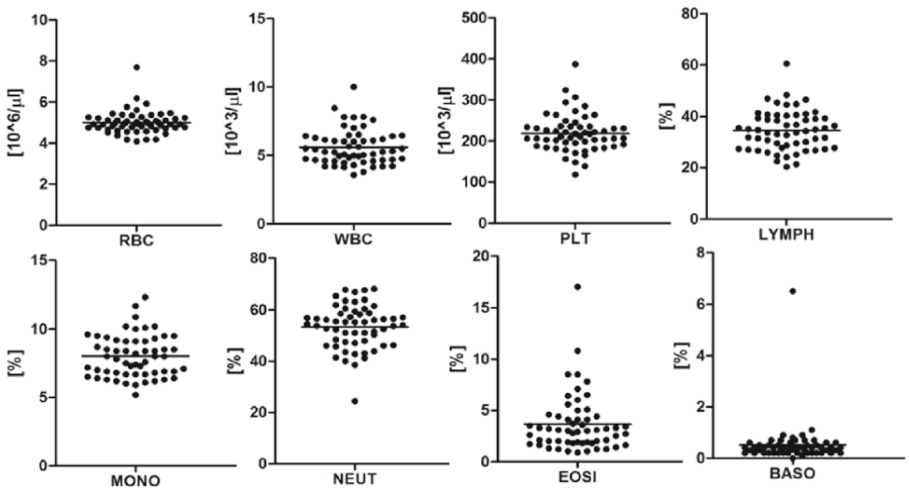

Figure 21. NBI allows to enrich in different EV lineages from blood. a) *Hematopoietic cells' antigens, biotinylated anti-CD41a, and CD235a antibodies were used to characterize plasma isolated EVs. Isolated EVs (2 × 108/ml), for a total of 15 samples, were divided into two volumes and incubated with biotinylated antibodies*

*(CD41a or CD235a) + streptavidin dynabeads. Supernatants were analysed at qNano instrument and the distribution of EVs left in solution are shown. * P-value < .05; ***P-value < .001.* ***b)*** *Correlation between the number of erythrocytes and small vesicles (Pearson r: 0.998) and between platelets and large vesicles (Pearson r: 0.989), analyzed in EV derived from plasma of 46 healthy donors.* ***c)*** *Blood cell counts of NBI-isolated EVs from the plasma of healthy volunteers.*

NBI allows recovering heterogeneous EVs derived by specific cell lineages

Next, we aimed at recognizing specific EV lineages from a heterogeneous pool of EVs isolated by NBI. This time we performed immune-capture experiments starting from the same number of EVs derived from melanoma cells (SK-MEL-28) and human plasma (10^9/mL) spiked in one mL of plasma after NBI procedure. We pooled the EVs derived from the different sources and incubated the mixture of isolated vesicles with varying combinations of CD235a, CD41a, and CD45 antibodies, the latter known to be expressed from leukocytes (Woodford-Thomas et al., 1993) but not from SK-MEL-28 cells (Cardi, Mastrangelo, & Berd, 1989). To target specifically the populations of melanoma-derived EVs, we used CD146 and CD166 antibodies. CD146 and CD166 are members of the cell adhesion molecule (CAM) family, a group of cell surface receptors that play a critical role in physiological and pathological conditions (Murray, Frampton, & Nelson, 1999; Lei, Guan, Song, & Wang, 2015). In particular, CD146 (Mel-CAM) and CD166 (Al-CAM) are considered target molecules in the monitoring of melanoma, given their role supporting the melanoma progression (Wang & Yan, 2013; Ordóñez, 2014; (Ruma et al., 2016).

After multiple combinations of immune-depletions with the markers as mentioned earlier, we measured by TRPS the number of EVs left in the supernatants. After immunoprecipitation of CD235a, CD41a, and CD45 positive vesicles, CD146 antibody still recognized the 64% of input EVs (light green vs. light grey bars) positive to the epithelial marker, in contrast to the CD166 antibody which resulted as an experimental negative control (shown in Fig. 19). We have shown that it is possible to assess the presence of specific hematopoietic-endothelial antigens on the surface of plasmatic EVs and that NBI allows an unbiased enrichment of different EV lineages.

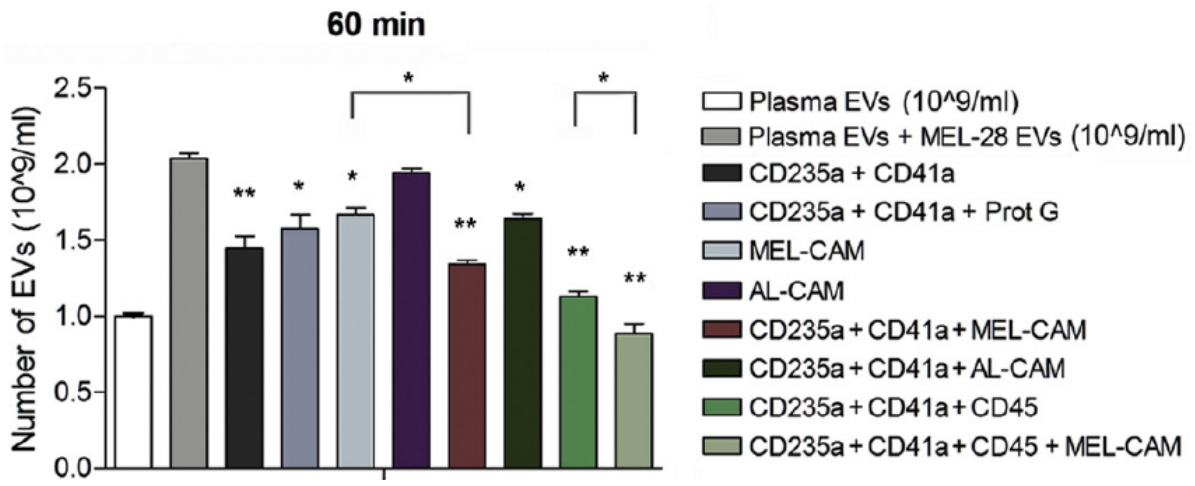

Figure 22. Identification of specific EV lineages in plasma. *10^9/ml plasma EVs and 10^9/ml EVs isolated from media of SK-MEL-28 cells were spiked in 1 ml of post-NBI human plasma. Indicated biotinylated antibodies were incubated for 60 min and, after streptavidin dynabeads precipitation, TRPS analyses were performed on EVs left in solution. One-way ANOVA-Bonferroni has been used to calculate the statistical significance (*P-value < .05; **P-value < .001).*

EXPLORING THE INNER AND OUTER CONTENT OF EVs: SENSITIVE DETECTION OF PROTEINS AND RNA BY NBI-BASED TECHNIQUES

Being abundantly present in biological fluids, EV can be captured and analyzed in liquid biopsies. Cancer diagnostic may take advantage of EVs since they represent a biological source to exploit for discovery and detection of biomarkers. To gain a profit from the uniqueness of EVs, the clinical studies require rigorous and sensitive analytical approaches to get high-quality diagnostic information about the heterogeneity of tumor cells. We demonstrated the advantages of NBI procedure to recover intact and polydisperse EVs, from cell supernatants and blood fractions, in a scalable and reproducible way. In the next steps, we exploited the potential of this novel method to optimize biochemical and molecular assays and reach ultra-sensitive biomarker detection via EVs.

Ultrasensitive detection of surface antigens by NBI-alpha assay

To detect surface antigens expressed on the EV-membrane, we exploited the versatility of NBI approach to optimize the amplified luminescent proximity homogeneous assay (alpha) technology. In this assay (illustrated in Fig. 23, top), streptavidin-coated donor beads recognize a biotinylated antibody specific for the antigen of interest, while positively-charged nickel-chelate acceptor beads interact with EVs and emit a fluorescent signal when in the proximity of excited donor beads (NBI-Alpha).

EVs isolated from two healthy volunteers and melanoma cells SK-MEL-28 were subjected to NBI-Alpha. EV counts, assessed by TRPS, were reported as a function of the signal, obtained after binding with CD235a, CD41a, and CD45 biotinylated antibodies. The expression of CD235a, markers of red blood cells, was efficiently detected on the surface of plasma-derived EVs, compared to CD41a and CD45 (Fig. 23, b) bottom), in barely 10^6 EVs. Conversely, in case of EV derived from melanoma cells, the signal of Mel-CAM protein was more enhanced compared to hematopoietic markers, with a peak corresponding at 10^5 vesicles, confirming the expression of this marker on the membrane of melanoma-derived EVs (Fig. 23, b) top).

a) **b)**

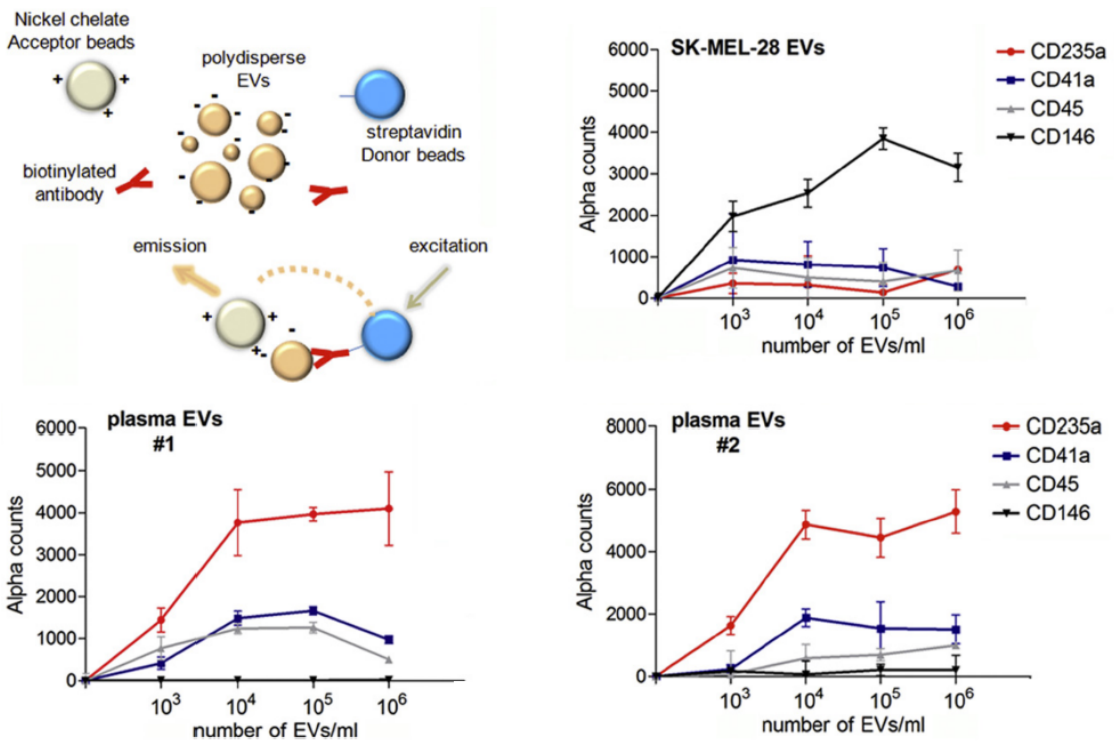

Figure 23. NBI-alpha as a new analytical tool to study EVs. a) *Diagram describing the alpha assay designed to detect surface antigens on individual, polydisperse EVs.* ***b)*** *Saturation curves were obtained as a*

function of the number of EVs purified by NBI from the plasma of two healthy donors (#1, #2) and SK-MEL-28 melanoma cells.

To test the assay in terms of sensitivity and accuracy, we compared the NBI-Alpha with two other techniques: ELISA (Smith et al., 2015) and ExoScreen (Yoshioka et al., 2014), which have been used to identify proteins associated to EVs with superior sensitivity. In particular, we evaluated the performance of the methods to detect CD146 levels in three cells lines, SK-MEL-28, HeLa and Jurkat, showing respectively, high, intermediate and low levels of endogenous CD146 (Fig. 24 b). To this end, EVs subjected to ELISA and ExoScreen were isolated by UC (10k and 100k pellet) while EVs for NBI-alpha were purified by NBI and UC, (10k and 100k pellet analyzed separately).

Generally, all the techniques were consistent in the detection of the relative cellular expression of CD146, although NBI-alpha showed the highest sensitivity in CD146 detection (>5 times), even when the antigen expression was low as in the case of Jurkat. Notably, the advantage of the optimized Alpha assay is superior when combined to NBI procedure rather than UC, as a possible consequence of particle aggregation, induced by g-force, on both ultracentrifuged samples (Fig. 24 a).

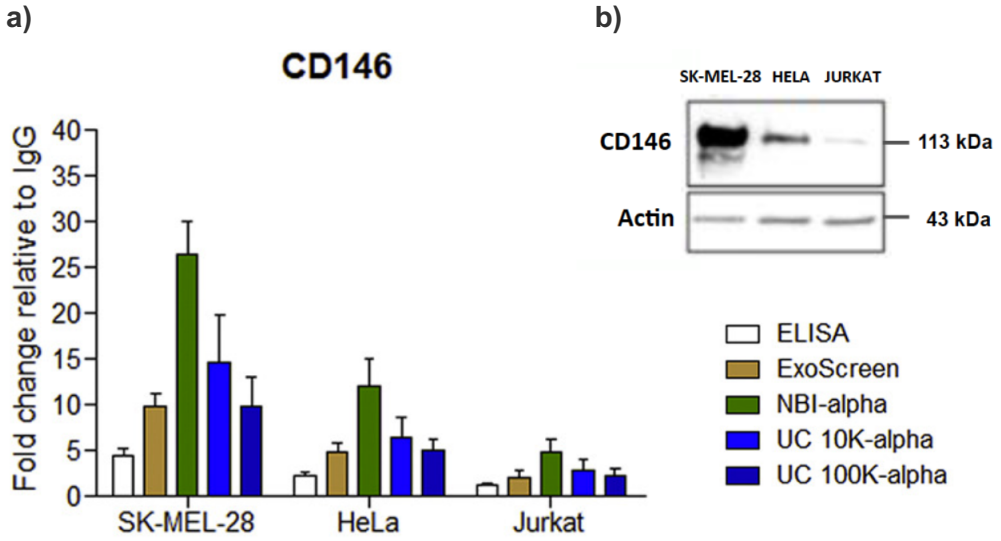

Figure 24. NBI-alpha detects the expression of EV surface proteins with enhanced sensitivity. a) *The relative performances of different detection methods have been then evaluated, using anti-CD81 biotinylated antibody for plate-coating in the case of ELISA (coupled with anti-CD146 and HRP-conjugated secondary antibodies) or conjugation with Acceptor beads in the case of ExoScreen. The specific, background-subtracted signals were normalized to IgG signals of individual experiments. 10 K and 100 K indicate the g forces applied in the two protocols of UC, respectively. SD refers to two independent experiments.* ***b)*** *Immune-blotting performed on cell lysates indicate cells lines expressing high, intermediate, or low levels of CD146 protein.*

Finally, we exploited the analytical potential of NBI-alpha in retrospective studies to detect cancer biomarkers in patients' fluids. We chose as target prostate specific marker antigen (PSMA), a protein expressed in all types of prostatic tissue, which is achieving a prominent role in diagnostics of prostate cancer (von Eyben, Baumann, & Baum, 2018). We isolated EVs from one milliliter of plasma of ten patients with advanced metastatic prostate cancer (>60 years) and seven healthy subjects (age of 50-55 years) as controls.

In agreement with other studies (Yoshioka et al., 2013) we found a statistically significant increase in the number of recovered EVs in the cancer patients (Fig. 25 a), as well as increased levels of PSMA in all patients' EVs, compared to healthy controls (mean *P* value <.001). The sensitivity of NBI-alpha allowed identifying a picomolar concentration of PSMA using 10^5 EVs (Fig. 25 b), as determined by a standard curve with His-tagged PSMA.

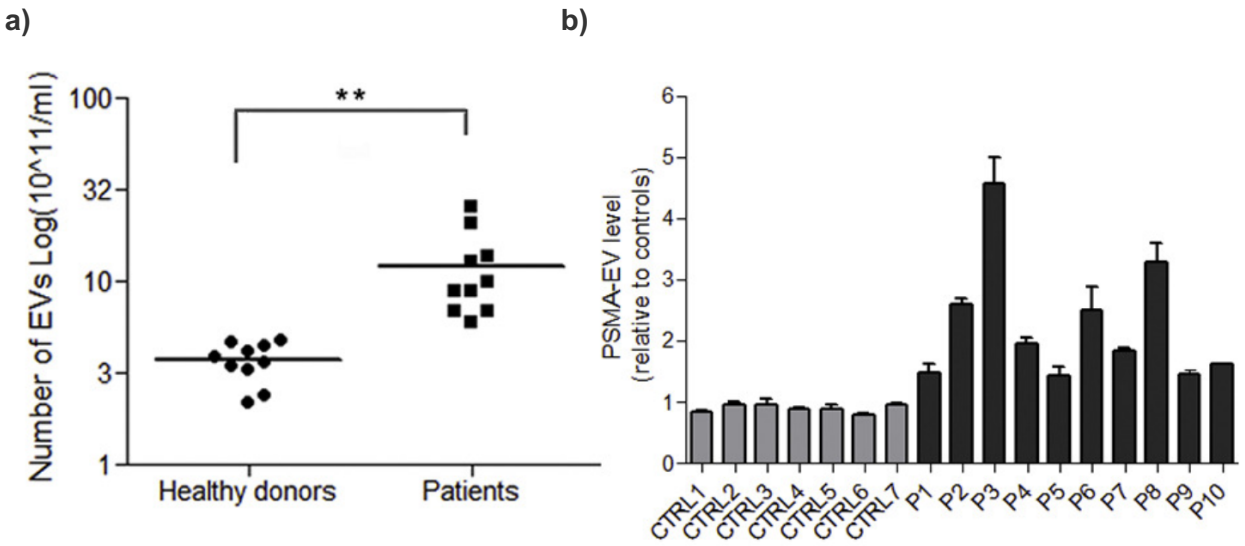

Figure 25. Detection of PSMA in NBI-EVs derived from patients and healthy controls. a) *The relative number of EVs is plotted for healthy donors (50–55 years) and prostate cancer patients (>60 years). One-way ANOVA-Bonferroni has been used to calculate the statistical significance. **P-value < .001.* ***b)*** *The relative levels of PSMA on 10^5 EVs were detected by NBI-alpha. According to the standard curve with purified recombinant histidine-PSMA, 1 in the Y-axis corresponds to ~35 pg/ml of PSMA in solution. SD refers to three independent experiments.*

Ultrasensitive detection of RNA in EV lineages by NBI-ddPCR assays

EVs are enriched in nucleic acids, which can be shuttled between cells and mirror the genetic diversity of the cells of origin. One of the most highly sensitive technologies used to detect RNA and mutated transcripts inside EVs is the droplet digital PCR (ddPCR) (Allenson et al., 2017). The sensitive power of ddPCR lies in the dilution and partition of the nucleic acids into separated droplets

which are simultaneously and independently amplified. In this way, the assay results in a more effective PCR amplification and a higher detection sensitivity (R. Zhang et al., 2018). With this assay, we analyzed the nucleic acid content of heterogeneous EVs isolated from plasma of forty-seven healthy donors, having a broad size range of 50–700 nm. We started from $3x10^9$ EVs per each sample and investigated the absolute number of glyceraldehyde 3-phosphate dehydrogenase (GAPDH) transcripts. We confirmed the correlation between the number of GAPDH mRNAs and the number of platelets (Pearson r: 0,623), given the abundance of MVs derived from platelets in the blood (Żmigrodzka, Guzera, Miśkiewicz, Jagielski, & Winnicka, 2016) expressing GAPDH (McDonald, Reep, Lapetina, & Molina y Vedia, 1993). Encouraged by these promising results, we exploited the versatility of NBI procedure, implementing the standard ddPCR protocol through direct encapsulation of NBI-EVs into the oil-droplets to skip the step of RNA extraction. Moreover, we optimized the assay adding a thermostable reverse transcriptase to the mix performing a one-step amplification of the RNA fragment of interest (Fig. 26 b). Interestingly, using particles isolated by UC, we did not observe an optimal number of oil droplets generated (>12000), suggesting that the eventual particle aggregation was a limiting factor to the direct encapsulation of EVs.

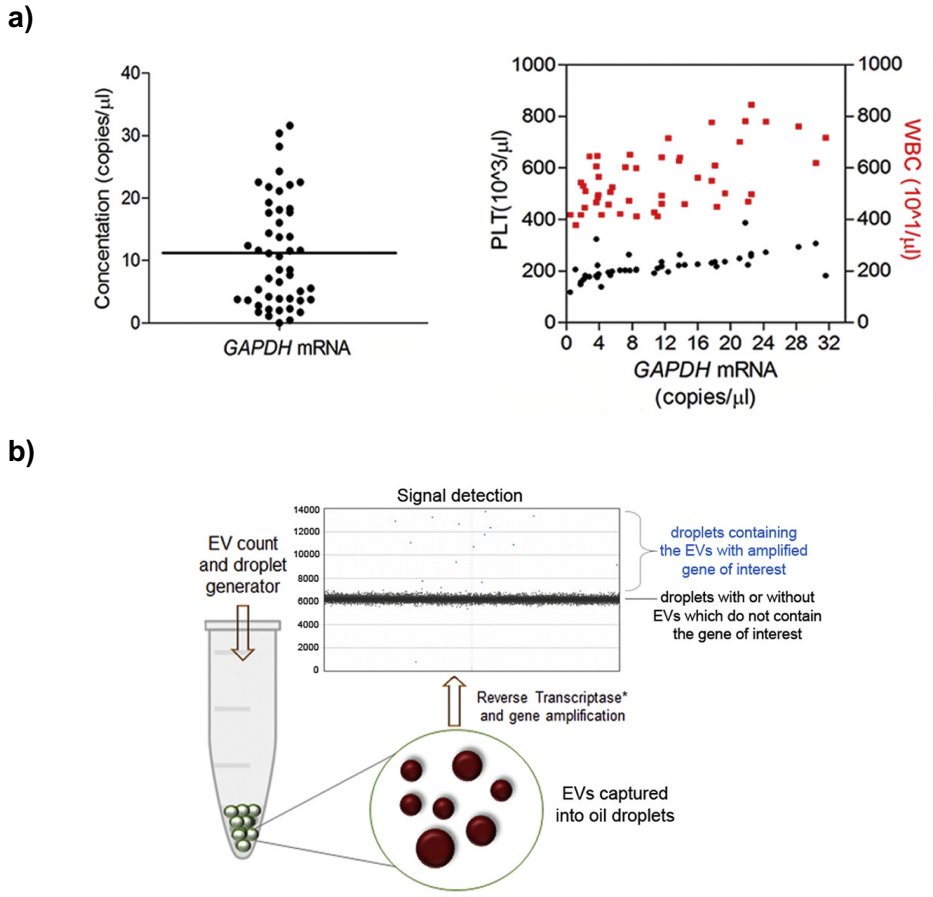

Figure 26. Detection of RNA species in plasmatic EVs and design of a new ddPCR assay for nucleic acids detection in NBI-isolated EVs. a) *EV-RNA were deriving from plasma samples of 47 healthy donors.*

ddPCR has been performed with EvaGreen chemistry. The absolute number of GAPDH mRNA copies has been analysed by QuantaSoft Analysis software (BIORAD). ***b)*** *Schematic representation of a new ddPCR assay to encapsulate EVs (50–700 nm) into oil droplets (1400–1600 nm). The number of copies of specific RNAs present in NBI-isolated EVs can be obtained as a function of EV titration. The stochastic entrapment of EVs into oil droplets allow the amplification of the target of interest upon supplementation of the EvaGreen mix with a thermostable Reverse Transcriptase enzyme.*

In the light of a clinical application, we tested the performances of the NBI-ddPCR in a retrospective analysis, detecting a mutation in a cohort of metastatic colorectal cancer patients. Colorectal cancer (CRC) is one of the deadliest types of cancer in the western countries, with 861,000 deaths in 2018, according to World Health Organization (Global Cancer Observatory). Despite a decline of about 50% in CRC mortality over the past four decades, thanks to the changes of dietary and smoking habits and advancements in early detection and treatment, the assessment of new diagnostic tools would help accelerate the progress against this type of cancer and predict early CRC (Siegel, Miller, & Jemal, 2019; X. Chen et al., 2019). Recently, many studies focused on the diagnostic potential of EV cargo for early detection of mutations and microRNA signatures have been proposed as useful biomarkers for diagnosis, prediction of prognosis, and treatment response. In this work we analyzed, in blind, the diagnostic utility of NBI-ddPCR to detect BRAF V600E mutation in plasma of twenty-one patients, previously enrolled in a randomized phase III clinical trial for chemotherapy alone or in combination with bevacizumab, plus 6 additional blood draws collected from one single patient during the treatment (longitudinal liquid biopsy), (Marisi et al., 2017; Ulivi et al., 2015). KRAS and BRAF are two key proteins investigated in CRC clinical management to indicate a correct therapeutic approach. The rare co-occurrence of mutated versions of these proteins is a reflection of the high degree of tumor heterogeneity that characterizes CRC and is associated with aggressive clinical manifestations (Larki et al., 2017). Notably, BRAFV600E is a single nucleotide mutation characterized by a substitution of glutamic acid for valine (nucleotide 1799 T > A; codon GTG > GAG), and it occurs in 15% of sporadic colorectal cancer (Bond & Whitehall, 2018).

On the analyzed CRC cases, the mutational status of these biomarkers has been assessed by pyrosequencing on formalin-fixed, paraffin-embedded (FFPE) tissue DNA, indicating the presence of the BRAF V600E mutation in 5 out of 21 patients (~24%, samples C02, C11, C14, C20, and C25) and further confirmed 5 months later in the sample C03, a posterior blood draw of the sample C20. Any mutation was reported in the KRAS gene, except for the variant K117N in the sample C07. We isolated EVs from the samples mentioned above and first of all, we observed, as for prostate cancer patients, a higher number of EVs recovered from the plasma of colon cancer patients in comparison to those of healthy donors (Fig. 27 a, on the left). Then we applied the NBI-ddPCR protocol starting from one thousand EVs per sample as input to amplify the allele fragment containing the BRAF V600E mutation. In figure 27 a) (on the right) it is shown the number of single droplets that have

encapsulated vesicles carrying the V600E mutated transcripts. In particular, the brownish dots detected in samples C02, C03, C11, C14, C20, and C25 an arbitrary threshold >1 indicate a relatively higher number of mRNA copies detected by NBI-ddPCR, matching 100% with data obtained by pyrosequencing on Formalin-Fixed Paraffin-Embedded (FFPE) tissue specimens, while the copies of mutated BRAF in samples C04, C09, C19, C21, and C24 (blue dots) were exclusively detected by NBI-ddPCR.

To further investigate the accuracy of these results, we assessed the number of BRAFV600E copies in the same patients, after immune-depletions of hematopoietic markers positive EVs, finding an ulterior increase in the number of detected copies, compared to the signal obtained in the total population of EVs (Fig. 27, b), on the left). Since we previously showed the feasible profiling of EV subpopulations by NBI, we analyzed the EVs immunodepleted of CD-147, a tetraspanin overexpressed in plasmatic EVs derived from CRC cases, (Tian et al., 2018), to evaluate the specificity and sensitivity of our approach. In this case, illustrated on the right of Fig. 24 b), we noticed a reduction of the number of mutated copies in the case of the sample C25 (0.25 vs. 4.48 and 20.05 copies, respectively obtained in the previous experiments), and just ~34% the concordance with exclusive NBI-ddPCR mutation-bearing samples (blue dots). These results showed that individual EVs negative for the CD147 antigen could effectively carry BRAF mutated transcripts, indicating that it is possible to capture the genetic tumoral heterogeneity with NBI combined approach, with unprecedented specificity compared to single antibody-mediated enrichment of tumor-derived vesicles.

a)

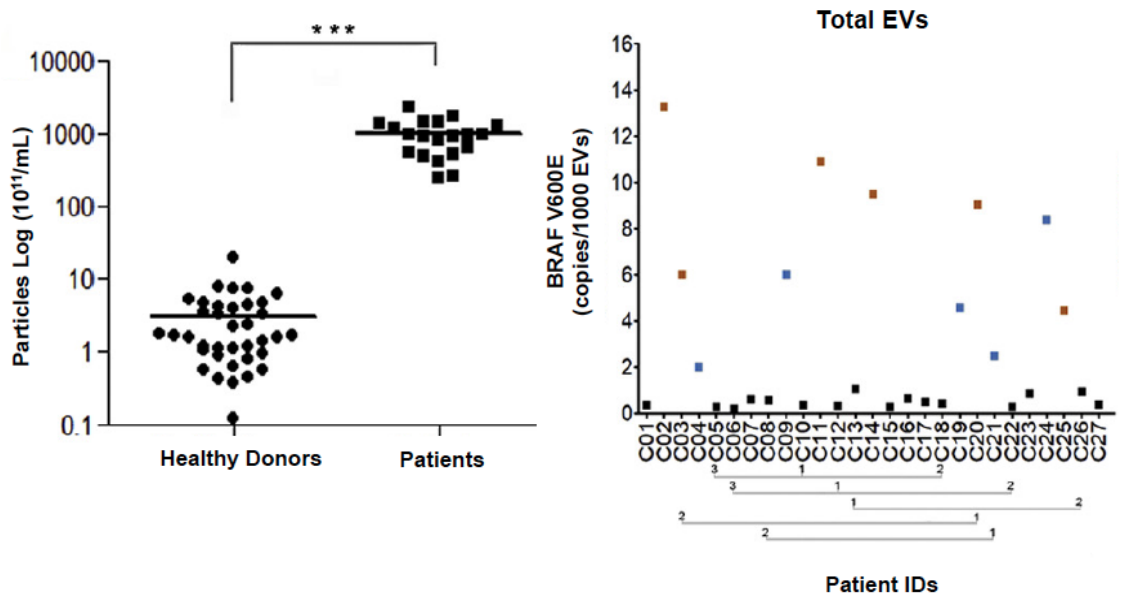

b)

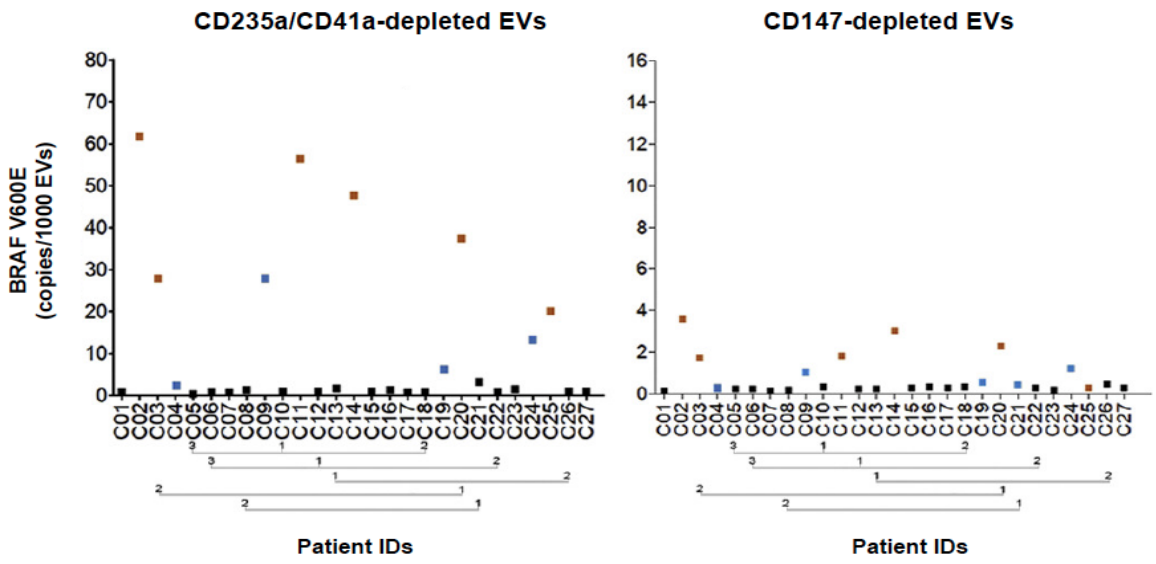

***Figure 27**. **Diagnostic application of the optimized NBI-ddPCR protocol on a retrospective study. a)** NBI was performed on 1 ml of plasma deriving from patients with colon cancer. The relative number of EVs is plotted for healthy donors (35–55 years) and colon cancer patients (64 ± 8 years). The correlation coefficient was 0.93, with relative counts of RBCs, WBCs, and PLTs. One-way ANOVA-Bonferroni has been used to calculate the statistical significance (on the left). ***P-value <.001. On the right the copy number of BRAF V600E enclosed in 1000 EVs isolated from 20 colon cancer patients is shown. **b)** the copy number of BRAF V600E enclosed in 1000 EVs upon immune depletion of CD235a/CD41a positive EVs is shown; on the right: the copy number of BRAF V600E in EVs isolated by CD147 antibody.*

Given the exciting findings obtained by NBI-ddPCR, we performed a diagnostic approved analysis, the allele-specific real-time PCR screen (EasyPCR), on the FFPE DNA of the samples from patients C04, C09, C19, C21, and C24 (blue dots), whose EVs resulted positive to BRAF mutation, contrarily to the tissue biopsy results. This time the sample C09 resulted positive to BRAF V600E mutation, indicating the correspondence of the mutation in DNA of the primary tumor and the effective presence of this cellular subpopulations. Furthermore, as shown in Fig.28, we were able to identify the mutation (a borderline A peak masked by the prevalence of the T allele) in the bulk of total EVs isolated by sample C09, stressing the sensitivity of EVs, analyzed by NBI-derived approaches, in detecting an unreported mutation by tissue biopsies standard methods.

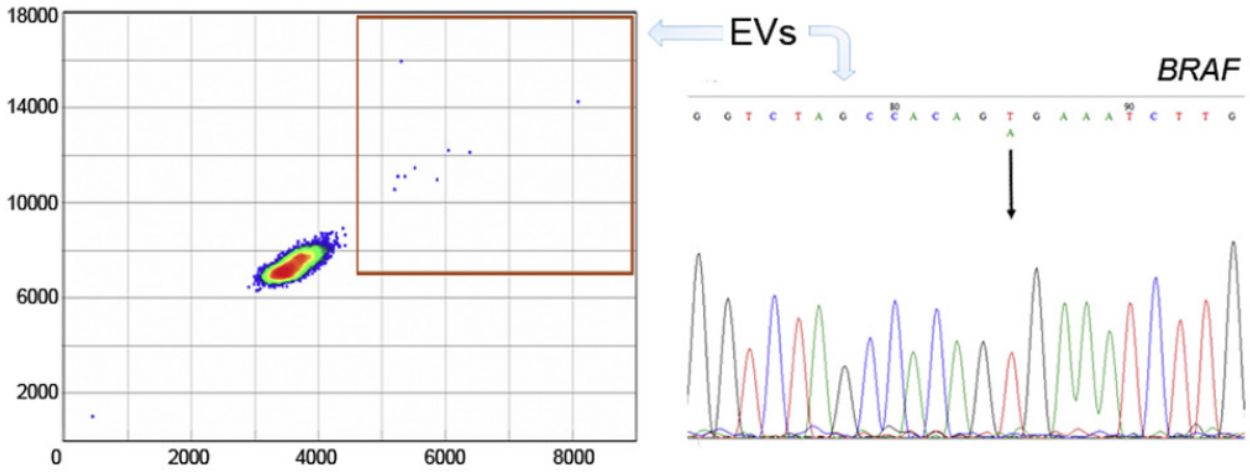

Figure 28. Validation of BRAFV600E detection by NBI-ddPCR in sample C09 by Sanger sequencing. *On the left, it is shown the original plot of the NBI-ddPCR results for the sample C09, whose RNA from the bulk of EVs has been amplified with BRAF exon-spanning primers and then sequenced, as shown in the electropherogram on the right.*

Confident in these validations, we additionally analyzed the mutational status of KRAS gene on the exon 2 in the pool of EVs isolated from the same cases. Interestingly, also in the case of KRAS, we were able to detect three samples positive to the G12C mutation and one sample positive to the G12D, and the last alteration (KRAS G12D) present in the sample C12 was indeed endorsed by a subsequent analysis on FFPE DNA (Fig.29).

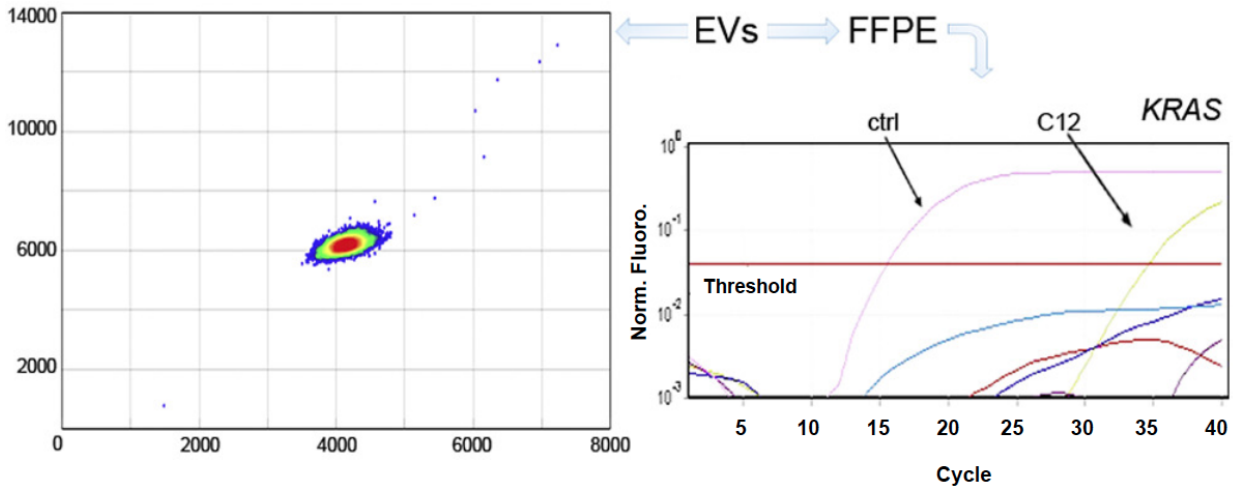

Figure 29. Validation of KRAS G12C mutation detected by NBI-ddPCR in sample C12 by EasyPCR analysis. *On the left, it is shown the original plot of the NBI-ddPCR results for the sample C12, while in the plot on the right it is illustrated the EasyPCR analysis, confirming the presence of the alteration on KRAS exon 2 in the sample C12.*

As I underlined in the introduction, extracellular RNA circulating in the bloodstream can also be associated with contaminants of non-vesicular origin (Douglas D Taylor & Gercel-Taylor, 2013). Apolipoprotein A-1 (APOA1) is the major constituent of high-density lipoproteins (HDL), while Apolipoprotein B100 (APOB100) is one of the most represented proteins of low-density lipoproteins (Frank & Marcel, 2000; Guevara, Romo, Hernandez, & Guevara, 2018). We chose these proteins because multiple studies evidenced the presence of apolipoproteins in EV preparations (Szatanek, Baran, Siedlar, & Baj-Krzyworzeka, 2015) and we wondered whether their presence could impact on the diagnostic potential of RNA derived from NBI-EVs.

To this aim, we analyzed a pool of plasmatic EVs of two healthy volunteers, before and after immune-depletion with APOA1 and APOB100 antibodies to verify their influence on the amplification of GAPDH and wild-type BRAF by NBI-ddPCR. Notably, the RNA extracted from particles recognized by APO A1 and APO B100 antibodies did not contribute to the signal observed for GAPDH or wild-type BRAF mRNAs.

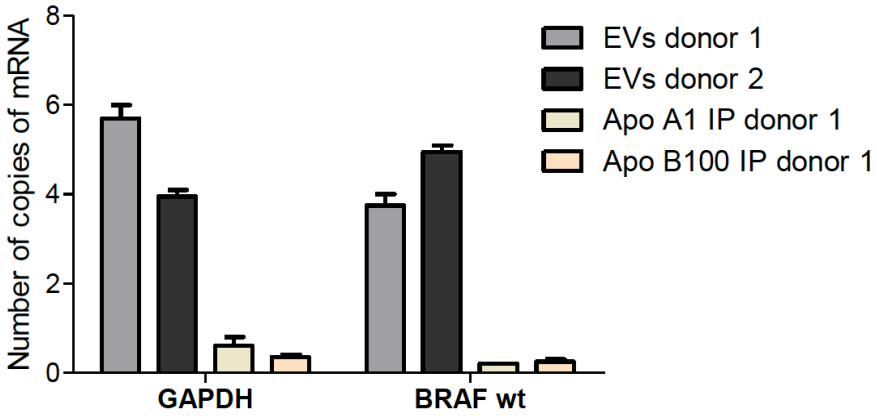

Figure 30. Analysis of the content of plasmatic EV-RNA by ddPCR. *NBI-ddPCR was performed on EVs isolated by NBI from the plasma of two healthy subjects and, in parallel, APO A1 and APO B100 immunoprecipitated particles. EvaGreen chemistry was used with PCR primers for amplification of GAPDH or wild-type BRAF mRNA fragments.*

Y- RNAs are enriched in EVs derived from glioblastoma stem cells compared to human IPSCs

In 2017, a paper from Wei and colleagues illustrated the content in extracellular RNA of glioma stem cells, providing useful indications for further studies on biomarker discovery. Interestingly, they found enrichment in Y-RNA and tRNA fragments in extracellular RNA associated with EVs and RNPs (Wei et al., 2017b). Given the expertise of my laboratory on Y-RNAs as

translational regulators, first of all, we approached the investigation of the content of Y-RNA in two cell lines of glioblastoma stem cells that were already employed and well characterized in our lab for other projects (COMI and 030616 cell lines). In particular, we compared the Y-RNA content of CSCs with a commercial cell line of human induced pluripotent stem cells (hIPSCs), resembling the stem-like characteristics of CSCs, without the characteristics of the disease. In this way, we could get a hint whether an elevated content of this RNA species inside EVs were attributable to the disease.

We cultured the CSCs as neurospheres in suspension, while human IPSCs were cultured in adhesion on a Geltrex coating (Thermo Fisher). We collected the media and isolated EVs according to NBI protocol. To proceed with the RNA extraction, we pelleted the total vesiculome isolated by NBI at 100000xg for 70 min and resuspended the pellet in Trizol. We assessed the RNA concentration at bioanalyzer, reverse-transcribed an equal amount of RNA, and normalized each sample to a standard curve to compensate for differences in the qPCR input quality and quantity. We detected an increased relative abundance of Y-RNAs associated with COMI EVs, compared to the other two cell lines, with Y3 as the most represented form in all the cell types. Both EVs released from glioblastoma stem-like cells displayed a higher content in Y-RNAs compared to hiPSCs.

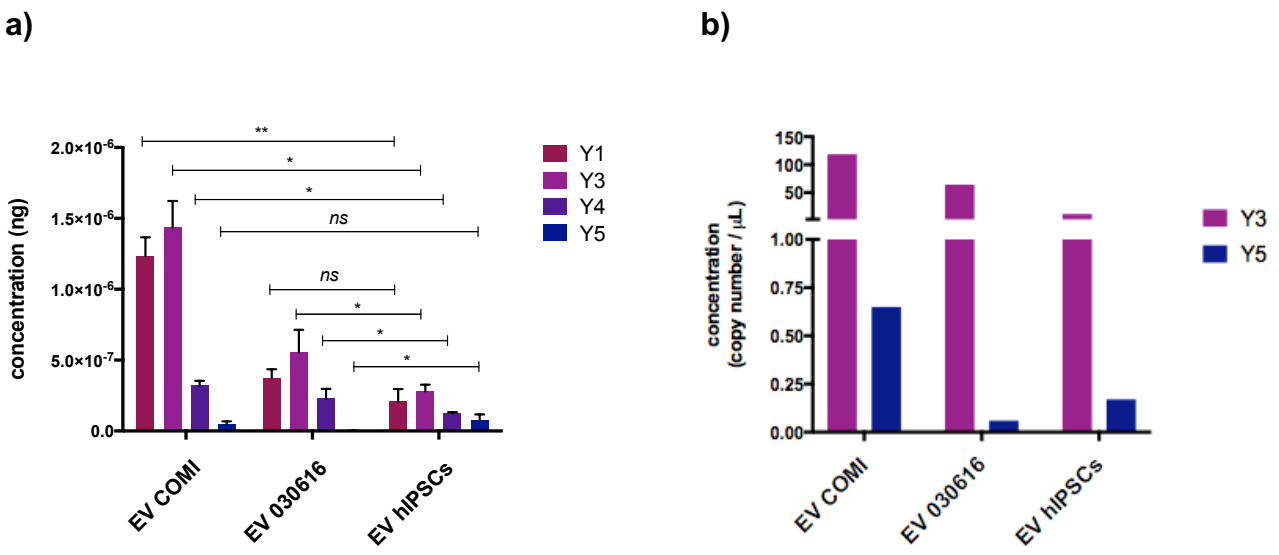

Figure 31. Evaluation of Y-RNA content in EVs derived from COMI, 030616, and GIBCO cells by RT-qPCR and validation in droplet digital PCR. a) *Data presented as concentration over a standard curve. n=3 biological replicates, mean ± SD. * P-value <0.05; **P-value <0.01.* ***b****) Validation of qPCR results by droplet digital PCR assay. Data refer to the most and less represented Y-RNA forms, respectively, Y3 and Y5. n=1 biological replicate.*

Y-RNA content of EVs is a reflection of the cellular transcriptome

A reliable biomarker should allow the monitoring of cell status during the entire disease course. To verify whether the vesicular content in Y-RNAs would serve to this purpose, we investigated in parallel the expression of Y-RNAs in RNA extracted from EVs and cells of origin, to assess if the EV cargo would mirror the cellular transcriptome. As for the previous experiment, we performed a reverse transcription reaction on the same quantity of RNA derived from cells and EVs and carried out an RT-qPCR. We observed a correspondence, between cells and EVs, of the expression of the four Y-RNAs in both cell lines, apart from Y3 and Y1 which were respectively more enriched in cells and EVs. Interestingly, Y5 was almost not expressed in both cases. These results suggest that Y-RNA associated with EVs is mostly reflecting the cellular transcriptome and could represent a potential biomarker for glioblastoma cancer stem cells.

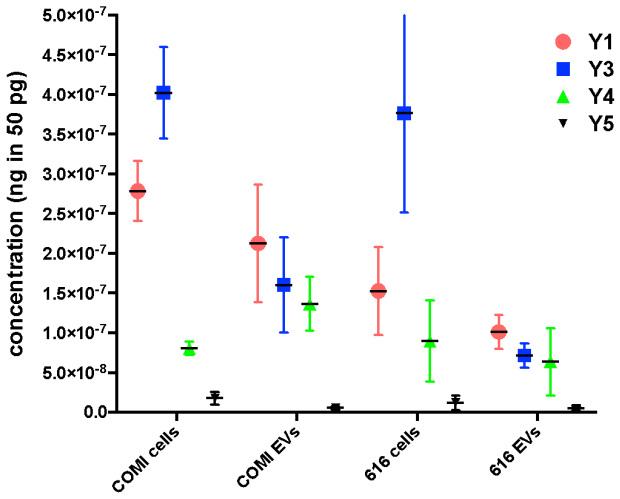

Figure 32. Assessment of Y-RNA expression in COMI and 030616 EVs by RT- qPCR. *Data presented as concentration over a standard curve, starting from 50 pg of RNA as input. n=3 biological replicates, mean ± SD.*

Y-RNAs are enriched in EVs derived from stem cells rather than EVs derived from differentiated cells

Y-RNAs are a peculiar class of RNAs because although non-coding, they play an essential role in DNA replication and bind to different RBPs (Driedonks & Nolte-'t Hoen, 2019; Krude, Christov, Hyrien, & Marheineke, 2009). Despite these facts, still little is known about their functions in vertebrates. It was previously demonstrated, from a project carried out in my laboratory, that Y3

silencing has been shown to modulate the neuronal differentiation counteracting the effect of HuD, an RNA binding protein (Tebaldi et al., 2018).

Since we observed that Y3 was one of the most expressed forms of Y-RNAs inside EVs, we wanted to investigate its expression, along with other Y-RNAs, in astrocytes derived from by differentiation of COMI. In detail, we chose COMI since they showed higher levels of Y-RNA expression compared to 030616 cells, and we differentiated cells in astrocytes according to a protocol already employed in our laboratory (Pollard et al., 2009). We validated the differentiation efficiency by immunofluorescence on stemness (SOX2, Nestin) and using GFAP protein as a marker of astrocytes (Fig. 33). We assessed the Y-RNA expression by qPCR, and we observed an enrichment in Y-RNAs in stem-like glioblastoma cells rather than in differentiated cells, suggesting that extracellular Y-RNAs could be evaluated as potential markers associated to stemness features in glioblastoma stem cells.

a)

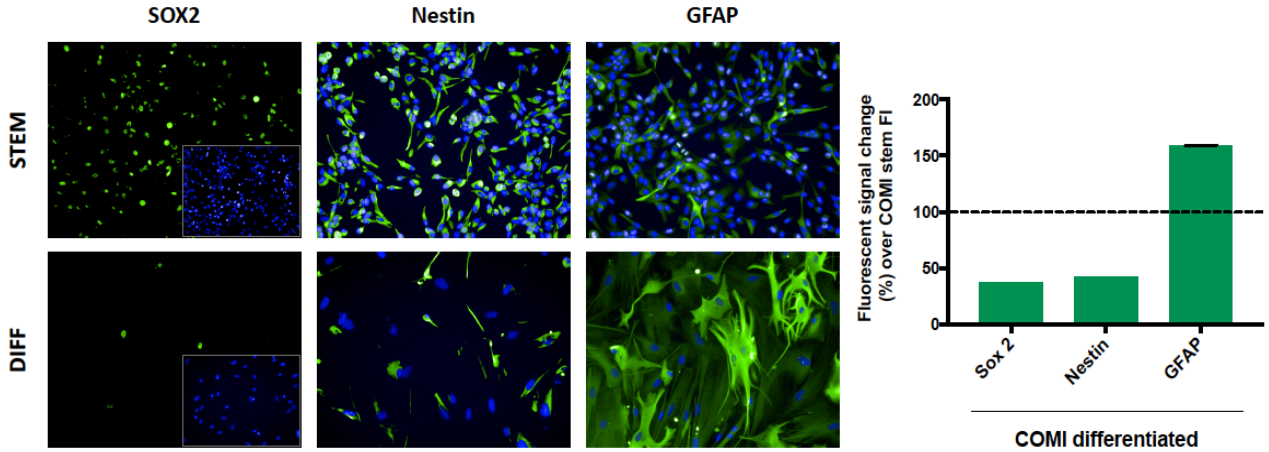

b)

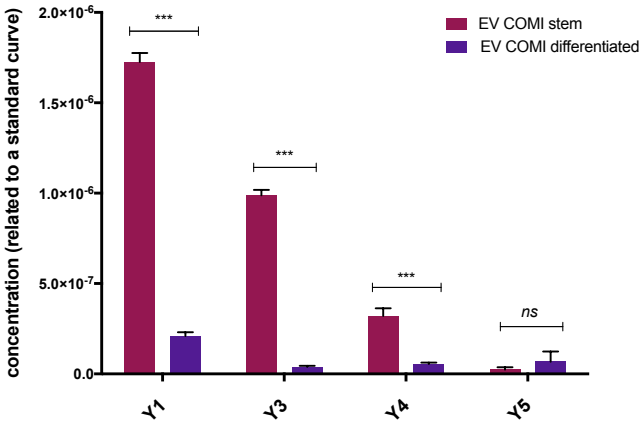

Figure 33. Assessment of Y-RNA expression levels in astrocytes derived from differentiation of glioma stem cells. a) *Representative images of differentiation of COMI by Immunofluorescence staining using*

stemness (Sox2 and Nestin) and differentiation (GFAP) markers. COMI were differentiated for 14-15 days in medium deprived of growth factors and supplemented with 10% FBS. On the right, quantification of the normalized intensity of immunostaining of Sox2, Nestin and GFAP over fluorescence intensity of COMI stem. n=6000 objects for stem cells and n=1000 objects for differentiated cells, mean, ± SEM. For this experiment, cells were cultured in adhesion with media supplemented with fetal bovine serum 10%, changed every other day (Pollard et al., 2009; Rahman et al., 2015)***. b)*** *Expression levels of different Y-RNAs in COMI stem and COMI differentiated. Data are presented as a function of concentration over a standard curve. n=2 biological replicates, mean ± SD. *** P-value <.001.*

EVs derived from glioblastoma stem cells can enhance the translation of differentiated glioblastoma stem cells

To understand the functional role of Y-RNAs carried by EVs derived from glioblastoma stem cells, we evaluated their potential to modulate the translation efficiency on astrocytes derived from differentiated COMI as receiving cells. We isolated EVs from undifferentiated and differentiated COMI, measured by TRPS and treated the receiving cells with EVs in ratio 1:100 for 24 hours. To assess the synthesis of nascent proteins, we exploited the Click-It chemistry using the AHA assay. We observed enhanced levels of protein synthesis when astrocytes are incubated with stem EVs. Even though the differences are not statistically significant, these results showed an effect on translational modulation mediated by EVs derived from stem-like GBM cells, implicating a potential impact on cell behavior.

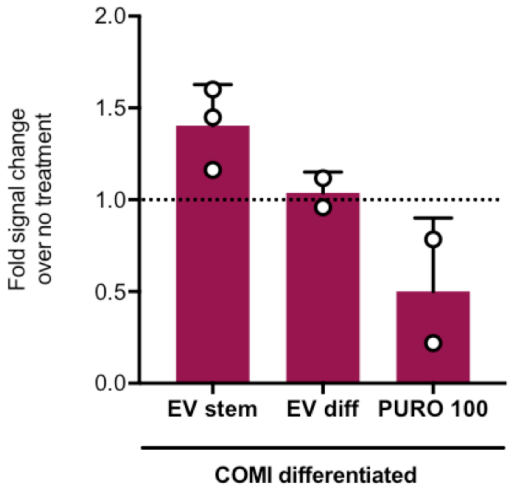

Figure 34. Translational modulation of astrocytes by EVs derived from glioblastoma stem cells. *Data are presented as fold signal change, over not treated cells. n=3 biological replicates, mean ± SD. Differences between conditions are not statistically significant.*

DISCUSSION

Cancer therapies become more effective when the tumor is diagnosed at early stages, and it is possible to monitor the evolution of the disease in real time. In this context, the analysis of circulating molecules in liquid biopsies can be useful to implement the information obtained by tissue biopsies. Tissue biopsies are very invasive, and for this reason, cannot be scheduled frequently. Moreover, deriving from a single tumor site, they do not recapitulate the tumor heterogeneity.

The interest on extracellular vesicles increased exponentially in the last decades since they are abundantly released by all the cellular types in biological fluids, and can shuttle bioactive molecules between cells, acting as important intercellular mediators. EVs can be analyzed as tumor biomarkers *per se* because their levels in liquid biopsies of patients are higher than healthy controls, and the relative abundance of EVs can change during the course of the disease, allowing to monitor the progression of pathological conditions. Likewise, their content in protein and nucleic acids, reflecting the cellular status, can be investigated for the presence of specific biomarkers or mutations. For all these reasons, EVs represent an ideal target to analyze in liquid biopsies of tumor patients, also because they are released from multiple sites of the tumor, mirroring the tumoral complexity.

The major obstacles to the application of EVs in the clinical practice are the lacks of protocol standardization and, as a consequence, reproducibility of the results (De Rubis, Rajeev Krishnan, & Bebawy, 2019). In the last decade, multiple technological tools have been developed to implement the isolation and analysis of EVs, but they are mostly impractical for daily clinical utilization. The majority of the available techniques is laborious, requires expensive equipment and, when time-effective, as in case of precipitation with polymeric agents, results in inadequate quality preparations.

At the beginning of my Ph.D. studies, I applied the gold standard procedures (i.e., ultracentrifugation techniques) to isolate extracellular vesicles but, in the light of a clinical application, it was soon clear to us that we needed more efficient assays for all the reason previously stated. Therefore, by exploiting the physical properties of EVs, we defined a novel procedure to isolate EVs, where nickel-charged beads are exploited to rapidly capture heterogeneous EVs (50–700 nm) directly from biological fluids, by affinity with the negative charge (zeta potential) of the EV membrane. Extracellular vesicles then are eluted by anion exchange with a combination of chelating agents in a physiological solution, and the concentration of citric acid and EDTA were adjusted in order to avoid a cytotoxic effect. Optimizing the composition of the elution buffer was of utmost priority for targeting EVs in solution. A common disadvantage of several methods is, in fact, the co-precipitation of other particles along with EVs. Especially proteins represent a persistent contaminant of

extracellular vesicles preparations. We evaluated the specificity of the buffer to target specifically EVs in physiological solutions, demonstrating that low concentrations of chelating agents are sufficient to elute EVs over proteins and nucleic acids. As a complementary approach, we demonstrated that the elution buffer could preferentially isolate EVs, even in a protein-enriched environment.

Previous works have already exploited the biophysical properties of the EV membrane. Other techniques such as charge-based precipitation and ion-exchange chromatography (AIEX) (Deregibus et al., 2016a; Heath et al., 2018) already took advantage of the negative charge of EVs to capture them. Although, in this case, the high concentration of salts required results in an increased ionic strength that would risk affecting the integrity of EVs. In this work we demonstrated that the integrity of heterogeneous EVs in solution is preserved, compared to ultracentrifuged samples, even in the presence of a high concentration of salts. In this context, isolating EVs under physiological conditions could represent an analytical advantage since the possibility of analyzing individual polydisperse particles, would limiting the bias in the results due to particle aggregations and creation of artifacts. Interestingly, we tested the stability of EVs isolated by Nickel Based over time, to assess the proper storage conditions, and we found out that NBI-EVs have a half-life of about 50 days at 4°C, with respect to 7 days for EVs obtained by ultracentrifugation. Here we hypothesized that the increased stability of NBI-EVs might be explained by the absence of external forces (i.e., high g forces in case of ultracentrifugation) that would destabilize the integrity of EV membranes and as a consequence, impact on the vesicle stability.

The presence of microvesicles and exosomes in NBI preparations was tested by immune blotting. We detected the expression of two cytosolic proteins and one tetraspanin, commonly enriched in exosomes and microvesicles, confirming the presence of these two types of vesicles in the mixture of heterogeneous particles isolated from U87 by NBI. Conversely, GM130, a marker of Golgi apparatus and therefore a negative EV marker, was not expressed. To further analyze the nature of NBI-EVs, we visualized U87-EVs by transmission electron microscopy. We could appraise the corporeity of EVs isolated by NBI in term of heterogeneity and reduced aggregation. By TEM analysis, we also detected an enrichment of EVs with a diameter of 80–120 nm, lower, compared to our previous analysis. We, therefore, interrogated the literature and learned that this phenomenon is a technical artifact occurring during the sample preparation, resulting in shrinkage in size (van Niel et al., 2018).

Profitably, NBI assay takes place in less than one hour, and we demonstrated that it is a scalable method, which is a desirable feature also for the use of EVs as therapeutics, requiring large volumes

of starting material. Furthermore, NBI is a cost-effective and easy procedure, which is a valuable quality for clinical utilization, not requiring expensive equipment and highly trained human resources.

I illustrated the advantages of NBI but every procedure presents its drawbacks. In case of *in vitro* assays, the presence of chelating agents in the NBI elution buffer might, in fact, sequestrate co-factors in culture media, risking to affect the cellular homeostasis. Furthermore, NBI allows to isolate a pool of heterogeneous particles, mostly comprised between 50 and 800 nm, and the study of subpopulations of vesicles based on their dimensions would require further separation passages, prolonging the process timeline. Finally, it would be interesting to test on a large scale the performance of NBI in comparison to other techniques based on anion exchange chromatography, to assess the relative benefits of choosing a Nickel-based approach because of the lower osmotic stresses on EVs.

To assess the accuracy of NBI for both research and clinical applications, we assessed its reproducibility of a panel of cell lines and on the plasma of healthy individuals. We observed an equal distribution of isolated EVs in terms of size and concentration in all the cells, made an exception for SH-SY5Y, a neuroblastoma cell line which released a lower number of EVs. We observed a similar trend in the distribution of large and small vesicles in plasma samples, and the presence of two distinct populations of EVs, with a prevalence of small vesicles over large ones in ratio 55:1. NBI is, therefore proposed as a reliable tool for liquid biopsy studies.

Notably, plasma was analyzed after platelet depletion. Generally, in the light of biomarker discovery, it is advisable to perform the platelet-depletion in plasma, prior EV isolation, to avoid confounding factors in the results (Max et al., 2018; Tao, Guo, & Zhang, 2017; Witwer et al., 2013). Platelets are abundant in the plasma fraction and share a dimensional similarity with EVs. Moreover, they release a massive amount of EVs, accounting for more than 50% of blood EVs, which several studies found containing RNA, bearing a potential therapeutic significance. Consistently, we observed a strong correlation between the number of plasmatic large vesicles and the platelet counts and, by droplet digital PCR, we detected a high number of GAPDH copies in RNA derived from plasmatic EVs of healthy volunteers, which was most probably encapsulated in platelet EVs, since platelets are indicated as major producers of GAPDH in the circulation (McDonald et al., 1993).

As I stressed in the introduction, the uniqueness of extracellular vesicles as promising diagnostic lies in the fact that they can reflect the cellular status in real time. Being released by potentially all the cells, they are also instrumental in catching the tumor heterogeneity. In this context, we demonstrated that NBI presents many technical advantages, which makes it valuable for a high-throughput study of EVs directed to research and clinical utilization. From a diagnostic perspective,

an excellent analytical tool should exploit the potential of EVs in reporting information derived from a specific subset of cells. A general pattern indicated that the correlation between polydisperse vesicles and the cell of origin is quite hard to depict since EVs can express multiple antigens on the membrane surface. We demonstrated that through NBI, it is possible to discriminate and enrich in EV lineages from a liquid biopsy. An approach of combined immunocapture proved to be helpful to characterize populations of EVs which were positive to hematopoietic markers such as CD41 (a marker of platelets) and CD235a (a marker of erythrocytes) or endothelial cell markers as in case of CAM proteins. In this manner, heterogeneous particles can be sorted based on a common parental origin. The most significant results were obtained using EVs derived from cell lines (i.e., SK-MEL-28), as spike-in in human plasma. Using well-characterized cells for the marker expression, as CD146 in case of SK-MEL-28 cells, it is possible to sort out specific EV lineages from a heterogeneous pool, to enrich in tumor-derived EVs. In light of this approach, we illustrated how the versatility of NBI could serve to implement the specificity of amplified luminescent proximity homogeneous assay (alpha). Following this promising indication, for the first time, we tested the specificity of NBI-Alpha in a retrospective study, on EVs released in plasma of prostate cancer patients.

Importantly, the quality of NBI-EVs in Alpha Screen Assay allowed detecting picomolar concentrations of prostate cancer specific membrane antigen (PSMA) on the surface of a small number of EVs. Notably, we compared the performance of the assays with two other highly sensitive methods, Exoscreen and ELISA, which are used as detection and biomolecular characterization of EVs. We showed that the specificity of NBI made possible the detection of a picomolar concentration of prostate cancer specific membrane antigen (PSMA) in the EVs derived from patients and, most importantly, the difference respect to controls was of about one order of magnitude. We reasoned that this level of sensitivity is attainable because NBI-EVs are less aggregated in solution, allowing us to exploit NBI-isolated EVs as individual particles in assays to detect cancer biomarkers. This result is of utmost importance if we consider that in this manner, it would be possible to perform a rapid biomarker detection on a limited number of EVs.

Moreover, NBI is advantageous because we reached this level of sensitivity in a bulk assay, in a faster way compared to single EV techniques. In this way, we can exploit the information carried by NBI in a high throughput manner. To understand the advantage of EVs in this context, we should considerate that in order to isolate 1- 10 circulating tumor cells we need at least 1 mL of blood (Miller, Doyle, & Terstappen, 2010).

Similarly, we took advantage of the versatility of NBI to employ EVs in an improved version of droplet digital PCR, a method already in use in many clinical laboratories, to investigate cell-free DNA

content in the circulation of cancer patients. In the optimized version of NBI-ddPCR, EVs are directly encapsulated into the oil droplets, avoiding the RNA extraction. A simplified protocol allows reducing the technical errors and eventual loss due to a prolonged sample manipulation. Furthermore, we maximize the sensitivity of the assay, starting from a known number of vesicles, taking advantage of the preserved integrity of NBI-EVs.

Using NBI-ddPCR for liquid biopsy analyses, we showed the detection of biomarkers in plasmatic EVs isolated from a cohort of colon cancer patients. We focused on KRAS and BRAF, two genes clinically relevant for their prognostic role in many types of solid tumors. In detail, we demonstrated the advantage of NBI in detecting mutated BRAF (V600E) and KRAS (G12C e G12D) transcripts in plasmatic EVs derived from patients upon immunodepletion of hematopoietic markers. Interestingly, some cases showed mutations only in the secreted EVs, suggesting that NBI-ddPCR could serve to deduce the presence of specific cell subpopulations, complementing the diagnostic information of tissue biopsies. These results were further confirmed by subsequent analysis on tissue biopsies, and the cases detected by NBI-ddPCR led to re-consider the mutational status in at least 10% of the patients analyzed. We have therefore shown that, through liquid biopsy, it is possible to identify fractions of secreted EVs carrying tumor biomarkers with unprecedented sensitivity and accuracy, opening new perspectives to reveal the extraordinary potential of the EVs towards clinical molecular diagnostics.

Importantly, the choice of plasma derived from patients enrolled in prospective studies generally represents a better choice for biomarker validation or discovery in liquid biopsies, to better understand whether molecules may have a predictive or prognostic significance along the disease course. Although, in retrospective studies, the possibility to obtain rapid information on patients whose molecular profile of the disease has been previously assessed by tissue sample analysis, could offer some advantages, in terms of time and information on the disease outcome. In our case, for instance, we needed to test the performance of our newly-designed assay to detect, in EVs, the expression of cancer biomarkers already employed in the clinical practice, with a high level of sensitivity and specificity to discriminate cancer patients from healthy individuals. To this purpose, the possibility to compare our technique with other sensitive methods, on samples whose signature of the disease had been already documented, represented an advantage. We find here that NBI is a reliable and sensitive tool to detect tumor biomarkers associated to EVs and discriminate between cancer patients and healthy subjects.

Notably, the immunoprecipitation combined with NBI-ddPCR was useful also to validate the nature of the analyzed extracellular RNA. Several studies pointed out that extracellular RNA can also be associated with lipoproteins, highly abundant in biological fluids, especially in plasma. To answer

this point, we demonstrated that wild type BRAF and GAPDH transcripts were still detectable in samples immunodepleted of particles positive to markers of HDL and LDL, corroborating the robustness of NBI approaches to target preferentially EVs.

In line with this approach, we moved towards an exploratory analysis of glioblastoma stem cells. Glioblastoma is a malignant tumor with a poor prognosis when diagnosed. The current therapies proved to fail in fighting this type of cancer. The standard of care relies massively on the surgical resection of the tumoral area and temozolomide, the only effective chemotherapy, has more side effects than benefits. For all these reasons, there is an urgent need for biomarkers associated with liquid biopsies, allowing to monitor the progression of disease in a less invasive way than tissue biopsies.

Most importantly, finding biomarkers to early detect glioblastoma multiforme, would constitute a giant step ahead in the management of glioblastoma patients, improving their chance of survival. In a recent report, Wei and colleagues analyzed the content in extracellular RNA of glioma stem cells, providing useful indications for further studies on biomarker discovery. Interestingly, they found enrichment in Y-RNA and tRNA fragments in extracellular RNA associated with EVs and RNPs (Wei et al., 2017b).

Given the expertise of my laboratory on the study of Y-RNAs as translational regulators, we wondered about its functional role in EVs, and their potential as biomarkers in glioblastoma. We started investigating the role of Y-RNAs in a rare subset of glioblastoma cells, with stem-like characteristics, showing enrichment in Y-RNAs compared to hiPSCs. This result encouraged us to verify the Y-RNAs expression levels also in the cells of origins since a reliable biomarker needs to reflect the status of the cell of origin, and we could demonstrate that EV-RNAs mirrored the cellular transcriptome. Encouraged by these data, we moved our attention towards a possible functional role of Y-RNAs in glioblastoma, to influence the fate of the neuronal differentiation, as it was shown previously in our lab. We demonstrated that Y-RNAs were enriched in stem-like glioblastoma cells rather than in astrocytes derived from by differentiation of COMI, suggesting a possible role as markers associated with stemness features in glioblastoma stem cells. Finally, preliminary results indicated an effect on translational modulation of astrocytes, mediated by EVs derived from stem-like GBM cells. We reasoned that this effect could be mediated by Y-RNA, which we found enriched in EVs derived from COMI, although this evidence is still at a preliminary stage. To demonstrate our hypothesis, we are currently working on the knock-out of Y-3 RNAs in COMI, to isolate EVs from these cells and understand whether the increased astrocytic translation could be mediated by COMI EVs enclosed Y-RNAs. In parallel, it would also be interesting to investigate the interactions of EVs derived from glioblastoma stem cells with RNA binding proteins, to understand their role on the

translational control. Later, we will perform these experiments on other glioblastoma stem cell lines to assess the robustness of these observations.

ONGOING EXPERIMENTS AND FUTURE DIRECTIONS

The work illustrated in this thesis is part of a bigger project, whose final goal is to discover novel biomarkers with a diagnostic, prognostic and predictive value in liquid biopsies, using non-invasive tests based on molecular analysis of circulating molecules. To this end, extracellular RNA and cell-free tumor DNA, derived from cancer patients' biofluids, would be interrogated for molecular alterations using next-generation sequencing tools.

As part of a collaboration with the Laboratory of Computational Oncology, in this project, my work focused on the analysis of extracellular vesicles. Nickel-based isolation proved so far to be a helpful tool to exploit the potential of EV for a clinical utilization, detecting biomarkers able to with extraordinary sensitivity.

After the optimization of the novel method, we had the opportunity to employ NBI in a longitudinal study, to identify biomarkers to predict response to chemotherapy. In particular, we focused our attention on a cohort of breast cancer patients, eligible for adjuvant treatment, having a tumoral mass greater than 1 cm (Chew et al., 2009), to identify markers which would help discriminate the patients who would get more benefits from these treatments. Patients' whole blood has been collected in three different time points: the first one at the diagnosis and before starting the adjuvant chemotherapy, then at the end of the therapy, generally after six months, and lastly after surgical asportation of the tumor mass.

Since 2017 we collected whole blood from sixty-four patients. We separated plasma, from which we isolated EVs by NBI, and isolated peripheral blood mononuclear cells (PBMCs). Then we focused on the RNA associated with EVs in order to investigate the presence of molecular alterations and understand whether they may have a diagnostic value.
In detail, we quantified EVs isolated by plasma of breast cancer patients by TRPS, to analyze the differences of EV distribution along with the therapeutic management of patients.
Subsequently, we analyzed RNA extracted by EVs derived from plasma of healthy donors and cell lines, to set up the most efficient condition for the detection of molecular alterations in plasma of patients. Multiple strategies are described in the literature for sequencing the RNA enclosed in EVs. The limited yield in RNA and the lack of standardized procedures require a targeted approach in order to maximize the diagnostic potential of EVs. To optimize the analysis of the expression levels of molecular markers by RNA sequencing derived from extracellular vesicles, we designed an experiment to define the ideal conditions for the sequencing of EV-RNA derived from the plasma of patients collected in the three time points. In this case, we added a known number of EVs deriving

from PC-3 and VCaP (prostate cancer cell lines) to a pool of EVs derived from plasma from two healthy donors. Later we extracted RNA from EVs to test the limits of sequencing analysis in the detection of translocations or mutations described in the two lines in a matrix (plasma of healthy donors) lacking these characteristics. To this end, we took advantage of the work done in collaboration with the Laboratory of Experimental Cancer Biology (Prof. Marina Mione) and the Laboratory of Transcriptional neurobiology (Prof. Manuela Basso) on the optimization of protocols to extract RNA from EVs, as described in Fig.8. As suggested from previous sequencing experiments, the most performant RNA extraction procedure started with the guanidine thiocyanate extraction, followed by purification on Norgen columns (Single Cells Kit) and DNAse treatment to avoid DNA contamination. Given the low amount of RNA as a template and the peculiar experimental design, we compared two different kits for libraries preparation. The choice of the kit, in fact, represents an essential step to determine the experimental outcome of a sequencing experiment by Next Generation Sequencing. In particular, we compared two kits SMARTer® Stranded RNA-Seq Kit (Clontech) and QIAseq® miRNA Library Kit. The achievement of an adequate level of mapping (coverage) of sequences on the reference genome, indicated the SMARTer® smRNA-Seq Kit (Clontech) kit as the best kit for preparing libraries using RNA isolated from vesicles as a template. Using this optimized pipeline, it is therefore possible to analyze the EVs RNA of patients in the best manner for biomarker discovery.

Summarizing the work done so far, I believe that these results could bring a relevant contribution to the growing field of EVs for the rational establishment of EV-based liquid biopsy studies for the future benefit of clinical diagnostics. Undoubtedly, more validation studies on larger cohorts of patients are needed to better define the performance and reproducibility of this approach on a large scale. Moreover, the possibility to ultra-sensitively detect RNA and protein associated with specific EV lineages could allow more in-depth characterization of tumor heterogeneity and its evolution during therapy, with a potential impact for the clinical management of patients.

EXPERIMENTAL PROCEDURES

CELL CULTURES

Glioblastoma cells U87-MG (ATCC® HTB-14™); breast adenocarcinoma cell lines MCF7 (ICLC; HTL95021) and MDA-MB-231 (ICLC; HTL99004), neuroblastoma SH-SY5Y (ATCC®CRL-2266™), prostate adenocarcinoma PC-3 (ATCC® CRL-1435™), and melanoma SK-MEL-28 (ATCC® HTB-72™) cells were grown in DMEM, except for PC-3 cell line that was cultured in RPMI 1640 Medium. Media were supplemented with 10% Fetal Bovine Serum (FBS), 2 mM L-glutamine, and 100 U/ml penicillin + 100 µg/ml streptomycin (all from Life Technologies, Carlsbad, CA, USA) to obtain a complete medium. Human glioblastoma stem cells COMI and 030616 were kindly donated from Antonio Daga (Azienda Ospedaliera Universitaria San Martino di Genova, Italy), and Rossella Galli (H. S. Raffaele, Milan, Italy), respectively. Glioblastoma initiating cancer stem cells (GCS) were cultured in DMEM/F-12 and Neurobasal media in 1:1 ratio (Thermo Fisher Scientific,), supplemented with GlutaMAX (2 mM; Thermo Fisher Scientific), B27 supplement (1%; Thermo Fisher Scientific), Penicillin G (100 U/mL; Sigma Aldrich), recombinant human fibroblast growth factor-2 (bFGF) (10 ng/mL; R&D Systems), recombinant human epidermal growth factor (EGF) (20 ng/mL; R&D Systems) and heparin (2 µg/mL; Sigma Aldrich) at kept at 37°C, 5% CO2. GCS were grown either as spheres in suspension or in adhesion on laminin-coated flasks, where they maintain intact self-renewal capacity (Pollard et al., 2009). The Gibco Human Episomal iPSC Line (Cat number: A18945, Thermo Fisher Scientific), was a kind gift of Prof. Conti (CIBIO, Trento) and cells were cultured in Essential 8™ Medium on Geltrex™ matrix-coated culture vessels (Thermo Fisher Scientific); cells were passaged using 0.5 mM EDTA prepared in Dulbecco's Phosphate-Buffered Saline (DPBS) without calcium or magnesium (Cat. no. 14190). For COMI differentiation, cells were grown on laminin-coated plates in the above media without growth factors and with the addition of 10% FBS (Thermo Fisher Scientific) for two weeks. Expression levels of stemness (Sox2 and Nestin) and differentiation (GFAP) markers were assessed by immunofluorescence. Generally, to obtain extracellular vesicles-containing media, cells were initially grown in the complete medium until reaching 75% confluence (usually 48 hours); then, after two gentle washes with PBS, cells were incubated with serum-free medium for 24 hours prior collection. Serum depletion is needed since it has been reported that the fetal bovine serum contains vesicles itself, therefore, it could affect the results quantitatively and qualitatively (Shelke, Lässer, Gho, & Lötvall, 2014). Alternatively, in case of GCS, since these cells are already cultured without serum, cells' confluence was monitored, and media were collected when cells reached 85% confluence, usually five days after seeding in case of cells growing as neurospheres and three days after seeding when cultured on laminin. Cells were plated in different plastic formats according to the experiments to be performed, but the density of them was kept constant at $3.2 \pm 0.2 * 10^4/cm^2$ otherwise differently stated in the figure legends. Before

starting the NBI procedure, collected media were centrifuged at 2800 *xg* for 10 minutes and carefully transferred to new tubes. For the experiments in Fig 15, the depleted FBS condition (dFBS) refers to NBI performed in media containing 100K ultracentrifuged FBS at a final concentration of 10%. These media have been diluted 1:10 with PBS to reduce the viscosity of the solution. For cell density experiments in Fig 19, U-87-MG, MDA-MB-231, SH-SY5Y, MCF7 and PC-3 cell lines were plated in triplicates in 6-well plates with these numbers per well: $3.4x10^5$; $1.7x10^5$; $8.5x10^4$; $4.2x10^4$; $2.1x10^4$ and $1.0x10^4$. After 48 hr of incubation in complete medium, cells were washed twice with PBS and then incubated for 24 hr with the serum-free medium before starting with NBI protocol. In this case, after removing EVs-containing media, adherent cells were fixed with 4% paraformaldehyde, stained with Hoechst-33342 and washed with PBS for high content imaging analysis using Operetta instrument (Perkin Elmer). Images were acquired at 10X magnification, and 50 fields/well were analyzed by Harmony software. EVs were analyzed by TRPS using qNano (IZON Science).

ISOLATION OF EXTRACELLULAR VESICLES BY DIFFERENTIAL ULTRACENTRIFUGATION

To isolate EVs from the U87-MG cell line, cells were cultured in T150 flasks (CLS430823-50EA), and EVs were processed by differential ultracentrifugation according to the protocol by Di Vizio (Di Vizio et al., 2012) with minor modifications. Briefly, after 24 hours of incubation of cells with serum-free media, the media were collected in falcon tubes and centrifuged at 2,800 *xg* at 4°C to remove cell debris. Then, the supernatants were transferred to ultracentrifuge tubes (Polyallomer Quick-Seal centrifuge tubes 25×89 mm, Beckman Coulter) and centrifuged for 30 minutes at 4°C at 10,000 *xg* in an Optima XE-90 (Beckman Coulter) instrument with SW 32 Ti rotor. This step allowed to preferentially precipitate large vesicles, that were gently resuspended in filtered PBS. After that, according to Théry C. et al 2006, the recovered supernatants were filtered through a 0.22 µm filter (Sarstedt, Numbrecht, Germany) to remove no vesicular contaminants or vesicle aggregates and centrifuged at 100,000 *xg* for 70 minutes at 4°C to precipitate small vesicles. Pellets were resuspended in filtered PBS. EVs obtained from differential centrifugations were pooled and stored a -80°C or kept at 4°C to proceed with TRPS analyses.

FLOW CYTOMETRY ANALYSIS OF EXTRACELLULAR VESICLES

Extracellular vesicles obtained by differential ultracentrifugation or NBI were diluted in 0.22 µm filtered PBS, and background signal was set up on filtered PBS, and the light scattering threshold

level was adjusted to allow an event rate of ≤5 events per second. Light scattering detection was performed in log mode, the assigned voltages for FSC and SSC were 300 and 310 volts, respectively, and the threshold was set at 200 for both signals. The acquisition was performed at a low flow rate, and samples were diluted correctly to avoid coincidence and swarm effects. Polystyrene bead standards of 1 and 10 µm (Invitrogen) were used to set gates for large vesicles. A number of 10,000 events was counted or at least 1-minute recording for each sample. Sample acquisition was performed on a FACS Canto flow cytometer (BD Biosciences) and data analysis using BD Diva software (BD Biosciences).

For the optimization of the staining conditions of large vesicle membranes in Fig.7, titration experiments were performed to determine optimal reagent amount. In detail, we compared Nile Red and Vybrant® CFDA-SE dyes. Nile Red is a lipophilic membrane dye, that stains intracellular lipid droplets; while carboxyfluorescein diacetate succinimidyl ester (Vybrant® CFDA SE Cell Tracer Kit, Thermo Fisher) is a cell-permeant dye, which passively diffuses into cells and emits fluorescence when its acetate groups are cleaved by intra-cellular esterases. A bulk of LVs, resuspended in filtered PBS, was incubated in CFDA-SE, and Nile Red solutions for 30 minutes in the dark, at room temperature in case of Nile Red and 37°C in case of CFDA-SE. Any unbound dye was removed after samples were centrifuged for 30 minutes at 10000xg. LVs were resuspended in 500 µL filtered PBS and sample acquisition was performed as previously described on a FACS Canto flow cytometer (BD Biosciences).

NICKEL-BASED ISOLATION (NBI) OF EXTRACELLULAR VESICLES

Commercial agarose beads of 34 µm size (GE Healthcare, 17-5268-01, 25 mL) were transferred to a 50 mL tube and centrifuged at 350 *xg* for 1 minute at room temperature, in order to remove their preserving solution. The positive charge of beads was neutralized washing the beads once with 1:1 bead volume of Stripping buffer (PBS 1X + 50 mM NaCl + 50 mM EDTA pH 8.0), and centrifuged at 350*xg* for 2 minutes. At this point beads were re-charged adding 1:1 bead volume of 190 mM of $NiSO_4$ (Sigma, 656895) in 0,22 µm-filtered PBS 1X, obtaining a suspension of 20 mg/mL nickel charged beads. A residual number of cations was removed by washing the beads twice with 1:1 bead volume of 0,22 µm-filtered PBS 1X and centrifuging them at 350*xg* for 2 minutes. After functionalization, NBI-beads can be stored at 4 °C for up to 1 month. The capture of EVs, entirely performed at room temperature, has been optimized using 20 µL of beads from the prepared suspension of 20 mg/mL nickel charged beads, per each mL of cell supernatant, serum, plasma or any other biological fluid. Briefly, after a centrifugation at 2800 *xg* for 10 minutes to get rid of cellular debris, beads were gently poured as drops on the upper surface of the EV-containing medium and the solution was incubated for 30 minutes on a tube rotator, in order to be well homogenized. After

that, tubes were gently centrifuged (600 *xg* for 2 minutes) and kept in a vertical position for 5 minutes, allowing beads to settle down by gravity, and the supernatant was carefully removed using a pipette, paying attention to not disturb the bead pellet. The elution buffer (referred in the text as 1X solution), was freshly prepared by diluting a Solution A (3.2 mM EDTA, ThermoFisher, UltraPure pH 8.0, 15575020) and a Solution B (10 mM NaCl, Sigma, 450006, 45 µM citric acid, Sigma, 251275), both concentrated 5X, in 0.22 µm-filtered PBS 1X. A 1:1 bead volume of elution buffer 1X was added to the bead pellet, and the mixture was transferred to a 1.5/2 mL tube. EVs were eluted during a 15-minute incubation at 28°C at 600*xg,* in orbital shaking to keep the beads in suspension, allowing a competitive dissociation of EVs from beads and their release in solution at physiological pH (7.4). After the incubation, beads were pelleted at 350 *xg* for 2 minutes and the EV-containing supernatant was carefully transferred to a new labelled 1.5 mL tube.

TRANSMISSION ELECTRON MICROSCOPY ANALYSIS

The vesicles were visualized using a conventional transmission electron microscope (TEM). Briefly, a 5 µl aliquot of a purified sample was fixed in elution buffer with 2.5% formaldehyde and applied to 300-square mesh copper-nickel grids coated with a thin carbon film (Agar Scientific). The grids were subsequently negatively stained with 1% buffered uranyl acetate, at pH 4.5, and observed using a TEM FEI Tecnai G2 Spirit microscope operating at 100 kV and equipped with an Olympus Morada side-mount 2Kx4K charge-coupled device camera (magnification used: 20500x and 87000x).

CHARACTERIZATION OF EXTRACELLULAR VESICLES BY TUNABLE RESISTIVE PULSE SENSING

Size and concentration of EVs were characterized by TRPS using qNano (IZON Science). An average of 500 particles was counted for each sample, except for experiments performed in 6-well plates, or in samples where the particle rate was below 100 particle/min, in which at least 2 minutes recording time was used. NP200 (A40948, A43545, A43667, A43667), NP400 (A43592, A44117, A44116), NP800 (A40542, A36164, A40548, A44118) and N1000 (A40572) nanopores, stretched between 45.5–47 mm were used. Voltage was set in between 0.12–0.68 to achieve and maintain a stable current in the range of 95–130 nA, noise below 7-12 pA and particle count rate linear. The calibration beads CPC100B (Batch ID: B8748N), CPC200B (Batch ID: B6481M), CPC500E (Batch ID: 659543B), CPC800E (Batch ID: 634561B) and CPC1000F (Batch ID: 669582B) with mean diameters of 114 nm, 210 nm, 500 nm, 710 nm and 940 nm, respectively, were from IZON Science. All the qNANO data were recorded and analyzed by IZON Control Suite v.3.

PROTEIN COMPETITIVE ASSAY

The specificity of the elution buffer for EVs has been challenged by a competitive assay in which 10 mL of medium containing EVs deriving from U87 was supplemented with 30 µg/ml of DH5α *E. coli* crude extract and with 15 µg/ml of purified histidine-tagged recombinant proteins (T7 RNA pol, 110 kDa; HuR, 36 kDa; YTH, 23 kDa). Briefly, DH5α cells were grown in LB medium until they reached an OD_{600} of 0.5 and were harvested by centrifugation at 6,000 *xg* for 5 minutes. Pellet was resuspended in 3 ml of DMEM medium + 1 µg/ml lysozyme and sonicated at 4°C in a water bath for seven cycles (40 amplitude, 7 sec *on*, 10 sec *off*). The lysate was clarified by centrifugation at 13,000 *xg* for 20 minutes and then filtered with 0.2 µm membrane disposals before being spiked to the EV-containing medium. Histidine-tagged recombinant T7 RNA polymerase was kindly provided by Dr. S. Mansy's lab (CIBIO, University of Trento); recombinant HuR[69] and YTH[70] proteins produced and purified as previously described.

NBI was performed with incubation times and reagents already described, except for the gradient of elution solutions as indicated in Fig.13. Protein samples were quantified using BCA and Bradford assays according to the manufacturer's instructions. An equal volume of solutions containing eluted EVs was loaded on 12% SDS-PAGE for subsequent Sypro Ruby staining or western blotting using a 1:1000 dilution of a primary anti-histidine antibody (Abcam, ab1187). Number and size of recovered particles were analyzed by TRPS, using NP800, NP400, and NP200 nanopores to cover all the vesicles subpopulations.

IMMUNOPRECIPITATION AND IMMUNOBLOTTING EXPERIMENTS

Immunodepletion experiments on plasmatic NBI-EVs were performed using biotinylated anti-CD235a (130-100-271) and anti-CD41a (130-105-608) from Miltenyl Biotec, anti-CD166 (sc-74558), anti-CD146 (sc-18837), anti-CD45 (sc-1187) from Santa Cruz Biotechnology, anti-Apo B100 (ab7616) and anti-Apo-A1 (ab7613) from Abcam, and streptavidin (11205D) or protein-G (10003D) Dynabeads from Thermo Fisher Scientific. The number of EVs in the supernatants after beads precipitation was measured by qNANO and normalized to the number of particles in the counterpart control samples with an equivalent amount of biotin (Sigma, B4501).

For western blotting experiments, the protein concentrations of U87-MG, SK-MEL28, HeLa, and Jurkat cell lines were quantified with Pierce™ BCA Protein Assay Kit (Thermo Fisher Scientific, cat. 23227). Thereafter, 15 µg of whole cell lysate and/or the lysate of EVs isolated from the media of 3 T75 flasks per each cell line, were separated by a pre-cast gradient SDS-PAGE (Bolt™ 4–12% Bis-Tris Plus Gels, 12-well, Invitrogen) and transferred to a polyvinylidene difluoride membrane

(Amersham Hybond P 0.2 μm PVDF) overnight. After blocking with 5% nonfat milk in TBS-T (10 mM Tris, pH 8.0, 150 mM NaCl, 0.1% Tween 20) for 60 minutes, the membrane was incubated in 1% milk TBS-T with antibodies against CD63 (Abcam, 1:1000), Flotillin-1 (BD Biosciences,1:1000), Alix (Abcam, 1:1000), GM130 (Abcam,1:1000) or anti-histidine antibody (Abcam, 1:1000) at 4 °C overnight. Membranes were washed three times for 5 minutes and incubated with horseradish peroxidase-conjugated anti-goat, anti-rabbit or anti-mouse secondary antibodies for 1–2 h. Blotted membranes were washed with TBS-T three times, and the immunoblot signal was revealed using a chemiluminescent ECL Select detection reagent (GE Healthcare Amersham, UK).

PREPARATION OF EXOSOME-LIKE VESICLES

The lipid composition of exosome-like vesicles was: 20% mol egg phosphatidylcholine, 10% mol egg phosphatidylethanolamine, 15% mol dioleoylphosphatidylserine, 15% mol egg sphingomyelin, 40% mol cholesterol (adapted from Llorente et al., 2013; Haraszti et al., 2016). Lipid films were formed by removing the organic solvent (i.e., chloroform) from a lipid solution by rotary evaporation and vacuum drying for at least one hour. Lipids at a final concentration of 1 mg/mL, were swollen in DPBS and vortexed vigorously to give multilamellar liposomes, which were further exposed to 6 cycles of freezing and thawing. Exosome-like liposomes were prepared by extruding a suspension of multilamellar liposomes with a two-syringes extruder (LiposoFast Basic Unit, Avestin Inc.). Thirty-one passages were performed through two stacked polycarbonate filters (Millipore) with pores of different average diameters to obtain differently sized vesicles[72], then measured by photon correlation spectroscopy with a Zeta Sizer instrument (Nano-ZS, Malvern Instruments).

COLLECTION AND PROCESSING OF BLOOD SAMPLES

Plasma samples derived from patients with metastatic colon cancer were provided by the IRST Cancer Center (Meldola, Italy). All patients gave informed consent before blood sampling, approved by the Local Ethics Committee. Patients' tumors were characterized for BRAF status by MassARRAY (Sequenom, San Diego, CA, USA) using the Myriapod Colon status (Diatech Pharmacogenetics, Jesi, Italy). Plasma was obtained from peripheral blood collected in EDTA-tubes, after centrifugation at 3000 rpm for 15 minutes, and stored at −80 °C until EV isolation.
Whole blood from healthy donors was collected at Meyer Children's University Hospital. Plasma samples were collected into commercially available anticoagulant-treated tubes EDTA-treated (lavender tops), serum samples in red-topped tubes. The venous blood in EDTA tube was shipped on cold packs from the hospital blood collection unit to the laboratory. Informed consent was obtained

from donors before the sample analysis. Plasma has been obtained by removing cells after centrifugation for 10 minutes at 2,000*xg* using a refrigerated (4°C) centrifuge (Eppendorf 5702 R, Milan, Italy). Serum samples have been obtained allowing the blood to clot by leaving it undisturbed at room temperature for 30 minutes. The clot has been removed by spin down at 2,000 *xg* using a refrigerated (4°C) centrifuge (Eppendorf 5702 R, Milan, Italy). Blood count was performed using a Sysmex XE-5000 hematology analyzer (Sysmex America, Mundelein, IL). The analytic procedure was conducted according to the manufacturer's instructions.
Blood from metastatic prostate cancer patients was obtained at Weill Cornell Medicine (WCM) after informed consent (IRB #1305013903). Whole blood (Streck Cell-Free DNA BCT) was centrifuged at 1,600xg for 10 minutes at 4°C within 3 hours after blood collection. The plasma layer was transferred to 2 mL microcentrifuge tubes and centrifuged at 16,000xg for 10 minutes at 4°C. The plasma was then collected and stored at -80°C. Complete blood counts (CBC) was performed in the WCM clinical lab and results obtained from chart review.

SURGICAL BIOPSIES ANALYSIS

Formalin-fixed and paraffin included (FFPE) patients' tumor samples, used for routinary molecular diagnostic, were selected for containing an area of at least 50% of tumor cells, based on hematoxylin and eosin staining. Tumor genomic DNA was extracted with QIAamp DNA Micro kit (QIAGEN, Hilden, Germany), following the manufacturer's protocol, and DNA quantity and quality were determined at Nanodrop (CELBIO, Milan, Italy). Pyrosequencing performed characterization of BRAF status with the anti-EGFR MoAb response® BRAF status assay (Diatech Pharmacogenetics, Jesi, Italy): 50 ng of starting FFPE genomic DNA were amplified, and reactions were run on the PyroMark Q96 ID system (QIAGEN), according to Diatech Pharmacogenetics protocol. For samples 7, 12, 13, 23, and 26, Qualitative detection of BRAF-V600E and KRAS-G12D/G12C mutations was repeated on 30 ng of tumor DNA, by using either the Easy®BRAF kit or the Easy®KRAS kit, on Corbett Rotor-Gene 6000 (QIAGEN), following manufacturer's instructions (Diatech Pharmacogenetics). The assay allows the detection of low percentages of a mutated allele by real-time amplification with sequence-specific probes: positivity for BRAF-V600E was considered over the internal BRAF control, as a delta Ct lover than 12.5 cycles, and setting the detection threshold on 0.04, according to the guidelines of Diatech Pharmacogenetics.

AMPLIFIED LUMINESCENT PROXIMITY HOMOGENEOUS ASSAY (AlphaScreen), ELISA AND EXOSCREEN

For NBI-Alpha, streptavidin-coated Donor beads recognize the antigen-specific biotinylated antibody while positively-charged nickel-chelate Acceptor beads interact with EVs and emit a fluorescent signal when in the proximity of excited Donor beads. Reactions were carried out in 384-Optiplate (Perkin Elmer) in a final volume of 20 µL. NBI-Alpha assay was optimized in PBS using 15 µg/mL of nickel-chelate AlphaLisa Acceptor beads and 10 µg/mL of streptavidin-Donor beads with serial dilutions of antibody to identify the maximum signal (hook point). The presence of surface markers was analyzed in dose-response with a serial dilution of EVs, previously characterized by TRPS. EVs were purified by NBI from the plasma of healthy donors or the serum-free medium of tumor cell lines. Alpha counts were revealed by Enspire instrument (Perkin Elmer) after 90 minutes of plate incubation in the dark at room temperature. We used a biotinylated antibody against human PSMA (Cusabio, CSB-PA018865LD01HU) and a recombinant His-tagged PSMA (Origene, NM_002786) for a standard curve quantification. In comparisons with other methods, the relative performances of different detection methods have been then evaluated, using anti-CD81 biotinylated antibody for plate-coating in the case of ELISA (coupled with anti-CD146 and HRP-conjugated secondary antibodies) or conjugation with Acceptor beads in the case of ExoScreen. The specific, background-subtracted signals were normalized to IgG signals of individual experiments.

RNA EXTRACTION

Total RNA was extracted using QIAzol reagent (QIAGEN) according to the manufacturer's instructions with several modifications. Briefly, NBI EVs were pelleted at 100000xg and the pellet was resuspended in 100 µl of QIAzol, vortexed and incubated for 5 minutes at room temperature. Samples were supplemented with 20 µl of chloroform, shaken vigorously for 15 sec and incubated at room temperature for 3 minutes. Phases were separated by centrifugation at 12,000 *xg* for 15 minutes at 4˚C, and the upper phase was recovered. After addition of 1 µl of glycogen (20 mg/ml) and 100 µl of isopropanol, RNA was precipitated overnight at -80˚C. After centrifugation at 12,000 *xg* for 10 minutes, RNA pellets were washed with 75% ethanol, centrifuged as above and resuspended in 10 µl RNase-free water. EV-RNA was quantified using the Bioanalyzer RNA 6000 Pico Kit (Agilent Technologies) following the manufacturer's instructions, while 1 µl of RNA extracted from cells was used for the quantification at NanoDrop™ Spectrophotometer. For the experiments described in Fig.8, Single Cell RNA Purification Kit (Norgen), miRCURY™ RNA Isolation Kit (Exiqon) and DNAse: Qiagen Rnase-Free Dnase (Qiagen) and TURBO DNase™ (ThermoFisher) were used according to the manufacturer's indications.

REVERSE TRANSCRIPTION

Reverse transcription was performed using miRCURY LNA Universal RT microRNA PCR, Universal cDNA Synthesis Kit II (Exiqon) following the manufacturer's instructions with the following reaction composition: 2.3 µl of 5X reaction buffer, 1.15 µl enzyme mix, 0.5 µl synthetic RNA spike-in and 7.5 µl of template total RNA for *GAPDH* and *BRAF* experiments on the C1000 Thermal Cycler (BioRad). To evaluate the expression of Y-RNAs in GCS derived EVs, RNA was treated with DNAse (Thermo Fisher) and incubated for 30 minutes at 37°C. Input EV-RNA of different cell lines was diluted before reverse transcription reaction, to obtain the same amount of cDNA to be used for quantitative PCR. Reverse transcription was performed with RevertAid First Strand cDNA Synthesis Kit (Thermo Fisher), according to manufacturer's protocol with the following reaction mix: 11 µL of DNAse treated RNA, 1 µL random primers, 4 µL of 5X reaction buffer, 2 µL of 10 mM dNTP Mix, 1 µL of RiboLock RNase Inhibitor and 1ul of RevertAid enzyme mix (200 U/µL) on a the C1000 Thermal Cycler (BioRad).

QUANTITATIVE POLYMERASE CHAIN REACTION (qPCR)

Quantitative real-time PCR was performed using KAPA SYBR® FAST Universal Kit (Roche), following the manufacturer's instructions on the CFX384 Real-Time System (BioRad). All the assays, except in case of the amplification of YRNAs in undifferentiated and differentiated COMI, were performed in triplicate in 3 independent experiments. Data were analysed using CFX Manager software (BioRad). Relative expression values of each target gene were normalized over a standard curve obtained from a gel-purified qPCR product of Hek cellular RNA. RNA has been quantified at NanoDrop™ Spectrophotometer, and a standard curve was built. The following primers were used at a 10 µM concentration: 5'-GGCTGGTCCGAAGGTAGTGA-3' and 5'-GCAGTAGTGAGAAGGGGGGA-3' for *human Y1;* 5'-CCGAGTGCAGTGGTGTTTAC-3' and 5'-AAGCAGTGGGAGTGGAGAA-3' for *human Y-3*; 5'-TCCGATGGTAGTGGGTTATCA-3' and 5'-AAAGCCAGTCAAATTTAGCAGT-3' for *human Y-4* and 5'-AGTTGGTCCGAGTGTTGTGG-3' and 5'AACAGCAAGCTAGTCAAGCG-3' for *human Y-5*.

DROPLET DIGITAL PCR

QX200TM Droplet Digital™ PCR System (BioRad) was used to quantify mRNA copies using EvaGreen chemistry. The following primers were used at 150 nM concentration: 5'-

CAACGAATTTGGCTACAGCA-3' and 5'-AGGGGTCTACATGGCAACTG-3' for *GAPDH*; 5'-GATTTTGGTCTAGCTACAGA and 5'-GGATTTTTATCTTGCATTC for *BRAF*; 5'-CCGAGTGCAGTGGTGTTTAC-3' and 5'-AAGCAGTGGGAGTGGAGAA-3' for *human Y-3*; 5'-AGTTGGTCCGAGTGTTGTGG-3' and 5'AACAGCAAGCTAGTCAAGCG-3' for *human Y-5*.
The standard protocol was performed using cDNA as an input sample, according to the manufacturer's protocol. The direct encapsulation of EVs into oil droplets has been performed using isolated EVs as input sample, EvaGreen master mix supplemented with 5 U/ml of WarmStart® RTX Reverse Transcriptase (NEB) and with 3 mM magnesium sulfate. The standard protocol of ddPCR included a starting 10 minutes step at 55°C followed by 5 minutes at 65°C. The procedure was optimized on a range of 10^2-10^6 polydisperse EVs to obtain at least 15,000 droplets in each assay.

CLICK-IT A-HA ASSAY

Newly synthesized proteins were measured using the Click-iT AHA Alexa Fluor Protein Synthesis HCS Assay (Life Technologies) according to the manufacturer's instructions. Click-iT® AHA is an amino acid analog of methionine containing an azido moiety. Similar to the radioactive 35S-methionine, Click-iT® AHA is fed to cultured cells and incorporated into proteins during active protein synthesis. Detection of the incorporated amino acid utilizes a chemoreceptive ligation or "click" reaction between an azide and an alkyne, where the azide modified protein is detected with the green-fluorescent Alexa Fluor® 488 alkynes. Briefly, EVs were isolated from COMI cells and COMI cultured in differentiated conditions. For the assay, COMI differentiated were plated at a density of 8000 and 10000 cells/plate. On the following day, cells were incubated with EVs derived from both cell lines for 24 hours in ratio 1:100. After 48 hours from the seeding, cells were washed, incubated with L-azidohomoalanine (AHA) 50 µM for 1h and fixed. When AHA is incorporated into cells, the modified protein can be detected through the fluorescence emitted from the binding with the green-fluorescent Alexa Fluor® 488 alkynes. Puromycin (100 µg/ml), a protein synthesis inhibitor, was used as a control to evaluate the efficiency of background incorporation of L-azidohomoalanine (AHA). Nuclei were stained with Hoechst dye. The fluorescent signals were analyzed by high content imaging with Operetta system (Perkin Elmer) by Harmony software (PerkinElmer).

STATISTICAL ANALYSIS

The data and the number of independent experiments are indicated in the relative figure legends. Anova, *t*-test, and Pearson r coefficient were calculated by GraphPad Prism Software v 7.1, and results were considered statistically significant when P value was <0.05 (*), <0.01 (**), <0.001 (***).

SCIENTIFIC PRODUCTION

- The main work described in the thesis has been published and reviewed as the following publications:

  Michela Notarangelo, Deborah Ferrara, Cristina Potrich, Lorenzo Lunelli, Lia Vanzetti, Alessandro Provenzani, Manuela Basso, Alessandro Quattrone, Vito G. D'Agostino*. **Rapid nickel-based isolation of extracellular vesicles from different biological fluids**. Under review. Bio-protocol 2019.

  Michela Notarangelo, Chiara Zucal, Angelika Modelska, Isabella Pesce, Giorgina Scarduelli, Cristina Potrich, Lorenzo Lunelli, Cecilia Pederzolli, Paola Pavan, Giancarlo la Marca, Luigi Pasini, Paola Ulivi, Himisha Beltran, Francesca Demichelis, Alessandro Provenzani, Alessandro Quattrone, Vito G. D'Agostino* **Ultrasensitive detection of cancer biomarkers by nickel-based isolation of polydisperse extracellular vesicles from blood.** Accepted: April 18, 2019. Published online: April 29, 2019. EBioMedicine, 2019. DOI: https://doi.org/10.1016/j.ebiom.2019.04.039

- The procedure "Nickel-based isolation (NBI)" has been filed for patenting:

  Vito Giuseppe D'Agostino, Alessandro Provenzani, Alessandro Quattrone**, Michela Notarangelo,** Chiara Zucal, Isabella Pesce. "**METHOD FOR ISOLATING EXTRACELLULAR VESICLES FROM BIOLOGICAL MATERIAL".** Patent n. P019950WO/2018.

- During my Ph.D. studies, I worked at a side project, which resulted in the following work, currently submitted to upper 1st quartile, high-impact factor journal.

  Angelika Modelska*, Denise Sighel*, **Michela Notarangelo,** Shintaro Aibara, Angela Re, Gianluca Ricci, Marianna Guida, Alessia Soldano, Valentina Adami, Mariachiara Buccarelli, Quintino Giorgio D'Alessandris, Stefano Giannetti, Simone Pacioni, Lucia Ricci-Vitiani, Joanna Rorbach, Roberto Pallini, Alexey Amunts, Ines Mancini, Alessandro Quattrone. **Suppressing glioblastoma stem cell growth by inhibition of mitochondrial translation.**

CONTRIBUTIONS

I contributed to the project since the beginning, starting from the optimization of all the techniques used in this research, until the most recent sequencing experiments (ongoing work). In detail, I performed the isolation of extracellular vesicles with different methods and analysis by Tunable Resistive Pulse Sensing. I processed the biological fluids of healthy donors and cancer patients for EV isolation. I characterized the content in protein and nucleic acids of EVs, using the described molecular assays. Finally, I co-wrote the manuscript related to Nickel-Based-Isolation.

All the experiments concerning extracellular vesicles have been performed in collaboration with my advisor, Dr. Vito D'Agostino. Importantly, Dr. Vito D'Agostino conceived the Nickel Based Isolation and supervised the experiments, together with my tutor Prof. Alessandro Quattrone, and I contributed to the experimental design and analysis of the data.

The optimization of protocols to extract RNA from EVs has been done in collaboration with the Laboratory of Experimental Cancer Biology (Prof. Marina Mione) and the Laboratory of Transcriptional neurobiology (Prof. Manuela Basso), while the sequencing workflow has been carried out by the Next Generation Sequencing Facility (CIBIO).

The experiments involving the Alpha Screen assay have been entirely performed by Dr. Vito D'Agostino.

The liposome preparation and Dynamic Light Scattering measurements were performed by Dr. Cristina Potrich and Dr. Lorenzo Lunelli (Fondazione Bruno Kessler).

The analysis of mutational status on genomic DNA extracted by tissue biopsies of colon cancer patients has been performed by Dr. Luigi Pasini (Istituto Scientifico Romagnolo per lo Studio e la Cura dei Tumori, Meldola).

Quantitative real-time PCR experiments have been performed in collaboration with Dr. Federica Alessandrini (CIBIO), while Dr. Chiara Zucal (CIBIO) helped with cell cultures for experiments regarding the integrity, stability and dynamic release of EVs isolated by NBI.

The analysis by Transmission Electron Microscopy of U87-MG has been carried out by Dr. Giorgina Scarduelli of Imaging facility (CIBIO) with the help of facility members Dr. Ilaria Ferlenghi and Fabiola Giusti at GlaxoSmithKline Vaccines in Siena.

The technical optimizations to study extracellular vesicles by flow cytometry have been accomplished with the assistance of Dr. Isabella Pesce, manager of Cell Analysis and Separation Facility (CIBIO).

ACKNOWLEDGMENTS

This Ph.D. thesis represents the work of almost four years, during which I had the opportunity to work on a very innovative project, oriented towards a translational clinical application. During this period, I had the opportunity to interact with many great researchers from which I tried to learn as much as possible, and I would like to emphasize in this last chapter how important they have been for me.

First of all, my sincere thanks go to my tutor Prof. Alessandro Quattrone, for allowing me to work on this project, for inspiring me with his hard work and passion for science, for encouraging my research, and of course for his essential advice.
I acknowledge my advisor Dr. Vito D'Agostino. First of all, for his brilliant idea of NBI, that upgraded my Ph.D. project, secondly for his guidance during all these years that helped me in all the time of this research, and for the stimulating discussions which have allowed me to grow as a researcher.
I have to express my gratitude to all our many internal and external collaborators for believing in this work; your contribution has been valuable.

Special thanks to all the past and present members of the great LTG group I had the pleasure to work with during these years. Thank you all for the scientific discussions and fun times!
A special acknowledgment to Chiara Zucal and Federica Alessandrini for the help in the lab and Alessia Soldano for proof-reading this manuscript and the interesting scientific discussions.
I cannot forget to acknowledge the staff scientists of the CIBIO facilities that helped me with some experiments.

These Ph.D. years have not always been easy, but the support of my family and fun moments with some great colleagues as Isabelle Bonomo and Denise Sighel, made the Ph.D. life very pleasant.
In particular, I enormously thank my dear family, whose support was essential during these years: a massive thank to my parents and my brother Francesco for really everything, you are my daily life inspiration and strength. Many thanks to my best friends forever Francesca (Pic), Jamaica (Cat), and Paola for encouraging me to follow my passions and achieve my goals, despite the geographical distances. I thank my boyfriend Duhan, one of the strongest persons I met so far, for all the support, stimulating discussions, and because he always encourages me to improve myself and never give up.

REFERENCES

Aatonen, M. T., Ohman, T., Nyman, T. A., Laitinen, S., Grönholm, M., & Siljander, P. R.-M. (2014). Isolation and characterization of platelet-derived extracellular vesicles. *Journal of Extracellular Vesicles*, *3*. https://doi.org/10.3402/jev.v3.24692

Abd Elmageed, Z. Y., Yang, Y., Thomas, R., Ranjan, M., Mondal, D., Moroz, K., … Abdel-Mageed, A. B. (2014). Neoplastic Reprogramming of Patient-Derived Adipose Stem Cells by Prostate Cancer Cell-Associated Exosomes. *STEM CELLS*, *32*(4), 983–997. https://doi.org/10.1002/stem.1619

Abels, E. R., & Breakefield, X. O. (2016). Introduction to Extracellular Vesicles: Biogenesis, RNA Cargo Selection, Content, Release, and Uptake. *Cellular and Molecular Neurobiology*, *36*(3), 301–312. https://doi.org/10.1007/s10571-016-0366-z

Ainsztein, A. M., Brooks, P. J., Dugan, V. G., Ganguly, A., Guo, M., Howcroft, T. K., … Venkatachalam, S. (2015). The NIH Extracellular RNA Communication Consortium. *Journal of Extracellular Vesicles*, *4*, 27493. https://doi.org/10.3402/jev.v4.27493

Al-Nedawi, K., Meehan, B., Micallef, J., Lhotak, V., May, L., Guha, A., & Rak, J. (2008). Intercellular transfer of the oncogenic receptor EGFRvIII by microvesicles derived from tumour cells. *Nature Cell Biology*, *10*(5), 619–624. https://doi.org/10.1038/ncb1725

Allenson, K., Castillo, J., San Lucas, F. A., Scelo, G., Kim, D. U., Bernard, V., … Alvarez, H. (2017). High Prevalence of Mutant *KRAS* in Circulating Exosome-derived DNA from Early Stage Pancreatic Cancer Patients. *Annals of Oncology*, *28*(4), mdx004. https://doi.org/10.1093/annonc/mdx004

Araldi, E., Krämer-Albers, E.-M., Hoen, E. N.-'t, Peinado, H., Psonka-Antonczyk, K. M., Rao, P., … Nazarenko, I. (2012). International Society for Extracellular Vesicles: first annual meeting, April 17-21, 2012: ISEV-2012. *Journal of Extracellular Vesicles*, *1*, 19995. https://doi.org/10.3402/jev.v1i0.19995

Aubertin, K., Silva, A. K. A., Luciani, N., Espinosa, A., Djemat, A., Charue, D., … Wilhelm, C. (2016). Massive release of extracellular vesicles from cancer cells after photodynamic treatment or chemotherapy. *Scientific Reports*, *6*(1), 35376. https://doi.org/10.1038/srep35376

Auffinger, B., Spencer, D., Pytel, P., Ahmed, A. U., & Lesniak, M. S. (2015). The role of glioma stem cells in chemotherapy resistance and glioblastoma multiforme recurrence. *Expert Review of Neurotherapeutics*, *15*(7), 741–752. https://doi.org/10.1586/14737175.2015.1051968

Aum, D. J., Kim, D. H., Beaumont, T. L., Leuthardt, E. C., Dunn, G. P., & Kim, A. H. (2014). Molecular and cellular heterogeneity: the hallmark of glioblastoma. *Neurosurgical Focus*, *37*(6), E11. https://doi.org/10.3171/2014.9.FOCUS14521

Baietti, M. F., Zhang, Z., Mortier, E., Melchior, A., Degeest, G., Geeraerts, A., … David, G. (2012). Syndecan–syntenin–ALIX regulates the biogenesis of exosomes. *Nature Cell Biology*, *14*(7), 677–685. https://doi.org/10.1038/ncb2502

Balaj, L., Atai, N. A., Chen, W., Mu, D., Tannous, B. A., Breakefield, X. O., … Maguire, C. A. (2015). Heparin affinity purification of extracellular vesicles. *Scientific Reports*, *5*(1), 10266. https://doi.org/10.1038/srep10266

Bao, G., Rhee, W. J., & Tsourkas, A. (2009). Fluorescent Probes for Live-Cell RNA Detection. *Annual Review*

of Biomedical Engineering, *11*(1), 25–47. https://doi.org/10.1146/annurev-bioeng-061008-124920

Batagov, A. O., Kuznetsov, V. A., & Kurochkin, I. V. (2011). Identification of nucleotide patterns enriched in secreted RNAs as putative cis-acting elements targeting them to exosome nano-vesicles. *BMC Genomics*, *12*(Suppl 3), S18. https://doi.org/10.1186/1471-2164-12-S3-S18

Bathini, S., Raju, D., Badilescu, S., Kumar, A., Ouellette, R. J., Ghosh, A., & Packirisamy, M. (2018). Nano–Bio Interactions of Extracellular Vesicles with Gold Nanoislands for Early Cancer Diagnosis. *Research*, *2018*, 1–10. https://doi.org/10.1155/2018/3917986

Bigay, J., & Antonny, B. (2012). Curvature, lipid packing, and electrostatics of membrane organelles: defining cellular territories in determining specificity. *Developmental Cell*, *23*(5), 886–895. https://doi.org/10.1016/j.devcel.2012.10.009

Bilkey, G. A., Burns, B. L., Coles, E. P., Mahede, T., Baynam, G., & Nowak, K. J. (2019). Optimizing Precision Medicine for Public Health. *Frontiers in Public Health*, *7*, 42. https://doi.org/10.3389/fpubh.2019.00042

Biomarkers Definitions Working Group. (2001). Biomarkers and surrogate endpoints: preferred definitions and conceptual framework. *Clinical Pharmacology and Therapeutics*, *69*(3), 89–95. https://doi.org/10.1067/mcp.2001.113989

Bond, C. E., & Whitehall, V. L. J. (2018). How the *BRAF* V600E Mutation Defines a Distinct Subgroup of Colorectal Cancer: Molecular and Clinical Implications. *Gastroenterology Research and Practice*, *2018*, 1–14. https://doi.org/10.1155/2018/9250757

Bonnet, D., & Dick, J. E. (1997). Human acute myeloid leukemia is organized as a hierarchy that originates from a primitive hematopoietic cell. *Nature Medicine*, *3*(7), 730–737. Retrieved from http://www.ncbi.nlm.nih.gov/pubmed/9212098

Bosch, S., de Beaurepaire, L., Allard, M., Mosser, M., Heichette, C., Chrétien, D., … Bach, J.-M. (2016). Trehalose prevents aggregation of exosomes and cryodamage. *Scientific Reports*, *6*(1), 36162. https://doi.org/10.1038/srep36162

Brescia, P., Ortensi, B., Fornasari, L., Levi, D., Broggi, G., & Pelicci, G. (2013). CD133 Is Essential for Glioblastoma Stem Cell Maintenance. *STEM CELLS*, *31*(5), 857–869. https://doi.org/10.1002/stem.1317

Brescia, P., Richichi, C., & Pelicci, G. (2012). Current strategies for identification of glioma stem cells: adequate or unsatisfactory? *Journal of Oncology*, *2012*, 376894. https://doi.org/10.1155/2012/376894

Buschmann, D., Kirchner, B., Hermann, S., Märte, M., Wurmser, C., Brandes, F., … Reithmair, M. (2018). Evaluation of serum extracellular vesicle isolation methods for profiling miRNAs by next-generation sequencing. *Journal of Extracellular Vesicles*, *7*(1), 1481321. https://doi.org/10.1080/20013078.2018.1481321

Cardi, G., Mastrangelo, M. J., & Berd, D. (1989). Depletion of T-cells with the CD4+CD45R+ phenotype in lymphocytes that infiltrate subcutaneous metastases of human melanoma. *Cancer Research*, *49*(23), 6562–6565. Retrieved from http://www.ncbi.nlm.nih.gov/pubmed/2479465

Casás-Selves, M., & Degregori, J. (2011). How cancer shapes evolution, and how evolution shapes cancer. *Evolution*, *4*(4), 624–634. https://doi.org/10.1007/s12052-011-0373-y

Castro-Giner, F., Gkountela, S., Donato, C., Alborelli, I., Quagliata, L., Ng, C. K. Y., … Aceto, N. (2018). Cancer Diagnosis Using a Liquid Biopsy: Challenges and Expectations. *Diagnostics (Basel, Switzerland)*, *8*(2). https://doi.org/10.3390/diagnostics8020031

Chang, S. F., Reich, B., Brunzell, J. D., & Will, H. (1998). Detailed characterization of the binding site of the

lipoprotein lipase-specific monoclonal antibody 5D2. *Journal of Lipid Research*, *39*(12), 2350–2359. Retrieved from http://www.ncbi.nlm.nih.gov/pubmed/9831623

Chen, G., Huang, A. C., Zhang, W., Zhang, G., Wu, M., Xu, W., … Guo, W. (2018). Exosomal PD-L1 contributes to immunosuppression and is associated with anti-PD-1 response. *Nature*, *560*(7718), 382–386. https://doi.org/10.1038/s41586-018-0392-8

Chen, X., Liang, H., Zhang, J., Zen, K., & Zhang, C.-Y. (n.d.). Horizontal transfer of microRNAs: molecular mechanisms and clinical applications. https://doi.org/10.1007/s13238-012-2003-z

Chew, H. K., Doroshow, J. H., Frankel, P., Margolin, K. A., Somlo, G., Lenz, H. J., … Albain, K. S. (2009). Phase II studies of gemcitabine and cisplatin in heavily and minimally pretreated metastatic breast cancer. *Journal of Clinical Oncology*, *27*(13), 2163–2169. https://doi.org/10.1200/JCO.2008.17.4839

Colombo, M., Raposo, G., & Théry, C. (2014). Biogenesis, Secretion, and Intercellular Interactions of Exosomes and Other Extracellular Vesicles. *Annual Review of Cell and Developmental Biology*, *30*(1), 255–289. https://doi.org/10.1146/annurev-cellbio-101512-122326

Crescitelli, R., Lässer, C., Szabó, T. G., Kittel, A., Eldh, M., Dianzani, I., … Lötvall, J. (2013). Distinct RNA profiles in subpopulations of extracellular vesicles: apoptotic bodies, microvesicles and exosomes. *Journal of Extracellular Vesicles*, *2*. https://doi.org/10.3402/jev.v2i0.20677

Crowe, J., Döbeli, H., Gentz, R., Hochuli, E., Stüber, D., & Henco, K. (1994). 6xHis-Ni-NTA Chromatography as a Superior Technique in Recombinant Protein Expressiod/Purification. In *Protocols for Gene Analysis* (Vol. 31, pp. 371–388). New Jersey: Humana Press. https://doi.org/10.1385/0-89603-258-2:371

D'Souza-Schorey, C., & Clancy, J. W. (2012). Tumor-derived microvesicles: shedding light on novel microenvironment modulators and prospective cancer biomarkers. *Genes & Development*, *26*(12), 1287–1299. https://doi.org/10.1101/gad.192351.112

De Rubis, G., Rajeev Krishnan, S., & Bebawy, M. (2019). Liquid Biopsies in Cancer Diagnosis, Monitoring, and Prognosis. *Trends in Pharmacological Sciences*, *40*(3), 172–186. https://doi.org/10.1016/j.tips.2019.01.006

Deregibus, M. C., Figliolini, F., D'antico, S., Manzini, P. M., Pasquino, C., De Lena, M., … Camussi, G. (2016a). Charge-based precipitation of extracellular vesicles. *International Journal of Molecular Medicine*, *38*(5), 1359–1366. https://doi.org/10.3892/ijmm.2016.2759

Deregibus, M. C., Figliolini, F., D'antico, S., Manzini, P. M., Pasquino, C., De Lena, M., … Camussi, G. (2016b). Charge-based precipitation of extracellular vesicles. *International Journal of Molecular Medicine*, *38*(5), 1359–1366. https://doi.org/10.3892/ijmm.2016.2759

Dhahbi, J. M., Spindler, S. R., Atamna, H., Boffelli, D., & Martin, D. I. (2014). Deep Sequencing of Serum Small RNAs Identifies Patterns of 5' tRNA Half and YRNA Fragment Expression Associated with Breast Cancer. *Biomarkers in Cancer*, *6*, 37–47. https://doi.org/10.4137/BIC.S20764

Di Vizio, D., Morello, M., Dudley, A. C., Schow, P. W., Adam, R. M., Morley, S., … Freeman, M. R. (2012). Large Oncosomes in Human Prostate Cancer Tissues and in the Circulation of Mice with Metastatic Disease. *The American Journal of Pathology*, *181*(5), 1573–1584. https://doi.org/10.1016/j.ajpath.2012.07.030

Driedonks, T. A. P., & Nolte-'t Hoen, E. N. M. (2019). Circulating Y-RNAs in Extracellular Vesicles and Ribonucleoprotein Complexes; Implications for the Immune System. *Frontiers in Immunology*, *9*, 3164. https://doi.org/10.3389/fimmu.2018.03164

Enderle, D., Spiel, A., Coticchia, C. M., Berghoff, E., Mueller, R., Schlumpberger, M., … Noerholm, M. (2015). Characterization of RNA from Exosomes and Other Extracellular Vesicles Isolated by a Novel Spin Column-Based Method. *PLOS ONE*, *10*(8), e0136133. https://doi.org/10.1371/journal.pone.0136133

Fais, S., O'Driscoll, L., Borras, F. E., Buzas, E., Camussi, G., Cappello, F., … Giebel, B. (2016). Evidence-Based Clinical Use of Nanoscale Extracellular Vesicles in Nanomedicine. *ACS Nano*, *10*(4), 3886–3899. https://doi.org/10.1021/acsnano.5b08015

Farris, A. D., O'Brien, C. A., & Harley, J. B. (1995). Y3 is the most conserved small RNA component of Ro ribonucleoprotein complexes in vertebrate species. *Gene*, *154*(2), 193–198. https://doi.org/10.1016/0378-1119(94)00823-B

Fidler, I. J. (2003). The pathogenesis of cancer metastasis: the "seed and soil" hypothesis revisited. *Nature Reviews Cancer*, *3*(6), 453–458. https://doi.org/10.1038/nrc1098

Finotti, A., Allegretti, M., Gasparello, J., Giacomini, P., Spandidos, D. A., Spoto, G., & Gambari, R. (2018). Liquid biopsy and PCR-free ultrasensitive detection systems in oncology (Review). *International Journal of Oncology*, *53*(4), 1395. https://doi.org/10.3892/IJO.2018.4516

Frank, P. G., & Marcel, Y. L. (2000). Apolipoprotein A-I: structure-function relationships. *Journal of Lipid Research*, *41*(6), 853–872. Retrieved from http://www.ncbi.nlm.nih.gov/pubmed/10828078

Gardiner, C., Vizio, D. Di, Sahoo, S., Théry, C., Witwer, K. W., Wauben, M., & Hill, A. F. (2016). Techniques used for the isolation and characterization of extracellular vesicles: results of a worldwide survey. *Journal of Extracellular Vesicles*, *5*(1), 32945. https://doi.org/10.3402/jev.v5.32945

Gerdes, M. J., Sood, A., Sevinsky, C., Pris, A. D., Zavodszky, M. I., & Ginty, F. (2014). Emerging understanding of multiscale tumor heterogeneity. *Frontiers in Oncology*, *4*, 366. https://doi.org/10.3389/fonc.2014.00366

Ghosh, A., Davey, M., Chute, I. C., Griffiths, S. G., Lewis, S., Chacko, S., … Ouellette, R. J. (2014). Rapid Isolation of Extracellular Vesicles from Cell Culture and Biological Fluids Using a Synthetic Peptide with Specific Affinity for Heat Shock Proteins. *PLoS ONE*, *9*(10), e110443. https://doi.org/10.1371/journal.pone.0110443

Giddings, J., Yang, F., & Myers, M. (1976). Flow-field-flow fractionation: a versatile new separation method. *Science*, *193*(4259), 1244–1245. https://doi.org/10.1126/science.959835

Goossens, N., Nakagawa, S., Sun, X., & Hoshida, Y. (2015). Cancer biomarker discovery and validation. *Translational Cancer Research*, *4*(3), 256–269. https://doi.org/10.21037/4536

Gould, S. J., & Raposo, G. (2013). As we wait: coping with an imperfect nomenclature for extracellular vesicles. *Journal of Extracellular Vesicles*, *2*(1), 20389. https://doi.org/10.3402/jev.v2i0.20389

Greening, D. W., & Simpson, R. J. (2018). Understanding extracellular vesicle diversity – current status. *Expert Review of Proteomics*, *15*(11), 887–910. https://doi.org/10.1080/14789450.2018.1537788

Gudbergsson, J. M., Johnsen, K. B., Skov, M. N., & Duroux, M. (2016). Systematic review of factors influencing extracellular vesicle yield from cell cultures. *Cytotechnology*, *68*(4), 579–592. https://doi.org/10.1007/s10616-015-9913-6

Guevara, J., Romo, J., Hernandez, E., & Guevara, N. V. (2018). Identification of Receptor Ligands in Apo B100 Reveals Potential Functional Domains. *The Protein Journal*, *37*(6), 548–571. https://doi.org/10.1007/s10930-018-9792-8

Guo, G., von Meyenn, F., Rostovskaya, M., Clarke, J., Dietmann, S., Baker, D., … Smith, A. (2017). Epigenetic resetting of human pluripotency. *Development (Cambridge, England)*, *144*(15), 2748–2763.

https://doi.org/10.1242/dev.146811

Guo, L., & He, B. (2017). Extracellular vesicles and their diagnostic and prognostic potential in cancer. *Translational Cancer Research*, *6*(3), 599–612. https://doi.org/10.21037/14169

Guo, S.-C., Tao, S.-C., & Dawn, H. (2018). Microfluidics-based on-a-chip systems for isolating and analysing extracellular vesicles. *Journal of Extracellular Vesicles*, *7*(1), 1508271. https://doi.org/10.1080/20013078.2018.1508271

György, B., Szabó, T. G., Pásztói, M., Pál, Z., Misják, P., Aradi, B., … Buzás, E. I. (2011). Membrane vesicles, current state-of-the-art: Emerging role of extracellular vesicles. *Cellular and Molecular Life Sciences*, *68*(16), 2667–2688. https://doi.org/10.1007/s00018-011-0689-3

H Rashed, M., Bayraktar, E., K Helal, G., Abd-Ellah, M. F., Amero, P., Chavez-Reyes, A., & Rodriguez-Aguayo, C. (2017). Exosomes: From Garbage Bins to Promising Therapeutic Targets. *International Journal of Molecular Sciences*, *18*(3). https://doi.org/10.3390/ijms18030538

Haber, D. A., & Velculescu, V. E. (2014). Blood-Based Analyses of Cancer: Circulating Tumor Cells and Circulating Tumor DNA. *Cancer Discovery*, *4*(6), 650–661. https://doi.org/10.1158/2159-8290.CD-13-1014

Haderk, F., Moussay, E., Paggetti, J., Göbel, M., Dürig, J., Zenz, T., … Seiffert, M. (2014). Chronic Lymphocytic Leukemia-Derived Extracellular Vesicles Contain a Distinctive Proteome, As Well As Specific Micro RNAs and Y RNAs. *Blood*, *124*(21). Retrieved from http://www.bloodjournal.org/content/124/21/1968?sso-checked=true

Hanahan, D., & Weinberg, R. A. (2011a). Hallmarks of cancer: The next generation. *Cell*, *144*(5), 646–674. https://doi.org/10.1016/j.cell.2011.02.013

Hanahan, D., & Weinberg, R. A. (2011b). Hallmarks of Cancer: The Next Generation. *Cell*, *144*(5), 646–674. https://doi.org/10.1016/j.cell.2011.02.013

Hanif, F., Muzaffar, K., Perveen, K., Malhi, S. M., & Simjee, S. U. (2017a). Glioblastoma Multiforme: A Review of its Epidemiology and Pathogenesis through Clinical Presentation and Treatment. *Asian Pacific Journal of Cancer Prevention : APJCP*, *18*(1), 3–9. https://doi.org/10.22034/APJCP.2017.18.1.3

Hanif, F., Muzaffar, K., Perveen, K., Malhi, S. M., & Simjee, S. U. (2017b). Glioblastoma Multiforme: A Review of its Epidemiology and Pathogenesis through Clinical Presentation and Treatment. *Asian Pacific Journal of Cancer Prevention : APJCP*, *18*(1), 3–9. https://doi.org/10.22034/APJCP.2017.18.1.3

Hannafon, B. N., Carpenter, K. J., Berry, W. L., Janknecht, R., Dooley, W. C., & Ding, W.-Q. (2015). Exosome-mediated microRNA signaling from breast cancer cells is altered by the anti-angiogenesis agent docosahexaenoic acid (DHA). *Molecular Cancer*, *14*(1), 133. https://doi.org/10.1186/s12943-015-0400-7

Haraszti, R. A., Didiot, M.-C., Sapp, E., Leszyk, J., Shaffer, S. A., Rockwell, H. E., … Khvorova, A. (2016). High-resolution proteomic and lipidomic analysis of exosomes and microvesicles from different cell sources. *Journal of Extracellular Vesicles*, *5*(1), 32570. https://doi.org/10.3402/jev.v5.32570

Hatoum, A., Mohammed, R., & Zakieh, O. (2019). The unique invasiveness of glioblastoma and possible drug targets on extracellular matrix. *Cancer Management and Research*, *Volume 11*, 1843–1855. https://doi.org/10.2147/CMAR.S186142

Heath, N., Grant, L., De Oliveira, T. M., Rowlinson, R., Osteikoetxea, X., Dekker, N., & Overman, R. (2018). Rapid isolation and enrichment of extracellular vesicle preparations using anion exchange

chromatography. *Scientific Reports*, *8*(1), 5730. https://doi.org/10.1038/s41598-018-24163-y

Hendrick, J. P., Wolin, S. L., Rinke, J., Lerner, M. R., & Steitz, J. A. (1981). Ro small cytoplasmic ribonucleoproteins are a subclass of La ribonucleoproteins: further characterization of the Ro and La small ribonucleoproteins from uninfected mammalian cells. *Molecular and Cellular Biology*, *1*(12), 1138–1149. https://doi.org/10.1128/mcb.1.12.1138

Hessvik, N. P., & Llorente, A. (2018). Current knowledge on exosome biogenesis and release. *Cellular and Molecular Life Sciences*, *75*(2), 193–208. https://doi.org/10.1007/s00018-017-2595-9

Hill, A. F., Pegtel, D. M., Lambertz, U., Leonardi, T., O'Driscoll, L., Pluchino, S., … Nolte-'t Hoen, E. N. M. (2013). ISEV position paper: extracellular vesicle RNA analysis and bioinformatics. *Journal of Extracellular Vesicles*, *2*, 1–8. https://doi.org/10.3402/jev.v2i0.22859

Hoshino, A., Costa-Silva, B., Shen, T.-L., Rodrigues, G., Hashimoto, A., Tesic Mark, M., … Lyden, D. (2015). Tumour exosome integrins determine organotropic metastasis. *Nature*, *527*(7578), 329–335. https://doi.org/10.1038/nature15756

Hurley, J. H. (2008). ESCRT complexes and the biogenesis of multivesicular bodies. *Current Opinion in Cell Biology*, *20*(1), 4–11. https://doi.org/10.1016/j.ceb.2007.12.002

Igami, K., Uchiumi, T., Ueda, S., Kamioka, K., Setoyama, D., Gotoh, K., … Kang, D. (2019). Characterization and function of medium and large extracellular vesicles from plasma and urine by surface antigens and Annexin V. *BioRxiv*, 623553. https://doi.org/10.1101/623553

Janas, T., Janas, M. M., Sapoń, K., & Janas, T. (2015). Mechanisms of RNA loading into exosomes. *FEBS Letters*, *589*(13), 1391–1398. https://doi.org/10.1016/j.febslet.2015.04.036

Jeppesen, D. K., Fenix, A. M., Franklin, J. L., Higginbotham, J. N., Zhang, Q., Zimmerman, L. J., … Coffey, R. J. (2019). Reassessment of Exosome Composition. *Cell*, *177*(2), 428-445.e18. https://doi.org/10.1016/j.cell.2019.02.029

Kalra, H., Drummen, G., & Mathivanan, S. (2016). Focus on Extracellular Vesicles: Introducing the Next Small Big Thing. *International Journal of Molecular Sciences*, *17*(2), 170. https://doi.org/10.3390/ijms17020170

Kanwar, S. S., Dunlay, C. J., Simeone, D. M., & Nagrath, S. (2014). Microfluidic device (ExoChip) for on-chip isolation, quantification and characterization of circulating exosomes. *Lab Chip*, *14*(11), 1891–1900. https://doi.org/10.1039/C4LC00136B

Karachaliou, N., Mayo-de-Las-Casas, C., Molina-Vila, M. A., & Rosell, R. (2015). Real-time liquid biopsies become a reality in cancer treatment. *Annals of Translational Medicine*, *3*(3), 36. https://doi.org/10.3978/j.issn.2305-5839.2015.01.16

Kastelowitz, N., & Yin, H. (2014). Exosomes and microvesicles: Identification and targeting by particle size and lipid chemical probes. *ChemBioChem*. https://doi.org/10.1002/cbic.201400043

Kawakami, K., Fujita, Y., Matsuda, Y., Arai, T., Horie, K., Kameyama, K., … Ito, M. (2017). Gamma-glutamyltransferase activity in exosomes as a potential marker for prostate cancer. *BMC Cancer*, *17*(1), 316. https://doi.org/10.1186/s12885-017-3301-x

Keerthikumar, S., Gangoda, L., Gho, Y. S., & Mathivanan, S. (2017). Bioinformatics Tools for Extracellular Vesicles Research. In *Methods in molecular biology (Clifton, N.J.)* (Vol. 1545, pp. 189–196). https://doi.org/10.1007/978-1-4939-6728-5_13

Khan, S., Jutzy, J. M. S., Aspe, J. R., McGregor, D. W., Neidigh, J. W., & Wall, N. R. (2011). Survivin is released from cancer cells via exosomes. *Apoptosis*, *16*(1), 1–12. https://doi.org/10.1007/s10495-010-

0534-4

Kim, K. M., Abdelmohsen, K., Mustapic, M., Kapogiannis, D., & Gorospe, M. (2017). RNA in extracellular vesicles. *Wiley Interdisciplinary Reviews. RNA*, e1413. https://doi.org/10.1002/wrna.1413

Kitange, G. J., Carlson, B. L., Schroeder, M. A., Grogan, P. T., Lamont, J. D., Decker, P. A., … Sarkaria, J. N. (2009). Induction of MGMT expression is associated with temozolomide resistance in glioblastoma xenografts. *Neuro-Oncology*, *11*(3), 281–291. https://doi.org/10.1215/15228517-2008-090

Köhn, M., Pazaitis, N., & Hüttelmaier, S. (2013). Why YRNAs? About Versatile RNAs and Their Functions. *Biomolecules*, *3*(1), 143–156. https://doi.org/10.3390/biom3010143

König, L., Kasimir-Bauer, S., Bittner, A.-K., Hoffmann, O., Wagner, B., Santos Manvailer, L. F., … Rebmann, V. (2018). Elevated levels of extracellular vesicles are associated with therapy failure and disease progression in breast cancer patients undergoing neoadjuvant chemotherapy. *OncoImmunology*, *7*(1), e1376153. https://doi.org/10.1080/2162402X.2017.1376153

Konoshenko, M. Y., Lekchnov, E. A., Vlassov, A. V., & Laktionov, P. P. (2018). Isolation of Extracellular Vesicles: General Methodologies and Latest Trends. *BioMed Research International*, *2018*, 1–27. https://doi.org/10.1155/2018/8545347

Kosanović, M., Milutinović, B., Goč, S., Mitić, N., & Janković, M. (2017). Ion-exchange chromatography purification of extracellular vesicles. *BioTechniques*, *63*(2). https://doi.org/10.2144/000114575

Kowal, J., Arras, G., Colombo, M., Jouve, M., Morath, J. P., Primdal-Bengtson, B., … Théry, C. (2016). Proteomic comparison defines novel markers to characterize heterogeneous populations of extracellular vesicle subtypes. *Proceedings of the National Academy of Sciences of the United States of America*, *113*(8), E968-77. https://doi.org/10.1073/pnas.1521230113

Kowal, J., Tkach, M., & Théry, C. (2014). Biogenesis and secretion of exosomes. *Current Opinion in Cell Biology*, *29*, 116–125. https://doi.org/10.1016/j.ceb.2014.05.004

Kowalski, M. P., & Krude, T. (2015a). Functional roles of non-coding Y RNAs. *The International Journal of Biochemistry & Cell Biology*, *66*, 20–29. https://doi.org/10.1016/j.biocel.2015.07.003

Kowalski, M. P., & Krude, T. (2015b). Functional roles of non-coding Y RNAs. *The International Journal of Biochemistry & Cell Biology*, *66*, 20–29. https://doi.org/10.1016/j.biocel.2015.07.003

Krebs, M. G., Hou, J.-M., Ward, T. H., Blackhall, F. H., & Dive, C. (2010). Circulating tumour cells: their utility in cancer management and predicting outcomes. *Therapeutic Advances in Medical Oncology*, *2*(6), 351–365. https://doi.org/10.1177/1758834010378414

Krude, T., Christov, C. P., Hyrien, O., & Marheineke, K. (2009). Y RNA functions at the initiation step of mammalian chromosomal DNA replication. *Journal of Cell Science*, *122*(16), 2836–2845. https://doi.org/10.1242/jcs.047563

Kucharzewska, P., Christianson, H. C., Welch, J. E., Svensson, K. J., Fredlund, E., Ringnér, M., … Belting, M. (2013). Exosomes reflect the hypoxic status of glioma cells and mediate hypoxia-dependent activation of vascular cells during tumor development. *Proceedings of the National Academy of Sciences of the United States of America*, *110*(18), 7312–7317. https://doi.org/10.1073/pnas.1220998110

Kusuma, G. D., Barabadi, M., Tan, J. L., Morton, D. A. V., Frith, J. E., & Lim, R. (2018). To Protect and to Preserve: Novel Preservation Strategies for Extracellular Vesicles. *Frontiers in Pharmacology*, *9*. https://doi.org/10.3389/FPHAR.2018.01199

Lane, R. E., Korbie, D., Trau, M., & Hill, M. M. (2017). Purification Protocols for Extracellular Vesicles (pp.

111–130). https://doi.org/10.1007/978-1-4939-7253-1_10

Langley, A. R., Chambers, H., Christov, C. P., & Krude, T. (2010). Ribonucleoprotein Particles Containing Non-Coding Y RNAs, Ro60, La and Nucleolin Are Not Required for Y RNA Function in DNA Replication. *PLoS ONE*, *5*(10), e13673. https://doi.org/10.1371/journal.pone.0013673

Larki, P., Gharib, E., Yaghoob Taleghani, M., Khorshidi, F., Nazemalhosseini-Mojarad, E., & Asadzadeh Aghdaei, H. (2017). Coexistence of KRAS and BRAF Mutations in Colorectal Cancer: A Case Report Supporting The Concept of Tumoral Heterogeneity. *Cell Journal*, *19*(Suppl 1), 113–117. https://doi.org/10.22074/cellj.2017.5123

Lathia, J. D., Mack, S. C., Mulkearns-Hubert, E. E., Valentim, C. L. L., & Rich, J. N. (2015). Cancer stem cells in glioblastoma. *Genes & Development*, *29*(12), 1203–1217. https://doi.org/10.1101/gad.261982.115

Laulagnier, K., Motta, C., Hamdi, S., Roy, S., Fauvelle, F., Pageaux, J.-F., … Record, M. (2004). Mast cell- and dendritic cell-derived exosomes display a specific lipid composition and an unusual membrane organization. *The Biochemical Journal*, *380*(Pt 1), 161–171. https://doi.org/10.1042/BJ20031594

Lei, X., Guan, C.-W., Song, Y., & Wang, H. (2015). The multifaceted role of CD146/MCAM in the promotion of melanoma progression. *Cancer Cell International*, *15*(1), 3. https://doi.org/10.1186/s12935-014-0147-z

Lerner, M. R., Boyle, J. A., Hardin, J. A., & Steitz, J. A. (1981). Two novel classes of small ribonucleoproteins detected by antibodies associated with lupus erythematosus. *Science (New York, N.Y.)*, *211*(4480), 400–402. Retrieved from http://www.ncbi.nlm.nih.gov/pubmed/6164096

Liang, K., Liu, F., Fan, J., Sun, D., Liu, C., Lyon, C. J., … Hu, Y. (2017). Nanoplasmonic quantification of tumour-derived extracellular vesicles in plasma microsamples for diagnosis and treatment monitoring. *Nature Biomedical Engineering*, *1*(4), 0021. https://doi.org/10.1038/s41551-016-0021

Llorente, A., Skotland, T., Sylvänne, T., Kauhanen, D., Róg, T., Orłowski, A., … Sandvig, K. (2013). Molecular lipidomics of exosomes released by PC-3 prostate cancer cells. *Biochimica et Biophysica Acta*, *1831*(7), 1302–1309. Retrieved from http://www.ncbi.nlm.nih.gov/pubmed/24046871

Logozzi, M., De Milito, A., Lugini, L., Borghi, M., Calabrò, L., Spada, M., … Fais, S. (2009). High Levels of Exosomes Expressing CD63 and Caveolin-1 in Plasma of Melanoma Patients. *PLoS ONE*, *4*(4), e5219. https://doi.org/10.1371/journal.pone.0005219

Louis, D. N., Perry, A., Reifenberger, G., von Deimling, A., Figarella-Branger, D., Cavenee, W. K., … Ellison, D. W. (2016). The 2016 World Health Organization Classification of Tumors of the Central Nervous System: a summary. *Acta Neuropathologica*, *131*(6), 803–820. https://doi.org/10.1007/s00401-016-1545-1

Maacha, S., Bhat, A. A., Jimenez, L., Raza, A., Haris, M., Uddin, S., & Grivel, J.-C. (2019). Extracellular vesicles-mediated intercellular communication: roles in the tumor microenvironment and anti-cancer drug resistance. *Molecular Cancer*, *18*(1), 55. https://doi.org/10.1186/s12943-019-0965-7

Marassi, V., Roda, B., Zattoni, A., Tanase, M., & Reschiglian, P. (2014). Hollow fiber flow field-flow fractionation and size-exclusion chromatography with multi-angle light scattering detection: A complementary approach in biopharmaceutical industry. *Journal of Chromatography A*, *1372*, 196–203. https://doi.org/10.1016/j.chroma.2014.10.072

Marca, V. La, Fierabracci, A., La Marca, V., & Fierabracci, A. (2017). Insights into the Diagnostic Potential of Extracellular Vesicles and Their miRNA Signature from Liquid Biopsy as Early Biomarkers of Diabetic Micro/Macrovascular Complications. *International Journal of Molecular Sciences*, *18*(9), 1974.

https://doi.org/10.3390/ijms18091974

Marisi, G., Scarpi, E., Passardi, A., Nanni, O., Ragazzini, A., Valgiusti, M., … Ulivi, P. (2017). Circulating VEGF and eNOS variations as predictors of outcome in metastatic colorectal cancer patients receiving bevacizumab. *Scientific Reports*, *7*(1), 1293. https://doi.org/10.1038/s41598-017-01420-0

Maroto, R., Zhao, Y., Jamaluddin, M., Popov, V. L., Wang, H., Kalubowilage, M., … Brasier, A. R. (2017). Effects of storage temperature on airway exosome integrity for diagnostic and functional analyses. *Journal of Extracellular Vesicles*, *6*(1), 1359478. https://doi.org/10.1080/20013078.2017.1359478

Mathai, R. A., Vidya, R. V. S., Reddy, B. S., Thomas, L., Udupa, K., Kolesar, J., & Rao, M. (2019). Potential Utility of Liquid Biopsy as a Diagnostic and Prognostic Tool for the Assessment of Solid Tumors: Implications in the Precision Oncology. *Journal of Clinical Medicine*, *8*(3). https://doi.org/10.3390/jcm8030373

Mathivanan, S., & Simpson, R. J. (2009). ExoCarta: A compendium of exosomal proteins and RNA. *PROTEOMICS*, *9*(21), 4997–5000. https://doi.org/10.1002/pmic.200900351

Max, K. E. A., Bertram, K., Akat, K. M., Bogardus, K. A., Li, J., Morozov, P., … Tuschl, T. (2018). Human plasma and serum extracellular small RNA reference profiles and their clinical utility. *Proceedings of the National Academy of Sciences of the United States of America*, *115*(23), E5334–E5343. https://doi.org/10.1073/pnas.1714397115

McDonald, B., Reep, B., Lapetina, E. G., & Molina y Vedia, L. (1993). Glyceraldehyde-3-phosphate dehydrogenase is required for the transport of nitric oxide in platelets. *Proceedings of the National Academy of Sciences of the United States of America*, *90*(23), 11122–11126. https://doi.org/10.1073/pnas.90.23.11122

Meldolesi, J. (2018). Exosomes and Ectosomes in Intercellular Communication. *Current Biology*, *28*(8), R435–R444. https://doi.org/10.1016/j.cub.2018.01.059

Melo, S. A., Luecke, L. B., Kahlert, C., Fernandez, A. F., Gammon, S. T., Kaye, J., … Kalluri, R. (2015). Glypican-1 identifies cancer exosomes and detects early pancreatic cancer. *Nature*, *523*(7559), 177–182. https://doi.org/10.1038/nature14581

Melo, S. A., Sugimoto, H., O'Connell, J. T., Kato, N., Villanueva, A., Vidal, A., … Kalluri, R. (2014). Cancer exosomes perform cell-independent microRNA biogenesis and promote tumorigenesis. *Cancer Cell*, *26*(5), 707–721. https://doi.org/10.1016/j.ccell.2014.09.005

Menard, J. A., Cerezo-Magaña, M., & Belting, M. (2018). Functional role of extracellular vesicles and lipoproteins in the tumour microenvironment. *Philosophical Transactions of the Royal Society of London. Series B, Biological Sciences*, *373*(1737), 20160480. https://doi.org/10.1098/rstb.2016.0480

Miller, M. C., Doyle, G. V, & Terstappen, L. W. M. M. (2010). Significance of Circulating Tumor Cells Detected by the CellSearch System in Patients with Metastatic Breast Colorectal and Prostate Cancer. *Journal of Oncology*, *2010*, 617421. https://doi.org/10.1155/2010/617421

Momen-Heravi, F., Balaj, L., Alian, S., Mantel, P.-Y., Halleck, A. E., Trachtenberg, A. J., … Kuo, W. P. (2013). Current methods for the isolation of extracellular vesicles. *Biological Chemistry*, *394*(10), 1253–1262. https://doi.org/10.1515/hsz-2013-0141

Monguió-Tortajada, M., Morón-Font, M., Gámez-Valero, A., Carreras-Planella, L., Borràs, F. E., & Franquesa, M. (2019). Extracellular-Vesicle Isolation from Different Biological Fluids by Size-Exclusion Chromatography. *Current Protocols in Stem Cell Biology*, *49*(1), e82. https://doi.org/10.1002/cpsc.82

Morales-Kastresana, A., Telford, B., Musich, T. A., McKinnon, K., Clayborne, C., Braig, Z., … Jones, J. C. (2017). Labeling Extracellular Vesicles for Nanoscale Flow Cytometry. *Scientific Reports*, *7*(1), 1878. https://doi.org/10.1038/s41598-017-01731-2

Morelli, A. E., Larregina, A. T., Shufesky, W. J., Sullivan, M. L. G., Stolz, D. B., Papworth, G. D., … Thomson, A. W. (2004, November 15). Blood. *Blood*. American Society of Hematology. https://doi.org/10.1182/blood-2004-03-0824

Mummery, C. L. (Christine L. ., Stolpe, A. van de, Roelen, B. A. J., & Clevers, H. (n.d.). *Stem cells : scientific facts and fiction*.

Muralidharan-Chari, V., Clancy, J., Plou, C., Romao, M., Chavrier, P., Raposo, G., & D'Souza-Schorey, C. (2009). ARF6-Regulated Shedding of Tumor Cell-Derived Plasma Membrane Microvesicles. *Current Biology*, *19*(22), 1875–1885. https://doi.org/10.1016/j.cub.2009.09.059

Murphy, D. E., de Jong, O. G., Brouwer, M., Wood, M. J., Lavieu, G., Schiffelers, R. M., & Vader, P. (2019). Extracellular vesicle-based therapeutics: natural versus engineered targeting and trafficking. *Experimental & Molecular Medicine*, *51*(3), 32. https://doi.org/10.1038/s12276-019-0223-5

Murray, P., Frampton, G., & Nelson, P. N. (1999). Cell adhesion molecules. Sticky moments in the clinic. *BMJ (Clinical Research Ed.)*, *319*(7206), 332–334. https://doi.org/10.1136/bmj.319.7206.332

Nolte-'t Hoen, E. N. M., Buermans, H. P. J., Waasdorp, M., Stoorvogel, W., Wauben, M. H. M., & 't Hoen, P. A. C. (2012). Deep sequencing of RNA from immune cell-derived vesicles uncovers the selective incorporation of small non-coding RNA biotypes with potential regulatory functions. *Nucleic Acids Research*, *40*(18), 9272–9285. https://doi.org/10.1093/nar/gks658

Nomura, S. (2017). Extracellular vesicles and blood diseases. *International Journal of Hematology*, *105*(4), 392–405. https://doi.org/10.1007/s12185-017-2180-x

Ogata-Kawata, H., Izumiya, M., Kurioka, D., Honma, Y., Yamada, Y., Furuta, K., … Tsuchiya, N. (2014). Circulating Exosomal microRNAs as Biomarkers of Colon Cancer. *PLoS ONE*, *9*(4), e92921. https://doi.org/10.1371/journal.pone.0092921

Oldenhuis, C. N. A. M., Oosting, S. F., Gietema, J. A., & de Vries, E. G. E. (2008). Prognostic versus predictive value of biomarkers in oncology. *European Journal of Cancer*, *44*(7), 946–953. https://doi.org/10.1016/j.ejca.2008.03.006

Ordóñez, N. G. (2014). Value of melanocytic-associated immunohistochemical markers in the diagnosis of malignant melanoma: a review and update. *Human Pathology*, *45*(2), 191–205. https://doi.org/10.1016/J.HUMPATH.2013.02.007

Osti, D., Del Bene, M., Rappa, G., Santos, M., Matafora, V., Richichi, C., … Pelicci, G. (2019). Clinical Significance of Extracellular Vesicles in Plasma from Glioblastoma Patients. *Clinical Cancer Research*, *25*(1), 266–276. https://doi.org/10.1158/1078-0432.CCR-18-1941

Ostrom, Q. T., Bauchet, L., Davis, F. G., Deltour, I., Fisher, J. L., Langer, C. E., … Barnholtz-Sloan, J. S. (2014). The epidemiology of glioma in adults: a "state of the science" review. *Neuro-Oncology*, *16*(7), 896–913. https://doi.org/10.1093/neuonc/nou087

Pan, B. T., & Johnstone, R. M. (1983). Fate of the transferrin receptor during maturation of sheep reticulocytes in vitro: selective externalization of the receptor. *Cell*, *33*(3), 967–978. Retrieved from http://www.ncbi.nlm.nih.gov/pubmed/6307529

Park, J. E., Tan, H. Sen, Datta, A., Lai, R. C., Zhang, H., Meng, W., … Sze, S. K. (2010). Hypoxic Tumor Cell

Modulates Its Microenvironment to Enhance Angiogenic and Metastatic Potential by Secretion of Proteins and Exosomes. *Molecular & Cellular Proteomics*, *9*(6), 1085–1099. https://doi.org/10.1074/mcp.M900381-MCP200

Park, S. J., Kim, J. M., Kim, J., Hur, J., Park, S., Kim, K., … Chwae, Y.-J. (2018). Molecular mechanisms of biogenesis of apoptotic exosome-like vesicles and their roles as damage-associated molecular patterns. *Proceedings of the National Academy of Sciences*, *115*(50), E11721–E11730. https://doi.org/10.1073/pnas.1811432115

Patel, A. P., Tirosh, I., Trombetta, J. J., Shalek, A. K., Gillespie, S. M., Wakimoto, H., … Bernstein, B. E. (2014). Single-cell RNA-seq highlights intratumoral heterogeneity in primary glioblastoma. *Science (New York, N.Y.), 344*(6190), 1396–1401. https://doi.org/10.1126/science.1254257

Peinado, H., Zhang, H., Matei, I. R., Costa-Silva, B., Hoshino, A., Rodrigues, G., … Lyden, D. (2017). Pre-metastatic niches: organ-specific homes for metastases. *Nature Reviews Cancer*, *17*(5), 302–317. https://doi.org/10.1038/nrc.2017.6

Pesenti, C., Navone, S. E., Guarnaccia, L., Terrasi, A., Costanza, J., Silipigni, R., … Marfia, G. (2019). The Genetic Landscape of Human Glioblastoma and Matched Primary Cancer Stem Cells Reveals Intratumour Similarity and Intertumour Heterogeneity. *Stem Cells International*, *2019*, 1–12. https://doi.org/10.1155/2019/2617030

Pollard, S. M., Yoshikawa, K., Clarke, I. D., Danovi, D., Stricker, S., Russell, R., … Dirks, P. (2009). Glioma Stem Cell Lines Expanded in Adherent Culture Have Tumor-Specific Phenotypes and Are Suitable for Chemical and Genetic Screens. *Cell Stem Cell*, *4*(6), 568–580. https://doi.org/10.1016/J.STEM.2009.03.014

Racila, E., Euhus, D., Weiss, A. J., Rao, C., McConnell, J., Terstappen, L. W., & Uhr, J. W. (1998). Detection and characterization of carcinoma cells in the blood. *Proceedings of the National Academy of Sciences of the United States of America*, *95*(8), 4589–4594. https://doi.org/10.1073/pnas.95.8.4589

Rahman, M., Reyner, K., Deleyrolle, L., Millette, S., Azari, H., Day, B. W., … Reynolds, B. A. (2015). Neurosphere and adherent culture conditions are equivalent for malignant glioma stem cell lines. *Anatomy & Cell Biology*, *48*(1), 25. https://doi.org/10.5115/acb.2015.48.1.25

Raposo, G., & Stoorvogel, W. (2013). Extracellular vesicles: Exosomes, microvesicles, and friends. *Journal of Cell Biology*, *200*(4), 373–383. https://doi.org/10.1083/jcb.201211138

Ropolo, M., Daga, A., Griffero, F., Foresta, M., Casartelli, G., Zunino, A., … Frosina, G. (2009). Comparative Analysis of DNA Repair in Stem and Nonstem Glioma Cell Cultures. *Molecular Cancer Research*, *7*(3), 383–392. https://doi.org/10.1158/1541-7786.MCR-08-0409

Ruma, I. M. W., Putranto, E. W., Kondo, E., Murata, H., Watanabe, M., Huang, P., … Sakaguchi, M. (2016). MCAM, as a novel receptor for S100A8/A9, mediates progression of malignant melanoma through prominent activation of NF-κB and ROS formation upon ligand binding. *Clinical & Experimental Metastasis*, *33*(6), 609–627. https://doi.org/10.1007/s10585-016-9801-2

Safaei, R., Larson, B. J., Cheng, T. C., Gibson, M. A., Otani, S., Naerdemann, W., & Howell, S. B. (2005). Abnormal lysosomal trafficking and enhanced exosomal export of cisplatin in drug-resistant human ovarian carcinoma cells. *Molecular Cancer Therapeutics*, *4*(10), 1595–1604. https://doi.org/10.1158/1535-7163.MCT-05-0102

Salgın, S., Salgın, U., & Bahadır, S. (2012). *Zeta Potentials and Isoelectric Points of Biomolecules: The Effects*

of Ion Types and Ionic Strengths. *Int. J. Electrochem. Sci* (Vol. 7). Retrieved from www.electrochemsci.org

Savina, A., Furlán, M., Vidal, M., & Colombo, M. I. (2003). Exosome release is regulated by a calcium-dependent mechanism in K562 cells. *The Journal of Biological Chemistry*, *278*(22), 20083–20090. https://doi.org/10.1074/jbc.M301642200

Schiller, M., Bekeredjian-Ding, I., Heyder, P., Blank, N., Ho, A. D., & Lorenz, H.-M. (2008). Autoantigens are translocated into small apoptotic bodies during early stages of apoptosis. *Cell Death & Differentiation*, *15*(1), 183–191. https://doi.org/10.1038/sj.cdd.4402239

Shao, H., Im, H., Castro, C. M., Breakefield, X., Weissleder, R., & Lee, H. (2018). New Technologies for Analysis of Extracellular Vesicles. *Chemical Reviews*, *118*(4), 1917–1950. https://doi.org/10.1021/acs.chemrev.7b00534

Shelke, G. V., Lässer, C., Gho, Y. S., & Lötvall, J. (2014). Importance of exosome depletion protocols to eliminate functional and RNA-containing extracellular vesicles from fetal bovine serum. *Journal of Extracellular Vesicles*, *3*, 1–8. https://doi.org/10.3402/jev.v3.24783

Shurtleff, M. J., Temoche-Diaz, M. M., Karfilis, K. V, Ri, S., & Schekman, R. (2016). Y-box protein 1 is required to sort microRNAs into exosomes in cells and in a cell-free reaction. *ELife*, *5*. https://doi.org/10.7554/eLife.19276

Siegel, R. L., Miller, K. D., & Jemal, A. (2019). Cancer statistics, 2019. *CA: A Cancer Journal for Clinicians*, *69*(1), 7–34. https://doi.org/10.3322/caac.21551

Simons, F. H. M., Rutjes, S. A., Van Venrooij, W. J., & Pruijn, G. J. M. (1996). *The interactions with Ro60 and La differentially affect nuclear export of hY1 RNA*. *RNA* (Vol. 2). Cambridge University Press. Retrieved from https://www.ncbi.nlm.nih.gov/pmc/articles/PMC1369369/pdf/8608450.pdf

Singh, S. K., Clarke, I. D., Terasaki, M., Bonn, V. E., Hawkins, C., Squire, J., & Dirks, P. B. (2003). Identification of a Cancer Stem Cell in Human Brain Tumors. *Cancer Research*, *63*(18), 5821–5828. Retrieved from http://cancerres.aacrjournals.org/content/63/18/5821.long

Siravegna, G., Marsoni, S., Siena, S., & Bardelli, A. (2017). Integrating liquid biopsies into the management of cancer. *Nature Reviews Clinical Oncology*, *14*(9), 531–548. https://doi.org/10.1038/nrclinonc.2017.14

Skog, J., Würdinger, T., van Rijn, S., Meijer, D. H., Gainche, L., Curry, W. T., … Breakefield, X. O. (2008). Glioblastoma microvesicles transport RNA and proteins that promote tumour growth and provide diagnostic biomarkers. *Nature Cell Biology*, *10*(12), 1470–1476. https://doi.org/10.1038/ncb1800

Skotland, T., Sandvig, K., & Llorente, A. (2017). Lipids in exosomes: Current knowledge and the way forward. *Progress in Lipid Research*, *66*, 30–41. https://doi.org/10.1016/J.PLIPRES.2017.03.001

Slamon, D. J., Leyland-Jones, B., Shak, S., Fuchs, H., Paton, V., Bajamonde, A., … Norton, L. (2001). Use of Chemotherapy plus a Monoclonal Antibody against HER2 for Metastatic Breast Cancer That Overexpresses HER2. *New England Journal of Medicine*, *344*(11), 783–792. https://doi.org/10.1056/NEJM200103153441101

Smith, Z. J., Lee, C., Rojalin, T., Carney, R. P., Hazari, S., Knudson, A., … Wachsmann-Hogiu, S. (2015). Single exosome study reveals subpopulations distributed among cell lines with variability related to membrane content. *Journal of Extracellular Vesicles*, *4*(1), 28533. https://doi.org/10.3402/jev.v4.28533

Sódar, B. W., Kittel, Á., Pálóczi, K., Vukman, K. V, Osteikoetxea, X., Szabó-Taylor, K., … Buzás, E. I. (2016). Low-density lipoprotein mimics blood plasma-derived exosomes and microvesicles during isolation and

detection. *Scientific Reports*, *6*(1), 24316. https://doi.org/10.1038/srep24316

Steffen, L. E., Boucher, K. M., Damron, B. H., Pappas, L. M., Walters, S. T., Flores, K. G., … Kinney, A. Y. (2015). Efficacy of a Telehealth Intervention on Colonoscopy Uptake When Cost Is a Barrier: The Family CARE Cluster Randomized Controlled Trial. *Cancer Epidemiology, Biomarkers & Prevention : A Publication of the American Association for Cancer Research, Cosponsored by the American Society of Preventive Oncology*, *24*(9), 1311–1318. https://doi.org/10.1158/1055-9965.EPI-15-0150

Szatanek, R., Baran, J., Siedlar, M., & Baj-Krzyworzeka, M. (2015). Isolation of extracellular vesicles: Determining the correct approach (Review). *International Journal of Molecular Medicine*, *36*(1), 11–17. https://doi.org/10.3892/ijmm.2015.2194

Takov, K., Yellon, D. M., & Davidson, S. M. (2019). Comparison of small extracellular vesicles isolated from plasma by ultracentrifugation or size-exclusion chromatography: yield, purity and functional potential. *Journal of Extracellular Vesicles*, *8*(1), 1560809. https://doi.org/10.1080/20013078.2018.1560809

Tang, Y.-T., Huang, Y.-Y., Zheng, L., Qin, S.-H., Xu, X.-P., An, T.-X., … Wang, Q. (2017). Comparison of isolation methods of exosomes and exosomal RNA from cell culture medium and serum. *International Journal of Molecular Medicine*, *40*(3), 834–844. https://doi.org/10.3892/ijmm.2017.3080

Tao, S.-C., Guo, S.-C., & Zhang, C.-Q. (2017). Platelet-derived Extracellular Vesicles: An Emerging Therapeutic Approach. *International Journal of Biological Sciences*, *13*(7), 828. https://doi.org/10.7150/IJBS.19776

Tauro, B. J., Greening, D. W., Mathias, R. A., Mathivanan, S., Ji, H., & Simpson, R. J. (2013). Two Distinct Populations of Exosomes Are Released from LIM1863 Colon Carcinoma Cell-derived Organoids. *Molecular & Cellular Proteomics*, *12*(3), 587–598. https://doi.org/10.1074/mcp.M112.021303

Taylor, D D, & Gerçel-Taylor, C. (2005). Tumour-derived exosomes and their role in cancer-associated T-cell signalling defects. *British Journal of Cancer*, *92*(2), 305–311. https://doi.org/10.1038/sj.bjc.6602316

Taylor, Douglas D., & Shah, S. (2015). Methods of isolating extracellular vesicles impact down-stream analyses of their cargoes. *Methods*, *87*, 3–10. https://doi.org/10.1016/j.ymeth.2015.02.019

Taylor, Douglas D, & Gercel-Taylor, C. (2013). The origin, function, and diagnostic potential of RNA within extracellular vesicles present in human biological fluids. *Frontiers in Genetics*, *4*, 142. https://doi.org/10.3389/fgene.2013.00142

Tebaldi, T., Zuccotti, P., Peroni, D., Köhn, M., Gasperini, L., Potrich, V., … Quattrone, A. (2018). HuD Is a Neural Translation Enhancer Acting on mTORC1-Responsive Genes and Counteracted by the Y3 Small Non-coding RNA. *Molecular Cell*, *71*(2), 256-270.e10. https://doi.org/10.1016/j.molcel.2018.06.032

Teunissen, S. W. M. (2000). Conserved features of Y RNAs: a comparison of experimentally derived secondary structures. *Nucleic Acids Research*, *28*(2), 610–619. https://doi.org/10.1093/nar/28.2.610

Théry, C., Clayton, A., Amigorena, S., & Raposo, G. (2006). Isolation and Characterization of Exosomes from Cell Culture Supernatants. *Cell Biology*, 1–29.

Théry, C., Zitvogel, L., & Amigorena, S. (2002). Exosomes: composition, biogenesis and function. *Nature Reviews Immunology*, *2*(8), 569–579. https://doi.org/10.1038/nri855

Tian, Y., Ma, L., Gong, M., Su, G., Zhu, S., Zhang, W., … Yan, X. (2018). Protein Profiling and Sizing of Extracellular Vesicles from Colorectal Cancer Patients *via* Flow Cytometry. *ACS Nano*, *12*(1), 671–680. https://doi.org/10.1021/acsnano.7b07782

Trajkovic, K., Hsu, C., Chiantia, S., Rajendran, L., Wenzel, D., Wieland, F., … Simons, M. (2008). Ceramide

Triggers Budding of Exosome Vesicles into Multivesicular Endosomes. *Science*, *319*(5867), 1244–1247. https://doi.org/10.1126/science.1153124

Tricarico, C., Clancy, J., & D'Souza-Schorey, C. (2017). Biology and biogenesis of shed microvesicles. *Small GTPases*, *8*(4), 220–232. https://doi.org/10.1080/21541248.2016.1215283

Ulivi, P., Scarpi, E., Passardi, A., Marisi, G., Calistri, D., Zoli, W., … Amadori, D. (2015). eNOS polymorphisms as predictors of efficacy of bevacizumab-based chemotherapy in metastatic colorectal cancer: data from a randomized clinical trial. *Journal of Translational Medicine*, *13*(1), 258. https://doi.org/10.1186/s12967-015-0619-5

United Nations Environment Programme., International Labour Organisation., World Health Organization., & International Program on Chemical Safety. (2001). *Biomarkers in risk assessment : validity and validation*. World Health Organization.

Vagida, M., Arakelyan, A., Lebedeva, A., Grivel, J.-C., Shpektor, A., Vasilieva, E., & Margolis, L. (n.d.). FLOW ANALYSIS OF INDIVIDUAL BLOOD EXTRACELLULAR VESICLES IN ACUTE CORONARY SYNDROME. https://doi.org/10.1080/09537104.2016.1212002

Vagner, T., Spinelli, C., Minciacchi, V. R., Balaj, L., Zandian, M., Conley, A., … Di Vizio, D. (2018). Large extracellular vesicles carry most of the tumour DNA circulating in prostate cancer patient plasma. *Journal of Extracellular Vesicles*, *7*(1), 1505403. https://doi.org/10.1080/20013078.2018.1505403

Valadi, H., Ekström, K., Bossios, A., Sjöstrand, M., Lee, J. J., & Lötvall, J. O. (2007). Exosome-mediated transfer of mRNAs and microRNAs is a novel mechanism of genetic exchange between cells. *Nature Cell Biology*, *9*(6), 654–659. https://doi.org/10.1038/ncb1596

Valkonen, S., van der Pol, E., Böing, A., Yuana, Y., Yliperttula, M., Nieuwland, R., … Siljander, P. R. M. (2017). Biological reference materials for extracellular vesicle studies. *European Journal of Pharmaceutical Sciences*, *98*, 4–16. https://doi.org/10.1016/J.EJPS.2016.09.008

Van Cutsem, E., Köhne, C.-H., Hitre, E., Zaluski, J., Chang Chien, C.-R., Makhson, A., … Rougier, P. (2009). Cetuximab and Chemotherapy as Initial Treatment for Metastatic Colorectal Cancer. *New England Journal of Medicine*, *360*(14), 1408–1417. https://doi.org/10.1056/NEJMoa0805019

Van Der Pol, E., Van Gemert, M. J. C., Sturk, A., Nieuwland, R., & Van Leeuwen, T. G. (2012). Single vs. swarm detection of microparticles and exosomes by flow cytometry. *Journal of Thrombosis and Haemostasis*, *10*(5), 919–930. https://doi.org/10.1111/j.1538-7836.2012.04683.x

Van Deun, J., Mestdagh, P., Agostinis, P., Akay, Ö., Anand, S., Anckaert, J., … Hendrix, A. (2017). EV-TRACK: transparent reporting and centralizing knowledge in extracellular vesicle research. *Nature Methods*, *14*(3), 228–232. https://doi.org/10.1038/nmeth.4185

Van Deun, J., Mestdagh, P., Sormunen, R., Cocquyt, V., Vermaelen, K., Vandesompele, J., … Hendrix, A. (2014). The impact of disparate isolation methods for extracellular vesicles on downstream RNA profiling. *Journal of Extracellular Vesicles*, *3*, 1–14. https://doi.org/10.3402/jev.v3.24858

van Niel, G., D'Angelo, G., & Raposo, G. (2018). Shedding light on the cell biology of extracellular vesicles. *Nature Reviews Molecular Cell Biology*, *19*(4), 213–228. https://doi.org/10.1038/nrm.2017.125

Villarroya-Beltri, C., Gutiérrez-Vázquez, C., Sánchez-Cabo, F., Pérez-Hernández, D., Vázquez, J., Martin-Cofreces, N., … Sánchez-Madrid, F. (2013). Sumoylated hnRNPA2B1 controls the sorting of miRNAs into exosomes through binding to specific motifs. *Nature Communications*, *4*(1), 2980. https://doi.org/10.1038/ncomms3980

von Eyben, F. E., Baumann, G. S., & Baum, R. P. (2018). PSMA diagnostics and treatments of prostate cancer become mature. *Clinical and Translational Imaging*, *6*(2), 145–148. https://doi.org/10.1007/s40336-018-0270-2

Wan, Y., Cheng, G., Liu, X., Hao, S.-J., Nisic, M., Zhu, C.-D., … Zheng, S.-Y. (2017). Rapid magnetic isolation of extracellular vesicles via lipid-based nanoprobes. *Nature Biomedical Engineering*, *1*(4), 0058. https://doi.org/10.1038/s41551-017-0058

Wang, Z., & Yan, X. (2013). CD146, a multi-functional molecule beyond adhesion. *Cancer Letters*, *330*(2), 150–162. https://doi.org/10.1016/j.canlet.2012.11.049

Wei, Z., Batagov, A. O., Carter, D. R. F., Krichevsky, A. M., Quinn, J. F., Landgraf, P., … Salony. (2016). Fetal Bovine Serum RNA Interferes with the Cell Culture derived Extracellular RNA. *Scientific Reports*, *6*, 31175. https://doi.org/10.1038/srep31175

Wei, Z., Batagov, A. O., Schinelli, S., Wang, J., Wang, Y., El Fatimy, R., … Krichevsky, A. M. (2017a). Coding and noncoding landscape of extracellular RNA released by human glioma stem cells. *Nature Communications*, *8*(1), 1145. https://doi.org/10.1038/s41467-017-01196-x

Wei, Z., Batagov, A. O., Schinelli, S., Wang, J., Wang, Y., El Fatimy, R., … Krichevsky, A. M. (2017b). Coding and noncoding landscape of extracellular RNA released by human glioma stem cells. *Nature Communications*, *8*(1), 1145. https://doi.org/10.1038/s41467-017-01196-x

Welch, J. L., Madison, M. N., Margolick, J. B., Galvin, S., Gupta, P., Martínez-Maza, O., … Okeoma, C. M. (2017). Effect of prolonged freezing of semen on exosome recovery and biologic activity. *Scientific Reports*, *7*(1), 45034. https://doi.org/10.1038/srep45034

Wick, W., Dettmer, S., Berberich, A., Kessler, T., Karapanagiotou-Schenkel, I., Wick, A., … Platten, M. (2019). N2M2 (NOA-20) phase I/II trial of molecularly matched targeted therapies plus radiotherapy in patients with newly diagnosed non-MGMT hypermethylated glioblastoma. *Neuro-Oncology*, *21*(1), 95–105. https://doi.org/10.1093/neuonc/noy161

Willms, E., Cabañas, C., Mäger, I., Wood, M. J. A., & Vader, P. (2018). Extracellular Vesicle Heterogeneity: Subpopulations, Isolation Techniques, and Diverse Functions in Cancer Progression. *Frontiers in Immunology*, *9*, 738. https://doi.org/10.3389/fimmu.2018.00738

Willms, E., Johansson, H. J., Mäger, I., Lee, Y., Blomberg, K. E. M., Sadik, M., … Vader, P. (2016). Cells release subpopulations of exosomes with distinct molecular and biological properties. *Scientific Reports*, *6*(1), 22519. https://doi.org/10.1038/srep22519

Witwer, K. W., Buzás, E. I., Bemis, L. T., Bora, A., Lässer, C., Lötvall, J., … Hochberg, F. (2013). Standardization of sample collection, isolation and analysis methods in extracellular vesicle research. *Journal of Extracellular Vesicles*, *2*, 1–25. https://doi.org/10.3402/jev.v2i0.20360

Wolf, P. (1967). The nature and significance of platelet products in human plasma. *British Journal of Haematology*, *13*(3), 269–288. Retrieved from http://www.ncbi.nlm.nih.gov/pubmed/6025241

Wright, P. K., Jones, S. B., Ardern, N., Ward, R., Clarke, R. B., Sotgia, F., … Lamb, R. (2014). 17β-estradiol regulates giant vesicle formation via estrogen receptor-alpha in human breast cancer cells. *Oncotarget*, *5*(10), 3055. https://doi.org/10.18632/ONCOTARGET.1824

Xu, R., Greening, D. W., Rai, A., Ji, H., & Simpson, R. J. (2015). Highly-purified exosomes and shed microvesicles isolated from the human colon cancer cell line LIM1863 by sequential centrifugal ultrafiltration are biochemically and functionally distinct. *Methods*, *87*, 11–25.

https://doi.org/10.1016/j.ymeth.2015.04.008

Xu, R., Greening, D. W., Zhu, H.-J., Takahashi, N., & Simpson, R. J. (2016). Extracellular vesicle isolation and characterization: toward clinical application. *The Journal of Clinical Investigation*, *126*(4), 1152–1162. https://doi.org/10.1172/JCI81129

Xu, R., Rai, A., Chen, M., Suwakulsiri, W., Greening, D. W., & Simpson, R. J. (2018). Extracellular vesicles in cancer — implications for future improvements in cancer care. *Nature Reviews Clinical Oncology*, *15*(10), 617–638. https://doi.org/10.1038/s41571-018-0036-9

Yoshioka, Y., Konishi, Y., Kosaka, N., Katsuda, T., Kato, T., & Ochiya, T. (2013). Comparative marker analysis of extracellular vesicles in different human cancer types. *Journal of Extracellular Vesicles*, *2*(1), 20424. https://doi.org/10.3402/jev.v2i0.20424

Yoshioka, Y., Kosaka, N., Konishi, Y., Ohta, H., Okamoto, H., Sonoda, H., … Ochiya, T. (2014). Ultra-sensitive liquid biopsy of circulating extracellular vesicles using ExoScreen. *Nature Communications*, *5*(1), 3591. https://doi.org/10.1038/ncomms4591

Yuana, Y., Böing, A. N., Grootemaat, A. E., van der Pol, E., Hau, C. M., Cizmar, P., … Nieuwland, R. (2015). Handling and storage of human body fluids for analysis of extracellular vesicles. *Journal of Extracellular Vesicles*, *4*, 29260. https://doi.org/10.3402/jev.v4.29260

Yuana, Y., Levels, J., Grootemaat, A., Sturk, A., & Nieuwland, R. (2014). Co-isolation of extracellular vesicles and high-density lipoproteins using density gradient ultracentrifugation. *Journal of Extracellular Vesicles*, *3*(1), 23262. https://doi.org/10.3402/jev.v3.23262

Zaborowski, M. P., Balaj, L., Breakefield, X. O., & Lai, C. P. (2015). Extracellular Vesicles: Composition, Biological Relevance, and Methods of Study. *BioScience*, *65*(8), 783–797. https://doi.org/10.1093/biosci/biv084

Zhang, H., & Lyden, D. (2019). Asymmetric-flow field-flow fractionation technology for exomere and small extracellular vesicle separation and characterization. *Nature Protocols*, *14*(4), 1027–1053. https://doi.org/10.1038/s41596-019-0126-x

Zhang, J., & Zhang, S. (2017). Discovery of cancer common and specific driver gene sets. *Nucleic Acids Research*, *45*(10), e86. https://doi.org/10.1093/NAR/GKX089

Zhang, L., Zhang, S., Yao, J., Lowery, F. J., Zhang, Q., Huang, W.-C., … Yu, D. (2015). Microenvironment-induced PTEN loss by exosomal microRNA primes brain metastasis outgrowth. *Nature*, *527*(7576), 100–104. https://doi.org/10.1038/nature15376

Zhang, R.-Q., Shi, Z., Chen, H., Chung, N. Y.-F., Yin, Z., Li, K. K.-W., … Ng, H.-K. (2016). Biomarker-based prognostic stratification of young adult glioblastoma. *Oncotarget*, *7*(4), 5030–5041. https://doi.org/10.18632/oncotarget.5456

Zhang, R., Chen, B., Tong, X., Wang, Y., Wang, C., Jin, J., … Li, W. (2018). Diagnostic accuracy of droplet digital PCR for detection of EGFR T790M mutation in circulating tumor DNA. *Cancer Management and Research*, *10*, 1209–1218. https://doi.org/10.2147/CMAR.S161382

Zhang, X., Yuan, X., Shi, H., Wu, L., Qian, H., & Xu, W. (2015). Exosomes in cancer: small particle, big player. *Journal of Hematology & Oncology*, *8*, 83. https://doi.org/10.1186/s13045-015-0181-x

Zhao, C., Wang, H., Xiong, C., & Liu, Y. (2018). Hypoxic glioblastoma release exosomal VEGF-A induce the permeability of blood-brain barrier. *Biochemical and Biophysical Research Communications*, *502*(3), 324–331. https://doi.org/10.1016/j.bbrc.2018.05.140

Żmigrodzka, M., Guzera, M., Miśkiewicz, A., Jagielski, D., & Winnicka, A. (2016). The biology of extracellular vesicles with focus on platelet microparticles and their role in cancer development and progression. *Tumor Biology*, *37*(11), 14391–14401. https://doi.org/10.1007/s13277-016-5358-6

Zong, H., Parada, L. F., & Baker, S. J. (2015). Cell of origin for malignant gliomas and its implication in therapeutic development. *Cold Spring Harbor Perspectives in Biology*, *7*(5). https://doi.org/10.1101/cshperspect.a020610

EBioMedicine 43 (2019) 114–126

Contents lists available at ScienceDirect

EBioMedicine

journal homepage: www.ebiomedicine.com

EBioMedicine
Published by THE LANCET

Ultrasensitive detection of cancer biomarkers by nickel-based isolation of polydisperse extracellular vesicles from blood

Michela Notarangelo [a], Chiara Zucal [a], Angelika Modelska [a], Isabella Pesce [b], Giorgina Scarduelli [c], Cristina Potrich [d], Lorenzo Lunelli [d], Cecilia Pederzolli [d], Paola Pavan [e], Giancarlo la Marca [f], Luigi Pasini [g], Paola Ulivi [g], Himisha Beltran [h], Francesca Demichelis [a], Alessandro Provenzani [a,1], Alessandro Quattrone [a,1], Vito G. D'Agostino [a,*,1]

[a] Department of Cellular, Computational and Integrative Biology (CIBIO), University of Trento, Via Sommarive 9, Trento 38123, Italy
[b] Cell Analysis and Separation Core Facility (CIBIO), University of Trento, Via Sommarive 9, Trento 38123, Italy
[c] Advanced Imaging Core Facility (CIBIO), University of Trento, Via Sommarive 9, Trento 38123, Italy
[d] Fondazione Bruno Kessler (FBK), Laboratory of Biomolecular Sequence and Structure Analysis for Health, Trento, Via Sommarive 14, Trento 38123, Italy
[e] Immunohematology and Cell Factory Unit, Meyer Children's University Hospital, Viale Pieraccini 24, Florence 50139, Italy
[f] Department of Experimental and Clinical Biomedical Sciences, Centro di Eccellenza Denothe, Aou Meyer University of Florence, Viale Pieraccini 6, 50139, Italy
[g] Istituto Scientifico Romagnolo per lo Studio e la Cura dei Tumori (IRST) IRCCS, Via Piero Maroncelli 40, Meldola 47014, Italy
[h] Department of Medical Oncology, Dana Farber Cancer Institute, Boston, MA, USA

ARTICLE INFO

Article history:
Received 18 January 2019
Received in revised form 6 April 2019
Accepted 18 April 2019
Available online 29 April 2019

Keywords:
Cancer
Biomarkers
Extracellular vesicles
Liquid biopsy
Nickel
Alpha
Droplet PCR

ABSTRACT

Background: Extracellular vesicles (EVs) are secreted membranous particles intensively studied for their potential cargo of diagnostic markers. Efficient and cost-effective isolation methods need to be established for the reproducible and high-throughput study of EVs in the clinical practice.
Methods: We designed the nickel-based isolation (NBI) to rapidly isolate EVs and combined it with newly-designed amplified luminescent proximity homogeneous assay or digital PCR to detect biomarkers of clinical utility.
Findings: From plasma of 46 healthy donors, we systematically recovered small EV (~250 nm of mean diameter; ~3×10^{10}/ml) and large EV (~560 nm of mean diameter; ~5×10^{8}/ml) lineages ranging from 50 to 700 nm, which displayed hematopoietic/endothelial cell markers that were also used in spike-in experiments using EVs from tumor cell lines. In retrospective studies, we detected picomolar concentrations of prostate-specific membrane antigen (PSMA) in fractions of EVs isolated from the plasma of prostate cancer patients, discriminating them from control subjects. Directly from oil-encapsulated EVs for digital PCR, we identified somatic *BRAF* and *KRAS* mutations circulating in the plasma of metastatic colorectal cancer (CRC) patients, matching 100% of concordance with tissue diagnostics. Importantly, with higher sensitivity and specificity compared with immuno-isolated EVs, we revealed additional somatic alterations in 7% of wild-type CRC cases that were subsequently validated by further inspections in the matched tissue biopsies.
Interpretation: We propose NBI-combined approaches as simple, fast, and robust strategies to probe the tumor heterogeneity and contribute to the development of EV-based liquid biopsy studies.
Fund: Associazione Italiana per la Ricerca sul Cancro (AIRC), Fondazione Cassa di Risparmio Trento e Rovereto (CARITRO), and the Italian Ministero Istruzione, Università e Ricerca (Miur).

1. Introduction

Extracellular vesicles (EVs) are membranous particles, composed of a lipid bilayer, that are massively secreted in biological fluids, where they are involved in cell-to-cell communication [1–3]. According to different mechanisms of biogenesis [4], EVs are classified into exosomes and microvesicles (or ectosomes), derivatives of the endosomal system or produced by outward budding of the plasma membrane, respectively

* Corresponding author at: Department of Cellular, Computational and Integrative Biology (CIBIO), University of Trento, Via Sommarive 9, Trento 38123, Italy.
E-mail addresses: himisha_beltran@dfci.harvard.edu (H. Beltran), vito.dagostino@unitn.it (V.G. D'Agostino).
[1] Co-last authors.

https://doi.org/10.1016/j.ebiom.2019.04.039

Research in context

Evidence before this study

The abundance and biological content of heterogeneous EVs in biological fluids qualify them as an attractive source of diagnostic markers. However, reproducible and efficient isolation methods need to be established for application in clinical practice. Rapid approaches that minimize protein contaminants exploited the surface charge of EVs to capture them.

Added value of this study

We designed a rapid and cost-effective procedure to obtain EVs in a physiological pH solution, while preserving vesicles' integrity/stability and minimizing particle aggregation. We exploited these advantages to combine this approach with highly sensitive immobilization-independent assays to detect cancer biomarkers, i.e. specific proteins or RNA species present in EVs. We show that a comprehensive isolation of EVs offers a strategic advantage for detecting tumor biomarkers from liquid biopsy.

Implications of all the available evidence

This study indicates the possibility of detecting, from circulating EVs, rare somatic alterations in driver genes that mirror the heterogeneity of tumor cells present in the matched tissue biopsies.

[4]. EVs are highly heterogeneous in size and molecular composition [5]: exosomes are generally smaller than 150 nm and microvesicles can overlap to some extent, ranging from 100 to 1000 nm; insights into their sub-cellular origin are usually obtained post-isolation by detecting the enrichment of specific markers [6]. For these reasons, the term small/large EVs can be also used to refer to a mixed population of vesicles with a defined range of size [7]. Recently, EVs have been studied in the frame of the modulation of the tumor microenvironment and inflammation [8]/immune surveillance [9], or also investigated as carriers of therapeutics [10]. The high abundance of circulating EVs and a biological composition reflecting the cell of origin [11] qualify them as attractive diagnostic tool [12]. This potential has been recently demonstrated from liquid biopsies by detecting cancer biomarkers with recognized clinical utility, for example in the case of circulating levels of *EGFR* in lung cancer [13] and breast cancer [14] patients or *EGFR* mutations in pulmonary adenocarcinoma patients [14,15]; in the case of $KRAS^{G12D}$ and $TP53^{R273H}$ mutations in patients with advanced or early-stage pancreatic cancer [16,17]; in the case of copy number variations that matched genes frequently altered in metastatic prostate cancer patients [18].

However, the application of EVs into the clinical practice is still limited by low-throughput, time-consuming isolation procedures and the sensitivity and specificity of the results are highly dependent on the methods used to enrich them. Given their nanoscale dimensions, many technical challenges have been addressed to isolate them with purity and reproducibility [19]. The methods more frequently employed include differential and/or density gradient ultracentrifugation, immunocapture, microfiltration/size exclusion, or precipitation with hydrophobic agents [20]. The differential ultracentrifugation (UC) is the most widely applied [21], as it concentrates the vesicles and allows for size-based sedimentation of EVs according to the *g*-force applied without interferences from chemical additives, especially in view of downstream applications. In this case, the yield and the purity of the obtained EVs [22] are influenced by different protocol settings and challenged by co-sedimentation of protein aggregates [19]. For these reasons, new antibody-based strategies or EV-targeting probes have been developed to recognize and immobilize the vesicles for subsequently detecting specific biomarkers [23–25]. These methods offer excellent throughput for identifying co-expression of antigens that decorate EVs, which should be deeply investigated in terms of quantitative/spatial distribution as potentially influenced by the cell status [5].

Alternative rapid EV-isolation procedures proven to reduce protein contaminants, in comparison with ultracentrifugation, exploited the negative surface charge of EVs [26–28]. These approaches are based on the principle that, under physiological conditions (pH > 5), heterogeneous EVs display negative fluctuations of zeta potential (ZP), which is a physicochemical parameter that quantifies the surface charge of biological particles [29]. ZP is highly dependent on pH, salt concentrations, temperature, and on the specific biochemical composition of the particles themselves [30]. Technologies like dynamic light scattering (DLS) [31] and tunable resistive pulse sensing (TRPS) [32] have been used to monitor the ZP of heterogeneous EVs, that encompasses −40 to −7 mV in PBS at pH 7.4 [33]. These values ensure the presence of a net negative surface charge that has been exploited to capture EVs and subsequently release them by modulating the pH and the ionic strength in the elution buffer.

In this work we describe an alternative strategy, named nickel-based isolation (NBI), that exploits a matrix of beads properly functionalized with nickel cations to capture heterogeneous EVs and the possibility to efficiently reverse the binding using a synergy of chelating agents (EDTA and citric acid) in PBS buffer (pH 7.4). NBI allowed a rapid enrichment of dimensionally heterogeneous (polydisperse) EVs in solution preserving their integrity and stability.

We characterized the performances of NBI in comparison with the gold standard differential ultracentrifugation and assessed the presence of specific hematopoietic-endothelial antigens on the surface of plasma-isolated EVs to ensure the unbiased enrichment of heterogeneous EV lineages by NBI. Importantly, the possibility to directly use NBI-isolated EVs as individual particles in no-wash, immobilization-independent assays allowed us to implement the amplified luminescent proximity homogeneous assay (alpha) and a new droplet digital PCR (ddPCR) protocol to detect cancer-specific markers on EVs from the plasma of oncological patients with an unprecedented resolution from liquid biopsy.

2. Materials and methods

2.1. Cell cultures

Glioblastoma cells U87-MG (ATCC® HTB-14™); breast adenocarcinoma cell lines MCF7 (ICLC; HTL95021) and MDA-MB-231 (ICLC; HTL99004), neuroblastoma SH-SY5Y (ATCC® CRL-2266™), prostate adenocarcinoma PC-3 (ATCC® CRL-1435™), and melanoma SK-MEL-28 (ATCC® HTB-72™) cells were grown in DMEM, except for PC-3 cell line that was cultured in standard conditions in RPMI 1640 Medium, supplemented with 10% Fetal Bovine Serum, 2 mM L-glutamine, and 100 U/ml penicillin +100 μg/ml streptomycin (all from Life Technologies, Carlsbad, CA, USA) to obtain complete medium. Generally, to obtain extracellular vesicles (EVs)-containing media, cells were initially grown in complete medium until reaching 75% confluence (usually 48 h); then, after two gentle washes with PBS, cells were incubated with serum-free medium for 24 h. Cells were plated in different plastic formats according to the experiments to be performed, but the density of them was kept constant at $3.2 \pm 0.2 \times 10^4/cm^2$ otherwise differently stated in the figure legends.

Before starting NBI procedure, collected media were centrifuged at 2800*g* for 10 min and carefully transferred to new tubes.

For the experiments in Fig. 2a, dFBS condition refers to NBI performed in media containing 100 K ultracentrifuged FBS at final concentration of 10%. These media have been diluted 1:10 with PBS to reduce viscosity of the solution.

For cell density experiments in Fig. 2B, U-87-MG, MDA-MB-231, SH-SY5Y, MCF7 and PC-3 cell lines were plated in triplicates in 6-well plates with these numbers per well: 3.4×10^5; 1.7×10^5; 8.5×10^4; 4.2×10^4; 2.1×10^4 and 1.0×10^4. After 48 h of incubation in complete medium, cells were washed twice with PBS and then incubated for 24 h with serum-free medium before starting with NBI protocol. In this case, after removing EVs-containing media, adherent cells were fixed with 4% paraformaldehyde, stained with Hoechst33342 and washed with PBS for high content imaging analysis using Operetta instrument (Perkin Elmer). Images were acquired at 10× magnification and 50 fields/well were analysed by Harmony software. EVs were analysed by TRPS using qNano (IZON Science).

2.2. EVs isolation by differential ultracentrifugation

EVs produced by U87-MG cells grown in T150 flasks (CLS430823-50EA) were isolated by differential ultracentrifugation according to the protocol by Di Vizio et al. [34] with minor modifications. Briefly, after 24 h of incubation with cells serum-free media were collected in falcon tubes and centrifuged at 2800*g* for 10 min at 4 °C to mainly remove cell debris and apoptotic bodies. Then, the supernatants were transferred to ultracentrifuge tubes (Polyallomer Quick-Seal centrifuge tubes 25 × 89 mm, Beckman Coulter) and centrifuged at 10,000*g* for 30 min at 4 °C in the Optima XE-90 (Beckman Coulter) instrument with SW 32 Ti rotor. This step allowed to preferentially precipitate larger particles (less apoptotic bodies, microvesicles), that were gently resuspended in filtered PBS (Res1). Thereafter, supernatants were further centrifuged at 100,000*g* for 70 min at 4 °C to pellet smaller particles. Pellets were resuspendend in filtered PBS (Res2). The volumes of Res1 and Res2 were pooled and stored a −80 °C or kept at 4 °C to proceed with TRPS analyses. For experiments involving OptiPrep density gradient (ODG) preparations, we followed the protocol reported by Van Deun et al. [35], but starting from a volume of 200 ul of PBS, that resuspended the pellet of 100,000 *g* ultracentrifuged particles, loaded on the top of 5–40% iodixanol gradient. After ultracentrifugation, we pooled the fractions 8 to 10 and analysed by immunoblotting the pellet obtained by re-centrifugation at 100,000*g* for 2 h from a 3 ml solution.

2.3. Flow cytometry analysis of microvesicles

Vesicles obtained by differential ultracentrifugation or NBI were diluted in 0.22 μm filtered PBS and background signal was set up on filtered PBS and the light scattering threshold level was adjusted to allow an event rate of ≤5 events per second.

Light scattering detection was performed in log mode, the assigned voltages for FSC and SSC were 300 and 310 V, respectively, and the threshold was set at 200 for both signals. Acquisition was performed at low flow rate and samples were properly diluted to avoid coincidence and swarm effects. Bead standards of 1 and 10 μm (Invitrogen) were used to set gates for microvesicles. A number of 10,000 events was counted or at least 1 min recording for each sample. Sample acquisition was performed on a FACS Canto flow-cytometer (BD Biosciences) and data analysis using BD Diva software (BD Biosciences).

2.4. Nickel-based isolation (NBI)

Positively charged agarose beads (GE Healthcare, 17-5268-01) were prepared with a suspension of 20 mg/ml in PBS containing 190 mM of $NiSO_4$ (Sigma, 656895). Residual amount of cations was removed by repeated PBS washing and centrifugation and beads were stored at 4 °C for up to 1 month.

The capture of EVs has been optimized using 20 μl/ml of beads from the prepared suspension and entirely performed at room temperature. An excess of beads ensured better reproducibility and maximal EVs recovery. Briefly, beads were gently added on the upper surface of the EVs-containing medium and the solution placed in orbital shaking for 30 min, well homogenized during incubation. Thereafter, tubes were gently centrifuged (~200*g*) and then maintained in vertical position for 5 min to allow beads to settle down by gravity. The elution buffer, freshly prepared by diluting solution A (3.2 mM EDTA, ThermoFisher, UltraPure pH 8.0, 15575020) and B (10 mM NaCl, Sigma, 450006, 45 μM citric acid, Sigma, 251275) in 0.22 μm-filtered PBS allowed competitive EVs-beads dissociation and release of EVs in solution at physiological pH (7.4).

2.5. Transmission electron microscopy (TEM)

The vesicles were visualized using conventional transmission EM (TEM). Briefly, a 5 μl aliquot of a purified sample, fixed in elution buffer with 2.5% formaldehyde, was applied to 300-square mesh copper-nickel grids coated with a thin carbon film. The grids were subsequently negatively stained with 1% buffered uranyl acetate, pH 4.5, and observed using a TEM FEI Tecnai G2 Spirit microscope operating at 100 kV and equipped with an Olympus Morada side-mount 2Kx4K charge-coupled device camera (magnification used: 20500× and 87,000×).

2.6. TRPS (tunable resistive pulse sensing)

Size and concentration of the EVs were characterized by TRPS using qNano (IZON Science). An average of 500 particles were counted for each sample, except for experiments performed in 6-well plates (Fig. 2B, Fig. 3, and Fig. S4) or in samples where the particle rate was below 100 particle/min, in which at least 2 min recording time was used. NP200 (A40948, A43545, A43667, A43667), NP400 (A43592, A44117, A44116), NP800 (A40542, A36164, A40548, A44118) and N1000 (A40572) nanopores, stretched between 45.5 and 47 mm were used. Voltage was set in between 0.12 and 0.68 to achieve and maintain a stable current in the range of 95–130 nA, noise below 7–12 pA and particle count rate linear. The calibration beads CPC100B (Batch ID: B8748N), CPC200B (Batch ID: B6481M), CPC500E (Batch ID: 659543B), CPC800E (Batch ID: 634561B) and CPC1000F (Batch ID: 669582B) with mean diameters of 114 nm, 210 nm, 500 nm, 710 nm and 940 nm, respectively, were from iZON Science. All the qNANO data were recorded and analysed by Izon Control Suite v.3.

2.7. Protein competitive assay

The step of EVs elution has been challenged by a competitive assay in which 10 ml of medium containing EVs deriving from U87 cells was supplemented with 30 μg/ml of DH5α *E. coli* crude extract and with 15 μg/ml of purified histidine-tagged recombinant proteins (T7 RNA pol, 110 kDa; HuR, 36 kDa; YTH, 23 kDa). Briefly, DH5α cells were grown in LB medium until they reached an OD_{600} of 0.5 and were harvested by centrifugation at 6000*g* for 5 min. Pellet was resuspended in 3 ml of DMEM medium +1 μg/ml lysozyme and sonicated at 4 °C in water bath for 7 cycles (40 amplitude, 7 s *on*, 10 s *off*). Lysate was clarified by centrifugation at 13,000*g* for 20 min and then filtered with 0.2 μm membrane disposals prior to be spiked to the EVs-containing medium. Histidine-tagged recombinant T7 RNA polymerase was kindly provided by Dr. S. Mansy's lab (CIBIO, University of Trento); recombinant HuR [36] and YTH [37] proteins produced and purified as previously described.

NBI was performed with incubation times and reagents already described, except for the gradient of elution solutions as indicated in Fig. 1b. Protein samples were quantified using BCA and Bradford assays according to the manufacturer's instructions. Equal volume of eluates were loaded on 12% SDS-PAGE for subsequent Sypro Ruby staining or western blotting using a 1:1000 dilution of a primary anti-histidine antibody (ab1187).

Number and size of recovered particles were analysed by TRPS, in all the fractions, using NP800, NP400, and NP200 nanopores.

For IP with apolipoproteins, 50 μg of whole cell lysate and the lysate of EVs isolated from the media of three T150 flasks per each condition: UC and NBI) were separated by a pre-cast gradient SDS-PAGE (Bolt™ 4–12% Bis-Tris Plus Gels, 12-well, Invitrogen) and transferred to a polyvinylidene difluoride membrane (Amersham Hybond P 0.2 μm PVDF) overnight. After blocking with 5% nonfat milk in TBS-T (10 mM Tris, pH 8.0, 150 mM NaCl, 0.1% Tween 20) for 60 min, the membrane was incubated in 1% milk TBS-T with antibodies against Apo B100 (ab7616, Abcam, 1:1000), Apo A1 (ab7613, Abcam, 1:1000), Syntenin (1:1000), Flotillin-1 (1:1000), Alix (1:1000) at 4 °C overnight. Membranes were washed three times for 5 min and incubated with horseradish peroxidase-conjugated anti-goat, anti-rabbit or anti-mouse secondary antibodies for 1–2 h. Blots were washed with TBS-T three times and the immunoblot signal was revealed using the chemiluminescent ECL Select detection reagent (GE Healthcare Amersham, UK).

2.8. Preparation of exosome-like liposomes

The lipid composition of exosome-like vesicles was: 20% mol egg phosphatidylcholine, 10% mol egg phosphatidylethanolamine, 15% mol dioleoylphosphatidylserine, 15% mol egg sphingomyelin, 40% mol cholesterol (adapted from literature [38,39]). Lipid films were formed by removing the organic solvent (i.e. chloroform) from a lipid solution by rotary evaporation and vacuum drying for at least 1 h. Lipids at a

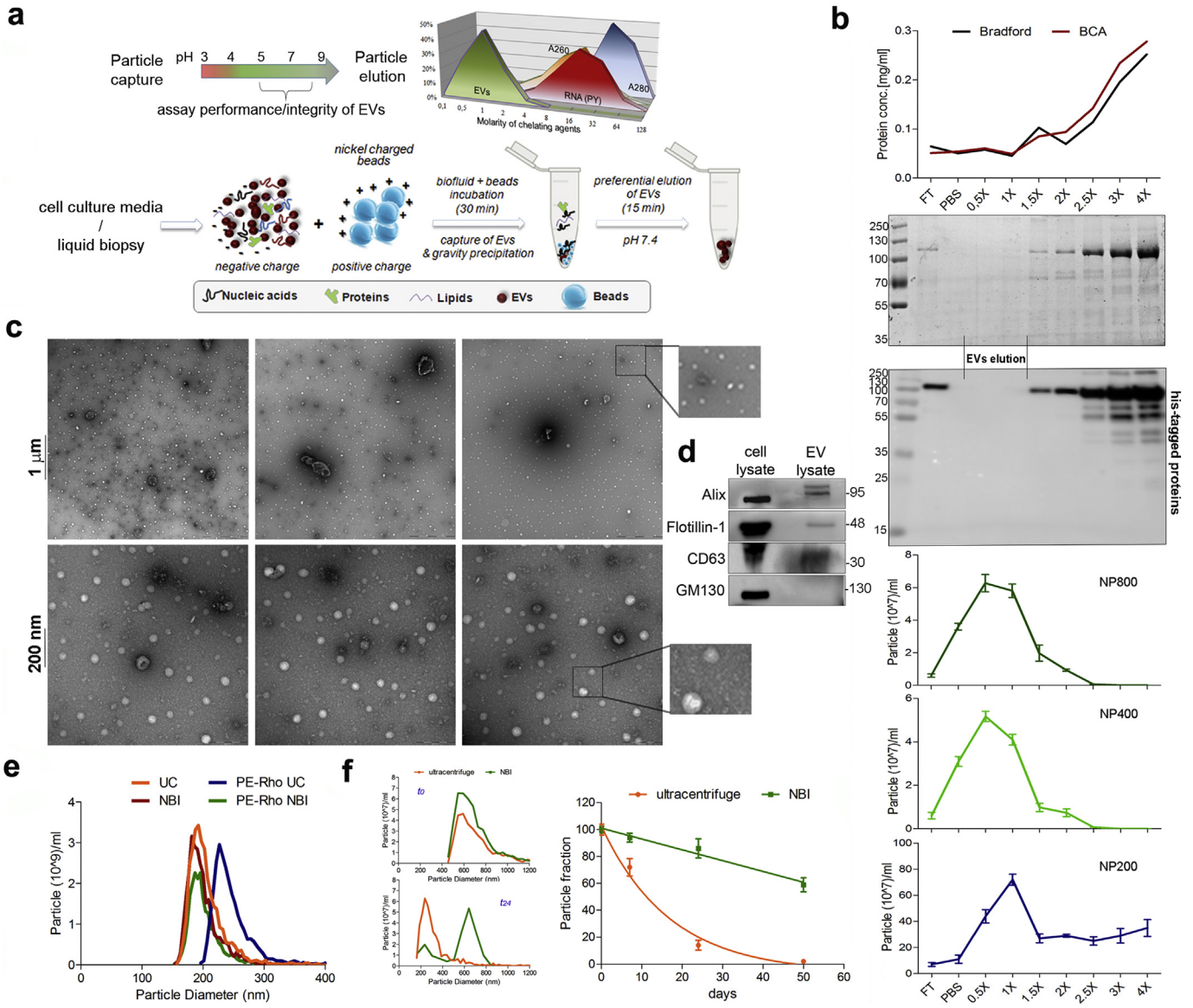

Fig. 1. Rapid purification of EVs by NBI preserving their integrity, dispersity, and stability in solution. a) At pH values >5 the net negative charge of membranous particles makes them susceptible to electrostatic interactions. Using 1–3 mM of chelating agents, TRPS analyses detected particles in the 500–700 nm range of size, selectively eluted from a functionalized stationary phase in contrast to nucleic acids (A260), proteins (A280), or pre-stained ssRNA (RNA Y) pre-incubated with nickel-agarose beads. The procedural steps highlighting the rapid NBI procedure are depicted. b) Competitive assay in serum-free medium containing 500 μg/ml of DH5α protein extract and of 50 μg/ml each of purified his-tagged proteins (T7p07, HuR, YTH domain). Two parallel gels were exposed to SYPRO Ruby or blotted on PVDF membrane to detect hstidine (tag known to confer the strongest interaction with Ni). The 1× solution is the optimized buffer and the flow-through (FT) is the medium after beads sedimentation. qNANO analyses with indicated nanopores were performed and *SD* refers to two independent experiments. c) Transmission electron microscopy (TEM) acquisitions, with 3 fields at 20.500× (1 μm) + 5× magnification and 3 fields at 87.000× (200 nm) + 5× magnification, of NBI samples fixed with 2.5% paraformaldehyde in the elution buffer. The original scale bars are embedded at the bottom right, but also added manually on the left side for better visualization. d) Western blot analyses on EV lysate (recovered by 14×10^6 cells) and on 1% total cell lysate (TCL) of U87 cells. e) Mixture of 4.2×10^9 liposomes with a diameter of 181 ± 23.8 nm recovered by ultracentrifugation (UC) or NBI. The same experiment has been replicated with phosphatidylethanolamine-rhodamine (5 ng/ml) stain (PE-Rho) of liposomes prior UC or NBI processing. f) EVs were isolated by UC or NBI from 3 ml of serum-free medium of U87 cells and analysed at (*t0*) or after 24 days (*t24*, stored at 4 °C). Repeated measurements by TRPS have been performed until 52 days post-purification and the relative half-live of the 600 nm populations have been calculated with GraphPad Prism software v.5.

final concentration of 1 mg/mL, were swollen in DPBS and vortexed vigorously to give multilamellar liposomes, which were further exposed to 6 cycles of freezing and thawing. Exosome-like liposomes were prepared by extruding a suspension of multilamellar liposomes with a two-syringes extruder (LiposoFast Basic Unit, Avestin Inc.). Thirty-one passages were performed through two stacked polycarbonate filters (Millipore) with pores of different average diameters to obtain differently sized vesicles [40], then measured by photon correlation spectroscopy with a Zeta Sizer instrument (Nano-ZS, Malvern Instruments).

2.9. Blood samples

Plasma samples derived from patients with metastatic colon cancer were provided by the IRST Cancer Center. All patients gave informed consent before blood sampling, approved by the Local Ethics Committee. Patients' tumors were characterized for BRAF status by MassARRAY (Sequenom, San Diego, CA, USA) using the Myriapod Colon status (Diatech Pharmacogenetics, Jesi, Italy). Plasma was obtained from peripheral blood collected in EDTA-tubes, after centrifugation at 3000 rpm for 15 min, and stored at −80 °C until EV isolation.

Whole blood from healthy donors were collected at Meyer Children's University Hospital. Plasma samples were collected into commercially available anticoagulant-treated tubes EDTA-treated (lavender tops), serum samples in red topped tubes. The venous blood in EDTA tube was shipped on cold packs from hospital blood collection unit to the laboratory. Informed consent were obtained from donors before the sample analysis.

Plasma has been obtained by removing cells after centrifugation for 10 min at 2000*g* using a refrigerated (4 °C) centrifuge (Eppendorf 5702 R, Milan, Italy). Serum samples have been obtained allowing the blood to clot by leaving it undisturbed at room temperature for 30 min. The clot has been removed by spin down at 2000*g* using a refrigerated (4 °C) centrifuge (Eppendorf 5702 R, Milan, Italy). Blood count were performed using a Sysmex XE-5000 hematology analyzer (Sysmex America, Mundelein, IL). The analytic procedure was conducted according to the manufacturer's instructions.

Blood from metastatic prostate cancer patients was obtained at Weill Cornell Medicine (WCM) after informed consent (IRB #1305013903). Whole blood (Streck Cell-Free DNA BCT) was centrifuged at 1600 $g \times 10$ min at 4 °C within 3 h after blood collection. The plasma layer was transferred to 2 ml microcentrifuge tubes and centrifuged at 16,000 $g \times 10$ min at 4 °C. The plasma was then collected and stored at −80 °C. Complete blood counts (CBC) was performed in the WCM clinical lab and results obtained from chart review.

Immunodepletion of NBI-purified vesicles has been performed using biotinylated anti CD235a (130-100-271) and anti CD41a (130-105-608) from Miltenyl Biotec, anti-AL-CAM (sc-74558), anti-MEL-CAM (sc-18837), anti CD45 (sc-1187) from SantaCruz Biotechnology, and streptavidin (11205D) or protein-G (10003D) dynabeads from Thermo Fisher Scientific. Vesicles after beads precipitation have been measured by qNANO and normalized to the number of particles in the counterpart control samples with equivalent amount of biotin (Sigma, B4501).

2.10. Tumor sample analysis

Formalin fixed and paraffin included (FFPE) patients' tumor samples, used for routinary molecular diagnostic, were selected for containing an area of at least 50% of tumor cells, based on hematoxylin and eosin staining. Tumor genomic DNA was extracted with QIAamp DNA Micro kit (QIAGEN, Hilden, Germany), following the manufacturer's protocol, and DNA quantity and quality was determined at Nanodrop (CELBIO, Milan, Italy). Characterization of BRAF status was performed by Pyrosequencing with the anti-EGFR MoAb response® BRAF status assay (Diatech Pharmacogenetics, Jesi, Italy): 50 ng of starting FFPE genomic DNA were amplified and reactions were run on the PyroMark Q96 ID system (QIAGEN), according to Diatech Pharmacogenetics protocol. For samples 7, 12, 13, 23, and 26, Qualitative detection of BRAF-V600E and KRAS-G12D/G12C mutations was repeated on 30 ng of tumor DNA, by using either the Easy®BRAF kit or the Easy®KRAS kit, on Corbett Rotor-Gene 6000 (QIAGEN), following manufacturer's instructions (Diatech Pharmacogenetics). The assay allows the detection of low percentages of mutated allele by real-time amplification with sequence-specific probes: positivity for BRAF-V600E was considered over the internal BRAF control, as a delta Ct lover than 12.5 cycles, and setting the detection threshold on 0.04, according to the guidelines of Diatech Pharmacogenetics.

2.11. RNA extraction

Total RNA was extracted using QIAzol reagent (QIAGEN) according to the manufacturer's instructions with several modifications. Briefly, 100 μl of QIAzol was added directly to the beads before the elution step of NBI, vortexed and incubated for 5 min at room temperature, supplemented with 20 μl of chloroform, shaken vigorously for 15 s and incubated at room temperature for 3 min. Phases were separated by centrifugation at 12,000*g* for 15 min at 4 °C, and the upper phase was recovered. After addition of 1 μl of glycogen (20 mg/ml) and 100 μl of isopropanol, RNA was precipitated overnight at −80 °C. After centrifugation at 12,000*g* for 10 min, RNA pellets were washed with 75% ethanol, centrifuged as above and resuspended in 10 μl RNase-free water. RNA was quantified using the Bioanalyzer RNA 6000 Pico Kit (Agilent Technologies) following the manufacturer's instructions.

2.12. Amplified luminescent proximity homogeneous assay (alpha)

Reactions were carried out in 384-Optiplate (Perkin Elmer) in a final volume of 20 μl. Assay was optimized in PBS using 15 μg/ml of nichel-chelate AlphaLisa Acceptor beads and 10 μg/ml of streptavidin-Donor beads with serial dilutions of antibody to identify hook point. The presence of surface markers was analysed in dose-response with serial dilution of EVs, previously characterized by TRPS. EVs were purified by NBI from plasma of healthy donors or from serum-free medium of tumor cell lines. Alpha counts were revealed by Enspire instrument (Perkin Elmer) after 90 min of plate incubation in the dark at room temperature. We used a biotinylated antibody against human PSMA (Cusabio, CSB-PA018865LD01HU) and a recombinant his-tagged PSMA (Origene, NM_002786) for a standard curve quantification.

2.13. Reverse transcription and droplet digital PCR

Reverse transcription was performed using miRCURY LNA Universal RT microRNA PCR, Universal cDNA Synthesis Kit II (Exiqon) following the manufacturer's instructions with the following reaction composition: 2.3 μl of 5× reaction buffer, 1.15 μl enzyme mix, 0.5 μl synthetic RNA spike-in and 7.5 μl of template total RNA.

QX200TM Droplet DigitalTM PCR System (BioRad) was used to quantify mRNA copies using EvaGreen chemistry and the following primers: 5′-CAACGAATTTGGCTACAGCA-3′ and 5′-AGGGGTCTACATGG CAACTG-3′ for *GAPDH*; 5′-GATTTTGGTCTAGCTACAGA and 5′-GGATTT TTATCTTGCATTC for *BRAF*.

The direct encapsulation of EVs into oil droplets has been performed using isolated EVs as input sample, EvaGreen master mix supplemented with 5 U/ml of WarmStart® RTx Reverse Transcriptase (NEB) and with 3 mM magnesium sulphate. The standard protocol of ddPCR included a starting 10 min step at 55 °C followed by 5 min at 65 °C.

We optimized the procedure working with 10^2–10^6 polydisperse EVs to obtain at least 15,000 droplets in each assay.

2.14. Statistical analyses

The data and the number of independent experiments are indicated in the relative figure legends. Anova, *t*-test, and Pearson r coefficient

were calculated by GraphPad Prism Software v5.1, and results were considered statistically significant when *P* value was <0.05 (*), <0.01 (**), <0.001 (***).

3. Results

3.1. Capture and competitive elution of extracellular vesicles by nickel-based isolation

The versatility of NBI is based on the scalable range of positive charge conferred by nickel cations and on the surface area of a stationary phase. We used a suspension of agarose beads functionalized by increasing concentrations of nickel sulphate (50–300 mM). To have an indication on the number of particles recovered from the beads, we analysed the particles obtained from 10 ml of serum-free media incubated with U87 glioma cells in parallel with differential ultracentrifugation (UC). As estimated by flow-cytometry and only for events ≥0.5 μm, we reached a condition where the observed number of particles was equivalent for the two approaches and, in case of NBI, dependent on nickel cations, since no particles were recovered by non-functionalized beads (Fig. S1). These results have been obtained by functionalizing a suspension 20 ml/ml of beads, 24 ± 7 μm in size, with 200 mM of nickel sulphate.

Since different molecules can efficiently interact with a nickel matrix, we next used TRPS (qNANO instrument) [41] and spectroscopic analyses to analyse the number of particles eluted from the beads in the presence of a phosphate buffered saline (PBS) solution containing chelating agents (elution buffers), i.e. EDTA and citric acid (CA), trying to design an elution buffer tailored for EVs. We used 10 ml of media containing U87-derived secretome and, in control experiments, we used nickel-beads pre-incubated with U87-purified input DNA, input proteins, or input RNA, to understand the specificity of the elution buffer in the reversible binding of the different biomolecules. We monitored, by absorbance and fluorescence scan, both elution buffers and beads (in this case by further normalizing the signal to the 350 nm peak of nickel beads). Since the absorbance of DNA and RNA molecules has the same peak at 260 nm, we pre-stained the beads with pyronin Y in order to measure a specific fluorescence signal for the RNA. We detected a significant number of particles (2–5 × 10^9/ml, 50–700 nm using 3 nanopores) with the elution buffer containing a low millimolar range of chelating agents (molar ratio EDTA:CA of ~1:70; elution buffer 1×), which resulted to an early dissociation of qNANO detected particles (Kd of 1.15 ± 0.37 mM^{-1} for EDTA in the presence of 45 μM of CA) at pH 7.4. Notably, no absorbance or relevant fluorescence signals were obtained using the elution buffer 1×, in contrast of elution buffers containing >3 mM of EDTA. Representative data and the steps of the procedure are schematically shown in Fig. 1a.

To validate these observations with complementary approaches, we challenged this selectivity by competitive assays in a protein-enriched system. We supplemented 10 ml of DMEM, containing the secretome of U87 cells, with crude extracts of DH5α *E. coli* cells (from pelleted bacteria) and with 3 purified histidine-tagged proteins of different molecular weight (MW, Fig. S2), since nickel matrices are conventionally exploited to purify 6xHis recombinant proteins. We performed NBI in the mixture and eluted the particles with a gradient of chelating agents in PBS, keeping the reference of the elution buffer 1× solution. Captured proteins started to be detected/eluted with a 1.5× solution, as evidenced by SDS-PAGE, SYPRO Ruby staining and immunoblotting using an anti-his antibody, that firstly detected the recombinant proteins with higher MW (Fig. 1b). In the same samples, TRPS analyses with 3 nanopores detected 50–700 nm particles with 0.5× and 1× elution buffers, confirming the competitive dissociation of EVs from the beads in the low millimolar range of chelating agents. According to Bradford or BCA assays, we quantified 20–25 μg/ml (0.5× + 1× condition, Fig. 1b) of proteins that mirrored a total of 2 × 10^9 particles detected by the nanopores.

The strategy of using EDTA combined with citric acid provided a valuable alternative to preserve the pH and the biological sample from high concentrations of salts [27] that can affect vesicles' integrity, as shown in Fig. S3.

We evaluated the extent of particles obtained with elution buffer 1× by transmission electron microscopy (TEM; 20,500× and 87,000× magnifications, Fig. 1c). Wide-field acquisitions of NBI samples showed a broad dispersity of vesicles with an enrichment at 80–120 nm in size. Although we optimized these experiments with reduced concentration of formaldehyde and dry time to minimize the shrinkage effects [5], we used DLS to calculate the polydispersity (index of 0.61 ± 0.05), which mirrored the data obtained by TRPS. Western blot analyses on those samples showed that NBI-isolated EVs were positive to endosome-associated proteins, such as Alix and CD63 markers [42], or also found to the plasma cell membrane, such as Flotillin-1 [43], and negative to Golgi markers (GM130, Fig. 1d) [20], at least indicating the presence of exosome and microvesicle markers in the mixed populations of the vesicles we isolate.

With the aim to investigate the impact of mechanical forces exerted during the NBI procedure, we produced liposomes with an "exosome-like" lipidic composition [39] and spiked them in 10 ml of DMEM (Fig. 1e). Similar to the EVs in the same conditions, the average zeta potential of these preparations was −15.2 mV, as determined by DLS. Testing a small volume (0.5 ml) of media, both NBI and UC allowed near full recovery (98.6%) of input liposomes with a mean size of ~190 nm, although with a slight shift of ~10 nm of diameter in UC samples (orange vs red curve). Additional experiments performed with liposomes that we pre-stained with the lipophilic phosphatidylethanolamine-rhodamine (PE-Rho) dye evidenced a coalescent effect (>40 nm shift) of PE-Rho UC vesicles, not observed with PE-Rho NBI vesicles. These data demonstrate that the elution buffer used for NBI minimizes particles aggregation. We next interrogated the turnover of vesicles stored at 4 °C after purification by NBI or UC (Fig. 1f, left). We focused on particles ≥300 nm, more vulnerable than smaller vesicles to different storage conditions [44]. In UC samples, at 24 days post-isolation (*t24*), the 600 nm population originally present was virtually replaced by a population of ~300 nm. Strikingly, NBI samples retained the 86% of the original EV population, still detectable using the same nanopore (Fig. 1f, middle). A kinetic analysis evaluating the size-shift of the 600 nm test population revealed a half-life of >50 days for NBI EVs, in contrast to 7.35 days for UC EVs (Fig. 1f, right). Collectively, these data indicate that polydisperse EVs can be selectively enriched by NBI preserving their integrity and stability in a near physiological pH solution.

3.2. Scalable and reproducible isolation of polydisperse EVs from cancer cell lines and the plasma of healthy volunteers

To assess the robustness of NBI in cell-based systems, we purified EVs secreted by U87 cells seeded at different densities, in 6-well plates, as indicated in Fig. 2a. We processed 1 ml of media and analysed the distribution of purified particles by TRPS using NP400, NP200, and NP100 nanopores. Isolated EVs displayed a continuous distribution, from approximately 50 to 700 nm in diameter (as compared with 3 different sets of iZON recommended calibration beads), characterized by at least two peaks of enriched vesicle populations showing ~200 and ~600 nm of mean diameter, respectively. We referred these two EV populations to as small EVs (sEVs) and large EVs (lEVs), respectively, while being aware of the unknown sub-cellular origin of individual NBI-isolated EVs [5]. The global number of isolated vesicles was proportional to the number of seeded cells, with a global coefficient of variation (*CV*) of 6.14% ($n = 9$ for NBI 1, 2, and 3) for both sEVs (197 ± 26 nm) and lEVs (595 ± 37 nm), underlying the high reproducibility of NBI. We did not observe a statistically significant variation ($P = .459$) comparing EVs from EV-depleted serum (dFBS) [45] and serum-free media (NBI 1), indicating that a reliable EV isolation can be started from relatively viscous solutions upon dilution with PBS. Interestingly, the efficient isolation of

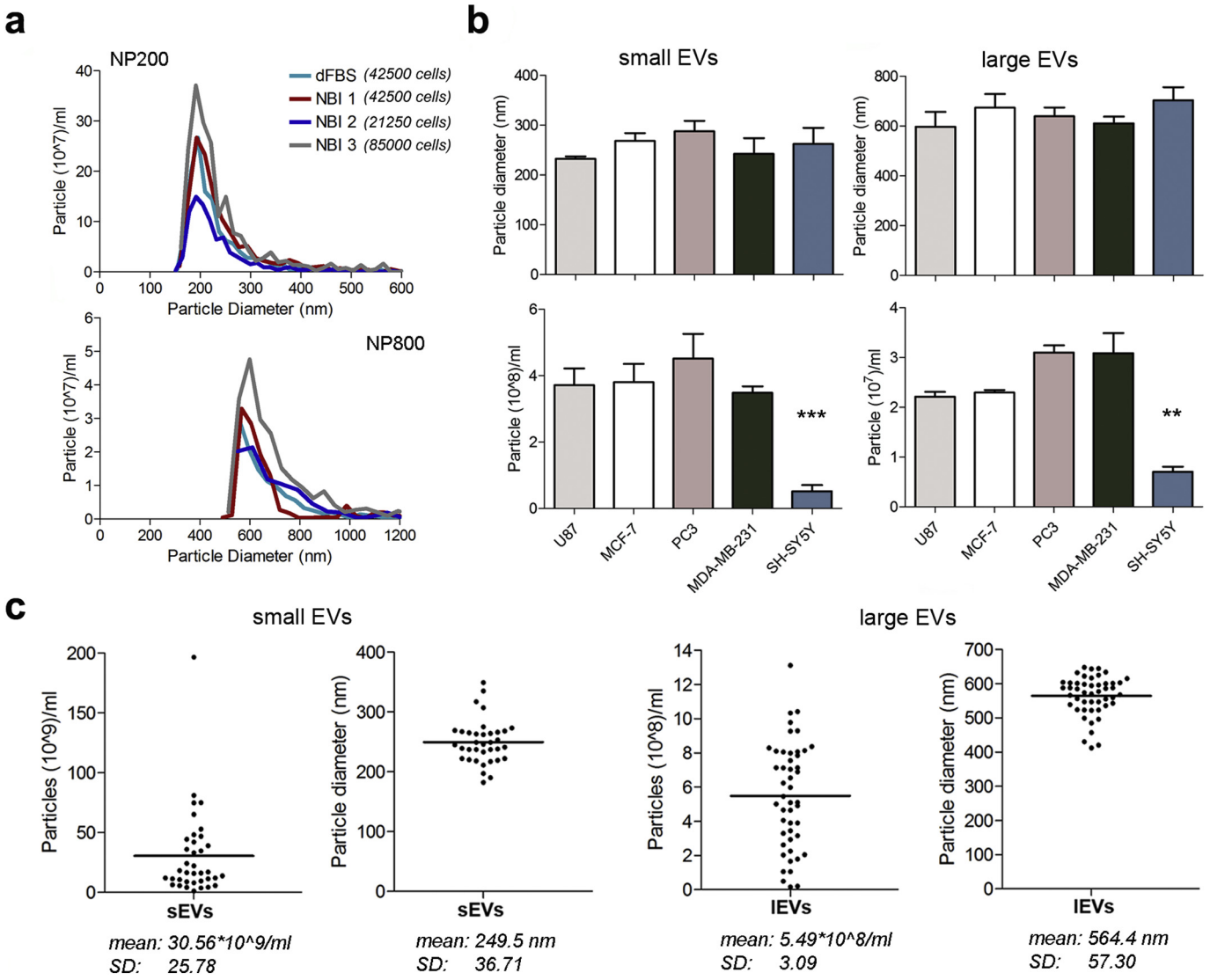

Fig. 2. NBI efficiently isolates EVs with high reproducibility from different biological fluids. a) The reproducibility of NBI has been tested in serum-free media of U87 cells seeded at different density, in 6-well plates, as indicated (NBI 1, 2, and 3). Ten % ultracentrifuged FBS (dFBS) condition showed substantial overlap with NBI-1 results. Plots are representative of 3 independent experiments and global *CV* was 6.1%. b) Distribution of NBI-isolated EVs have been analysed for different cell lines, as indicated. SH-SY5Y cells showed substantial reduction in releasing both vesicle populations ($^{**}P$ value = .006, F = 70.13, and $^{***} < 0.0001$, F = 30.84, using one-way ANOVA and Bonferroni's post-test). *SD* refers to 3 independent experiments. c) NBI was applied to 0.5 ml of plasma obtained from healthy volunteers. The relative distribution of EVs (representative original profiles are shown in Fig. S5b) has been evaluated by TRPS analyses using 3 nanopores with the obtained concentrations, per milliliter of plama, of the small and large EV populations.

EVs from small volumes allowed us to follow the release of vesicles using as low as 10^3 cells/cm^2 (Fig. S3). We observed a linear release of sEVs as a function of cell density, and an faster release of lEVs, as already suggested for microvesicles [5], possibly related with different biogenetic mechanism, intrinsic stability and/or cell-mediated turnover that correlate with particle size or composition [46]

We next characterized the EVs recovered from MCF-7, PC3, MDA-MB-231, and SH-SY5Y tumor cell lines (Fig. 2b). We observed an equivalent distribution of isolated EVs in terms of size and concentration, with the exception of the SH-SY5Y cells that demonstrated lower propensity to release both vesicle populations.

Since EVs are secreted in the blood by many cell types [47], we applied NBI to isolate EVs from the blood of healthy volunteers (Fig. S4). We analysed the abundance of isolated EVs in plasma and in the serum ($n = 9$) and clearly observed a 6-fold enrichment of EVs purified from plasma (Fig. S5a). We therefore performed NBI on (0.5 ml) plasma of 46 donors to assess the general distribution of EVs isolated from healthy subjects. The mean age of the volunteers was 45 ± 10 years. The profile of NBI-isolated EVs (Fig. S5b) was characterized by at least two enriched populations showing a quantitative ratio of ~55:1: the first one with a mean diameter of 249.5 ± 36.71 nm (sEVs) and a concentration of 30.56 ± 25.78 × 10^9 per milliliter of plasma; the second one with a mean size of 564.4 ± 57.3 nm (lEVs) and a concentration of 5.49 ± 3.09 × 10^8 per milliliter of plasma, as indicated in Fig. 2c.

3.3. Characterization of plasma EV lineages by combined immunocapture

In line with other reports [48,49], mixed populations of circulating vesicles in healthy individuals are positive to hematopoietic or endothelial cell markers. We therefore investigated whether specific hematopoietic surface markers can be instrumental for the characterization of isolated EVs. We measured the number of plasma-isolated EVs left in solution after incubation with CD235a (marker of erythrocytes [50]) or CD41a (marker of platelets [51]) antibodies, i.e. immunodepleted samples. We observed a reduction of about 20% of the original population of microvesicles and of about 60% of sEVs using the CD235a. On the other hand, this trend was opposite using the CD41a, which showed preferential recognition of lEVs (Fig. 3a). These results indicate that plasma

isolated EVs expose markers that are specific of distinct cell lineages, underlying the derivation from different cells/progenitors. In addition, these results are in line with other reports indicating that platelet-derived microvesicles (range of size >300 nm) are abundant in the blood of healthy individuals [52,53].

With the aim to recognize specific EV lineages from a mixture of NBI-isolated polydisperse vesicles, we performed combined immunocapture experiments with a known amount of tumor-derived EVs spiked in the human plasma. We added 10^9/ml EVs isolated from plasma to 10^9/ml EVs isolated from the media of melanoma SK-MEL-28 cells. After NBI, we incubated the mixture of isolated vesicles with CD235a, CD41a, and CD45 antibodies (known to be expressed from leukocytes [54] but not from SK-MEL-28 cells [55]). After the immunoprecipitation (or immunodepletion) of CD235a, CD41a, and CD45 vesicles, the MEL-CAM antibody (CD146, expressed on the surface of SK-MEL-28 cells) still recognized the 64% of input EVs (light green vs light grey bars) positive to the epithelial marker, in contrast to the AL-CAM (CD166) antibody which resulted as an experimental negative control (Fig. 3b).

Therefore, specific hematopoietic markers could be instrumental to fractionate plasma NBI-isolated EVs into distinct EV lineages. Importantly, the results obtained by these experiments indicated that intact, polydisperse EVs obtained by NBI form a homogeneous suspension of individual particles that could be exploited in no-wash, immobilization-independent assays.

3.4. Ultrasensitive detection of surface antigens on plasma EV lineages from healthy subjects and prostate cancer patients by NBI-alpha assay

Given their abundance in the blood, EVs can offer immediate advantage in liquid biopsy analyses for biomarker detection [56]. By NBI we can recover polydisperse EVs from biological samples and obtain a suspension of individual particles in solution. We therefore verified the possibility of applying NBI-extracted EVs to versatile homogeneous assays to perform ultrasensitive biomarker detection.

We adapted the amplified luminescent proximity homogeneous assay (alpha) [57] technology to detect surface antigens on NBI-isolated EVs. Following the notions obtained on the dispersity of NBI-isolated EVs, we designed the alpha assay using nickel-charged Acceptor beads in combination with streptavidin-Donor beads recognizing the antigen of interest through biotinylated antibodies (NBI-alpha,

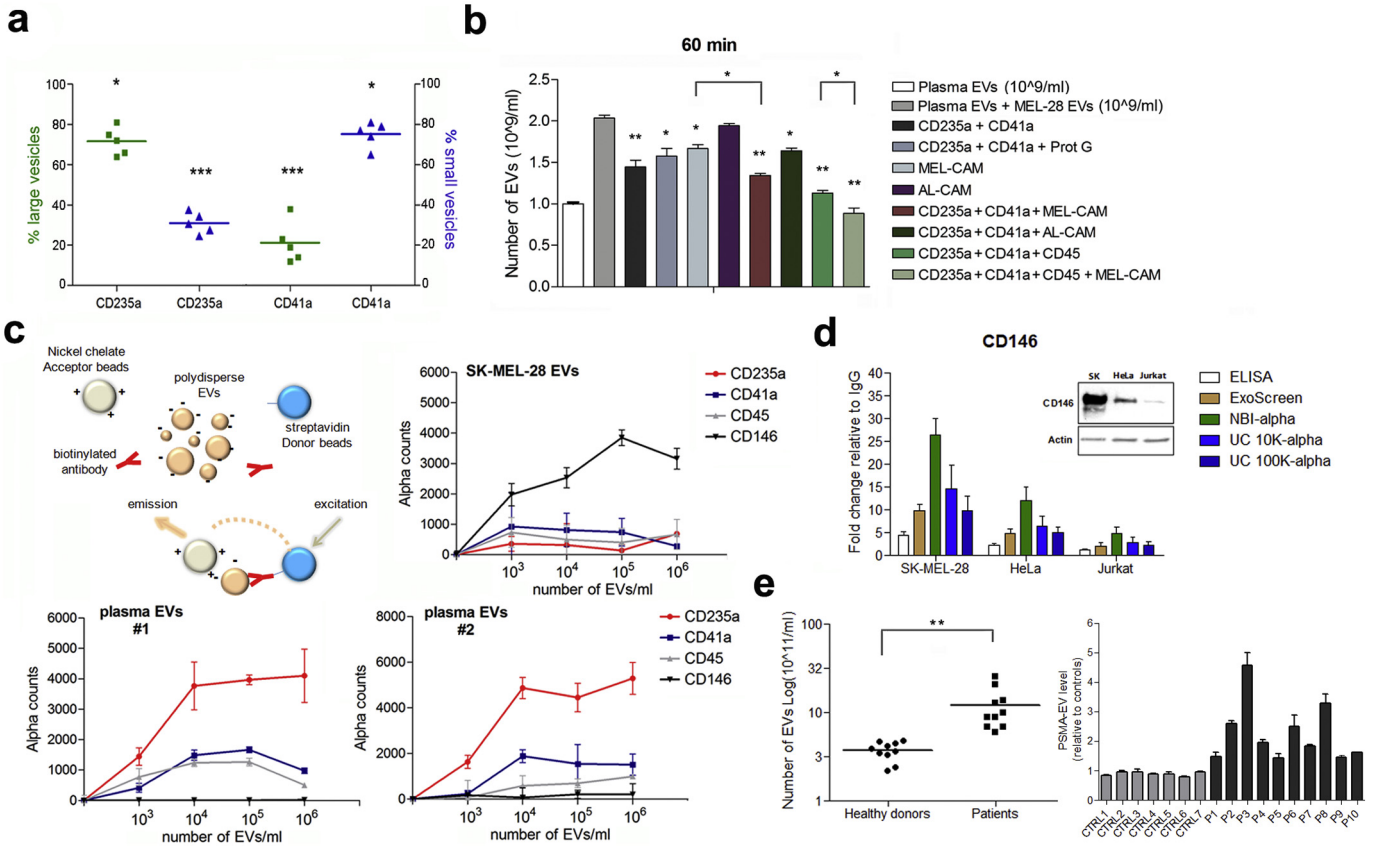

Fig. 3. NBI unbiasedly isolates different EV lineages from blood and allows to use EVs as individual particles in homogeneous assays to detect surface antigens. a) Hematopoietic cells' antigens, biotinylated anti-CD41a and CD235a antibodies, were used to characterize plasma isolated EVs. Isolated EVs (2×10^8/ml), for a total of 15 samples, were divided in 2 volumes and incubated with biotinylated antibodies (CD41a or CD235a) + streptavidin dynabeads. Supernatants were analysed by qNano instrument and the distribution of EVs left in solution are shown. * *P value* < .05; ***P value* < .001. b) 10^9/ml plasma EVs, together with 10^9/ml EVs isolated from media of SK-MEL-28 cells were spiked in 1 ml of post-NBI human plasma. Indicated biotinylated antibodies were incubated for 60 min and, after streptavidin-dynabeads precipitation, TRPS analyses were performed on EVs left in solution. One-way ANOVA-Bonferroni have been used to calculate the statistical significance (**P value* < .05; ***P value* < .001). c) Diagram describing the alpha assay designed to detect surface antigens on individual, polydisperse EVs. Streptavidin-coated Donor beads recognize the antigen-specific biotinylated antibody; positively-charged nickel-chelate Acceptor beads interact with EVs and emit a fluorescent signal when in proximity of excited Donor beads. Saturation curves were obtained as function of number of EVs purified by NBI from plasma of two healthy donors (#1, #2) and from SK-MEL-28 melanoma cells. d) Cells lines expressing high, intermediate, or low levels of CD146 protein are indicated by immunoblotting performed on cell lysates. EVs were isolated by NBI or UC from the corresponding media of the three cell lines. The relative performances of different detection methods have been then evaluated, using anti-CD81 biotinylated antibody for plate-coating in the case of ELISA (coupled with anti-CD146 and HRP-conjugated secondary antibodies) or conjugation with Acceptor beads in the case of ExoScreen. The specific, background-subtracted signals were normalized to IgG signals of individual experiments. EVs for ELISA and ExoScreen have been isolated by UC. 10 K and 100 K indicate the *g* forces applied in the two protocols of UC, respectively. SD refers to two independent experiments. e) NBI was performed on 1 ml of plasma deriving from patients with advanced prostate cancer. Left: The relative number of EVs is plotted for healthy donors (50–55 years) and for prostate cancer patients (>60 years). One-way ANOVA-Bonferroni have been used to calculate the statistical significance. Right: the relative levels of PSMA on 10^5 EVs were detected by NBI-alpha. According to the standard curve with purified recombinant histidine-PSMA, 1 in the Y axis corresponds to ~35 pg/ml of PSMA in solution. SD refers to 3 independent experiments.

Fig. 3c). In these settings, we titrated the number of plasma-isolated EVs (#1 and #2) and of SK-MEL-28-isolated EVs as function of the signal obtained with biotinylated CD235a, CD41a, and CD45 antibodies. In the case of plasma EVs, the saturation curves obtained showed three to four times enhanced binding of CD235a with respect to CD41a and CD45, with a background signal for the epithelial marker CD146 eve using 10^6 EVs (Fig. 3c, bottom left and right). Consistently with results in Fig. 2c,d, the CD235a antibody was the most efficient in recognizing a significant fraction of plasma-isolated EVs. In the case of EVs released from SK-MEL-28 cells, the signal of the CD146 antibody showed a dose-response curve, in contrast to the CD235a, CD45, and CD41a antibodies (Fig. 3c, top right), confirming the exposure of the CD146 protein on the EVs deriving from melanoma cells. All these experiments were performed in 20 μl, using ~2% of the solution containing plasma EVs and ~20% of the solution containing EVs recovered from 3×10^5 SK-MEL-28 cells.

To challenge this approach in terms of sensitivity and accuracy, we used three cell lines expressing high (SK-MEL-28), intermediate (HeLa), or low (Jurkat) levels of the CD146 protein (see immunoblot in Fig. 3d). We isolated EVs using NBI or UC and evaluated 2 additional techniques (ELISA [58], ExoScreen [57]) for CD146 detection on EVs. Globally, all the results obtained were consistent with relative expression levels of endogenous CD146. The NBI-alpha demonstrated a higher dynamic range and the most performant detection (>5 times) of CD146 on EVs isolated from the most challenging Jurkat cells (FC = 4.6, Fig. 3d). By comparing the alpha assay results with samples enriched in large EVs (sedimented at 10,000 *g*) or in small EVs (sedimented at 100,000 *g*), respectively obtained by UC) [59], we attributed the advantage of NBI-alpha in detecting the antigens on less aggregated particles (Fig. 1e).

We validated the NBI-alpha approach by detecting the prostate cancer specific membrane antigen (PSMA) on EVs isolated from plasma of prostate cancer patients (Fig. 3e). First, we analysed the distribution of EVs isolated from plasma of healthy subjects (age of 50–55 years) and from plasma of ten patients (>60 years) with metastatic prostate cancer (Fig. 3e). In line with other reports [60,61], we found a statistically significant increase (of about one order of magnitude) in the number of recovered EVs in the cancer patients (Fig. 3e, left). The Pearson r value of the correlation with counts of RBCs/WBCs/PLTs was 0.88 (Table S2). Using 10^5 EVs in the NBI-alpha assay, we detected higher levels of PSMA (mean *P* value < .001) in patients' EVs with respect to the healthy controls, reaching the sensitivity of picomolar concentration of PSMA (Fig. 3e, right) as determined by standard curve with his-tagged PSMA. Therefore, we specifically detected the enrichment of this surface marker on a fraction of the EVs isolated from the plasma of prostate cancer patients.

3.5. Ultrasensitive detection of RNA enclosed in EV lineages from plasma of healthy subjects and colon cancer patients by NBI-ddPCR assay

EVs can selectively or stochastically entrap nucleic acids [5]. The growing interest in exploiting EVs for cancer diagnostics relies with the potential identification of new biomarkers and of clues mirroring the genetic heterogeneity of tumor cells. Therefore, the potential clinical application requires a sensitive approach to distinguish EV subpopulations and to infer, at least qualitatively, the diversity of tumor cells that have originated them. We analysed the nucleic acid content of polydisperse EVs (50–700 nm) isolated from the plasma of healthy donors ($n = 47$) and we detected RNA, as demonstrated by automated electrophoresis profile following RNAse treatment (Fig. S7a). One of the most highly sensitive reported technology to detect fractions of mutated transcripts enclosed within EVs is the droplet digital PCR (ddPCR) [17,62]. We therefore applied a standard ddPCR protocol to calculate the absolute number of *GAPDH* mRNAs in all the samples starting from ~3×10^9 EVs (Fig. 4a and Fig. S7b). The system was sensitive enough to correlate the number of mRNA copies with the relative counts of PLTs (Pearson r: 0.623; Fig. 4b), blood components already recognized as major producer of *GAPDH* [63]. Interestingly, given the quality of the EV samples obtained by NBI (in terms of non-coalescent particles), we had a chance to implement the ddPCR assay by directly encapsulating NBI-isolated EVs into the oil droplets, with a reaction mix containing a thermostable reverse transcriptase to perform a one-step amplification of the RNA fragment of interest (Fig. 4c). In these experimental conditions, specific nucleic acids can be rapidly detected from a discrete number of individual EVs and without the step of RNA extraction. Notably, particles isolated by UC failed to generate the expected number of oil droplets (>12,000), indicating that a direct encapsulation can be in this case hampered by aggregated vesicles.

We challenged the diagnostic performances of this NBI-ddPCR protocol by a retrospective analysis of a cohort of metastatic colon cancer patients. Patients were previously enrolled in a randomized phase III clinical trial for chemotherapy alone or in combination with bevacizumab [64,65]. All of the patients were analysed for the *KRAS* and *BRAF* status, two biomarkers that have a profound impact for patients in terms of clinical management and therapeutic options for CRC patients. We isolated EVs by NBI from the plasma of 21 cases with 6 additional blood draws collected from one single patient during the treatment (longitudinal liquid biopsy). The molecular characterization was performed by pyrosequencing on formalin-fixed, paraffin-embedded (FFPE) tissue DNA and indicated the presence of the *BRAF* V600E mutation in 5 out of 21 patients (~24%, samples C02, C11, C14, C20, and C25). The mutation was confirmed in the sample C03, a 5 months' later blood draw of the sample C20. In the samples we received, no mutations in *KRAS* were reported, except for the variant K117N in the sample C07. We analysed the samples in blind as in the order reported in Table S3.

First, we report that the levels of EVs recovered from plasma of colon cancer patients were strikingly higher in comparison to those of healthy donors (Fig. 4d). The correlation coefficient was 0.93 with relative counts of RBCs, WBCs, and PLTs. We then applied our RNA-extraction free ddPCR protocol in a reaction volume of 20 μl and 10^3 isolated EVs as input to amplify the allele fragment containing the *BRAF* V600E mutation. As shown in Fig. 4e, the dots above an arbitrary threshold >1 indicate a relative higher number of mRNA copies detected by NBI-ddPCR, resulting from single droplets that have encapsulated vesicles carrying the V600E mutated transcripts. Indeed, samples C02, C03, C11, C14, C20, and C25 (orange dots) showed 100% matching with data obtained by pyrosequencing on FFPE tissues, while the samples C04, C09, C19, C21, and C24 (blue dots) indicated potential new insights on *BRAF* status only detected by NBI-ddPCR. To challenge the specificity and sensitivity of these results, we evaluated the extent of mRNA amplification upon immunodepletion of CD235a/CD41a positive EVs (Fig. 4e, middle). Unexpectedly, the number of *BRAF* V600E copies in the same patients' samples were found 4 to 5 fold increased with respect to the signal obtained from the bulk population of EVs, specifically increasing the dynamic range of sensitivity of the NBI-ddPCR. We also performed another experiment to analyse EVs isolated by anti-CD147, one of the most well-recognized approaches to enrich for colon cancer derived EVs [57] [66]. In this case, the diagnostic power was reduced to 83% as compared with the tissue biopsy results, with a number of copies <<1 in the case of the sample C25 (0.25 vs 4.48 and 20.05 copies, respectively obtained in the previous experiments), and to ~34% the concordance with blue dots. These data show that a significant fraction of EVs negative for the CD147 antigen can effectively carry *BRAF* mutated transcripts. Consequently, NBI is more efficient in comparison to single antibody-mediated enrichment of tumor-derived vesicles.

In order to validate the accuracy of the NBI-ddPCR results, we performed further inspections to the FFPE DNA of the samples from patients C04, C09, C19, C21, and C24, which resulted *BRAF* mutation positive in the EVs but not in the original tumor. These DNAs were subjected to a more sensitive, and clinically approved, allele-specific real-time PCR (EasyPCR) screen. The sample C19, that showed a value of

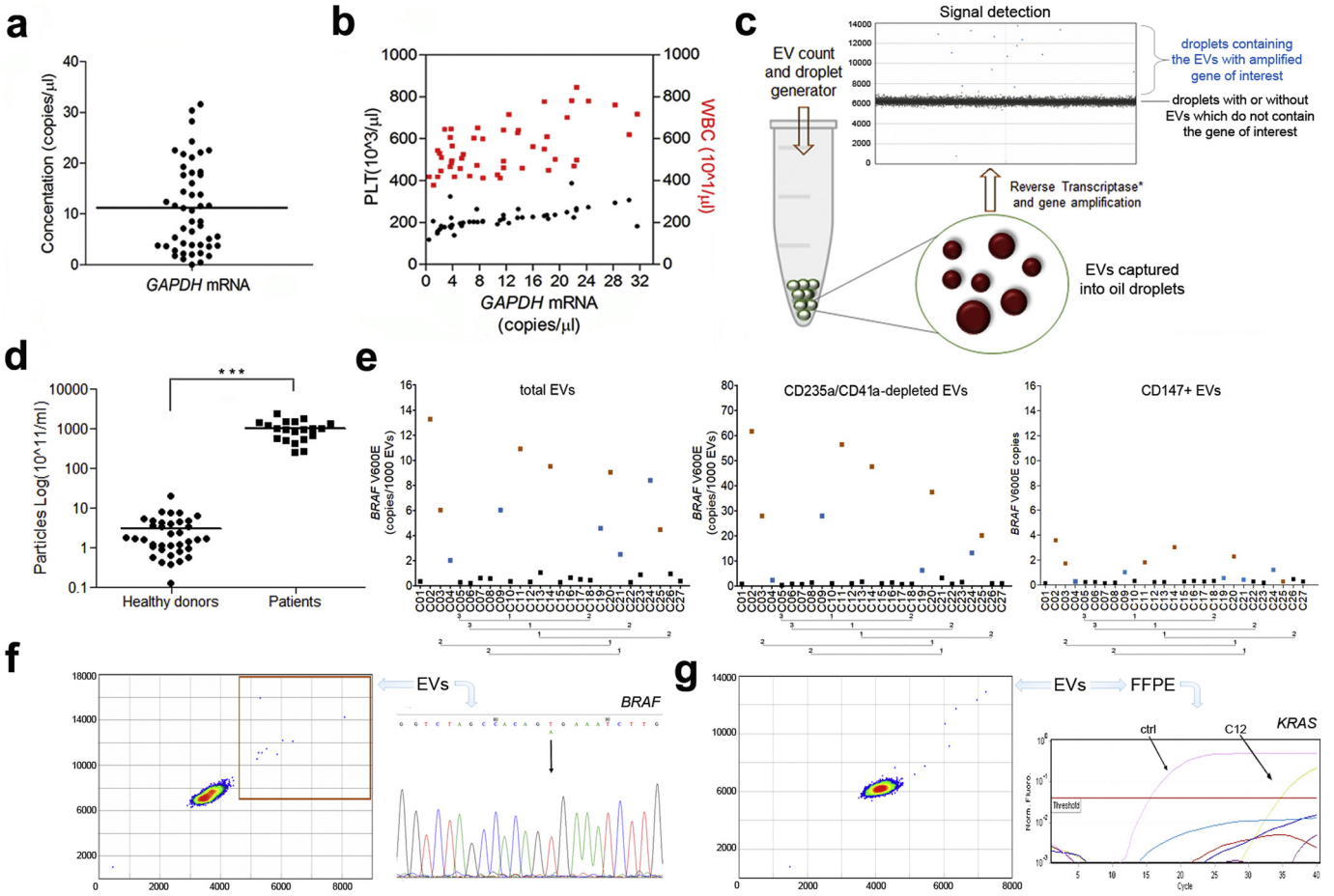

Fig. 4. Detection of RNA species enclosed into plasma-isolated EVs and design of a new ddPCR assay to exploit individual, polydisperse EVs for nucleic acids detection. a) Two µl out of 20 of cDNA synthesized from 0.1–4 ng RNA. EV-RNA were deriving from plasma samples of 47 healthy donors. ddPCR has been performed with EvaGreen chemistry. Absolute number of *GAPDH* mRNA copies has been analysed by QuantaSoft Analysis software (BIORAD). b) The number of *GAPDH* mRNA copies positively correlated with number of PLTs ($r = 0.62$), major producer of circulating *GAPDH* mRNA and of microvesicles. c) Design of a new ddPCR assay to encapsulate EVs (50–700 nm) into oil droplets (1400–1600 nm). The number of copies of specific RNAs present in NBI-isolated EVs can be obtained as function of EV titration. The stochastic entrapment of EVs into oil droplets allow the amplification of the target of interest upon supplementation of the EvaGreen mix with a *thermostable Reverse Transcriptase enzyme. d) NBI was performed on 1 ml of plasma deriving from patients with colon cancer. The relative number of EVs is plotted for healthy donors (35–55 years) and for colon cancer patients (64 ± 8 years). One-way ANOVA-Bonferroni have been used to calculate the statistical significance. e) Left: the copy number of *BRAF* V600E enclosed in 1000 EVs isolated from 20 colon cancer patients is shown; middle: the copy number of *BRAF* V600E enclosed in 1000 EVs upon imunodepletion CD235a/CD41a positive EVs is shown; right: the copy number of *BRAF* V600E in EVs isolated by CD147 antibody. See the Table S3 to evaluate the matching with *BRAF* sequencing results performed in tissue biopsy. Numbered lines refer to longitudinal liquid biopsies from the same patient. f) Original plot of the NBI-ddPCR results for the sample C09, whose RNA from the bulk of EVs has been amplified with *BRAF* exon-spanning primers and then sequenced. g) Original plot of the NBI-ddPCR results for the sample C12 showing KRAS G12C mutation, subsequently verified by EasyPCR kit.

4.57 *BRAF* copies by NBI-ddPCR, resulted indeed positive to *BRAF* V600E mutation, indicating correspondence of the mutation at DNA level and the effective presence of this cell sub-populations in the tumor. In the efforts to highlight the presence of the mutated allele by standard sequencing in the sample C09, that showed a value of ~6 in the bulk EVs, we obtained a borderline A peak masked by the prevalence of the T allele present in the majority of the isolated EV (Fig. 4f). Therefore, by NBI-ddPCR we identified a previously unreported mutation in *BRAF* in at least the 7.5% of the colon cancer patients analysed. Notably, to investigate also the possibility of detecting a non-vesicular RNA proportion potentially bound by apolipoproteins that could be present in NBI-isolated samples, we performed immunoprecipitation with APO A1 and APO B100 antibodies on NBI-isolated EVs from the plasma of two healthy volunteers [67]. Fig. S7c shows that RNA extracted from particles recognized by APO A1 and APO B100 antibodies does not contribute to the signal observed for *GAPDH* or wild-type *BRAF* mRNAs.

Next, we succeeded to assess on the EVs from the same patients the prevalent mutations at the level of the exon 2 of *KRAS*. Remarkably, 3 samples resulted positive to the G12C mutation and 1 sample to the G12D: the presence of the G12D allele in the sample C12 (with a value of 1.79 copies/10^4 EVs) was clearly confirmed by a re-analysis on FFPE DNA (Fig. 4g). Even in the case of *KRAS*, by NBI-ddPCR we revealed a previously undetected mutation for at least 3.8% of the patients analysed.

Collectively, these data show that NBI-ddPCR can be used for liquid biopsy analyses and to detect clinically relevant predictive and prognostic biomarkers (such as *KRAS* and *BRAF*) and open new perspectives to reveal the extraordinary potential of the EVs towards clinical molecular diagnostics.

4. Discussion

In this study, we describe the nickel-based isolation (NBI) as a new approach to selectively enrich heterogeneous (50–700 nm) extracellular vesicles from biological fluids in timely and cost-effective manner. We found that EVs captured through electrostatic interactions can be efficiently dissociated from a nickel-functionalized matrix using chelating agents as excipients, maintaining the properties of a physiological, PBS-like solution in the elution buffer. This aspect is particularly important not only to preserve the integrity of EVs which determines at the end the efficiency in the recovery, but also in view of downstream qualitative and quantitative analyses of the vesicles, as evidenced by

immunocapture-based studies [68,69], or ion-exchange chromatograpy [28] with a modulation of the ionic strength which can impact fractions of EVs. By contrast, the concentration of EDTA and citric acid could be detrimental for chelating calcium /magnesium ions or cofactors important for cell phenotype/viability or in vitro assays involving the incubation with NBI-isolated EVs. We did not observe variations on the viability (MTT assay) of U87 or colon cancer HCT116 cells exposed for 24 or 48 h to elution buffer 1× or PBS (data not shown). Technically, we present an optimized procedure that can be readily exploited for research in clinical settings and that could be combined with HPLC or size-exclusion procedure to fractionate EVs within the range of 50–800 nm.

The use of an accurate method to isolate vesicles is mandatory for correlation analyses since the assessment of particle distribution can be of relevance for liquid biopsy studies on health and disease states [47]. The quantitative characterization of NBI-isolated EVs from human plasma indicated that polydisperse vesicles can expose surface antigens of different progenitor cells, making difficult any correlation between the vesicle size and the cell of origin. For this reason, we refer to EV lineages indicating all the mixed vesicle populations that are positive to a cell type-distinctive marker and therefore assumed to have a common parental origin. This concept is corroborated by other studies that have investigated the presence or absence of specific antigens on plasma-derived or tumor-derived EVs [56].

The proof-of-principle experiments performed with human plasma including EVs isolated from SK-MEL-28 cells and the melanoma cell-adhesion molecule CD146 demonstrated that different EV lineages are unbiasedly recovered by NBI, resulting to a homogeneous suspension of polydisperse EV lineages. In this context, a targeted immunodepletion of hematopoietic EV lineages in NBI samples can facilitate the discovery and characterization of tumor-derived EV lineages. We have formally proven this possibility by detecting the *BRAF* V600E mutated mRNA, whose copy number was enriched in EVs isolated from plasma of colon cancer patients upon CD235a/CD41a immunodepletion (Fig. 4e and Table S3).

Early detection is a key challenge that could enable specific interventions to reduce patient mortality and morbidity [70]. First, we designed a new ddPCR assay in which the step of RNA extraction can be bypassed, with the important implications of reducing chances of sample contamination, simplifications of the steps towards the results and the sensitivity obtained. In this context, the sensitivity over DNA analysis can be favored by the higher relative number of RNA molecules present in the sample. Second, the advantage of NBI in detecting mutated *BRAF* and *KRAS* transcripts in comparison with CD147-positive EVs and the use of a label-free method can provide better sensitivity for tumor-derived vesicles.

KRAS and *BRAF* are two genes clinically relevant for the prognostic role [71,72], and therapeutic options [73] not only for colon cancer. We have shown that, through liquid biopsy, it is possible to identify fractions of secreted EVs carrying tumor biomarkers with a sensitivity and accuracy that led to re-consider the mutational status in at least 10% of the patients analysed. Currently, the analysis of circulating tumor biomarkers, based on cell-free DNA, shows incomplete sensitivity in lung cancer [74]. In our proof-of-concept study, despite the small number of cases analysed, we reached a complete concordance with the tumor-derived data in detecting *BRAF* and *KRAS* mutations from liquid biopsy. Importantly, some cases showed mutations only in the secreted EVs, suggesting that NBI-ddPCR could serve to infer the presence of specific cell sub-populations hardly detectable in tissue biopsy. This possibility could allow a deeper characterization of tumor heterogeneity and/or its evolution during therapy, with potential impact for the clinical managements of patients. Addressing the low fraction of cells that could generate the EV sub-populations detectable by NBI-ddPCR, systematic studies are needed to understand the threshold specificities and the potential clinical relevance. We believe these findings can relevantly contribute to the rational establishment of EV-based liquid biopsy studies for the future benefit of clinical diagnostics.

Ackowledgements

We are grateful to Drs. Ilaria Ferlenghi and Fabiola Giusti (SBAD, GSK Vaccines, Siena, Italy) for their assistance in structural microscopy. We thank Dr. D. Di Vizio (Cedars-Sinai Medical Center, USA) for providing suggestions and helpful comments on the manuscript, and Dr. Manuela Basso (CIBIO, University of Trento) for precious discussions on EVs biology.

This research was supported by Associazione Italiana per la Ricerca sul Cancro (to A.P.), Fondazione Cassa di Risparmio Trento e Rovereto (to F.D. and A.Q.), and the Italian Miur (FFABR, to V.G.D.).

Funding sources

Associazione Italiana per la Ricerca sul Cancro (AIRC, N. 21548), Fondazione Cassa di Risparmio Trento e Rovereto (CARITRO), and the Italian Ministero Istruzione, Università e Ricerca (Miur).

Declaration of interests

The authors declare competing interests. The procedure of NBI reported in this manuscript is currently under consideration for patenting.

Author contributions

V.G.D., A.P. and A.Q. conceived NBI, the project and the experimental design. V.G.D and M.N. optimized the NBI protocol, performed the experiments and analysed the data; M.N. and C.Z. did cell cultures; I.P. performed FACS experiments and qNANO measurements for EV integrity; G.S. performed TEM experiments; C.P., L.L. and C.P. prepared liposomes and performed spectroscopic analyses; A.M. did RNA extraction from EVs; P.P., G.L.M., selected human plasma samples and recorded blood count data; H.B. provided plasma samples of prostate cancer patients and, together with F.D., shared her expertise on prostate cancer markers; L.P. provided plasma samples of colon cancer patients and, together with P.U., performed EasyPCR on FFPE samples; V.G.D., M.N., A.Q., A.P. wrote the manuscript and all the authors revised it.

Appendix A. Supplementary data

Supplementary data to this article can be found online at https://doi.org/10.1016/j.ebiom.2019.04.039.

References

[1] Raposo G, Stoorvogel W. Extracellular vesicles: exosomes, microvesicles, and friends. J Cell Biol 2013 Feb 18;200(4):373–83 Internet. cited 2017 Jan 17. Available from http://www.jcb.org/lookup/doi/10.1083/jcb.201211138.

[2] Antonyak MA, Cerione RA. Microvesicles as mediators of intercellular communication in cancer. Methods Mol Biol 2014;1165:147–73 Internet. cited 2017 Jan 31. Available from http://link.springer.com/10.1007/978-1-4939-0856-1_11.

[3] Al-Nedawi K, Meehan B, Micallef J, Lhotak V, May L, Guha A, et al. Intercellular transfer of the oncogenic receptor EGFRvIII by microvesicles derived from tumour cells. Nat Cell Biol 2008;10(5):619–24.

[4] Colombo M, Raposo G, Thery C. Biogenesis, secretion, and intercellular interactions of exosomes and other extracellular vesicles. Annu Rev Cell Dev Biol 2014 Oct 11; 30(1):255–89 Internet. cited 2017 Jun 27. Available from http://www.ncbi.nlm.nih.gov/pubmed/25288114.

[5] van Niel G, D'Angelo G, Raposo G. Shedding light on the cell biology of extracellular vesicles. Nat Rev Mol Cell Biol 2018;19(4):213–28 Internet. Available from http://www.nature.com/doifinder/10.1038/nrm.2017.125.

[6] Théry C, Amigorena S, Raposo G, Clayton A. Isolation and characterization of exosomes from cell culture supernatants and biological fluids. Curr Protoc Cell Biol 2006 Apr. https://doi.org/10.1002/0471143030.cb0322s30 Internet. [cited 2017 Jan 17];Chapter 3:Unit 3.22. Available from:.

[7] Tkach M, Théry C. Communication by extracellular vesicles: where we are and where we need to go. Cell 2016;164(6):1226–32.

[8] Nogués L, Benito-Martin A, Hergueta-Redondo M, Peinado H. The influence of tumour-derived extracellular vesicles on local and distal metastatic dissemination. Mol Aspects Med 2018;60:15–26.
[9] Kahlert C, Kalluri R. Exosomes in tumor microenvironment influence cancer progression and metastasis. J Mol Med 2013;91(4):431–7.
[10] Yáñez-Mó M, Siljander PR-M, Andreu Z, Zavec AB, Borràs FE, Buzas EI, et al. Biological properties of extracellular vesicles and their physiological functions. J Extracell Vesicles 2015;4:27066 Internet. cited 2017 Jan 17. Available from: http://www.ncbi.nlm.nih.gov/pubmed/25979354.
[11] Wiklander OPB, Nordin JZ, O'Loughlin A, Gustafsson Y, Corso G, Mäger I, et al. Extracellular vesicle in vivo biodistribution is determined by cell source, route of administration and targeting. J Extracell Vesicles 2015;4 (26316).
[12] Fais S, O'Driscoll L, Borras FE, Buzas E, Camussi G, Cappello F, et al. Evidence-based clinical use of nanoscale extracellular vesicles in nanomedicine. ACS Nano 2016;10 (4):3886–99.
[13] Chen J, Xu Y, Wang X, Liu D, Yang F, Zhu X, et al. Rapid and efficient isolation and detection of extracellular vesicles from plasma for lung cancer diagnosis. Lab Chip 2019;19(3):432–43 Internet. [cited 2019 Jan 11]; Available from: http://xlink.rsc.org/?DOI=C8LC01193A.
[14] Ortega FG, Piguillem SV, Messina GA, Tortella GR, Rubilar O, Jiménez Castillo MI, et al. EGFR detection in extracellular vesicles of breast cancer patients through immunosensor based on silica-chitosan nanoplatform. Talanta 2019 Mar 1;194: 243–52 Internet. cited 2019 Jan 11. Available from: https://www.sciencedirect.com/science/article/pii/S0039914018310464?via%3Dihub.
[15] Lee JS, Hur JY, Kim IA, Kim HJ, Choi CM, Lee JC, et al. Liquid biopsy using the supernatant of a pleural effusion for EGFR genotyping in pulmonary adenocarcinoma patients: a comparison between cell-free DNA and extracellular vesicle-derived DNA. BMC Cancer 2018 Dec 10;18(1):1236 Internet. cited 2019 Jan 11. Available from: https://bmccancer.biomedcentral.com/articles/10.1186/s12885-018-5138-3.
[16] Yang S, Che SPY, Kurywchak P, Tavormina JL, Gansmo LB, Correa de Sampaio P, et al. Detection of mutant KRAS and TP53 DNA in circulating exosomes from healthy individuals and patients with pancreatic cancer. Cancer Biol Ther 2017 Mar 4;18(3): 158–65 Internet. cited 2019 Jan 11. Available from: https://www.tandfonline.com/doi/full/10.1080/15384047.2017.1281499.
[17] Allenson K, Castillo J, San Lucas FA, Scelo G, Kim DU, Bernard V, et al. High prevalence of mutant KRAS in circulating exosome-derived DNA from early-stage pancreatic cancer patients. Ann Oncol 2017;28(4):741–7.
[18] Vagner T, Spinelli C, Minciacchi VR, Balaj L, Zandian M, Conley A, et al. Large extracellular vesicles carry most of the tumour DNA circulating in prostate cancer patient plasma. J Extracell Vesicles 2018 Dec 7;7(1):1505403 Internet. cited 2019 Jan 11. Available from: https://www.tandfonline.com/doi/full/10.1080/20013078.2018.1505403.
[19] EV-TRACK Consortium J, Van Deun J, Mestdagh P, Agostinis P, Akay Ö, Anand S, et al. EV-TRACK: transparent reporting and centralizing knowledge in extracellular vesicle research. Nat Methods 2017 Feb 28;14(3):228–32 Internet. cited 2017 May 18. Available from: http://www.nature.com/doifinder/10.1038/nmeth.4185.
[20] Gardiner C, Di Vizio D, Sahoo S, Théry C, Witwer KW, Wauben M, et al. Techniques used for the isolation and characterization of extracellular vesicles: results of a worldwide survey. J Extracell Vesicles 2016 Oct 31;5(0) Internet. cited 2017 Jan 17. Available from: http://www.journalofextracellularvesicles.net/index.php/jev/article/view/32945.
[21] Momen-Heravi F, Balaj L, Alian S, Mantel P-Y, Halleck AE, Trachtenberg AJ, et al. Current methods for the isolation of extracellular vesicles. Biol Chem 2013 Jan 1;394 (10):1253–62 Internet. cited 2017 Jan 17. Available from: http://www.ncbi.nlm.nih.gov/pubmed/23770532.
[22] Cvjetkovic A, Lötvall J, Lässer C. The influence of rotor type and centrifugation time on the yield and purity of extracellular vesicles. J Extracell Vesicles 2014 Jan 24;3 (1):23111 Internet. cited 2017 May 18. Available from: https://www.tandfonline.com/doi/full/10.3402/jev.v3.23111.
[23] Liang K, Liu F, Fan J, Sun D, Liu C, Lyon CJ, et al. Nanoplasmonic quantification of tumour-derived extracellular vesicles in plasma microsamples for diagnosis and treatment monitoring. Nat Biomed Eng 2017 (pii: 0021).
[24] Wan Y, Cheng G, Liu X, Hao SJ, Nisic M, Zhu CD, et al. Rapid magnetic isolation of extracellular vesicles via lipid-based nanoprobes. Nat Biomed Eng 2017 (pii: 0058).
[25] Oliveira-Rodríguez M, López-Cobo S, Reyburn HT, Costa-García A, López-Martín S, Yáñez-Mó M, et al. Development of a rapid lateral flow immunoassay test for detection of exosomes previously enriched from cell culture medium and body fluids. J Extracell Vesicles 2016;5:31803.
[26] Deregibus MC, Figliolini F, D'Antico S, Manzini PM, Pasquino C, De Lena M, et al. Charge-based precipitation of extracellular vesicles. Int J Mol Med 2016 Nov 29;38 (5):1359–66 Internet. cited 2017 Jan 17. Available from: http://www.spandidos-publications.com/10.3892/ijmm.2016.2759.
[27] Kosanović M, Milutinović B, Goč S, Mitić N, Janković M. Ion-exchange chromatography purification of extracellular vesicles. Biotechniques 2017;63(2):65–71.
[28] Heath N, Grant L, De Oliveira TM, Rowlinson R, Osteikoetxea X, Dekker N, et al. Rapid isolation and enrichment of extracellular vesicle preparations using anion exchange chromatography. Sci Rep 2018 Dec 10;8(1):5730 Internet. cited 2019 Jan 11. Available from: http://www.ncbi.nlm.nih.gov/pubmed/29636530.
[29] Předota M, Machesky ML, Wesolowski DJ. Molecular origins of the zeta potential. Langmuir 2016;32(40):10189–98.
[30] Salgin S, Salgin U, Bahadir S. Zeta potentials and isoelectric points of biomolecules: the effects of ion types and ionic strengths. Int J Electrochem Sci 2012;7(12): 12404–14.
[31] Kaszuba M, Corbett J, Watson FM, Jones A. High-concentration zeta potential measurements using light-scattering techniques. Philos Trans R Soc A Math Phys Eng Sci 2010;368(1927):4439–51.
[32] Vogel R, Pal AK, Jambhrunkar S, Patel P, Thakur SS, Reátegui E, et al. High-resolution single particle zeta potential characterisation of biological nanoparticles using tunable resistive pulse sensing. Sci Rep 2017;7(1):17479.
[33] Rupert DLM, Claudio V, Lässer C, Bally M. Methods for the physical characterization and quantification of extracellular vesicles in biological samples. Biochim Biophys Acta 2017 Jan;1861(1 Pt A):3164–79 Internet. cited 2017 Jan 17. Available from: http://linkinghub.elsevier.com/retrieve/pii/S0304416516302756.
[34] Di Vizio D, Morello M, Dudley AC, Schow PW, Adam RM, Morley S, et al. Large oncosomes in human prostate cancer tissues and in the circulation of mice with metastatic disease. Am J Pathol 2012 Nov;181(5):1573–84 Internet. cited 2017 Jun 27. Available from http://www.ncbi.nlm.nih.gov/pubmed/23022210.
[35] Van Deun J, Mestdagh P, Sormunen R, Cocquyt V, Vermaelen K, Vandesompele J, et al. The impact of disparate isolation methods for extracellular vesicles on downstream RNA profiling. J Extracell Vesicles 2014 Sep 18;3(0) Internet. cited 2017 Jan 17. Available from: http://www.journalofextracellularvesicles.net/index.php/jev/article/view/24858.
[36] D'Agostino VG, Adami V, Provenzani A. A novel high throughput biochemical assay to evaluate the HuR protein-RNA complex formation. PLoS One 2013 Jan;8(8): e72426 Internet. cited 2014 Jul 25. Available from: http://www.pubmedcentral.nih.gov/articlerender.fcgi?artid=3741180&tool=pmcentrez&rendertype=abstract.
[37] Xu C, Liu K, Ahmed H, Loppnau P, Schapira M, Min J. Structural basis for the discriminative recognition of N^6-methyladenosine RNA by the human YT521-B homology domain family of proteins. J Biol Chem 2015 Oct 9;290(41):24902–13 Internet. cited 2017 May 25. Available from http://www.ncbi.nlm.nih.gov/pubmed/26318451.
[38] Llorente A, Skotland T, Sylvänne T, Kauhanen D, Róg T, Orłowski A, et al. Molecular lipidomics of exosomes released by PC-3 prostate cancer cells. Biochim Biophys Acta 2013 Jul;1831(7):1302–9 Internet. cited 2017 May 25. Available from http://www.ncbi.nlm.nih.gov/pubmed/24046871.
[39] Haraszti RA, Didiot M-C, Sapp E, Leszyk J, Shaffer SA, Rockwell HE, et al. High-resolution proteomic and lipidomic analysis of exosomes and microvesicles from different cell sources. J Extracell Vesicles 2016 Jan 24;5(1):32570 Internet. cited 2017 May 25. Available from: https://www.tandfonline.com/doi/full/10.3402/jev.v5.32570.
[40] MacDonald RC, MacDonald RI, Menco BP, Takeshita K, Subbarao NK, Hu LR. Small-volume extrusion apparatus for preparation of large, unilamellar vesicles. Biochim Biophys Acta 1991;1061(2):297–303 Internet. Jan 30 [cited 2017 Jun 27. Available from http://www.ncbi.nlm.nih.gov/pubmed/1998698.
[41] Vogel R, Coumans FAW, Maltesen RG, Böing AN, Bonnington KE, Broekman ML, et al. A standardized method to determine the concentration of extracellular vesicles using tunable resistive pulse sensing. J Extracell Vesicles 2016 Jan 24;5(1):31242 Internet. cited 2017 May 18. Available from https://www.tandfonline.com/doi/full/10.3402/jev.v5.31242.
[42] Colombo M, Moita C, van Niel G, Kowal J, Vigneron J, Benaroch P, et al. Analysis of ESCRT functions in exosome biogenesis, composition and secretion highlights the heterogeneity of extracellular vesicles. J Cell Sci 2013 Dec 15;126(24):5553–65 Internet. cited 2017 Jun 27. Available from http://www.ncbi.nlm.nih.gov/pubmed/24105262.
[43] Meister M, Tikkanen R. Endocytic trafficking of membrane-bound cargo: a flotillin point of view. Membranes (Basel) 2014 Jul 11;4(3):356–71 Internet. cited 2019 Jan 14. Available from: http://www.ncbi.nlm.nih.gov/pubmed/25019426.
[44] Yuana Y, Böing AN, Grootemaat AE, van der Pol E, Hau CM, Cizmar P, et al. Handling and storage of human body fluids for analysis of extracellular vesicles. J Extracell Vesicles 2015;4:29260.
[45] Wei Z, Batagov AO, Carter DRF, Krichevsky AM. Fetal bovine serum RNA interferes with the cell culture derived extracellular RNA. Sci Rep 2016 Aug 9;6(1):31175 Internet. cited 2017 May 18. Available from: http://www.nature.com/articles/srep31175.
[46] Abels ER, Breakefield XO. Introduction to extracellular vesicles: biogenesis, RNA cargo selection, content, release, and uptake. Cell Mol Neurobiol 2016 Apr 6;36 (3):301–12 Internet. cited 2017 May 18. Available from http://link.springer.com/10.1007/s10571-016-0366-z.
[47] Nomura S. Extracellular vesicles and blood diseases. Int J Hematol 2017 Apr 27;105 (4):392–405 Internet. cited 2017 May 18. Available from: http://link.springer.com/10.1007/s12185-017-2180-x.
[48] Wolf P. The nature and significance of platelet products in human plasma. Br J Haematol 1967;13(3):269–88.
[49] Wisgrill L, Lamm C, Hartmann J, Preißing F, Dragosits K, Bee A, et al. Peripheral blood microvesicles secretion is influenced by storage time, temperature, and anticoagulants. Cytom Part A 2016 Jul;89(7):663–72 Internet. cited 2019 Jan 14. Available from http://www.ncbi.nlm.nih.gov/pubmed/27442840.
[50] Valkonen S, van der Pol E, Böing A, Yuana Y, Yliperttula M, Nieuwland R, et al. Biological reference materials for extracellular vesicle studies. Eur J Pharm Sci 2017 Feb 15;98:4–16 Internet. cited 2017 May 18. Available from http://linkinghub.elsevier.com/retrieve/pii/S0928098716303578.
[51] Vagida M, Arakelyan A, Lebedeva A, Grivel J-C, Shpektor A, Vasilieva E, et al. Flow analysis of individual blood extracellular vesicles in acute coronary syndrome. Platelets 2017 Mar 17;28(2):165–73 Internet. cited 2017 May 18. Available from https://www.tandfonline.com/doi/full/10.1080/09537104.2016.1212002.
[52] Melki I, Tessandier N, Zufferey A, Boilard E. Platelet microvesicles in health and disease. Platelets 2017;28(3):214–21.
[53] Aatonen MT, Ohman T, Nyman TA, Laitinen S, Grönholm M, Siljander PR-M. Isolation and characterization of platelet-derived extracellular vesicles. J Extracell Vesicles 2014;3 Internet. cited 2017 Feb 8. Available from http://www.ncbi.nlm.nih.gov/pubmed/25147646.
[54] Woodford-Thomas T, Thomas ML. The leukocyte common antigen, CD45 and other protein tyrosine phosphatases in hematopoietic cells. Semin Cell Biol 1993 Dec;4(6):

409–37 Internet. cited 2017 Jul 31. Available from http://www.ncbi.nlm.nih.gov/pubmed/8305680.

[55] Cardi G, Mastrangelo MJ, Berd D. Depletion of T-cells with the CD4+CD45R+ phenotype in lymphocytes that infiltrate subcutaneous metastases of human melanoma. Cancer Res 1989 Dec 1;49(23):6562–5 Internet. cited 2017 Jul 31. Available from: http://www.ncbi.nlm.nih.gov/pubmed/2479465.

[56] Belov L, Matic KJ, Hallal S, Best OG, Mulligan SP, Christopherson RI. Extensive surface protein profiles of extracellular vesicles from cancer cells may provide diagnostic signatures from blood samples. J Extracell Vesicles 2016;5:25355 Internet. cited 2017 Aug 1. Available from http://www.ncbi.nlm.nih.gov/pubmed/27086589.

[57] Yoshioka Y, Kosaka N, Konishi Y, Ohta H, Okamoto H, Sonoda H, et al. Ultra-sensitive liquid biopsy of circulating extracellular vesicles using ExoScreen. Nat Commun 2014;5:3591.

[58] Smith ZJ, Lee C, Rojalin T, Carney RP, Hazari S, Knudson A, et al. Single exosome study reveals subpopulations distributed among cell lines with variability related to membrane content. J Extracell Vesicles 2015;4:28533.

[59] Jeppesen DK, Hvam ML, Primdahl-Bengtson B, Boysen AT, Whitehead B, Dyrskjï¿½t L, et al. Comparative analysis of discrete exosome fractions obtained by differential centrifugation. J Extracell Vesicles 2014;3:25011.

[60] Yoshioka Y, Konishi Y, Kosaka N, Katsuda T, Kato T, Ochiya T. Comparative marker analysis of extracellular vesicles in different human cancer types. J Extracell Vesicles 2013;2.

[61] Tatischeff I. Innovative approach of prostate cancer by the way of tumour cell-derived extracellular vesicles. J Extracell Vesicles 2016. https://doi.org/10.0.13.74/jev.v5.31552.

[62] Chen WW, Balaj L, Liau LM, Samuels ML, Kotsopoulos SK, Maguire CA, et al. Beaming and droplet digital pcr analysis of mutant idh1 mrna in glioma patient serum and cerebrospinal fluid extracellular vesicles. Mol Ther Nucleic Acids 2013;2 (e109).

[63] McDonald B, Reep B, Lapetina EG, Molina y Vedia L. Glyceraldehyde-3-phosphate dehydrogenase is required for the transport of nitric oxide in platelets. Proc Natl Acad Sci U S A 1993 Dec 1;90(23):11122–6 Internet. cited 2017 May 18. Available from http://www.ncbi.nlm.nih.gov/pubmed/7902582.

[64] Ulivi P, Scarpi E, Passardi A, Marisi G, Calistri D, Zoli W, et al. eNOS polymorphisms as predictors of efficacy of bevacizumab-based chemotherapy in metastatic colorectal cancer: data from a randomized clinical trial. J Transl Med 2015;13:258.

[65] Marisi G, Scarpi E, Passardi A, Nanni O, Ragazzini A, Valgiusti M, et al. Circulating VEGF and eNOS variations as predictors of outcome in metastatic colorectal cancer patients receiving bevacizumab. Sci Rep 2017;7(1):1293.

[66] Tian Y, Ma L, Gong M, Su G, Zhu S, Zhang W, et al. Protein profiling and sizing of extracellular vesicles from colorectal cancer patients via flow cytometry. ACS Nano 2018;12(1):671–80.

[67] Ramakrishnaiah V, Thumann C, Fofana I, Habersetzer F, Pan Q, de Ruiter PE, et al. Exosome-mediated transmission of hepatitis C virus between human hepatoma Huh7.5 cells. Proc Natl Acad Sci 2013;110(32):13109–13.

[68] Nakai W, Yoshida T, Diez D, Miyatake Y, Nishibu T, Imawaka N, et al. A novel affinity-based method for the isolation of highly purified extracellular vesicles. Sci Rep 2016 Sep 23;6:33935 Internet. cited 2017 Jan 17. Available from: http://www.nature.com/articles/srep33935.

[69] Kim D, Nishida H, An SY, Shetty AK, Bartosh TJ, Prockop DJ. Chromatographically isolated CD63+CD81+ extracellular vesicles from mesenchymal stromal cells rescue cognitive impairments after TBI. Proc Natl Acad Sci U S A 2016 Jan 5;113(1):170–5 Internet. cited 2019 Jan 14. Available from http://www.pnas.org/lookup/doi/10.1073/pnas.1522297113.

[70] Srinivas PR, Kramer BS, Srivastava S. Trends in biomarker research for cancer detection. Lancet Oncol 2001;2(11):698–704.

[71] Phipps AI, Limburg PJ, Baron JA, Burnett-Hartman AN, Weisenberger DJ, Laird PW, et al. Association between molecular subtypes of colorectal cancer and patient survival. Gastroenterology 2015;148(1) (77-87.e2).

[72] Thomsen M, Skovlund E, Sorbye H, Bolstad N, Nustad KJ, Glimelius B, et al. Prognostic role of carcinoembryonic antigen and carbohydrate antigen 19-9 in metastatic colorectal cancer : a BRAF -mutant subset with high CA 19-9 level and poor outcome. Br J Cancer 2018. https://doi.org/10.1038/s41416-018-0115-9 Internet. (March). Available from:.

[73] El-Deiry WS, Vijayvergia N, Xiu J, Scicchitano A, Lim B, Yee NS, et al. Molecular profiling of 6,892 colorectal cancer samples suggests different possible treatment options specific to metastatic sites. Cancer Biol Ther 2015;16(12):1726–37.

[74] Rolfo C, Mack PC, Scagliotti GV, Baas P, Barlesi F, Bivona TG, et al. IASLC statement paper: liquid biopsy for advanced non-small cell lung cancer (NSCLC). J Thorac Oncol 2018;13(9):1248–68.